

2000

## Well Integrity Mechanism, Failure, and Testing in Shallow Marine Sediments.

Desheng Zhou  
*Louisiana State University and Agricultural & Mechanical College*

Follow this and additional works at: [https://repository.lsu.edu/gradschool\\_disstheses](https://repository.lsu.edu/gradschool_disstheses)

---

### Recommended Citation

Zhou, Desheng, "Well Integrity Mechanism, Failure, and Testing in Shallow Marine Sediments." (2000). *LSU Historical Dissertations and Theses*. 7405.  
[https://repository.lsu.edu/gradschool\\_disstheses/7405](https://repository.lsu.edu/gradschool_disstheses/7405)

This Dissertation is brought to you for free and open access by the Graduate School at LSU Scholarly Repository. It has been accepted for inclusion in LSU Historical Dissertations and Theses by an authorized administrator of LSU Scholarly Repository. For more information, please contact [gradetd@lsu.edu](mailto:gradetd@lsu.edu).

## INFORMATION TO USERS

This manuscript has been reproduced from the microfilm master. UMI films the text directly from the original or copy submitted. Thus, some thesis and dissertation copies are in typewriter face, while others may be from any type of computer printer.

**The quality of this reproduction is dependent upon the quality of the copy submitted.** Broken or indistinct print, colored or poor quality illustrations and photographs, print bleedthrough, substandard margins, and improper alignment can adversely affect reproduction.

In the unlikely event that the author did not send UMI a complete manuscript and there are missing pages, these will be noted. Also, if unauthorized copyright material had to be removed, a note will indicate the deletion.

Oversize materials (e.g., maps, drawings, charts) are reproduced by sectioning the original, beginning at the upper left-hand corner and continuing from left to right in equal sections with small overlaps. Each original is also photographed in one exposure and is included in reduced form at the back of the book.

Photographs included in the original manuscript have been reproduced xerographically in this copy. Higher quality 6" x 9" black and white photographic prints are available for any photographs or illustrations appearing in this copy for an additional charge. Contact UMI directly to order.

**UMI<sup>®</sup>**

Bell & Howell Information and Learning  
300 North Zeeb Road, Ann Arbor, MI 48106-1346 USA  
800-521-0600



**WELL INTEGRITY MECHANISM, FAILURE, AND TESTING  
IN  
SHALLOW MARINE SEDIMENTS**

**A Dissertation**

**Submitted to the Graduate Faculty of the  
Louisiana State University and  
Agricultural and Mechanical College  
in partial fulfillment of the  
requirements for the degree of  
Doctor of Philosophy**

**in**

**The Department of Petroleum Engineering**

**by**

**Desheng Zhou**

**B.S., Beijing University of Aeronautics & Astronautics, P. R. China, 1985**

**M.S., Southwest Petroleum Institute, P. R. China, 1988**

**Doctor of Engineering, Southwest Petroleum Institute, P. R. China, 1992**

**December, 2000**

UMI Number: 9998724

UMI<sup>®</sup>

---

UMI Microform 9998724

Copyright 2001 by Bell & Howell Information and Learning Company.

All rights reserved. This microform edition is protected against  
unauthorized copying under Title 17, United States Code.

---

Bell & Howell Information and Learning Company  
300 North Zeeb Road  
P.O. Box 1346  
Ann Arbor, MI 48106-1346

## ACKNOWLEDGMENTS

I express my gratitude and appreciation to my major professor, Dr. Andrew K. Wojtanowicz, professor of Department of Petroleum Engineering, under whose continuous guidance and supervision this work was completed.

Sincere thanks and appreciation are also extended to Dr. Adam Bourgoyne, Dr. Zaki Bassiouni, Dr. Julius P. Langlinais, Dr. John Smith and Dr. Jeff Nunn for their professional advice and kind support. Special thanks are extended to the other faculty and student members of the Petroleum Engineering Department who were directly or indirectly involved with this work.

I would like to thank Craft & Hawkins Department of Petroleum Engineering at Louisiana State University and Mineral Management Services (MMS) for providing financial support for this work. Finally, Amoco, Unocal, and Amerada Hess companies are to be thanked for providing the field test data.

## TABLE OF CONTENTS

ACKNOWLEDGMENTS.....	ii
LIST OF TABLES.....	vi
LIST OF FIGURES.....	vii
NOMENCLATURE.....	xii
ABBREVIATIONS.....	xvi
ABSTRACT.....	xvii
CHAPTER 1 INTRODUCTION.....	1
1.1 Estimation of Formation Fracture Pressure.....	3
1.2 Leak-off Test Data Base.....	5
1.3 Leak-off Test.....	5
1.4 Cement Fracturing and Relation .....	8
1.5 Objectives and Methodologies.....	9
CHAPTER 2. LITERATURE REVIEW.....	12
2.1 Rock Mechanics.....	12
2.1.1 Stress Tensor.....	12
2.1.2 Stress-Strain Relation.....	15
2.2 Yield and Fracture Mechanism.....	16
2.2.1 Yield Criterion.....	16
2.2.2 Fracture Mechanism.....	20
2.3 In-Situ Underground Stress.....	22
2.3.1 Overburden Pressure.....	23
2.3.2 Formation Pore Pressure.....	26
2.4 Open Hole Stress Distribution.....	26
2.4.1 Elastic Well.....	27
2.4.2 Plastic Well.....	29
2.5 Formation Fracture Prediction Methods.....	31
2.5.1 Horizontal to Vertical Stress Ratio.....	32
2.5.2 Water Effect.....	35
2.6 Leak-off Test Procedures And Analysis Techniques.....	35
2.6.1 Leak-off Test Procedures.....	36
2.6.2 Leak-off Test Plots.....	43
2.6.3 Interpretation Techniques.....	47
2.6.4 Modeling Leak-off Test Results.....	58
CHAPTER 3. DATA ANALYSIS IN SHALLOW MARINE SEDIMENTS.....	61
3.1 Soil Properties in Green Canyon of Gulf of Mexico.....	61
3.2 Leak-off Test Plots.....	68

3.3 Leak-off Pressure (Formation Fracture Pressure) Analysis.....	78
3.4 Leak-off Test Database.....	84
<b>CHAPTER 4. ANALYTICAL MODEL IN SHALLOW MARINE</b>	
<b>SEDIMENTS.....</b>	<b>87</b>
4.1 In-situ Stress Model for Shallow Marine Sediments.....	88
4.1.1 In-situ Elastic Stresses.....	88
4.1.2 In-situ Plastic Stress Model.....	89
4.1.3 In-Situ Stresses of Green Canyon in Gulf of Mexico.....	90
4.2 Stress Distribution around A Wellbore due to Drilling Operation.....	91
4.2.1 Condition of Forming Plastic Annular.....	92
4.2.2 Stress Distribution in Plastic Zone.....	95
4.3 Stress Distribution around A Wellbore due to Leak-off Test.....	101
4.4 Fracture Pressure.....	103
4.4.1 Vertical Fracture of Elastic Wellbore.....	104
4.4.2 Vertical Fracture of Plastic Wellbore.....	105
<b>CHAPTER 5. FINITE ELEMENT ANALYSES OF LEAK-OFF TEST.....</b>	<b>109</b>
5.1 Mechanical Models.....	110
5.1.1 Basic Relation.....	110
5.1.2 Constitutive Equation.....	111
5.2 Finite Element Method.....	113
5.2.1 Finite Element Models.....	113
5.2.2 Procedures.....	114
5.3 Using ABAQUS/Standard-A Finite Element Software.....	115
5.3.1 ABAQUS functions.....	115
5.3.2 Parameters of Drucker-Prager Criterion.....	117
5.4 Finite Element Model for Leak-off Test.....	118
5.4.1 Geometry.....	118
5.4.2 Divided Nodes and Elements.....	119
5.4.3 Boundary Conditions.....	120
5.4.4 Sample Rocks.....	121
5.5 Results from Finite Element Analysis.....	122
5.5.1 Case 1-Elastic Wellbore.....	124
5.5.2 Case 2-Plastic Wellbore.....	125
5.5.3 Case 3-Plastic Formation.....	127
5.6 Horizontal Fracture.....	128
5.7 Cement Parting.....	135
5.8 Finite Element Validation of In-situ Stress Model.....	139
5.8.1 Analytical Results.....	140
5.8.2 Finite Element Model.....	141
5.8.3 Simulated Results.....	142
<b>CHAPTER 6. CEMENT PARTING.....</b>	<b>146</b>
6.1 Contact Stress Model.....	146
6.1.1 Contact Stress Concept.....	147

6.1.2 Cement Slurry Pressure Reduction.....	147
6.1.3 Mathematical Model.....	148
6.2 Cement Parting Pressure.....	150
6.3 Field Example.....	152
6.4 Sensitivity Analysis.....	157
CHAPTER 7. MODELING LEAK-OFF TEST IN SHALLOW MARINE SEDIMENTS.....	159
7.1 Wellbore Expanded Volume.....	160
7.2 Loss into Rock.....	162
7.3 Plastic Fracture in Plastic Zone.....	164
7.4 Cement Parting between Cement and Rock.....	168
7.5 Modeling Leak-off Test.....	171
7.6 Model Analysis.....	174
7.7 Developed Software-LOTUMS.....	175
CHAPTER 8. INTERPRETATION OF LEAK-OFF TEST IN SHALLOW MARINE SEDIMENTS.....	181
8.1 Leak-off Test Plot in Shallow Marine Sediments.....	181
8.2 Analysis of Leak-off Test with Rock Fracturing.....	183
8.2.1 Overburden and Maximum Hydrostatic Pressure Lines.....	184
8.2.2 Examples.....	186
8.3 Pressure Level-off Section Analysis.....	188
8.3.1 Normalizing Time Unit Scale.....	189
8.3.2 Construction of Level-off Section.....	190
8.4 Interpretation Using Graphic Technique.....	193
8.4.1 Cement Parting.....	194
8.4.2 Leaking.....	195
CHAPTER 9. SUMMARY AND CONCLUSIONS.....	198
REFERENCES.....	203
APPENDIX	
A. IN-SITU STRESS IN PLASTIC FORMATION .....	209
B. ELASTO-PLASTIC BOUNDARY.....	217
C. PART OF FINITE ELEMENT ANALYSIS RESULTS.....	219
D. CEMENT CONTACT STRESS AT CASING SHOE.....	236
E. WELLBORE EXPANSION.....	246
F. FORMATION FRACTURE WIDTH AND VOLUME.....	249
G. ANNULAR CRACK.....	253
H. LOTUMS SOFTWARE.....	255
I. OVERBURDEN PRESSURE IN SHALLOW MARINE SEDIMENTS.....	260
VITA.....	267

## LIST OF TABLES

Table 2.1	LOT record (courtesy of Amoco).....	45
Table 3.1	Summary of deformation-controlled simple shear test results, boring 1, Block 184, Green Canyon Area.....	63
Table 3.2	Major Soil Strata in Green Canyon.....	63
Table 3.3	Values of yield pressure gradients from LOTs in UMS.....	71
Table 3.4	Offshore LOT data file record example.....	84
Table 3.5	Onshore LOT data file record example.....	85
Table 3.6	Symbols of fields of Table 3.4.....	85
Table 5.1	Data for horizontal fracture simulation study.....	134
Table 5.2	Data for annular channeling simulation study.....	137
Table 5.3	Stress Ratio in Elastic State.....	142
Table 5.4	Stress Ratio in Plastic State.....	143
Table 5.5	Stress Ratio From Elastic To Plastic State.....	144
Table 6.1	Example data.....	154
Table 6.2	Cement fracture calculations: Case 1 (shale) and Case 2 (sand).....	155
Table 6.3	Compensation sensitivity in 30” and 20” examples.....	158

## LIST OF FIGURES

Figure 1.1	Casing shoe sets based upon formation fracture pressure.....	2
Figure 1.2	Fracture mechanism.....	3
Figure 1.3	Fractures in formation or cement.....	6
Figure 1.4	Typical leak-off test plot.....	7
Figure 1.5	Relation among LOT, LOT data, Predicted FFP and Set Casing.....	9
Figure 2.1	Schematic representation of the nine stress components acting in a cubic element (Jaeger, 1979).....	13
Figure 2.2	Mohr-Coulomb and Drager-Prager criteria in principle stress space (Chen and Han, 1988).....	19
Figure 2.3	Fluid pressure distribution around a well.....	21
Figure 2.4	Underground stress distribution in relatively young deltaic sediments (Bourgoyne et al, 1991).....	23
Figure 2.5	Stress distribution around a wellbore.....	27
Figure 2.6	Leak-off Test.....	36
Figure 2.7	Preparing guide lines for leak-off test (Postler, 1997).....	39
Figure 2.8	Typical Leak-off Test Plot (Postler, 1997).....	43
Figure 2.9	Typical leak-off test with reference lines. ....	44
Figure 2.10	A more complete record example of leak-off test result (courtesy of Amoco).....	46
Figure 2.11	Stopping pump during leak-off test.....	47
Figure 2.12	Common interpretation of leak-off test result.....	48
Figure 2.13	Casing integrity test result (courtesy of Amoco).....	49
Figure 2.14	Pumping rate effect (Postler, 1997).....	50
Figure 2.15	Rock fracture and fracture propagation under leak-off test (Morita et al. , 1991).....	52

Figure 2.16	Effect of pre-existing crack length (Ishijima and Roegiers, 1983).....	52
Figure 2.17	Leak-off test under different rocks (courtesy of HESS).....	53
Figure 2.18	Interpretation of leak-off test result (courtesy of Amoco).....	54
Figure 2.19	Effect of channels on leak-off test result (Postler, 1997).....	56
Figure 3.1	Borings location map (Block 184, Green Canyon in Gulf of Mexico).....	62
Figure 3.2	Effective vertical stress vs. depth below sea floor.....	64
Figure 3.3	Poisson's ratio vs. depth below sea floor.....	65
Figure 3.4	Shear modulus vs. depth below sea floor.....	66
Figure 3.5	Cohesion strength vs. depth below sea floor.....	66
Figure 3.6	Friction angle vs. depth below sea floor.....	67
Figure 3.7	Typical LOT in deep formation.....	68
Figure 3.8	Non-linear LOT in shallow marine sediments.....	69
Figure 3.9	Nonlinear LOT in UMS with "yield" pressure.....	70
Figure 3.10	Fewer tested points to maximum pressure.....	72
Figure 3.11	Almost no pressure drop of maximum pressure.....	73
Figure 3.12	Pressure drop after shut-in and level-off.....	74
Figure 3.13	Traditional method based on straight line fails.....	74
Figure 3.14	Leak-off test result in UMS.....	75
Figure 3.15	Non-linear LOT.....	75
Figure 3.16	LOT and stabilized LOT.....	76
Figure 3.17	LOT and stabilized LOT.....	77
Figure 3.18	LOT and stabilized LOT in SMS.....	77
Figure 3.19	Typical formation fracture pressure curve for deep wells.....	78

Figure 3.20	Shallow scatter LOT data from West Cameron.....	79
Figure 3.21	Narrower scatter of LOT data with depth from High Island.....	80
Figure 3.22	No correlation, impossible to use minimum data, and average data at depth having high risk (North Sea, UK).....	81
Figure 3.23	Scatter in shallow with one almost equals mud density (Eugene Island).....	81
Figure 3.24	A LOP at 1000 ft is almost 2 ppg greater than those around 1500 ft...	82
Figure 3.25	Minimum LOP is too conservative and average LOP has high risk (SES, Brazil).....	82
Figure 3.26	No trend for shallow marine sediments (Main Pass).....	83
Figure 3.27	LOT gradient versus depth.....	86
Figure 3.28	Fracture gradient distribution from 7658 shallow LOTs.....	86
Figure 4.1	Stresses around a wellbore.....	92
Figure 4.2	Stress distribution around an elastic wellbore.....	93
Figure 4.3	Stress distribution around a wellbore with largest tangential stress....	98
Figure 4.4	Stress distribution around a wellbore with largest vertical stress.....	99
Figure 4.5	Formation fracturing when tangential stress gets tensile (negative)...	104
Figure 4.6	Tangential stress cannot be reduced to tensile and formation re-yield.....	108
Figure 5.1	Calculation part geometry: (a). Geometry; (b). Division.....	118
Figure 5.2	Finite element analytical nodes and elements.....	120
Figure 5.3	Special analytical places.....	123
Figure 5.4	Finite element results for Case 2 during LOT.....	124
Figure 5.5	Model of vertical fracture initialization during LOT.....	128
Figure 5.6	Concentration of tangential stress at top/bottom of open hole shows no tension during LOT.....	130

Figure 5.7	Model for horizontal fracture initiation during LOT.....	132
Figure 5.8	Vertical stress change shows initiation of horizontal fracture at casing shoe during LOT.....	133
Figure 5.9	Contact stress change shows initiation of channel at bottom of cemented casing during LOT.....	136
Figure 6.1	Cement parting.....	150
Figure 6.2	Case 1 (30") well configuration.....	153
Figure 6.3	Case 2 (20") well configuration.....	153
Figure 6.4	LOT at 20" casing shoe.....	156
Figure 7.1	Expansion of wellbore with plastic zone is controlled by outer elastic zone.....	160
Figure 7.2	Horizontal (plastic, non-penetrating) fracture in plastic zone around wellbore.....	164
Figure 7.3	Width of plastic fracture vs. radial distance.....	166
Figure 7.4	Volume taken by rock fracture in plastic zone.....	167
Figure 7.5	Annular cement parting between cement and rock is opened by increasing LOT pressure.....	169
Figure 7.6	Non-linear behavior of annular crack.....	170
Figure 7.7	Leak-off test software main interface.....	176
Figure 7.8	Data input form.....	177
Figure 7.9	Stress analysis form.....	178
Figure 7.10	Set printer.....	179
Figure 7.11	Fracture analysis form.....	179
Figure 7.12	Leak-off test analysis.....	180
Figure 8.1	Conceptual/typical leak-off test result in shallow marine sediment for interpretation.....	182

Figure 8.2	Rock fracture.....	186
Figure 8.3	Cement parting or leaking.....	187
Figure 8.4	Level-off section DE level-off ?.....	188
Figure 8.5	Normalizing time and volume scale by making the length of per minute equal to the length of a pumping rate value.....	189
Figure 8.6	Graphic expression of pressure build-up.....	191
Figure 8.7	Construction of level-off section.....	192
Figure 8.8	Interpretation Example I.....	194
Figure 8.9	Interpretation Example II.....	196
Figure 8.10	Constructing level-off section for Example II.....	197

## NOMENCLATURE

A	- area, [L <sup>2</sup> ]
A <sub>cs</sub>	- cross section area, [L <sup>2</sup> ]
C	- compressibility [LT <sup>2</sup> /M]
D	-depth, [L]
D <sub>s</sub>	-sediment depth, [L]
D <sub>w</sub>	-water depth, [L]
E	-Young's modulus, [M/(LT <sup>2</sup> )]
F <sub>σ</sub>	-ratio of horizontal to vertical stresses
H	- open hole height for leak-off test, [L]
h	- open hole height for cementing, [L]
h <sub>csg</sub>	- casing length, [L]
h <sub>mc</sub>	- mud cake thickness, [L]
K	- permeability, [L <sup>2</sup> ]
N	-rock property
p	- pressure, [M/(LT <sup>2</sup> )]
p <sub>f</sub>	- fracture pressure, [M/(LT <sup>2</sup> )]
p <sub>i</sub>	- pressure inside the casing, [M/(LT <sup>2</sup> )]
p <sub>LOT</sub>	-effective leak-off pressure, [M/(LT <sup>2</sup> )]
p <sub>o</sub>	- pore pressure, [M/(LT <sup>2</sup> )]
p <sub>w</sub>	-effective wellbore pressure, [M/(LT <sup>2</sup> )]
p' <sub>w</sub>	-critical wellbore pressure, [M/(LT <sup>2</sup> )]
q	- rate, [L <sup>3</sup> /T]

$R$	-radial distance in plastic zone, [L]
$r_c$	-radial distance of elasto-plastic boundary, [L]
$r_i$	- inner casing radius, [L]
$r_o$	- outer casing radius, [L]
$r$	- radius, [L]
$r_w$	- well radius, [L]
$t$	- time, [T]
$T$	- temperature
$u_w$	-radial displacement of wellbore wall, [L]
$V$	- volume, [L <sup>3</sup> ]
$V_{csg}$	- casing expansion volume, [L <sup>3</sup> ]
$V_w$	- borehole expansion volume, [L <sup>3</sup> ]
$V_f$	- leak volume, [L <sup>3</sup> ]
$V_o$	- initial system volume, [L <sup>3</sup> ]
$w$	-fracture width, [L]

**Greek Letters:**

$\Delta$	- difference or increment
$\varepsilon$	- strain, [L/L]
$\varepsilon_d$	- diametral strain, [L/L]
$\varepsilon_r$	- radial strain, [L/L]
$\varepsilon_\theta$	- tangential strain, [L/L]
$\varepsilon_z$	- vertical strain, [L/L]
$\phi$	- porosity, angle of internal friction

$\lambda$	-Lame's constant
$\mu$	- Poisson's ratio
$\mu_p$	-mud plastic viscosity, [M/(LT)]
$\pi$	- constant (3.141593)
$\theta$	- angle (radian), tangential (circumferential)
$\rho$	- density, [M/L <sup>3</sup> ]
$\rho_b$	- bulk density, [M/L <sup>3</sup> ]
$\rho_m$	- mud density, [M/L <sup>3</sup> ]
$\sigma_0$	-unconfined axial compressive strength, [M/(LT <sup>2</sup> )]
$\sigma_1$	-maximum principal stress, [M/(LT <sup>2</sup> )]
$\sigma_2$	-middle principal stress, [M/(LT <sup>2</sup> )]
$\sigma_3$	-minimum principal stress, [M/(LT <sup>2</sup> )]
$\sigma_h$	- effective horizontal stress, [M/(LT <sup>2</sup> )]
$\sigma_r$	- radial stress, [M/(LT <sup>2</sup> )]
$\sigma_v$	- vertical stress, [M/(LT <sup>2</sup> )]
$\sigma_\theta$	- tangential stress, [M/(LT <sup>2</sup> )]
$\sigma_z$	- vertical stress, [M/(LT <sup>2</sup> )]
$\tau$	- shear stress, [M/(LT <sup>2</sup> )]
$\tau_0$	-cohesive strength, [M/(LT <sup>2</sup> )]
$\tau_y$	-mud yield point

**Subscripts:**

**b** - bulk

**c** - contact stress  
**cs** - cross section  
**csg** - casing  
**de** - reduction  
**f** - filtration  
**ff** - formation fracture  
**m** -mud  
**o** - outer, initial, surface  
**over** - overburden  
**T** - temperature  
**v** - vertical  
**w** - wellbore  
**ww** -wellbore wall  
**x** - direction  
**y** - direction  
**z** - direction

## ABBREVIATIONS

FEA:	Finite Element Analysis
FFP:	Formation Fracture Pressure
LOP:	Leak-off Pressure
LOT:	Leak-off Test
SMS:	Shallow Marine Sediments
SGS:	Static Gel Strength
UPS:	Upper Marine Sediments

## ABSTRACT

The leak-off test (LOT) is an in-situ method for testing casing shoe integrity in a well. It is used to evaluate the cement and formation integrity relative to the well plan specifications. The results determine whether any remedial cementing or corrective actions are required and are a basis for planning future wells in the area. Typical analysis of LOTs assumes an elastic wellbore and involves identification of linear trends on the recorded plots. However, LOTs recorded in shallow marine sediments (SMS) are inherently nonlinear and their analysis is a problem.

Starting from the analyses of shallow soil properties, LOT plots, and leak-off pressure data, the dissertation presents the results of a theoretical study (analytical and numerical-finite element analysis) into potential for damage to cement integrity at the casing shoe resulting from leak-off test in SMS. Stress, strain and displacement around the open hole are analyzed before and during LOT. Three types of possible failures from LOTs were considered: vertical fracture, horizontal fracture, and cement parting.

It is proved that vertical fracture is the most unlikely failure of the three. Although horizontal fractures are initiated at low pressure in the plastic zone around the wellbore, they cannot propagate beyond the plastic zone until wellbore pressures exceed overburden pressures. Cement parting, on the other hand, may propagate upwards at pressures lower than overburden pressure. The study identifies two factors, related directly to drilling technology, that control critical pressure of cement parting: contact stress and drilling fluid penetration. It is shown in the study that changes in cementing and drilling practices can improve casing shoe integrity and reduce the need for remedial cement squeezes.

A general pressure-volume model of a LOT is presented including volumetric effects of wellbore expansion, mud loss into the rock, and propagation of both cement parting and plastic fracture. Software entitled LOTUMS was developed to simulate LOTs in SMS. A method is also proposed to identify the mechanisms controlling LOT results using known overburden pressure and the shape of LOT plot.

# CHAPTER 1

## INTRODUCTION

Safety and economy drilling needs knowing formation fracture pressure. Formation fracture pressure is the hydrostatic wellbore pressure at which the exposed formation will be ruptured and take into wellbore fluid. It determines the upper limit of drilling mud weight. Cautions should be taken during drilling since if mud hydrostatic pressure exceeds formation fracture pressure expensive drilling fluid will lose through the fractured formation. Further, problems such as wellbore collapse, gas kick, and even blowout may follow for the wellbore pressure reduction due to drilling fluid lose.

Formation fracture pressure is also a predominant factor in well control. When formation pressure exceeds mud pressure, formation fluid will flow into the well from a permeable formation. This is called a kick. Kick can be control by increasing drilling fluid pressure (well control). Failure of well control is so called blowout. For a successful well control, the wellbore pressure must be increased higher than formation pressure to prevent further kick but maintain lower than formation fracture pressure for prevent blowout. Blowout may be the worst disaster during drilling operation. It can cause loss of life, drilling equipment, the well, oil and gas reserves, and damage to environment.

Formation fracture pressure is also the major factor for well planning. Fig. 1.1 shows the method of determining casing depth. Formation pore pressure and formation fracture pressure are plotted with depth on the figure. Drilling fluid density is determined from formation pressure by adding a trip margin, generally 0.5 lb/gal.

Allowable maximum pressure is taken from formation fracture pressure by subtracting 0.5 lb/gal for safety. The design starts from the bottom hole of the well (Point A). The mud weight of Point A will fracture the exposed formation at Point B. Consequently, to reach Point A, a casing must be set to cover the exposed formation above Point B. Find the mud density (Point A') at the depth of Point B and find the casing shoe depth of Point B' follow the same procedure, and so on. Inaccurate formation fracture pressure may result in more casing string setting or blowout and increase drilling cost.

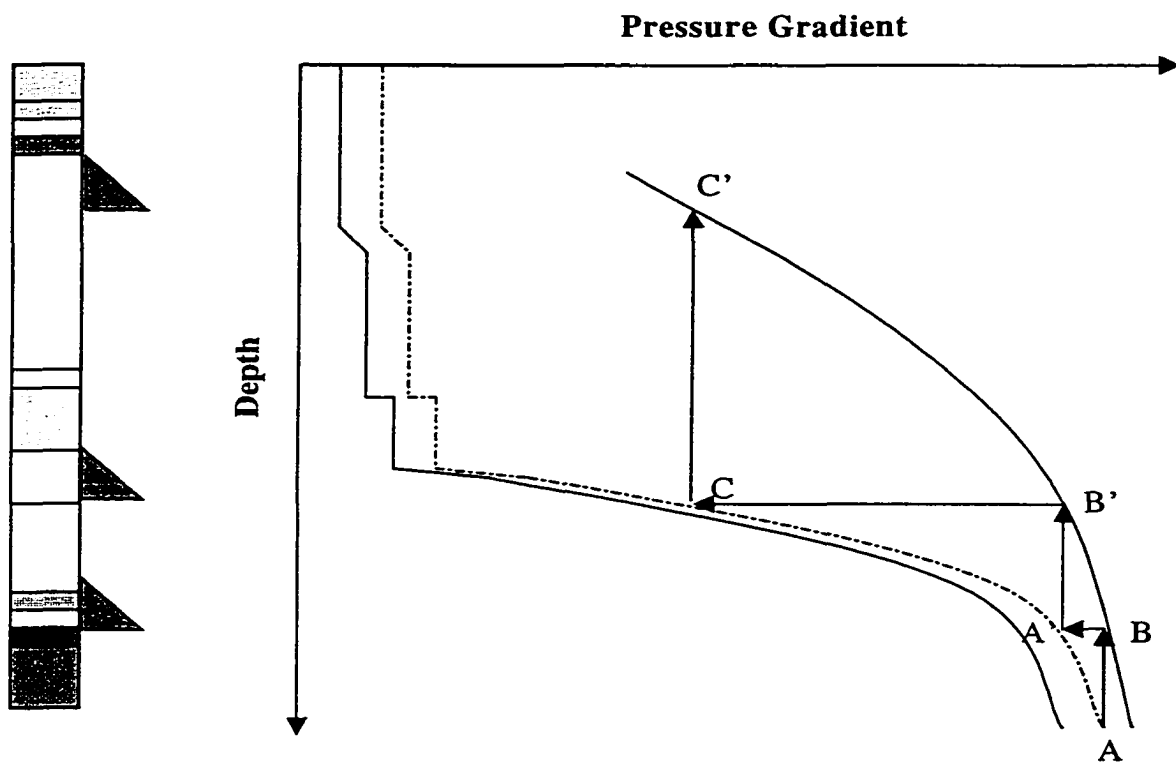


**Figure 1.1 Casing shoe sets based upon formation fracture pressure.**

The three reasons listed above illustrate the study of formation fracture pressure will never be overemphasized. Furthermore, cementing slurry weight and operation also depends on formation fracture pressure. Many methods have been developed to estimate formation fracture pressure.

## 1.1 Estimation of Formation Fracture Pressure

Fracture mechanism is shown in Fig. 1.2. When fluid pressure overcomes the closing pressure (minimum principle stress for 3-D case) and formation tensile strength, fracture is formed perpendicular to the closing pressure. Since formation is a porous fluid fills the pores. The pore fluid pressure is so called formation (pore) pressure. Pore pressure may change with stress change but this change is generally ignored in FFP analyses. Pore pressure should be subtracted from both the fluid pressure and the closing pressure for porous medium. This is so called effective stress.

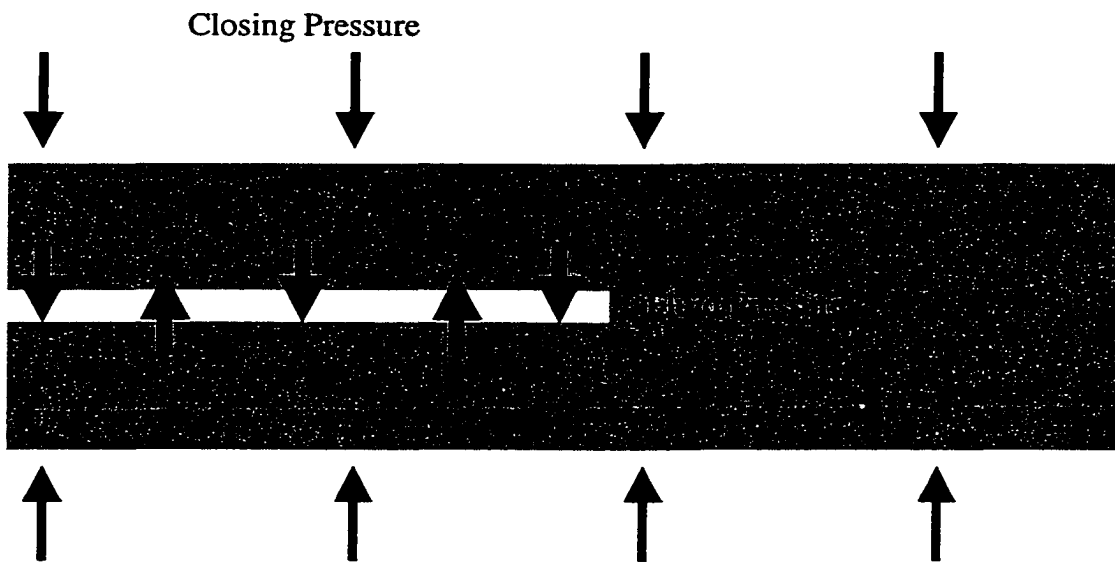


**Figure 1.2 Fracture mechanism.**

The minimum principle stress is expressed as a fraction of overburden stress. The fraction is generally called stress ratio—the ratio of horizontal to vertical effective stresses. Therefore, effective FFP is the product of the stress ratio and effective overburden pressure. The method is the basis of estimation FFP proposed by Hubbert and Willis in 1957.

The prediction of FFP consists of estimations of overburden pressure, formation pore pressure and stress ratio. The estimation of formation pore pressure comes from overburden pressure. Certainly, the accurate way is the integration of bulk densities if they are measured from well log. In the side of predicting overburden pressure, the simplest estimations of overburden pressure assumes a constant pressure gradient, 1.0 psi/ft. Pnnebaker (1968) noticed the variation of overburden pressure gradient versus depth and presented a correlation based on geologic age. Using a porosity compaction model, Bourgoyne et al. (1986) proposed an integration model.

For the estimation of the stress ratio, Hubbert and Willis (1957) assumed a constant of  $1/3$  in the regions of normal faulting, such as the U. S. Gulf Coast area. Matthews and Kelly (1967) and Pnnebaker (1968) presented correlations of stress ratio with depth back calculated from LOT results. Eaton (1969) used formation Poisson's ratio as a middle parameter between stress ratio and depth. His Poisson's ratio was also back calculated from LOT data. Christman (1973) correlated stress ratio with formation bulk density, while Holbrook et al (1995) proposed the stress ratio equal to formation solidity,  $1-\phi$ . For SMS, Rocha and Bourgoyne introduced a "pseudo-overburden" concept with stress ratio equal to one (geo-hydrostatic sediment) which gave fracture pressure equal to the pseudo-overburden pressure.

The common feature of the FFP estimation methods is their one parameter (the stress ratio) should be calculated back from known FFP data. Leak-off test is the only in-situ method to provide the data. Leak-off test data or called FFP data scatter even in the same area. The back-calculated parameter should be the best fitness to all the data in the same region.

## **1.2 Leak-off Test Data Base**

LOT data are kept and input in a data base for reference recently. Detail input information of a LOT depends on company. Generally, leak off pressure, mud density, formation depth, water depth (if any), and well size are enrolled for a LOT record.

Except the usage of LOT data for the estimation models stated in Chapter 1.1, LOT data can be used directly to estimate the FFP in the same area, especially from those of nearby wells. Logically, a new well should have the same or approximate FFP with a nearby well if the two wells have the same formation, at the same formation depth and water depth, same casing string, same cement slurry, same mud and same wellbore size. Generally, the average FFP from LOT data at an interested depth is used. LOT data are interpreted from leak-off tests.

## **1.3 Leak-off Test**

In-situ measurement may be the most accurate and persuade method in getting formation fracture pressure. In a drilled hole, separating the interested depth by top and bottom pluggers and increasing pressure by pumping fluid into the separated section, one can get the formation fracture pressure at the interested depth. This is so called formation stress test.

In drilling operation, generally, formation fracture pressure is measured after setting casing string and cementing since the fracture pressure at casing shoe is the weakest point. In contrast to formation stress test, leak-off test actually tests the integrity of casing shoe. As shown in Fig. 1.3, fracture may be created in formation or in cement. Obviously, what we need for well planning should be formation fracture pressure.

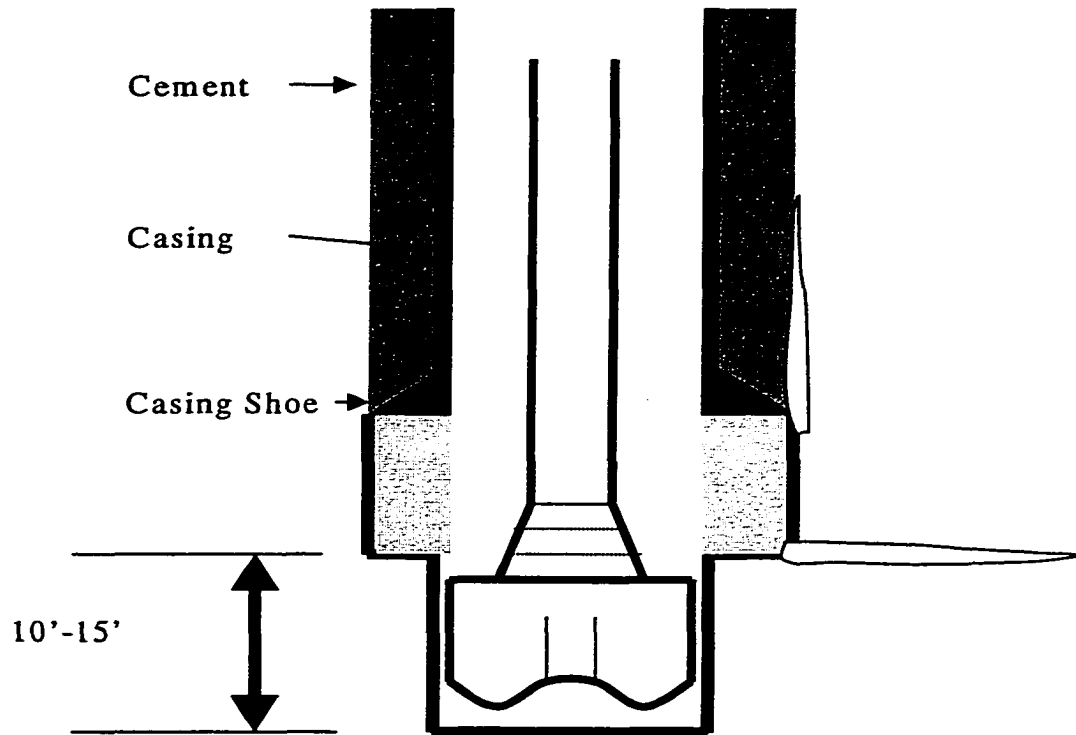


**Figure 1.3 Fractures in formation or cement.**

This is so called leak-off test in petroleum engineering. Bottom hole is used as lower plugger and closed blowout preventers (BOP) at surface is used as the upper plugger in this kind of test. Drilling fluid is pumped into the closed well at a constant rate (1/4 bbl/min) until the well begins to take whole mud. The pump is then stopped and pressure is observed for a few minutes (10 minutes). Casing string is tested for leaks in this manner before the cement is drilled from the bottom joints. This is called casing test. The cement and formations just below the casing shoe are tested in this manner after the cement is drilled from the bottom joints of casing and about 10 ft into the formations below the casing shoe. Leak-off test is also called pressure integrity test since it measures not only the fracture of formation but also the pressure at which drilling fluid leaks into cement channel.

Figure 1.4 shows a typical leak off test results. As shown, there is a constant pressure increase for each incremental drilling fluid volume pumped. The pressure is increased continuously until leaking occurs at point A. At this point, formation grains start to move apart and the formation begins to take whole mud. Pumping is continued during the leak off test long enough to ensure that the fracture pressure has been reached (Point B). The pump is stopped at Point B, and the well left shut in to observe the rate of pressure decline for about 10 minutes. The pressure at Point A is the leak-off pressure (LOP) and is taken as the formation fracture pressure at the casing shoe.

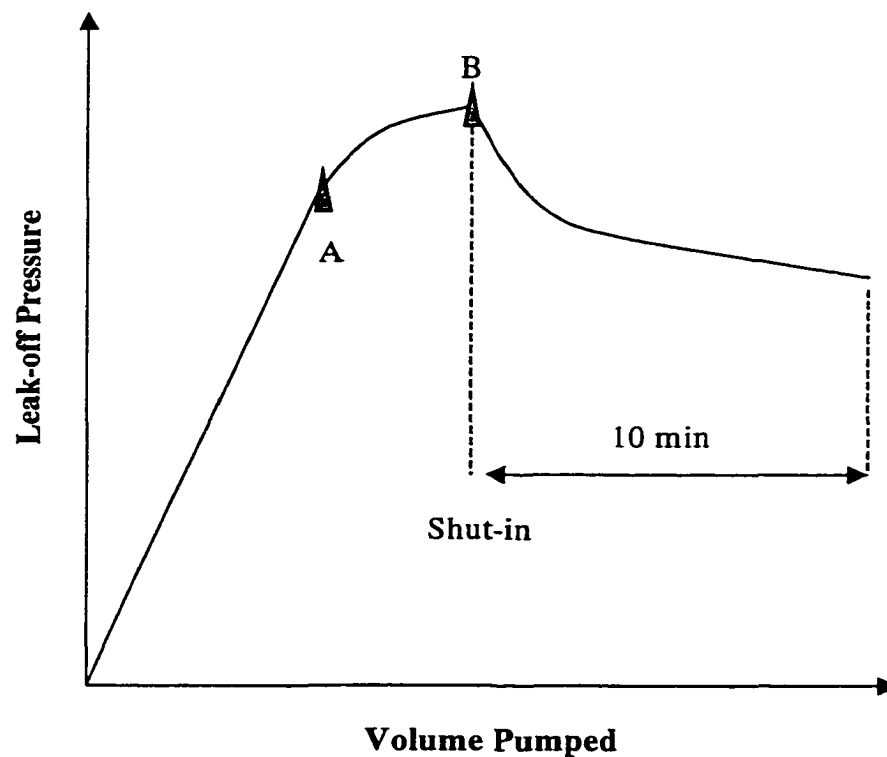


**Figure 1.4** Typical leak-off test plot.

The rock fracture mechanism due to leak-off test is the basis of interpretation of LOTs. Modeling LOT provides further technique for LOT interpretation. Chenevert and McClure (1978) discussed the mud gelation effect on LOT and provided a model

of LOT considering mud compressibility. Almeida (1986) set up a computer program simulating LOT pressure versus pumped volume by using a system overall compressibility. The overall compressibility consists of the compressibility of mud column, drill pipe and collar expansion, casing expansion (cemented and not cemented), filtration, borehole expansion. Using the whole compressibility, Altun (1999) modeled the non-linear behavior of pressure versus volume by using Darcy's law for filtration into pre-existed channel.

Combined existed analyses of LOT and field experience, Postler (1997) presented an interpretation technique of LOT which, as my knowledge, is the first published interpretation technique.

#### **1.4 Cement Fracturing and Relation**

Drilling fluid may leak into rock and channel in cement or its bonds with casing string and rock at casing shoe. Leak-off test (LOT) tests the integrity of casing shoe. Cement channel is generally regarded as pre-existed. As rock fracturing, there may be cement parting round casing shoe. This kind of cement fracture may occur before rock fracturing and should be discussed in the research of casing shoe integrity. Two fractures may occur at a casing shoe during LOT: formation fracture and cement fracture.

Finding out cement parting is important for cement squeezing. Cement squeezing is a re-medical method for cement channeling after LOT. The leak-off pressure at casing shoe can be increased to desired values by squeezing cement. As stated in above section, formation fracture pressure (FFP) is needed in well planning. The FFP can be estimated from models or LOT data especially those from near-by

wells. To verify the estimated FFP, LOT is conducted as setting casing and cementing. The LOT result is the real fracture pressure around the casing shoe. However, strictly speaking, LOT result is not only the FFP there. It tests the casing shoe integrity including cement channeling.

Figure 1.5 summaries the researches in the related areas and their relationship.

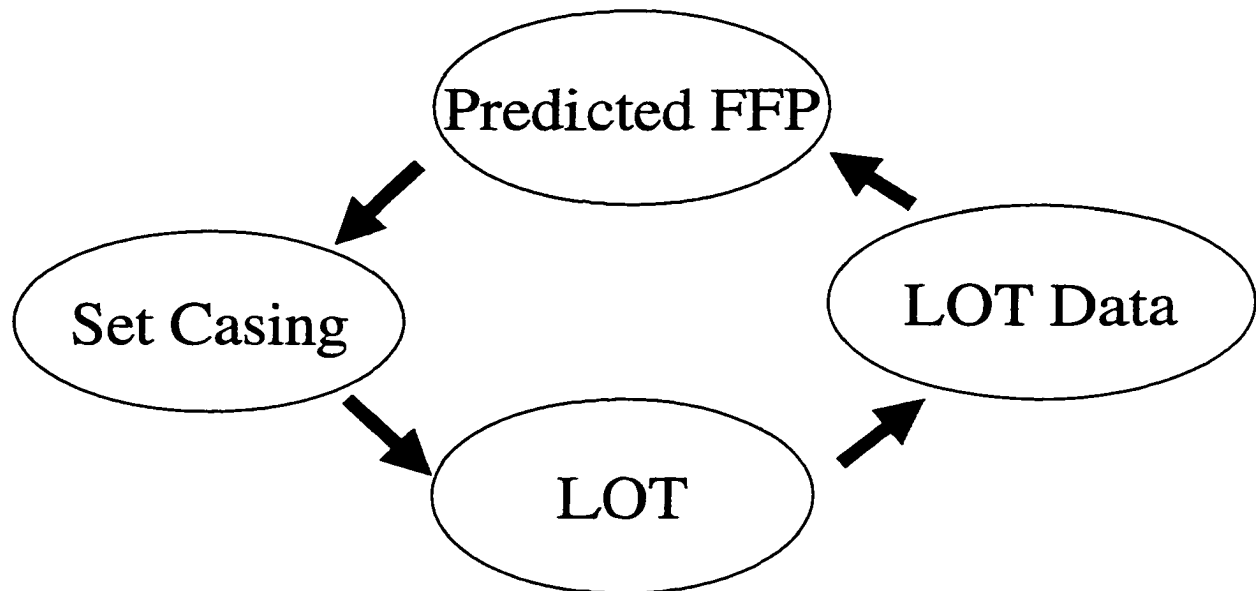


**Figure 1.5 Relation among LOT, LOT data, Predicted FFP and Set Casing.**

### **1.5 Objectives and Methodologies**

From the above analyses, a lot of achievements associating with FFP has been got and used in drilling operation and guarded the normal operation. However, problems in shallow marine sediments (SMSs) puzzle engineers. The specific characteristics from SMSs are:

- (1). Much higher formation fracture pressure gradient than those in deep wells;
- (2). Non-linear LOT plot;

(3). Less tested points on LOT plot.

(4). Horizontal fracturing.

Shallow marine sediments are defined as:

- Water depth:  $\cong 10'+$
- Sediment depth:  $\cong 100-3,000$  ft
- Young's model:  $\cong 200-200,000$  psi
- Poisson ratio:  $\cong 0.2-0.48$
- Angle of friction:  $\cong 10-30$  degree
- Cohesive strength:  $\cong 1-100$  psi

The understanding of problems in SMS is crucial because, besides the importance of FFP mentioned at the beginning of this chapter, it is more difficult to detect shallow gas kick and shallow gas kick may result in un-controllable outside casing flow and cratering. Unfortunately, except Rocha and Bourgoyne (1996) and Bender and Bourgoyne (1995) presented research in the estimation of shallow FFP and field observed horizontal fracturing phenomenon (Gidley et al., 1989), shallow fracture mechanism just stop at the knowledge of soft or plastic sediments and no research has been done about the analyzing, modeling, and interpreting LOTs. This work is going to focus on the problems in shallow marine sediments in the following aspects:

- Elastoplastic analysis of rock around wellbore

The elastic stress and deformation analyses in deep wells have been fully discussed and founded the basis of understanding rock fracture. Soft properties of SMSs may result in a plastic zone around a wellbore. The stress and deformation for soft SMS will be analyzed.

The methodology to solve this problem is analytical and numerical (finite element) analyses based on elastoplastic theory.

- **Elastioplastic analysis of the whole open hole section**

The open hole section for LOT is bonded by the bottomhole at the bottom and casing and cement at the top. The effect of the bonds on LOT is going to be analyzed by finite element method. The effect of the bonds on LOT for deep wells (elastic cases) will also be analyzed for it has not been analyzed.

- **Cement parting behavior**

Cement may be parted due to high LOT pressure. The parting condition will be discussed from the point of displacement and force using finite element method.

- **Modeling non-linear behavior**

Models of rock fracturing and cement parting will be set up to simulate the non-linear relation of pressure and pumped volume. To make the model applicable, analytical mathematical models will be given.

- **Interpretation of LOT results in SMS**

Interpretation of LOT plot is required to make on the site immediately. Different operation may be conducted based on the interpretation result. No interpretation technique is available up to now. Interpretation method will be developed based on the mechanism analysis and models.

## CHAPTER 2

### LITERATURE REVIEW

Formation fracture pressure (FFP) can be subdivided into four interrelated aspects: LOT, LOT data, predictive FFP and cement channeling as stated in Figure 1.5 in Chapter 1. Every aspect consists of a few major factors that affect its behavior. Understanding the whole related areas and their interactions helps us focus on the major problems and their solutions. In the chapter, we summary achievements in those areas by factors up to now. Also, some important basic concepts and formulas are reviewed. This chapter provides not only the research progress in our research areas, but basic theory, principles, and techniques used up to now.

#### 2.1 Rock Mechanics

The basic mechanism to understand FFP is rock mechanics. This brief overview is compiled from various sources with the objective of giving appropriate background to support parts of this research. For more information or detail, the reader may use the references accompanying this dissertation (books of Obert and Duvall, 1967, Jaeger and Cook, 1976, and Fjear et al., 1992).

##### 2.1.1 Stress Tensor

Stress  $\sigma$ , is defined as the limiting of the ratio of a force  $F$  and the area  $A$  on which it is acting when the area goes to zero.

$$\sigma = \lim\left(\frac{F}{A}\right) \quad (2.1)$$

Strain  $\varepsilon$  is the elongation,  $\Delta L$ , of a unit length,  $L$ , under the action of stress.

$$\varepsilon = \Delta L / L \quad (2.2)$$

Stress and strain are defined as positive for compressive action and negative for tensile action here. Stress and strain are vectors. A complete definition of the stress state acting in a body can be made only by the use of a tensor quantity with nine components (Jaeger, 1979) as shown in Fig. 2.1 and expressed as Eq. 2.3.

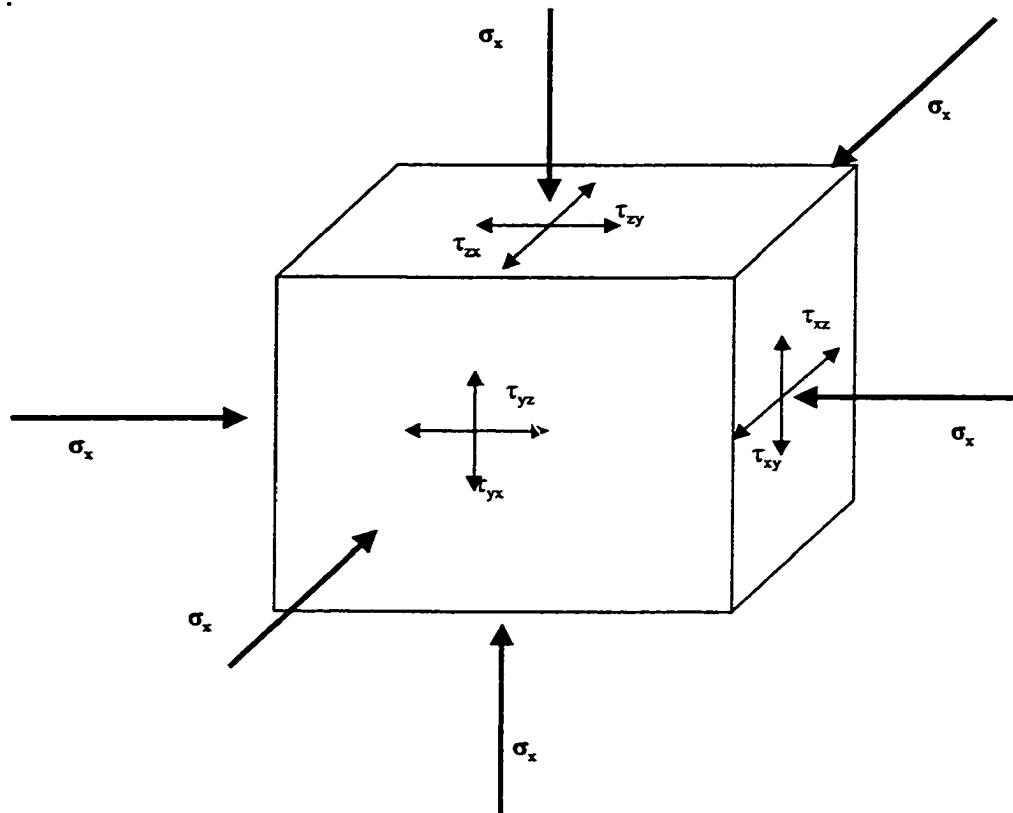


**Figure 2.1** Schematic representation of the nine stress components acting in a cubic element (Jaeger, 1979).

$$\sigma_{ij} = \begin{bmatrix} \sigma_x & \tau_{xy} & \tau_{xz} \\ \tau_{yx} & \sigma_y & \tau_{yz} \\ \tau_{zx} & \tau_{zy} & \sigma_z \end{bmatrix} \quad (2.3)$$

Where  $\sigma$  represents a normal component of stress, and  $\tau$  represents a shearing component of stress. It is always possible to find a coordinate system based on three

directions, called principle directions, in which all the shear stresses vanish. In this coordinate system, the stresses are called principle stresses. Generally,  $\sigma_1$ ,  $\sigma_2$ ,  $\sigma_3$  are used to present the principle stresses respectively. Using the three principle stresses as coordinate axes constructs so-called stress space.

The values of the stresses in Eq. 2.3 depend on the coordinates. Invariants of the stress tensor are stress combination of Eq. 2.3 which would be the same regardless of the rotation of the coordinate axes. Three stress invariants are:

$$\begin{aligned}
 I_1 &= \sigma_1 + \sigma_2 + \sigma_3 \\
 I_2 &= \sigma_1 \sigma_2 + \sigma_2 \sigma_3 + \sigma_3 \sigma_1 \\
 I_3 &= \sigma_1 \sigma_2 \sigma_3
 \end{aligned}
 \tag{2.4}$$

It is convenient in material modeling to decompose the stress tensor into two parts, one called the spherical or the hydrostatic stress tensor and the other called the stress deviator tensor. The hydrostatic stress tensor  $\sigma_p$  is the mean stress and it is the same for all possible orientations of the axes:

$$\sigma_p = 1/3(\sigma_x + \sigma_y + \sigma_z) = 1/3 I_1
 \tag{2.5}$$

The stress deviator tensor  $s_{ij}$  is defined by subtracting the spherical state of stress from the actual state of stress in Eq. 2.3.

$$s_{ij} = \begin{bmatrix} (\sigma_x - p) & \tau_{xy} & \tau_{xz} \\ \tau_{yx} & (\sigma_y - p) & \tau_{yz} \\ \tau_{zx} & \tau_{zy} & (\sigma_z - p) \end{bmatrix}
 \tag{2.6}$$

Same as for the invariants of stress tensor, the invariants of stress deviator tensor are:

$$J_1 = 0$$

$$J_2 = 1/3(I_1^2 - 3I_2)$$

$$J_3 = 1/27(2I_1^3 - 9I_1I_2 + 27I_3) \quad (2.7)$$

### 2.1.2 Stress-Strain Relation

Strain will be formed under any stress. If a linear relationship exists between stress and strain, the material is called as linearly elastic, or

$$\sigma = E\varepsilon \quad (2.8)$$

This equation is known as Hook's law. Coefficient  $E$  is called Young's modulus, and it is a measure of the stiffness of the sample (Fjaer et al., 1992). Another important parameter is Poisson's ratio defined as

$$\mu = -\frac{\varepsilon_x}{\varepsilon_z} \quad (2.9)$$

Where  $\varepsilon_x$  is the strain in lateral and  $\varepsilon_z$  is the strain in axial for a uniaxial test. The deformation caused by shear stress has the same treatment, in which it is also assumed that the material will deform linearly due to shear stress. The general relation between shear stress and shear strain is given by

$$\tau = G\gamma \quad (2.10)$$

Where  $G$  is shear modulus of the material.

The above three equations (Eqs. 2.8-2.10) form the basis of the so-called one-dimensional theory of linear elasticity. We restrict this discussion to isotropic material, that is, materials whose properties are independent of direction. For such material the principal axes of stresses and strains are coincide. According to Jaeger (1979) and Fjaer et al. (1992), the general relations between stresses and strains for a linear elastic material is:

$$\begin{aligned}
\sigma_x &= (\lambda + 2G)\varepsilon_x + \lambda(\varepsilon_y + \varepsilon_z) \\
\sigma_y &= (\lambda + 2G)\varepsilon_y + \lambda(\varepsilon_x + \varepsilon_z) \\
\sigma_z &= (\lambda + 2G)\varepsilon_z + \lambda(\varepsilon_x + \varepsilon_y) \\
\tau_{xy} &= 2G\gamma_{xy} \\
\tau_{yz} &= 2G\gamma_{yz} \\
\tau_{zx} &= 2G\gamma_{zx}
\end{aligned} \tag{2.11}$$

Where  $\varepsilon$  represents strains in coordinate directions and  $\gamma$  represents shear strains (same as those in Fig. 2.1).

## 2.2 Yield and Fracture Mechanism

Yield criterion is used to describe the critical value of elastic deformation. It is the value that material starts plastic deformation under continuous loading. Yield criterion is also called failure criterion or fracture criterion since a body is generally thought as failure when it turns into plastic state. However, it is distinguished in the work that yield criterion is used to describe the transition from elastic behavior to plastic. Different deformation formula will be used for elastic and plastic deformation respectively. Fracture means formation grains apart from each other and well fluid flows into the separated space.

### 2.2.1 Yield Criterion

A lot of yield criteria have been presented. Some of yield criteria are used in engineering fields and familiar to us. However, it should be pointed out failure mechanism of a solid is still not understand thoroughly by physicists. No a yield criterion works for all materials. Every criterion has its own application area. All

proposed criteria are set up based on the same thought: using some stress/strain, or some group of stresses/strains tested when yield in lab under simple loading condition as the yield value of actual irregular body which endures complex stresses.

The simplest criteria are maximum tensile stress theory and maximum tensile strain theory. Maximum tensile stress theory states that a body will yield if the maximum tensile stress in the body gets the tested maximum tensile stress of the specimen of the same material when it yields. A lot of research show that this theory is of poor agreement with experiments, especially when a body is in a complex stress state. However, it is widely used as a fracture criterion such as our formation fracture study. This is acceptable since micro-cracks are always existed in rock and tensile rock strength is relatively small.

Using maximum tensile strain as the condition of failure or yield is the theory of maximum tensile strain. It has also lost its application for not fitting the results of more complicated experiments. However, this theory agrees thick-walled cylinders and is still used such as the design of gun. Maximum tensile stress criterion and maximum tensile strain criterion can be expressed as

$$\begin{aligned}\sigma_{ten} &= -S_{ten} \\ \varepsilon_{ten} &= -\varepsilon_{ten}\end{aligned}\tag{2.12}$$

Where  $S_{ten}$  and  $\varepsilon_{ten}$  are the maximum tensile strength and tensile strain before failure.

Maximum shear theory uses the maximum shear stress as the failure/yield condition. This is the famous Tresca criterion. Associating with this theory, octahedral shear criterion and maximum strain energy criterion are also available. These theories have wider application field, especially for metal. If use  $S_{shear}$  as the maximum shear stress, Tresca's criterion is

$$\sigma_1 - \sigma_3 = 2S_{shear} \quad (2.13)$$

Another famous theory widely used in the field of metal is Von Mises' criterion. The distortion energy in a body is used as the indication of yield or failure, so this theory is sometimes called distortion energy theory. It assumes a cylinder surface as a failure surface. Therefore, this criterion can be expressed as:

$$(\sigma_1 - \sigma_2)^2 + (\sigma_1 - \sigma_3)^2 + (\sigma_2 - \sigma_3)^2 = c^2 \quad (2.14)$$

The term of the left side is called octahedral shear stress,  $\tau_{\text{ox}}$ . Therefore, failure will occur when the octahedral shear stress reaches a value  $c$ .

Mohr-Coulomb criterion can be regarded as coming from Tresca criterion. Both criteria are based on the assumption that the maximum shear stress is the only decisive measure of impending failure. The difference is that the Tresca criterion assumes that the critical value of the shear stress is a constant, but Mohr-Coulomb criterion assumes that the critical shear stress depends on the normal stress. Mohr-Coulomb criterion is used in many fields especially about granular materials, such as soil and rock.

Mohr-Coulomb criterion consists of a linear envelope tangent to all Mohr's circles representing critical combinations of principal stresses. The necessary stress to generate the Mohr-Coulomb envelope can be easily obtained from tri-axial tests. Mohr-Coulomb criterion can be expressed as:

$$\tau = \tau_0 + \sigma_n \tan \phi \quad (2.15)$$

Where  $\tau_0$  is cohesion. If  $\tau_0$  is equal to zero, the material is called cohesionless. Shallow marine sediments have a very small cohesive strength. Some rock's cohesive strength approaches to zero such as unconsolidated rocks.

As Mohr-Coulomb theory comes from Tresca's criterion by introducing the effect of normal stress. Drucker-Prager proposed a criterion that can be regarded as a modification of Von Mises' criterion. Actually, it introduces a more item of hydrostatic stress than Von Mises' criterion. The Mohr-Coulomb's hexagonal failure surface in principal stress space (as shown in Fig. 2.2) is mathematically convenient only in problems where it is obvious which one of the six sides is to be used. If this information is not known in advance, the corners of the hexagon can cause considerable difficulty and give rise to complications in obtaining a numerical solution (convergence problem).

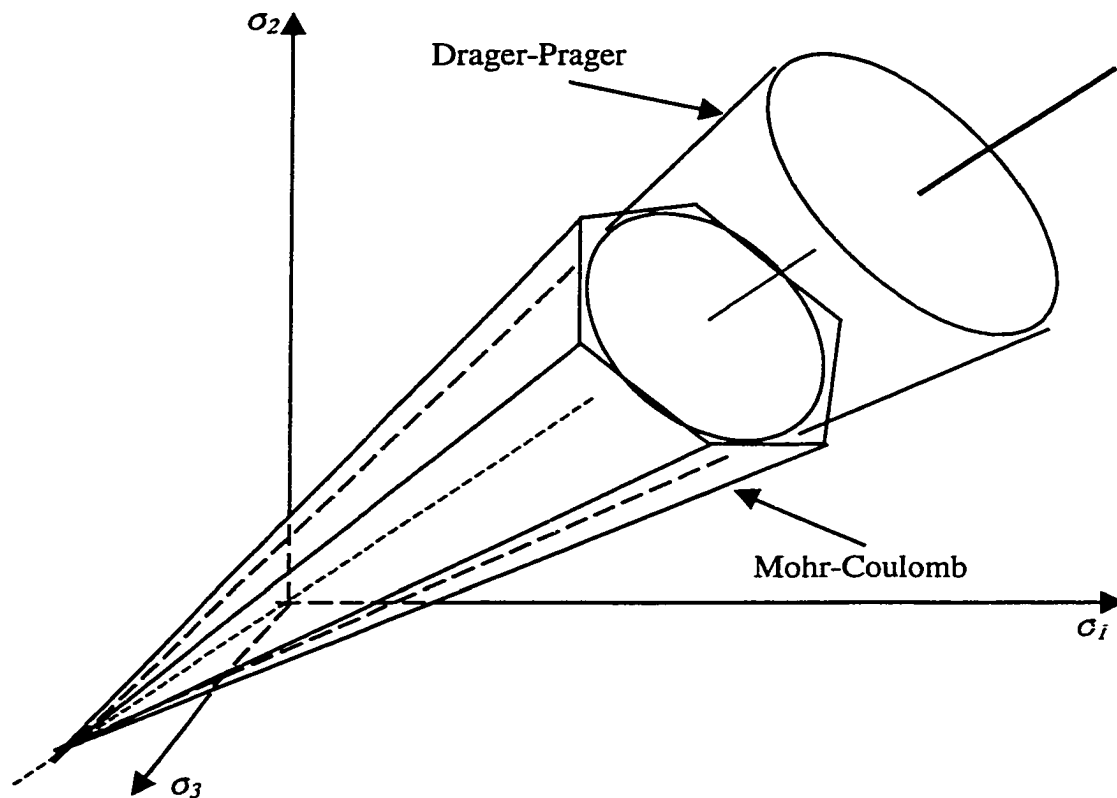


**Figure 2.2 Mohr-Coulomb and Drucker-Prager criteria in principle stress space (Chen and Han, 1988).**

Drucker-Prager criterion has the same application field as that of Mohr-Coulomb criterion and overcomes the mathematics troubles the latter meets in the analysis of complex stresses (cone shape as shown in Fig. 2.2). Therefore, Drucker-Prager criterion is widely used in complex stress analysis. Drucker-Prager criterion may be expressed as (Chen and Han, 1988):

$$\alpha I_1 + \sqrt{J_2} - k = 0. \quad (2.16)$$

Where  $\alpha$  and  $k$  are material constants. When  $\alpha$  is zero, this criterion reduces to the Von Mises criterion.

All those criteria are based on themselves experiments and have their own application fields. There is no theory suitable for all materials. Although Mohr-Coulomb criterion has been widely in the field of soil or rock, its internal friction theory has not been proved by state-in-art physicists. New criteria such as critical state model and capped model and Modified models of Mohr-Coulomb and Drucker-Prager criteria are introduced to compensate its shortcomings. Generally speaking, the more the parameters of material properties is used, the more precise a criterion is. However, the more the parameters are, the complex and difficulty the model is.

### 2.2.2 Fracture Mechanism

Formation fracture is defined as the formation grains apart and drilling fluid flows into the fractured space. Although drilling fluid will flow into permeable formation, the simple displacement of drilling fluid to pore fluid is not thought as fracture. Hydraulic fracturing of rock is a complex phenomenon that is very difficult to describe mathematically. Physically process can be understood as drilling fluid flows into pores or micro fractures of a rock and pushes the surrounding grains away.

Since drilling fluid may flow through pores, non-penetration and penetration fluid is discussed first here. Fig. 2.3 shows a possible distribution of pressure around the borehole with a penetrating and a non-penetrating type of fluid.

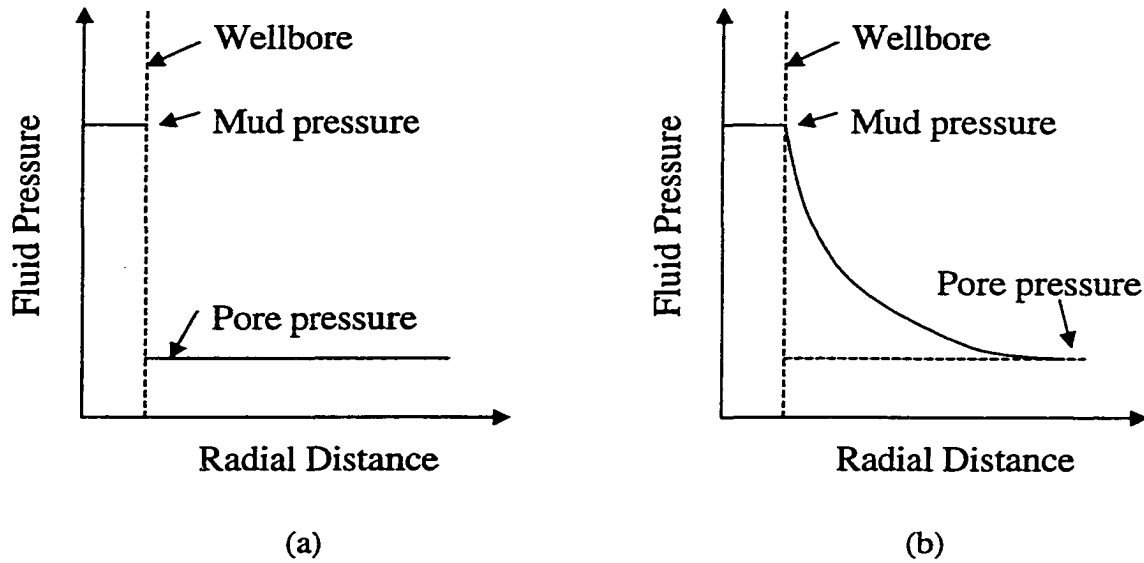


**Figure 2.3 Fluid pressure distribution around a well.**

A non-penetration fluid is a fluid that can not penetrate the pore of a rock formation (Fig. 2.3a). Whether a fluid is penetrate or nonpenetrate with respect to a certain rock depends on the sizes of the interconnected pores and naturally occurring micro fractures in the rock. An ordinary drilling mud forming a relatively impermeable filter cake on a rock is usually assumed to be a nonpenetrating fluid (Bourgoyne et al., 1991), even though there may be small amount of filtration taking place. The rates of any filtration taking place are small enough to be neglected is that they do not have a significant effect on the length or width of the fracture formed.

In the case of penetrating fluid, the pressure difference between the drilling fluid and the pore fluid in the formation will cause an outward radial flow from the well into the formation (Fig. 2.3b). Timoshenko and Goodier (1951) and Geertsma

(1957) applied the theory of thermoelasticity, modified to solve problems in elastic material, to show that fluid flow through porous media causes stresses that affect the rupturing pressure of permeable formations. When this happens, the fluid intrusion reduces the breakdown pressure.

The basic idea for formation fracture may be described as (Bourgoyne et al, 1991): a small cavity is assumed in a rock that is zero tensile strength. For drilling fluid to enter the cavity, the pressure of the drilling fluid must exceed of the pressure of the formation fluid in the pore spaces of the rock. As the pressure of drilling fluid is increased above the formation pore pressure, the rock matrix begins to be compressed. The compression is greatest in the direction of the minimum matrix stress. When the drilling fluid pressure exceeds the sum of the minimum matrix stress,  $\sigma_{min}$ , and pore pressure ( $p_p$ ), parting of the rock matrix occurs and the fracture propagates. The preferred fracture orientation is perpendicular to the least principle stress.

$$p_{ff} = \sigma_{min} + p_p \quad (2.17)$$

Basically, this fracture mechanism is the maximum tensile criterion. It is accepted and used in all the formation fracture analyses.

### **2.3 In-situ Underground Stress**

To understand the underground stresses that tend to resist formation fracture, we must consider the geologic processes that have occurred. A simple and common subsurface stress state generally encountered in sedimentary basins containing oil and gas often occurs in a tectonically relaxed area. As the deposition of sediments continues over geologic time, the vertical matrix stress increases owing to the increased loading at the grain to grain contacts. Under the influence of this vertical

stress, the rock's natural tendency is to expand laterally, but it is prevented from doing so by the surrounding rock. The tendency to expand introduces horizontal stress. If we designate as principle matrix stresses those stresses that are normal to planes in which no shear occurs, the general state of stress underground can be defined in terms of  $\sigma_x$ ,  $\sigma_y$ , and  $\sigma_z$ . Figure 2.4 shows underground stress distribution.

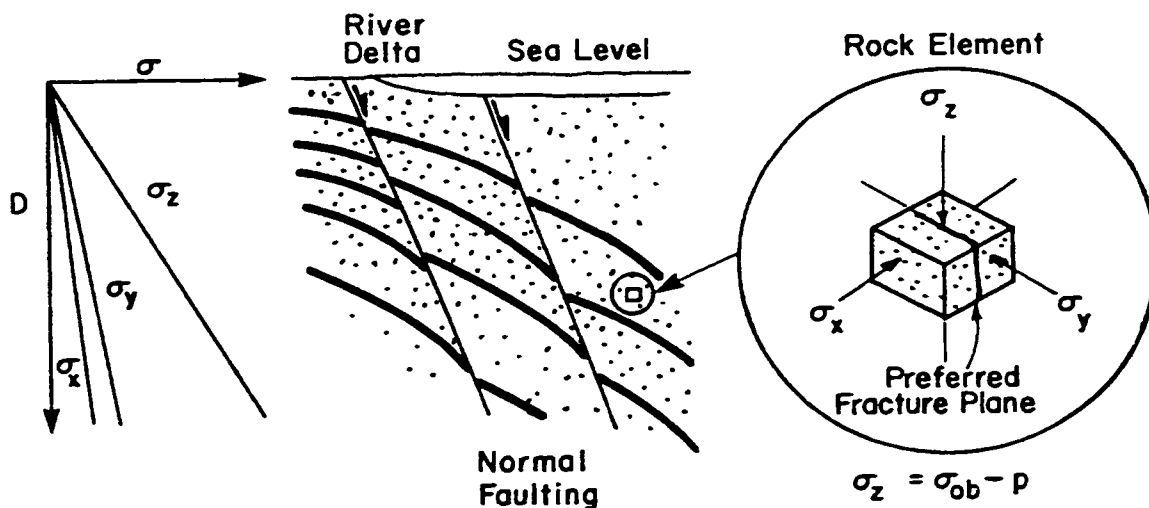


**Figure 2.4** Underground stress distribution in relatively young deltaic sediments (Bourgoyne et al, 1991).

### 2.3.1 Overburden Pressure

Overburden pressure,  $p_{over}$  is the pressure caused in a given point underground by the overburden load or geostatic load of the sediments above this point. This geostatic load is supported at a given depth by the grain to grain contact points of the rock material and by the pressure of the fluid inside the pore spaces. The vertical principle matrix stress,  $\sigma_z$ , is the result of this grain to grain supported load, and the overburden stress can be expressed by

$$p_{over} = \sigma_z + p_p \quad (2.18)$$

The vertical overburden pressure being equal to the geostatic load at a given point is a function of the bulk densities of the materials overlying the point under consideration. The correct value of the vertical overburden pressure is therefore the sum of the overlying load of each layer of different formations. However, the total state of stress of the rock at the depth of interest is not always adequately described by the vertical overburden pressure calculation. Common geologic processes other than simple sedimentation, like the upward movement of low density salt or plastic shale domes, can alter the vertical state of stress. It is sometimes possible to find the vertical stress state at depth exceeding the geostatic load. In the west Coast area, for example, the continental drift is causing a collision of the North American and Pacific plates, which results in large lateral compressive stresses. This can also be caused by the internal grain friction in sediments immediately above a salt dome. However, rocks generally are quite weak in tension, and faulting will occur, which tends to relieve the buildup of stresses significantly above the geostatic load.

Vertical overburden pressure is often assumed to be equal to 1.0 psi/ft of depth (Harrison et al, 1954; Hubbert and Willis 1957). Principally, this is the same as assuming a constant value of bulk density over the entire sediment section. This simplification may be helpful in some areas when planning wells deeper than 10,000 ft. However, it can lead to significant errors in the computation of overburden pressure, especially for shallow sediments beneath deepwater offshore.

This approximation generally is used when the change in bulk density with respect to depth is not known. The most accurate estimates of pore pressure and overburden pressure gradient can be made using density or porosity data available

from well logs. If the bulk density ( $\rho_b$ ) is known as a function of depth, the overburden pressure for each depth interval is calculated by integrating the bulk density for each depth interval, and the overburden pressure is determined by the following equation using this procedure.

$$p_{over} = \int_0^{D_w} g \rho_w dD + \int_{D_w}^D g \rho_b dD \quad (2.19)$$

Where  $D_w$  and  $\rho_w$  are water depth and density,  $D$  and  $\rho_b$  are the vertical depth and formation density which is function of depth.

Bourgoyne et al (1991) introduced another overburden pressure determination method using porosity variation with depth. This method basically assumes that the formation porosity declines exponentially with increasing sediment depth and given as

$$\phi = \phi_0 e^{-KD_s} \quad (2.20)$$

Where constants  $\phi_0$  and  $K$  are surface porosity and porosity decline constant.

Substitution of porosity into Eq. 2.19 yields

$$p_{over} = g\rho_w D_w + g\rho_g D_s - \frac{(\rho_g - \rho_{fl})g\phi_0}{K} (1 - e^{-KD_s}) \quad (2.21)$$

Overburden pressures in offshore areas are significantly affected by water depth. Based on water depths, the variation of overburden pressure and the fracture gradient was studied by Eaton (1969), Christman (1973), and Eaton and Eaton (1997). Increasing water depth reduces the total overburden pressure and results in lower formation fracture gradient. Eq. 2.21 shows this effect. It should be pointed out that overburden pressure at an interested place will increase with the increase of its over sea water depth. However, overburden gradient will decrease.

### **2.3.2 Formation Pore Pressure**

During the sediment deposition, the weight of solid particles supported grain-to-grain contact points does not under the influence of the fluid hydrostatic. When deposition continues with time and burial, the former deposited sediment particles get under the influence of geostatic loads and try to reorient themselves in order to minimize the load effect. This means that the sediment becomes more compacted and, as a result, pore space to fluid starts decreasing. Therefore, pore water tends to escape through the permeable paths from the decreasing pore space. This process continues as long as a permeable path is available; otherwise, the pore water is kept in the pore space. This trapped pore fluid will be pressurized with time and additional sediment burial and results in higher pore pressures. Since the overburden pressure is constant by definition, this process will induce low vertical matrix stress to keep the pressure balance. In addition, the lower vertical stress also results in smaller horizontal matrix stress, which controls the formation strength or the formation fracture pressure. The main challenge in this field is to detect and compute the abnormal pore pressures and zones. Numerous publications to predict pore pressure variations are available in literature. Since the pore pressure is not the concern of this study, the detailed summary of methods on the pore pressure aspect will not be covered. The pore pressure at point of interest depth will be assumed to known when it is necessary.

### **2.4 Open Hole Stress Distribution**

Drilling operation break the in-situ stress balance underground. Stresses will re-distribute to form a new balance for the new formed hole by drilling action. Understand the stress distribution is the basis for the research in this topic. Effective

stress principle is important in the analysis of porous media (Steiger and Leung, 1988). Effective stress is defined as the total stress at a interest point subtracts the pore pressure there.

#### 2.4.1 Elastic Well

Generally, the stress distortion by drilling operation is theoretically calculated by assuming that the rock is in elastic, the borehole is smooth and cylindrical, and the borehole axis is vertical and parallel to one of the pre-existing regional principle stresses. Figure 2.5 is a typical plot of stress distribution around a wellbore.

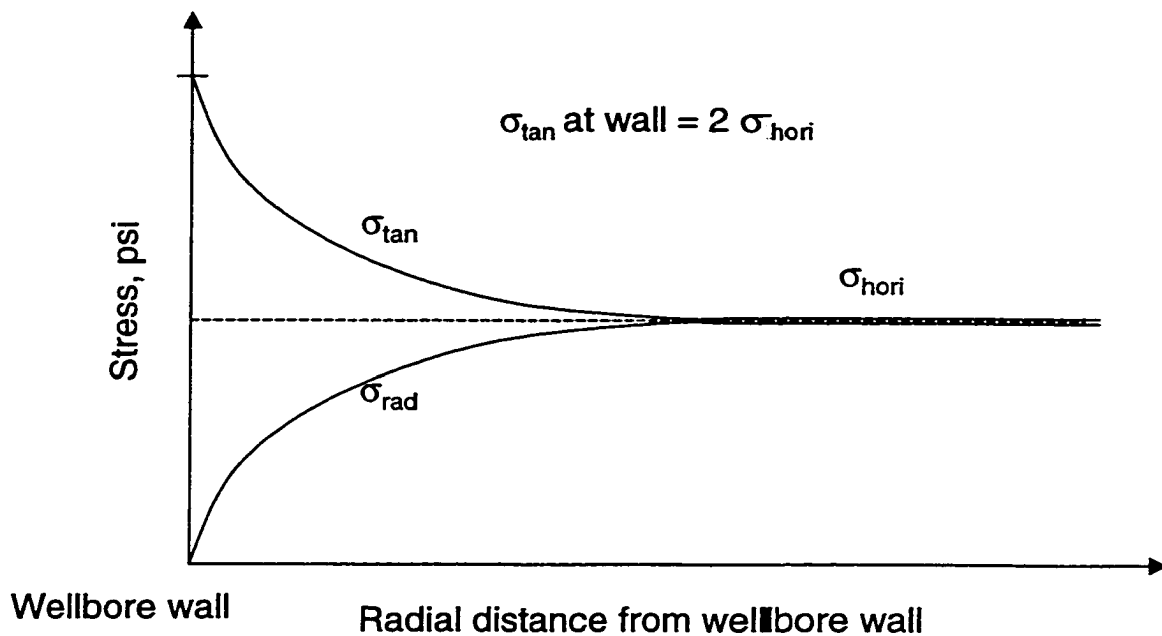


**Figure 2.5** Stress distribution around a wellbore.

Hubber and Willis (1957) pointed out that these stress concentration around a wellbore are local and that the stresses rapidly approach the undisturbed regional stress area within a few hole diameters. Different stress ratios of the two principle stresses in horizontal have different stress values in the vicinity of the wellbore. The distortion of the stress field is not only in the horizontal direction. However, the

magnitude of the distortion in the vertical direction is very small compared to the concentrations of the horizontal stresses.

Since the presence of the borehole affects the state of stress within its vicinity, it also affects the pressure needed to rupture the formation. It has been shown (Timoshenko and Goodier, 1951) that the tangential stress,  $S_t$ , on the periphery of the hole is equal to twice the homogeneous compressive stress,  $\sigma_h$ , of the undisturbed area away from the well bore (as shown in Fig. 2.5). A vertical plane will fracture only when the effective tangential stress passes from compression to tension. Thus, the pressure required to rupture the wellbore vertically is

$$P_{ff} = 2\sigma_h - S_t + P_p \quad (2.22)$$

Where  $P_{ff}$  is formation fracture pressure,  $P_p$  is formation pore pressure,  $S_t$  is the tensile strength of the rock.

Equation 2.22 is derived using elastic theory for the stresses in an infinite plate containing a circular hole, with its axes perpendicular to the plate (Haimson and Fairhurst, 1967). The stress distribution around a drilled open hole is shown in Fig. 2.5.

To determine the effect of well diameter on the fracture pressure, Scott et al. (1953) did some experimental work using a fluid that could not penetrate the cylinder walls significantly. They found that little change in the internal rupturing pressure occurred when ratios of outside to inside radii of the cylinder walls were greater than ten. In experiments performed in shallow wells, no effect on fracture pressure was observed when the well diameter was varied from 0.19 to 6.0 in., regardless the type of fluid used.

For a formation with different horizontal stresses, the stress distribution around a wellbore is more complex. A typical treatment used by most authors (Hubbert and Willis, 1957, Haimson and Fairhurst, 1967, Hagoort et al., 1980, Campos, 1983) is to solve a classical problem of stress concentration in a very large rectangular plate with a small circular hole at its center using elastic theory. The additional stress fields introduced by the fluid being pumped into the well and by borehole fluid movement into the formation are added based on the principle of superposition (Hubbert and Willis (1957). The final solution is

$$P_{ff} = (3\sigma_y - \sigma_x - S_{ten}) / (2 - \alpha(1 - 2\mu) / (1 - \mu)) + P_p \quad (2.23)$$

Where  $\alpha$  is the Biot's constant (Geertsma 1957).

If drilling fluid is penetrate, Eq. 2.23 reduces to.

$$P_{ff} = 3\sigma_y - \sigma_x - S_{ten} + P_p \quad (2.24)$$

The unequal horizontal stress model is rarely used in petroleum industry since we don't know the two stresses. Petroleum engineering generally focus on relaxed normal fault sediments that have almost equal horizontal principal stresses.

#### 2.4.2 Plastic Well

Unlike deeper formations, no correlation of shallow marine sediment (SMS) properties with depth exists for shallow marine sediments. Therefore, the problem is open to speculations. Many agree that upper marine sediments are soft and ductile compared to sediments at depth. Also, many mentioned that "soft shales and unconsolidated sands frequently found in the Texas and Louisiana Gulf Coast can be considered to exist in a plastic state of stress (Harrison et al., 1954)", or, "soft, clay-rich materials like shale often act as plastic (Warpinski and Smith, 1989)", or,

“shallow marine sediment behaves plastic (Rocha, 1993)”. It is widely believed that these sediments may exist in both an elastic and a plastic state of stress. Therefore, whether or not a wellbore wall in SMS will turn into plasticity depends on the sediment properties. Also, it is not a rule that the wellbore wall in SMS is always in the plastic state while in a deep well it is in an elastic state. It is well known fact that the deep sediments become ductile with depth and increasing stress.

In the study of wellbore stability, stress distribution around a wellbore has been analyzed widely (Cheatham, 1984). It was pointed out that a plastic annular might be formed around a wellbore for some sediments due to drilling action (Gnirk, 1972, 1991, Risnes, 1982), especially for shallow marine sediment (Rocha and Bourgoyne, 1994, Bender et al., 1995).

If a plastic zone is formed, it is the zone near the wellbore wall. The region outside the plastic annular is still in elastic state. The plastic annular will affect the stress distribution sharply in this area (Gnirk, 1972, Jeager and Cook, 1976, Risnes et al., 1982). Since the stress distribution around wellbore is different from those in elastic state, the interpretation method, theoretical or empirical relations or in-situ test based on elastic theory, can not be extrapolated to most shallow marine sediment. Some discusses are mainly caused by taking the upper and the deeper sediment as the same situation (Ward et al., 1995). Rocha and Bourgoyne (1994) and Bender et al. (1995) have noticed the difference between shallow and deep rocks and assumed the stresses in shallow marine sediment as hydrostatic.

Certainly, the properties of shallow marine sediments depend upon region, soil type and depth. As will be stated below, whether or not a wellbore wall turn into plasticity depends on rock properties. It is not absolute that the wall in shallow

sediments is in plastic state and that of a deep well is in elastic state. Generally speaking, shallow marine sediment is relatively soft and therefore easy to be turned into plastic state.

To study the plastic deformation of a wellbore, Mohr-Coulomb yield criterion may be used. It is necessary to distinguish the largest and smallest stresses to use Mohr-Coulomb yield criterion. Tangential stress is usually assumed as the largest stress in the analysis of a plastic wellbore (Obert and Duvall, 1967, Gnirk, 1972, , Jaeger and Cook, 1976, Vardoulakis et al., 1988, Wang and Dusseault, 1991). However, vertical stress may be the largest for most normal fault sediments (Harrison et al., 1954, Hubbert and Willis, 1957, Mathews and Kelly, 1967, Eaton, 1969, Christman, 1973, Constant and Bourgoyne, 1988). To soft sediments, tangential stress may become the largest stress near a wellbore (Risnes et al., 1982).

## **2.5 Formation Fracture Prediction Methods**

Equation 2.22 is widely used as the interpretation of formation fracture pressures. A formation fracture will be initialized if wellbore pressure is higher than the right side of the equation according to the equation. However, the tensile strength in the equation is generally ignored since micro fractures are popular in rocks. The parameter 2 reflects stress concentration but it is also ignored since it has been thought that the pre-existing micro fractures pass through the range of the stress concentration. Therefore, formation fracture is regarded as the minimum in-situ stress.

Minimum in-situ stress is difficult to calculate mathematically if three stresses are not equal. However, since the two principal stresses in horizontal plane are generally equal for a normal fault sediment region, a relation could be set up to

connect the two equal horizontal stresses to overburden stress which may be calculated from the integration of rock density versus depth. A stress ratio,  $F_{\sigma}$ , is defined as the ratio of horizontal effective stress to overburden effective stress. Therefore, formation fracture pressure is expressive as

$$P_{ff} = F_{\sigma}(P_{over} - P_p) + P_p \quad (2.25)$$

Overburden and pore pressures have been discussed in Chapter 2.3. Fracture pressure prediction is actual the prediction of the stress ratio. Follows are reviews of the achievements in the prediction of the stress ratio. Also, the effect of water depth is discussed.

### 2.5.1 Horizontal to Vertical Stress Ratio

Hubbert and Willis's pioneering paper (1957) established the theoretical basis for subsequent work in fracture-gradient prediction techniques. They described the effect that variations in the three principle stresses can have on fracture gradient and fracture orientation. They point out that the pressure to fracture a given formation should overcome the local stress concentration at the borehole wall. This stress concentration was found to be twice the least principle stress of an undisturbed region. In addition, they stated that under conditions of incipient normal faulting, such as those in the Gulf Coast area, the horizontal matrix in the X and Y direction are equal, then the pressure required to initiate fracture in a homogeneous, isotropic formation should be Eq. 2.25.

On the basis of laboratory experiments, Hubbert and Willis concluded that in unconsolidated shallow sediments, the horizontal matrix stress would be approximately one-third the vertical matrix stress. Drilling experience has shown that

formation fracture gradients generally increase with depth, even in normally pressured formations. Matthews and Kelly (1967) replaced Hubbert and Willis's (1957) assumption that the minimum matrix stress was one-third the overburden with stress ratio, that is a function of depth. The stress ratio was determined empirically from field data collected at the south Texas and Louisiana Gulf Coast, in normally pressured formations only.

Pennebaker (1968) presented a correlation similar to that of Matthews and Kelly. The effective stress ratio was correlated with depth, regardless of pore pressure ratio. Eaton (1969) developed a correction assuming that the relationship between horizontal and vertical matrix stress is accurately described by

$$F_{\sigma} = \frac{\mu}{1-\mu} \quad (2.26)$$

Where  $\mu$  is the Poisson's ratio of the formation.

Using observed fracture gradient data from western Texas and the Texas and Louisiana Gulf Coast, he computed values of Poisson's ratio as a function of depth. However, he didn't make any distinction between fracture pressure gradient and fracture extension pressure gradient. Eaton's equation is

$$P_{ff} = \frac{\mu}{1-\mu} (P_{over} - P_p) + P_p \quad (2.27)$$

Christman (1973) examined some bulk density logs of the Santa Barbara channel off the California coast. He found that in wells having low fracture pressures zones of unusually low density were exposed in the wellbore, and high fracture gradients were accompanied throughout the well bore by rocks of greater than normal

density. The finding suggests that formation bulk density correlates with stress ratio and can serve as a measure of the degree of compaction. Fracturing is assumed to be at the depth of highest stress ratio and lowest rock density. This approach emphasizes that different types of rocks can have different initiation gradients, if all other factors are equal. This then reinforces the concept that the weakest formation is not necessarily at the casing shoe.

Anderson et al. (1973) utilized Biot's (1957) stress strain relations for elastic porous media and certain other assumptions to develop the following theoretical expression for fracture gradient prediction:

$$p_{ff} = \frac{2\mu}{1-\mu} p_{over} + \frac{1-3\mu}{1-\mu} \alpha p_p \quad (2.28)$$

In addition to the fracture pressure equation, Anderson et al. (1973) developed an empirical relationship between Poisson's ratio and shale content of sand. The shale content, together with pore and overburden pressures, was estimated by using acoustic and density logging devices.

Compiling a database on each well including overburden pressure, pore pressure, and formation fracture pressures, Brennan and Annis (1984) performed an analysis to investigate previously published depth based corrections. They found that the inadequacy of the results obtained was primarily attributable to the variation from well to well of the top of abnormal pressure and of pore pressure with respect to overburden pressure. By assuming a variable overburden pressure from formation properties and including seawater pressure, they developed an equation through curve fitting of a plot of  $(p_{ff}-p_p)$  versus  $(p_{over}-p_p)$  using 57 leak-off test data.

### **2.5.2 Water Effect**

Christman (1973) discussed the effect of water depth on formation fracture gradient. Offshore fracture gradients are calculated in fundamentally the same manner as those on shore as stated above. However, since the upper-most interval is water, which is considerable less dense than rock, the overburden pressure is less than that of a comparable onshore location. As a result, fracture gradients are also lower especially in deep water and shallow formation.

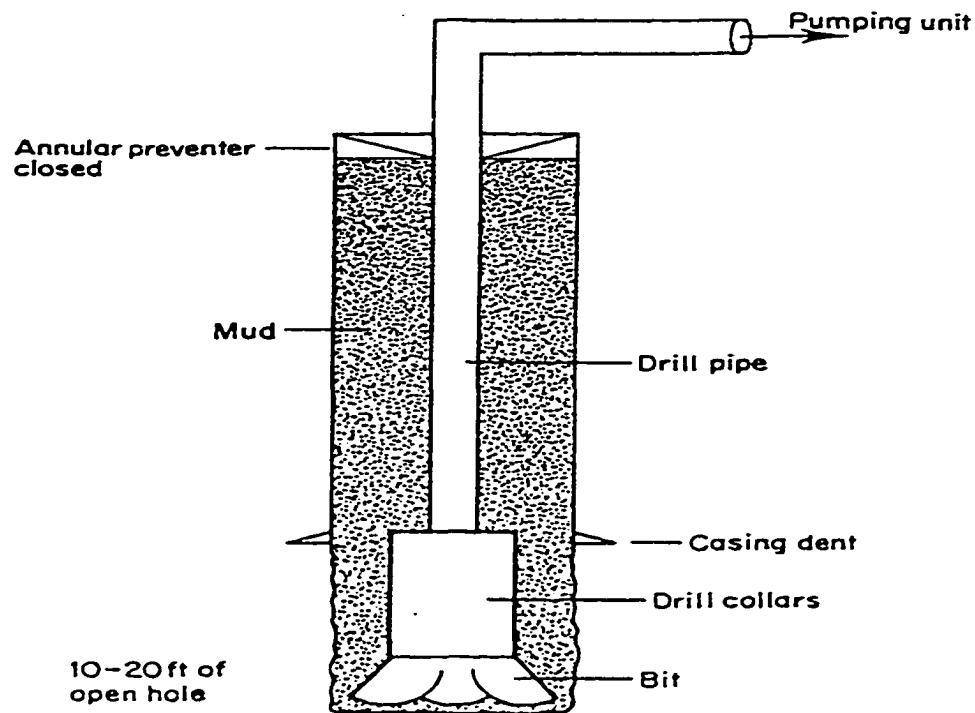
Water depth effect is a little bit confused. Logically, formation fracture pressure isn't decrease with the increase of water depth. Effective stress concept explains the point very well.

### **2.6 Leak-off Test Procedures And Analysis Techniques**

In-situ measurement is the most accurate and persuade method in getting formation fracture pressure. In a drilled hole, separating the interested depth by top and bottom pluggers and increasing pressure by pumping fluid into the separated section, one can get the formation fracture pressure at the interested depth. This method is called formation stress test and is used to measure formation stresses.

In drilling operation, generally, formation fracture pressure is measured after setting casing string and cementing since the fracture pressure at casing shoe is generally the weakest point according to well planning. Bottom hole is used as the lower plugger and closed blowout preventers (BOP) at surface is used as the upper plugger in petroleum engineering. The test is called leak-off test. Certainly, the result of the test is not only associated with formation stress but may reflect casing shoe failure through cement sheath.

Figure 2.6 shows a leak-off test. Mud is pumped into the closed well to increase wellbore pressure. Once the pressure is increased to the limit value the casing shoe could stand, fractures occur around casing shoe and pressure drops.



Schematic drawing of a small fracturing, leak-off or casing seat test assembly.

## Figure 2.6 Leak-off Test.

### 2.6.1 Leak-off Test Procedures

In general, Leak-off tests are done immediately beneath cemented casing in order to test the integrity of the set cement and determine the drilling fluid density that can be withstood by the formation. The bottom of the casing is usually set in shale as summarized by Aadnoy and Soteland (1989), Kunze and Steiger (1992). After waiting an appropriate time for the cement to harden, cement plug and 5-20 feet of fresh formation are drilled very carefully (almost zero weight on bit) to prevent damage of

casing shoe integrity. Drilling bit is pulled into casing before conditioning the mud. Mud circulation time should be longer enough to decrease gas effect and make uniform weight mud. Close BOP and pump mud down drill pipe at a constant rate between  $\frac{1}{4}$  - 1 bbls/min until the pressure stops increase. Afraid of damage of LOT on casing shoe integrity, some operators stops pumping once pressure gets what they are looking for. Finally, shut in the well an monitor the pressure for 10 minutes.

Many authors presented similar procedures. Following is an old procedure presented by Chenevert and McClure (1978).

1. Construct a graph with dashed lines indicating a “minimum volume” line and the anticipated leak-off pressure line.
2. While coming out of the hole, position the bit in the casing above the shoe.
3. If the mud is not of a known, uniform density it should be circulated until it is.  
Two common causes of non-uniform density are barite slugs in the drill pipe and formation cuttings in the annulus.
4. Close the ram preventer above the drilling spool.
5. Using a small pump (such as a cementing pump) begin pumping mud down the drill pipe at a constant rate of 0.25-1.50 bbl/min. The rate depends on conditions. With no open hole use 0.25-0.33 bbl/min. With sandstone formation exposed use 0.75-1.5 bbl/min depending on the amount of open hole. Data obtained should fall very close (within 0.5 bbl) to the “minimum volume” line at leak-off.
6. Record on the graph the pressure after each 0.25 or 0.50 bbl increment is pumped.

7. Continue pumping until the curve bends over, or until the anticipated leak-off pressure line is exceeded. Exceeding this line is often caused by only shale being exposed in the open hole.
8. When the pumping is shut off, keep the well shut in and read an instantaneous pressure. Then read pressure values each minute for about 10 min. These should also be plotted on the graph.
9. Release the pressure and record the volume of testing fluid recovered in the trip tank if one is available. The volume of fluid recovered should approximate the volume of fluid pumped.
10. Compare the graph with typical plots to be sure it is a good test.

Postler (1997) presented a newly procedure combining leak-off test and interpretation technique:

1. Reference Guidelines: prepare test graph before leak-off test. Label the horizontal axis in  $\frac{1}{4}$  bbl increments and vertical axis in 100-psi increments. Draw predicted leak-off pressure, minimum leak-off pressure, maximum pressure and maximum volume lines on the graph for interpretation as shown in Figure 2.7.
2. Proper Rig-up: Use low-volume high-pressure pump such as the cementing pump. Install shut-in valve between pump and pressure gauge. Install a bleed valve between the pump and the shut-in valve. Install purge valve for purging air from the test lines. Use good quality cement unit gauge. Pump down the drill pipe.
3. Use Clean, Uniform Mud.

- Plot Data During the Test: Record and plot data every  $\frac{1}{4}$  bbl regardless of pumping rate.

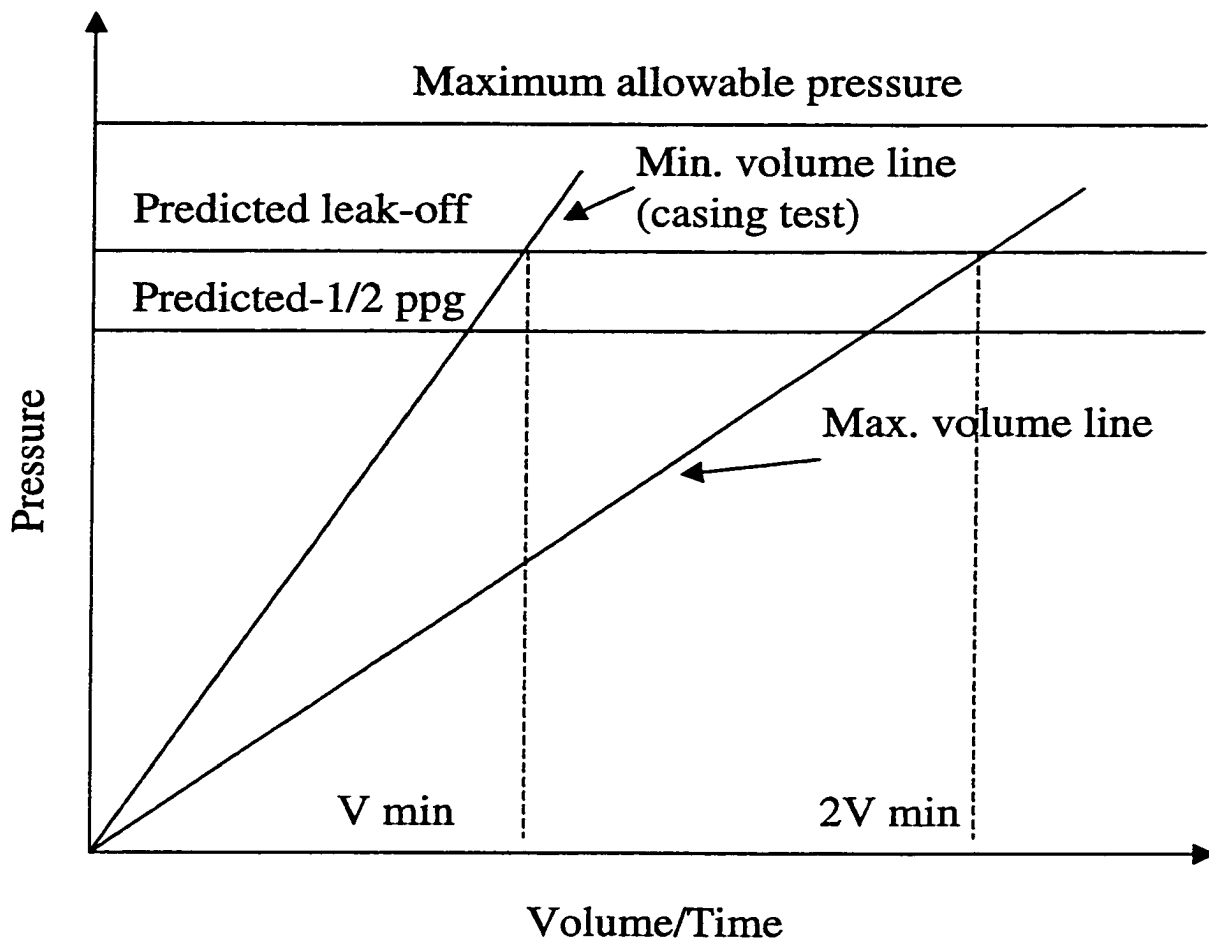


**Figure 2.7** Preparing guide lines for leak-off test (Postler, 1997).

Leak-off test procedures used by operators focus on the operating procedures and there are some differences among them. Amoco uses the following procedures.

Pick up drill bottom hole assembly (BHA) and trip in hole. Tag cement. If casing is full of seawater, displace seawater with mud that will be used in subsequent drilling to perform LOT.

1. Circulate and condition mud until mud weight is even in and out.
2. Casing Integrity Test – CIT: Pressure test casing recording pressures every 0.125 bbl (or every 0.25 bbl maximum). Shut-in and monitor pressure for 10 min. Input pumped volumes and pressures on CIT sheet.
3. Drill out Float Shoe, rat hole, and 10-15 ft (3-5m) of new hole. Circulate and condition the mud until mud weight is even in/out, checking in triplicate with pressurized mud balance.
4. Pull out of hole until bit is about 10-15 ft (~3-5m) inside casing shoe.
5. Rig up cementing unit and test lines. Close blow out preventers, BOP (Annular or pipe ram) and prepare to monitor volume/pressures on the cement unit, and also monitor pressures at the choke (via the casing pressure gauge on the choke console).
6. Pump mud (via cement unit) at 0.25 – 0.5 bpm constant rate, recording pressures every 0.25 bbl, regardless of pump rate until the pressure increase shows a definite deviation from a linear trend (leak-off pressure – LOP) or until hard break down. Hard break down occurs if the pressure abruptly drops while pumping. Record data on LOT sheet and follow plot. If pressure plot falls below maximum volume line, during pumping, before leak-off, the bleed –off pressure and start over using 0.25 bpm faster pump.
7. Confirm leak-off: Pump an additional volume (0.75 to 1.0 bbl) into the formation while frequently monitoring injection pressure behavior to ensure that the pressure increases at a smaller slope. Note: If hard break down has occurred, there is no need to pump this additional volume.

8. Shut down pump and record the instantaneous shut in pressure (ISIP). Then continue to monitor the pressure decline for 20 minutes, or until the shut in pressure stabilizes, whichever time is least. Look for surface leaks.
9. If a pressure decline is observed and the pressure stabilizes then the test is probably of good quality.
10. Bleed off pressure and record recovered drilling fluid volume. Record the injected and recovered fluid volumes.
11. Retest before squeezing. Retest if pressure abruptly dropped significantly while pumping (hard break down) to determine a valid LOP; do not use peak pressure as the LOP.

Amerada Hess emphasizes the stable of pumping pressure since leak-off pressure decreases with time. The LOT procedure is:

1. Drill cement, float equipment, and 10' of new formation or clean out rathole.
2. Circulate and condition mud until mud weight in and out is uniform (within 0.1 ppg).
3. Pull back into casing shoe. Make up cementing lines ensuring they are filled with mud (avoiding pumping air into drill pipe). Break circulation. Close annular.
4. Pump mud at  $\frac{1}{4}$  bpm until a pressure response is observed. Record volume pumped.
5. Begin pumping at  $\frac{1}{4}$  bpm until increments at  $\frac{1}{4}$  bpm rate. Stop pumps after each  $\frac{1}{4}$  bbl and wait until pressure stabilizes. Record volume of mud pumped, final pumping (dynamic) pressure and stabilized (static) pressure at each  $\frac{1}{4}$  barrel increment.

6. Plot both dynamic and static pressures vs. cumulative mud volume pumped.
7. Continue in ¼ barrel increments until the static pressure indicates a “leak-off” is occurring or the maximum specified pressure is reached (jug test).
8. A final shut-in pressure should be recorded 5 minutes after pumping has ceased.
9. Slowly bled off pressure and record the volume of mud bled back.

Dowell use the following procedures to do leak-off test.

1. Record Casing Test pressure each 0.25 bbl while pumping @ 0.25 bpm, and plot on Leak-Off Test Chart.
2. Drill out all cement and float equipment and +/- 10' of new formation.
3. Circulate the well with the mud pumps until the mud is conditioned (uniform density and rheology throughout the well). If mud does not have good fluid loss properties, a viscous, low fluid loss pill may be spotted across the O.H.
4. Pull drill bit into cased hole.
5. Pump mud with Dowell to fill treating line and remove any air from pump and lines before rigging up to drill pipe. Break circulation with Dowell pump. Close BOP.
6. Perform LOT with the cement pump. Level mud in the displacement tanks with a barrel marker, and reset volume to zero.
7. Perform LOT by pumping at a consistent 0.25 bpm and plotting the pressure every 0.25 bbl of volume pumped. The actual LOT is established when the plot of pressure vs. volume injected falls away from the straight line trend. When leak-off is established, stop pumping.

8. At this time, plot shut-in pressure on the same chart. This pressure should be plotted every minute until it levels out, or for about 5 minutes. If ISIP is less than  $\frac{1}{2}$  the leak-off pressure, a possible problem exists. Re-perform the leak-off test. If the same leak-off test is obtained on the new test, then it should be considered an accurate leak-off pressure.
9. Once pressure is stabilized, the well should be bled off into the displacement tanks and volume recorded.

### 2.6.2 Leak-off Test Plots

Leak-off test plot is what we said leak-off test result. Recorded pressures and pumped volumes are plotted on a graph describing the relationship of pressure versus pumped volume. On the graph, Y axis represents pressure and X axis volume pumped. The pressure after shutting-in might also be observed and plot on the X axis in minute from the time of shut-in. Figure 2.8 shows a typical leak-off test plot. The pressure-volume relation plot is the basic requirement of leak-off plot.

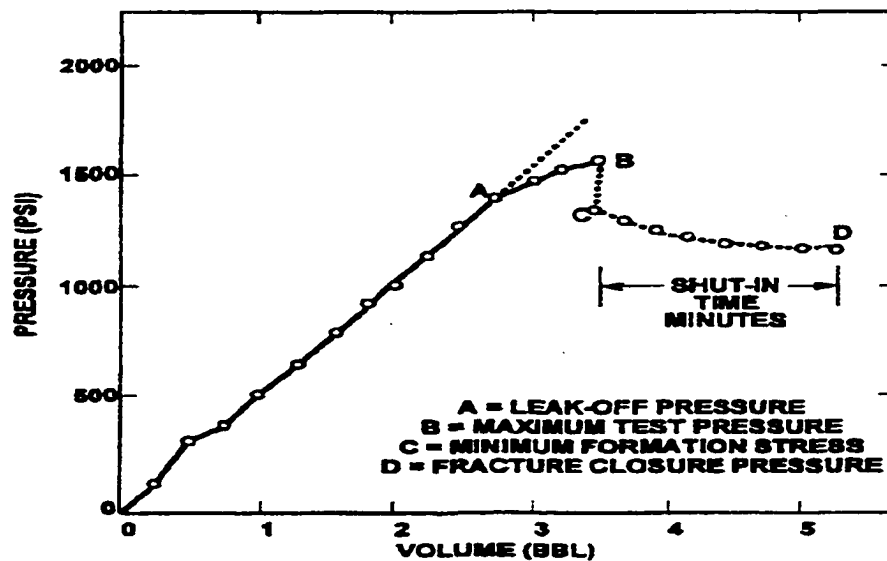
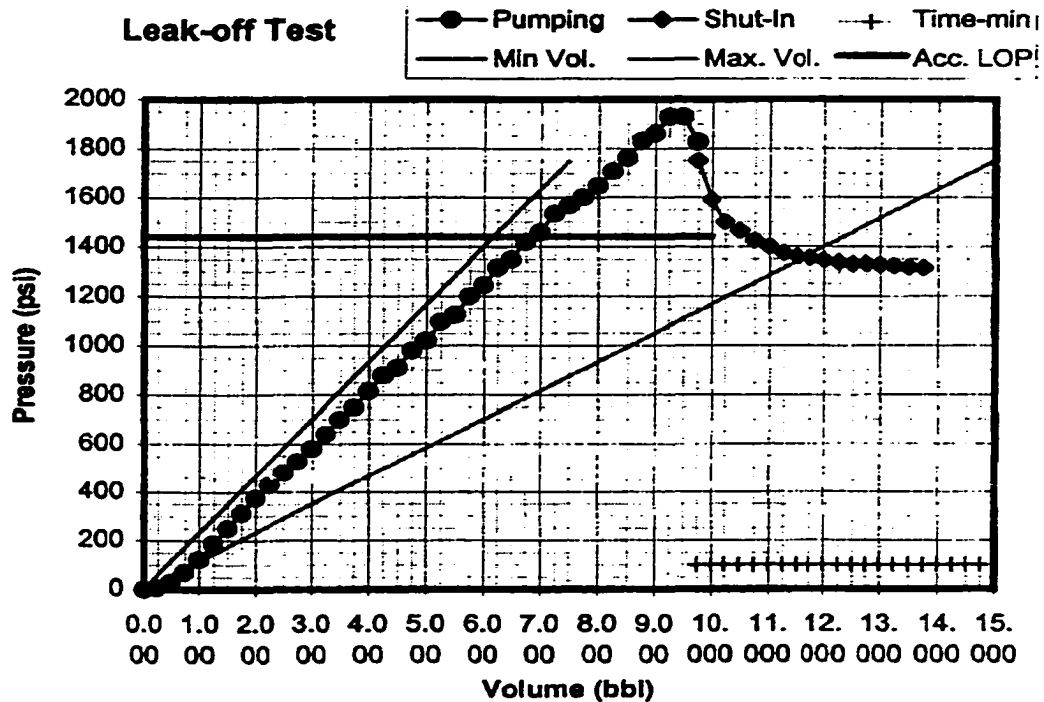


Figure 2.8 Typical Leak-off Test Plot (Postler, 1997).

Further more, some operator like to plot reference lines such as maximum, minimum pressure lines, and maximum and minimum volume lines on a plot as shown in Fig. 2.7 for interpretation. Figure 2.9 shows a typical LOT plot with such lines.



**Figure 2.9** Typical leak-off test with reference lines.

Most leak-off plots are recorded as Figure 2.8 or Figure 2.9. However, it is a good idea to record the well information and leak-off condition together with leak-off test data. The condition of a LOT gives interpreter more information and may be helpful for some unusual results.

Table 2.1 is an example of well information for a LOT. Generally, well name, date, air gap, water depth, casing shoe depth, mud (weight, viscosity, yield point et al.) should be recorded. More detail, estimated maximum pressure and predicted LOT pressure, together minimum and maximum volumes, should be listed. They are used for drawing the reference lines (as shown in Fig. 2.7).

**Table 2.1 LOT record (courtesy of Amoco).**

Date: 22-Mar-96		Water Depth ft	Air Gap ft	Max. TVD (ft)	Max. MD (ft)				
Well: XXXXXX									
Location: XXXXXX									
Rig: XXXXXX						300.00	70.00	5734.00	
LOP Criteria		Mud Properties							
Estimated Ppg	Min. Acc. Ppg	Mud Wt. ppg	WBM/ OBM	VIS. cp	PV cp	YP lbs/100sqf	API WL cc	Gels. 0/10	
16.50	15.75	13.00	WBM	50.00	21.00	13.00	13.00	4/19	
Casing Shoe					Top of 1st Below Casing Sand				
Csg. Size	MD ft.	TVD ft.	Incl. deg.	Azimuth deg.	MD ft.	TVD ft.	Incl. deg.	Azimuth deg.	
13.38		5686.00	0.00	N/A	N/A	N/A	N/A	N/A	

LOT Chart Guidelines					
Min. Volume (last point of CIT)		Max. Volume (twice Min. Vol.)		Accepted LOP (horiz. line)	
(bbl)	(psi)	(bbl)	(psi)	(bbl)	(psi)
0.00	0.00	0.00	0.00	0.00	813.10
2.50	1600.00	5.00	1600.00	10.00	813.10

 Required Input

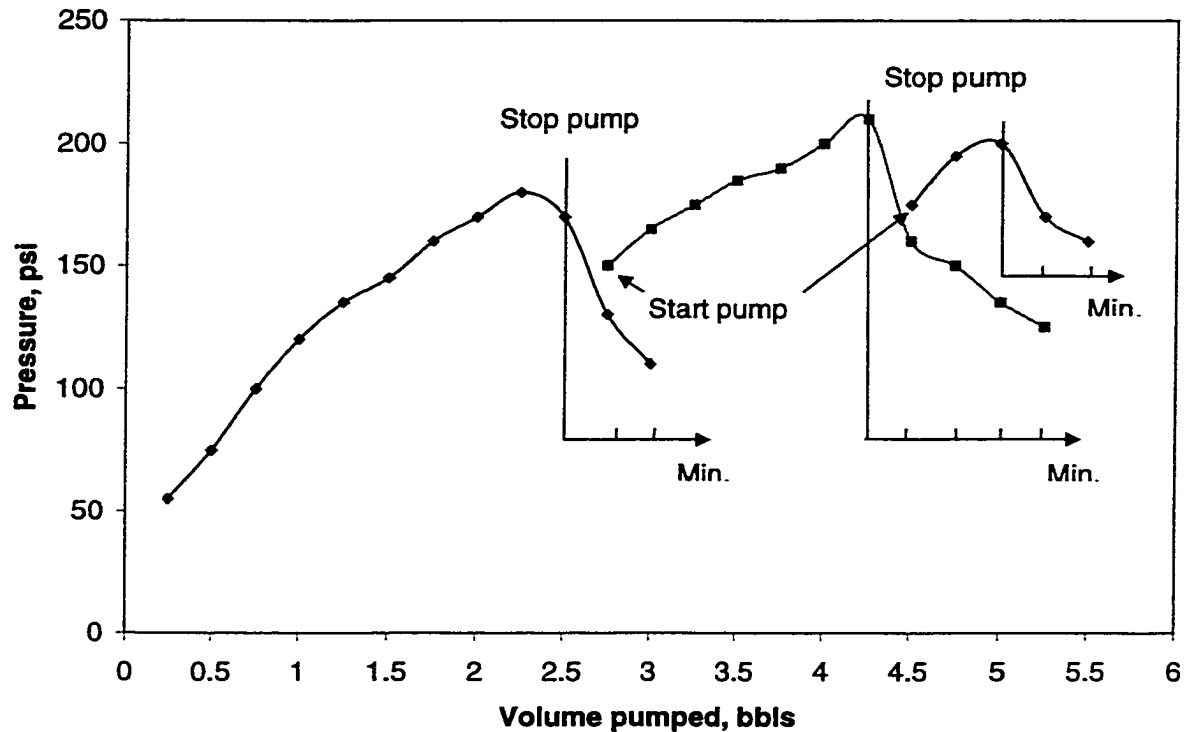
 Optional Input

Figure 2.10 shows an example of a completed record of a leak-off test. The figure should be used and stored together with Table 2.1. Pressures per ¼ bbl pumped volume should be recorded. Also recorded are the pressures per minute after shut-in the well. It is better to record mud return after releasing wellbore pressure. LOT plot is drawn for interpretation.

Slightly different from the procedures stated previously, operators in South China Sea stop pump in the middle of leak-off test. Pressures are monitored during the stop pump period. Continue pumping until break-down after a stopping pump period. Two or more stop pumping during LOT may be used depending on operators. As an example, Fig. 2.11 gives a leak-off test in South China Sea.



psi after pumped 4.25 bbls. stopped pump for 4 minutes and re-start pump got a pressure of 175 psi after 0.25 bbls was pumped getting the total volume of 4.5 bbls.



**Figure 2.11 Stopping pump during leak-off test.**

### 2.6.3 Interpretation Techniques

The propose of leak-off test is to determine whether the casing shoe is strong enough for following heavier mud or high pressure form formation fluid kick. The pressure the casing shoe can stand is the result of interpretation of leak-off test plot. As shown in Figure 2.12, the pressure at point A is the leak-off pressure (LOP) for the leak-off test. Point A is the point at which the pressure-volume plot deviated from a straight line (linear relation). Point B is the maximum pressure point at which pressure no longer increase with further pumping. After the maximum pressure B, the well is shut-in (Point C in Figure 2.7). Section DE is the level-off section of the leak-off test.

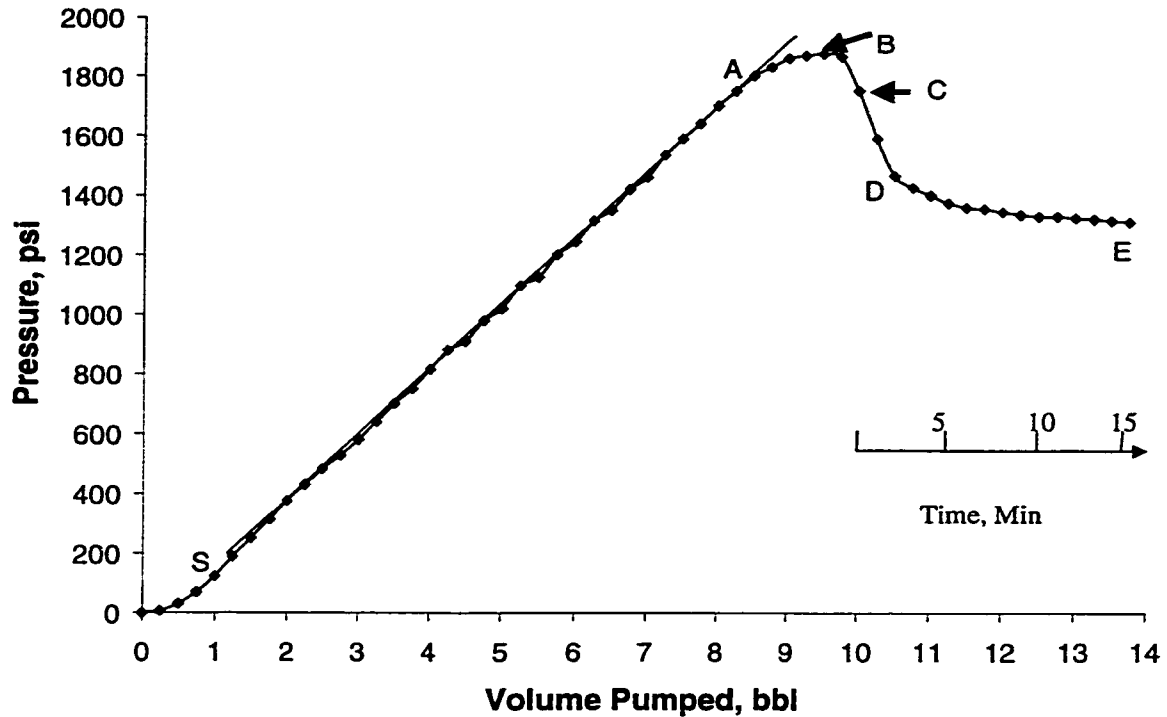


**Figure 2.12 Common interpretation of leak-off test result.**

For the leak-off test in Figure 2.12, the common interpretation techniques are summarized as the following. A straight line (line SA) can be drawn matching most of the points representing a linear pressure-volume relationship for most of wells. The beginning exponentially increasing part (section OS) represents the effect of gas. Fracture appears at point A. The fracture propagates at section AB as new drilling fluid is pumped. After Point B, the pumped mud as well as mud in the well flows into the fracture. Section SA is called pressure build-up section. Section AB is fracture propagation section. Point A is leak-off point and Point B is breakdown point. Section BC is the breakdown section. The sharp pressure drop (section CD) represents the loss the kinetic energy (loss friction of mud) and filtration of mud. The level-off section DE represents the filtration loss of mud.

Chenevert and McClure (1978) suggested using a minimum volume line and the anticipated LOP lines, shown in Figure 2.7, as a guide for determining the pump rates. The minimum volume line can be estimated from mud compressibility as the authors suggested. In practice it is the casing test line. Figure 2.13 gives a casing test result. Casing test is used to test casing integrity. The procedure is the same as that of LOT except drilling through cement plug and 10 to 15 ft new formation.

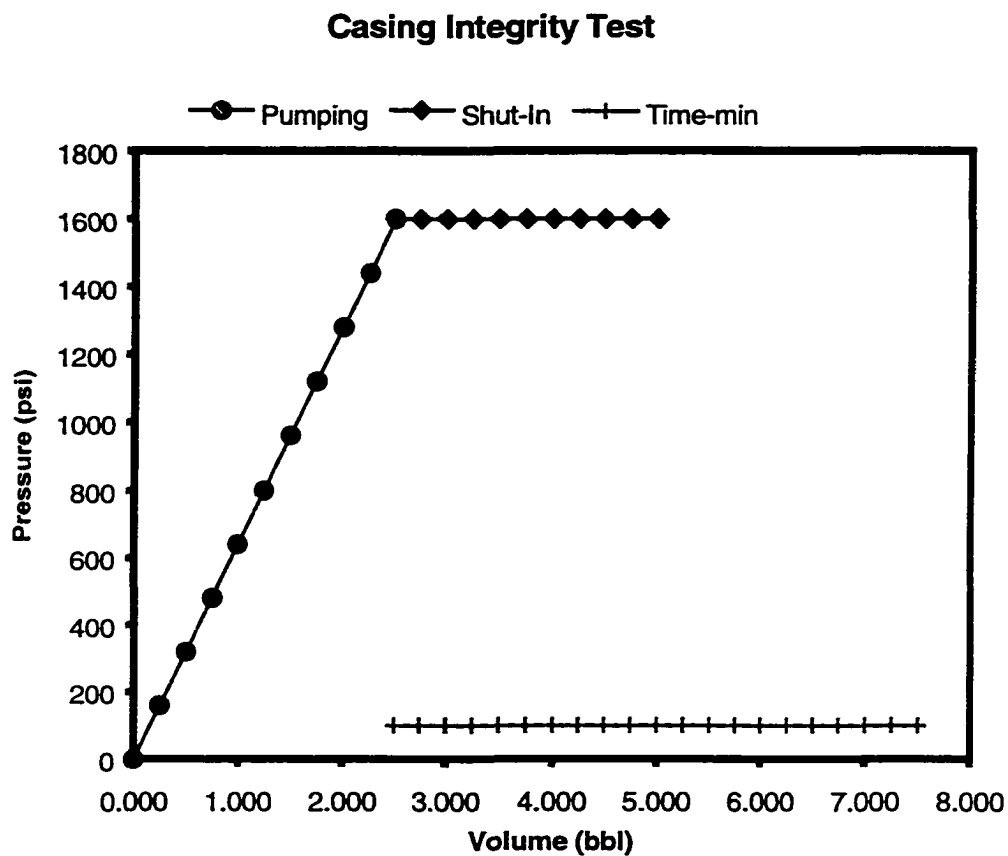


**Figure 2.13 Casing integrity test result (courtesy of Amoco).**

According to Chenevert and McClure (1978), straight-line data of a LOT should stay equal to or very close to the minimum volume line values; otherwise, the pump rate is inadequate. However, they did not mention the data limit that may

deviate from the minimum volume line. This limit is known as the maximum volume line, also shown in Figure 2.7.

Postler (1997) presented the determination of the reference guidelines as shown in Figure 2.7 and their interpretation is shown in Figure 2.14 and following procedures.

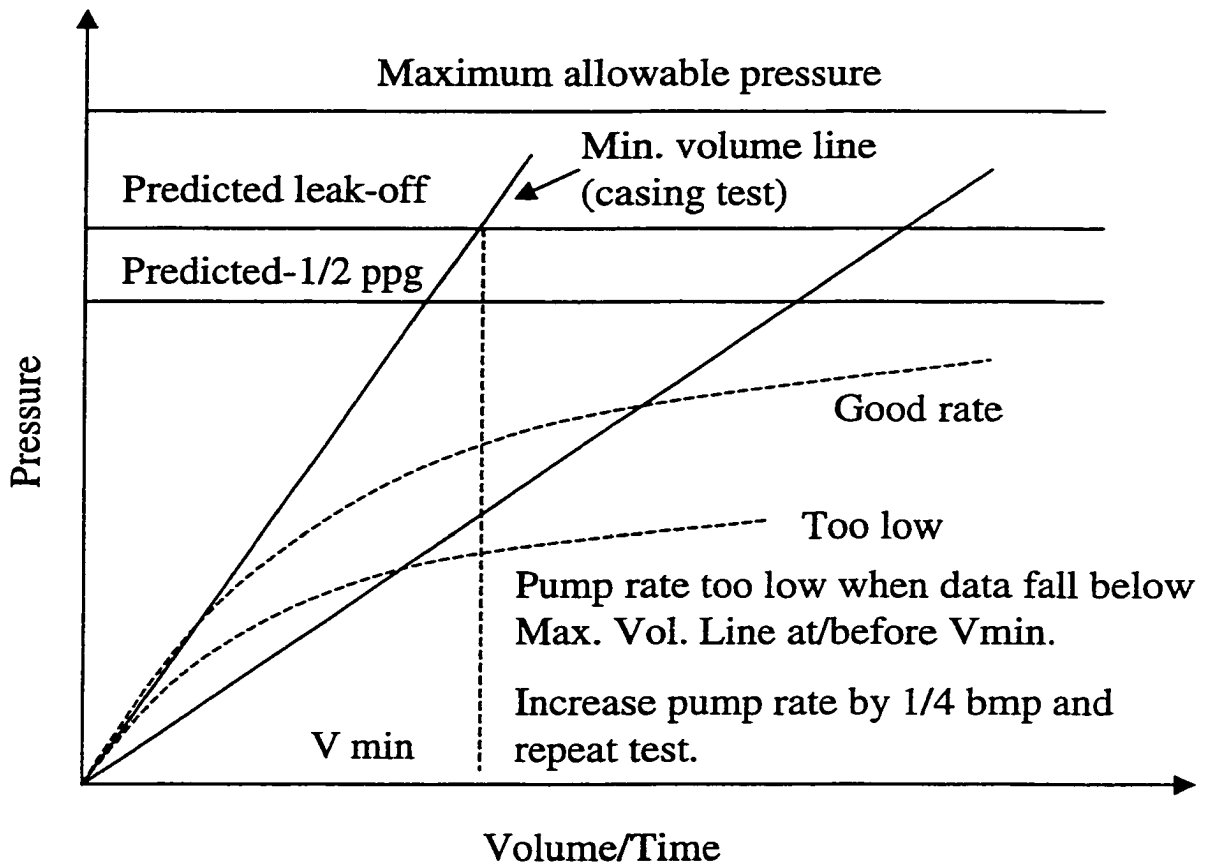


**Figure 2.14 Pumping rate effect (Postler, 1997).**

1. Predicted leak-off pressure line: the value comes from the analysis of offset well data and/or local overburden and pore pressure, not guesswork or the need for a certain value to reach the next casing shoe. A rightward bend in the plot

near this pressure probably indicates leak-off. A bend significantly below this line is probably not leak-off, and pumping should continue (Figure 2.14).

2. **Minimum leak-off pressure line:** less than  $\frac{1}{2}$  ppg of equivalent mud weight of the predicted leak-off pressure line. The  $\frac{1}{2}$  ppg represents error from experience.
3. **Maximum pressure line:** maximum pressure based on equipment limitations or lost circulation experience.
4. **Minimum volume line:** a diagonal line represents the mud compressibility and may be taken by casing integrity test line.
5. **Maximum volume line:** a diagonal line represents lower limit reference. It is two times the minimum volume as a rule of thumb. LOT data deviating below the line are usually caused by high formation permeability and a too-low pump rate.

Not all the lines are used by operators. In the case of Figure 2.9, only minimum pressure line (horizontal), the minimum and maximum volume lines were used.

Morita et al. (1991) studied the occurrence of formation fracture and its propagation during LOT. They concluded that no damage of leak-off test on formation fracture since the fracture is controlled by minimum rock stress and it will recover after leak-off test. Their interpretation of formation fracture is shown in Figure 2.15.

Some operators attribute unusual LOT results to pre-existing channels or so-called mini-fractures. Ishijima and Roegiers (1983) studied the effect of the length of pre-existing cracks on the pressures. They concluded that different crack length might give different initiation and breakdown pattern as shown in Figure 2.16.

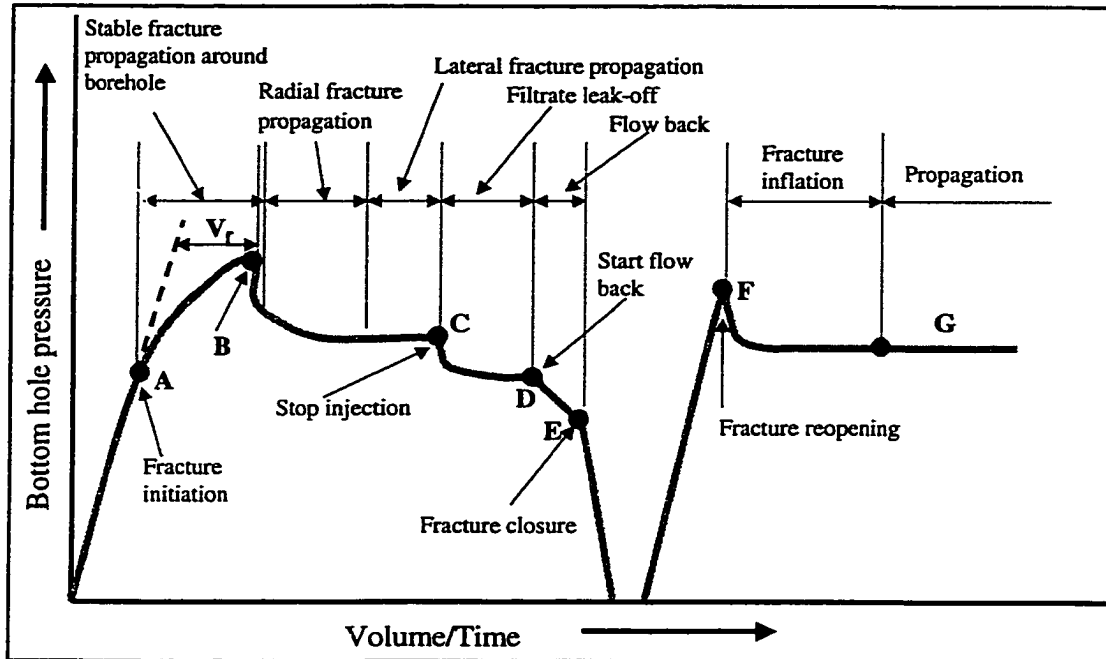
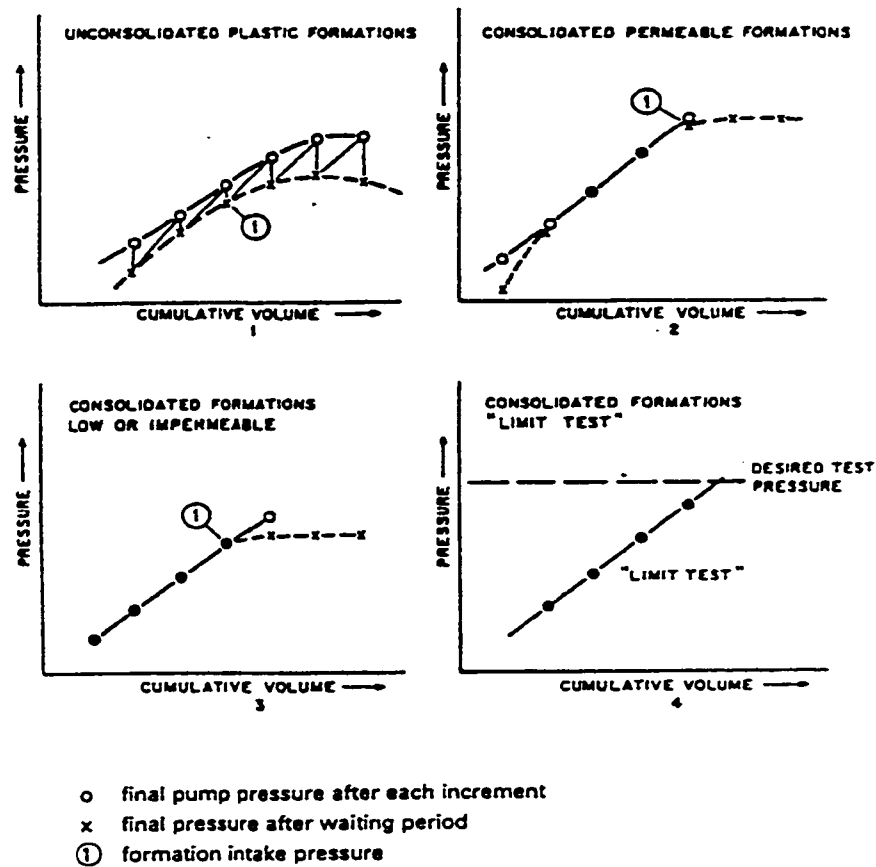


Figure 2.15 Rock fracture and fracture propagation under leak-off test (Morita et al. , 1991).



Figure 2.16 Effect of pre-existing crack length (Ishijima and Roegiers, 1983).

Most of the studies of rock fracturing hasn't been used by since detail rock properties are needed but usually not available. HESS summarized the possible LOT results form different formations. Their schematic representations are shown in Fig. 2.17. Rock plasticity and permeability are the major factors affecting leak-off test results according the figure.



**Figure 2.17 Leak-off test under different rocks (courtesy of HESS).**

The goal of the interpretation of leak-off test is to decide whether to drill ahead or to squeeze cement. The interpretation techniques used by operators are rather easy to follow. The general interpretation technique used by Amoco is shown in (Figure 2.18).

Date: 22-Mar-96		Casing Shoe				
Well: XXXXXX		Csg. Size	MD ft	TVD ft	Incl. deg	Azimuth deg
Location: XXXXXX		13.38		5686.00	0.00	N/A
Fig: XXXXX						
Mud Properties						
Mud Wt. ppg	WBM/ OBM	VIS. cp	PV cp	YP lbs/100sq	API WL cc	Gels. 0/10
13.00	WBM	50.00	21.00	13.00	13.00	4/19
LOT Test Results				Channel Indicators		
LOP (psi)	MS (psi)	LOF <sub>EMW</sub> (ppg)	MS <sub>EMW</sub> (ppg)	LOF <sub>EMW</sub> /MS <sub>EMW</sub>	1. LOF <sub>EMW</sub> < Minimum Acceptable Value 2. Shut-in pressure not leveling off 3. LOF <sub>EMW</sub> /MS <sub>EMW</sub> > 1.10 when leak-off occurs without abrupt pressure drop (hard breakdown)	
920.00	860.00	16.11	15.91	1.01		

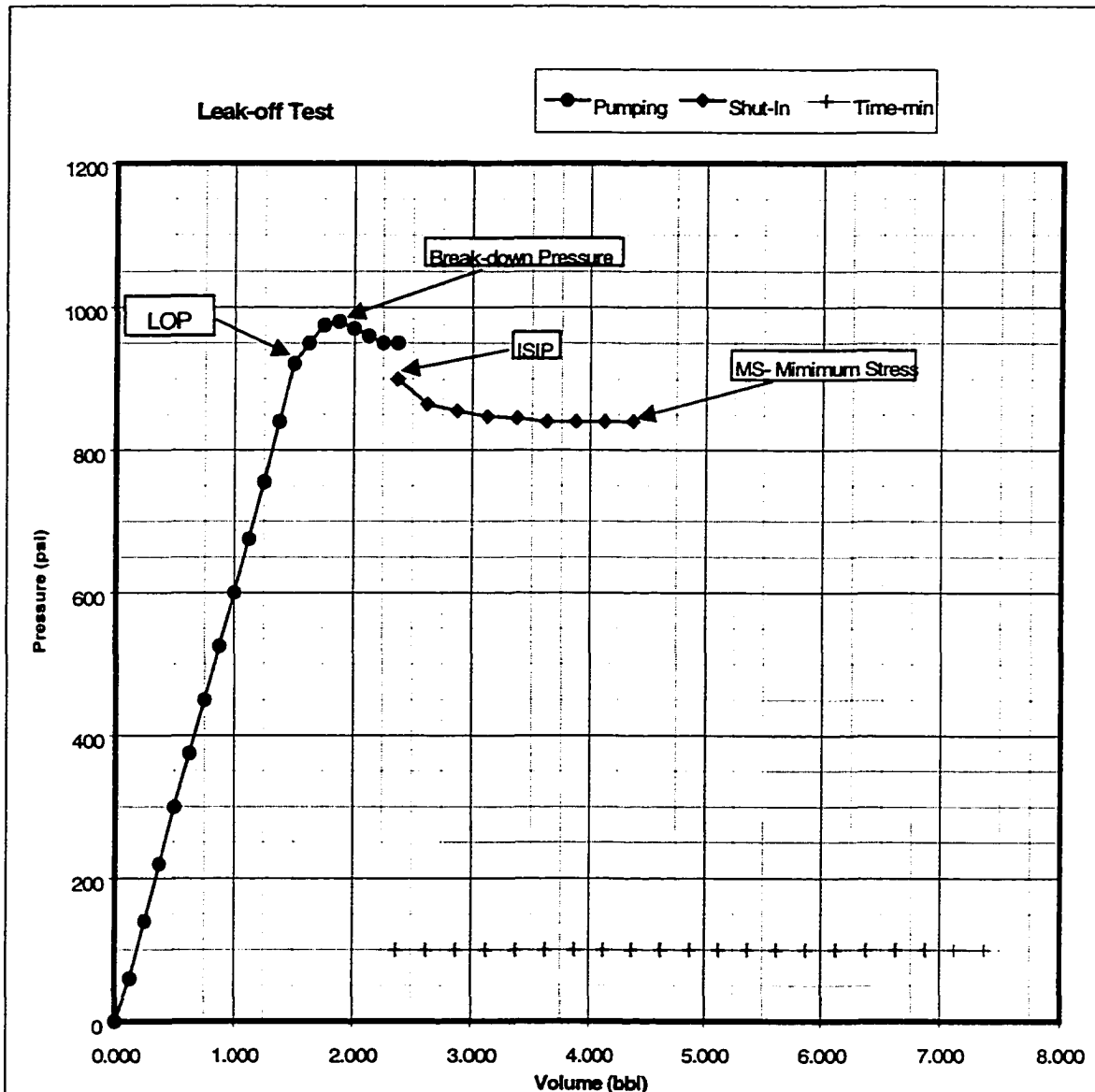


Figure 2.18 Interpretation of leak-off test result (courtesy of Amoco).

Squeezing cement is required if the leak-off pressure is less than minimum acceptable value to the next casing, shut-in pressure is not level-off, or the ratio of leak-off pressure (LOP) to minimum stress (MS) is greater than 1.1.

Another interpretation techniques are:

1. A concave upward slope early, then constant slope to leak-off indicates trapped air in the system.
2. A concave upward slope throughout the leak-off test indicates high fluid loss to a permeable formation.
3. A concave downward slope at a much earlier than expected fracture pressure indicates a cement or a casing leak.
4. A leak-off test that does not go through the origin indicates a pressure loss due to friction or the gel strength of mud.
5. After bleeding pressure back into displacement tanks, if significantly less volume returned than was pumped (+/- 1 bbl), then a possible channel exists. This assumes that pressure can be bled off through drill pipe (i.e. no check valves).

Postler (1997) presented a good summary of LOT guidelines and interpretation techniques based on published theory. The authors suggested to evaluation of both the build-up and shut-in portions of the test plot, as well as the judicious use of repeat tests during interpretation of LOT results. The proposed basic interpreting guidelines were: 1. estimate the leak off, 2. evaluate LOP, 3. evaluate shut-in, 4. check for cement channel, 5. retest when in double.

Postler (1997) also presented patterns for leak-off test plots from different channels. Large open channel around casing shoe gives a lower leak-off pressure than

predicted. Small open channel results in two slopes and therefore two leak-off points. The two slope plots also have two small level-off parts in the whole level-off section. The third case is plugged channel. Large pressure drops after shut-in well. Figure 2.19 shows the patterns.

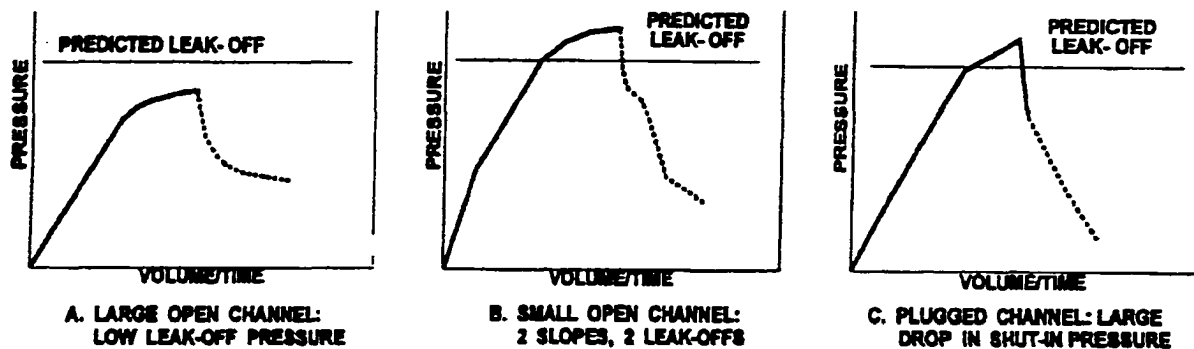


**Figure 2.19** Effect of channels on leak-off test result (Postler, 1997).

Many researches focused on some specific problems in LOT. These researches provided helpful materials for LOT interpretation. Two research results are summarized here.

Chenevert and McClure (1978) studied mud gelation effect of pressure-volume relation. Gelation effect caused friction pressure loss. They suggested that subtracting the mud gelation pressure from the LOP. The authors proposed using field circulation data to get mud gelation pressure.

However, pressures due to mud gelation are relatively small and can be ignored without resulting significant error when calculating the LOP and the fracture pressure. Following the procedure would result in overestimation of the LOP and the fracture pressure. Thus, the industry simply ignores the mud gelation effect during analyzing test results.

Hazov and Hushudov (1993) studied the effect of plastic formation on leak-off test since it has been thought that wellbore ballooning may be the major reason to take a lot of pumped volume. The authors calculated the wellbore compressibility in shale formations based on LOTs in the eastern North Caucasus of the former Soviet Union. It was observed that the measured and calculated volumes from the LOT and the drilling fluid compressibility were quite different. They also reported that calculated volume results for cased hole with 100% cement bond and those without cement bond were significantly different. In their example, all the pumped volume returned to mud pits after the pumps were stopped. When the wells were shut in immediately after the pumps were stopped, the wells had a slight pressure of about 2-MPa, indicating considerable gas entry, also confirmed by the mud logging.

The authors also stated that the non-linear LOT curves were the result of fluid loss and filtration. One possible explanation to this non-linearity was postulated to be the result of plastic deformation of the well. However, plastic deformation in shales takes considerable time (10 to 20 hours), and the time needed to pressurize shales during a LOT takes only 10 to 15 minutes. Therefore, the authors concluded that plastic deformation might not be the main factor there.

The authors concluded this big volume change came from elastic hydrofractures. They considered fractures as pre-existed. As pressure increased, the fractures took mud in. The fractures would be closed under the action of rock stress and returned the mud without any losses as the pressure was reduced.

Based upon Hazov and Hushudov's observations, it can be concluded that borehole expansion or so-called ballooning has a negligible effect on LOT behavior

since borehole wall displacement would be insignificant, resulting in trivial wellbore volume expansion.

#### 2.6.4 Modeling Leak-off Test Results

Leak-off test plot is the relation of pressure versus volume pumped. To model leak-off test result is to set up the pressure-volume relation. Chenevert and McClure (1978) presented a model for their minimum pressure line using basic mud compressibility equation.

$$\Delta V_I = C_m V_m P_i \quad (2.29)$$

Where:  $\Delta V_I$  = Volume of mud injected, bbl;

$C_m$  = Mud compressibility,  $\text{psi}^{-1}$ ;

$V_m$  = Volume of wellbore (drill pipe plus annulus), bbl;

$P_i$  = Injection pressure, psi.

The mud compressibility can be calculated from the components of the mud.

$$C_m = C_w \times \% \text{water} + C_s \times \% \text{solid}, \text{psi}^{-1} \quad (2.30)$$

Where  $C_w$  and  $C_s$  are water compressibility ( $3 \times 10^{-6} \text{psi}^{-1}$ ) and solid compressibility ( $0.2 \times 10^{-6} \text{psi}^{-1}$ ).

If the well mud volume does not include the part below cement plug, the pressure-volume relation given by Eq. 2.29 should be the result of casing integrity test.

Almeida (1986) did a good work in modeling leak-off test. He developed a computer simulation model of leak off test. The model included many factors that affect pressure behavior during the test, and could predict the LOT curve.

In his model, Almeida (1986) divided LOT into four phases: (1). pressure increase due to overall compressibility of the system, (2). fracture initiation, (3).

fracture expansion, and (4). pressure decline and fracture closure after the pump is shut in.

The major contribution in modeling LOT of Almeida's (1986) work is the concept of overall or whole compressibility of the well system. System overall compressibility included the mud compressibility, drilling pipe and drill collar expansion, casing expansion for un-cemented casing, filtration, wellbore expansion. Therefore the whole mud compressibility is the compressibility from Eq. 2.29 if the left volume (compressed mud volume) after all the effect is used instead of volume pumped.

$$\left( \begin{array}{c} \textit{Volume} \\ \textit{Pumped} \end{array} \right) = \left( \begin{array}{c} \textit{Compressed} \\ \textit{Mud} \\ \textit{Volume} \end{array} \right) + \left( \begin{array}{c} \textit{Casing} \\ \textit{Expanded} \\ \textit{Volume} \end{array} \right) + \left( \begin{array}{c} \textit{Wellbore} \\ \textit{Expanded} \\ \textit{Volume} \end{array} \right) + \left( \begin{array}{c} \textit{Leaked} \\ \textit{Volume} \end{array} \right) \quad (2.31)$$

In his work, Almeida (1986) divided casing expansion due to leak-off pressure into two categories: cemented casing and un-cemented casing. Casing expansion is negligible for cemented casing. Wellbore expansion also divided into elastic and plastic wellbores. His formula works for elastic wellbore. Basic formula of dynamic filtration (filtrated volume depends on square root of time) was used for mud leakage. According to his simulated results, perfect straight lines (linear pressure-volume relation) appeared in pressure build-up section.

Similarly, Hazov and Hurshudov (1993) considered the effect of wellbore expansion (open hole) and combined with mud compressibility. That is two terms in Eq. 2.31 was used. His result works since his casing was cemented (zero expansion) and casing shoe was set in shale with 100% bond cement sheath according to them.

Altun (1999) analyzed the non-linear behavior of LOTs in deep wells. Based on the whole compressibility concept, he proposed models to simulate non-linear curving. Using his model, Altun modeled the latter part of LOT curves supposing the early test part was known. His major contribution in modeling LOT is he used static filtration equation (Darcy's law) to calculate volume lost instead of using dynamic filtration equation for mud leak used by Almeida (1986). Using the basic filtration equation, Altun (1999) successfully modeled the non-linear behavior for deep wells.

## **CHAPTER 3**

### **DATA ANALYSES IN SHALLOW MARINE SEDIMENTS**

Data analyses are always the basis of researches. The mechanical properties of soils in Green Canyon of the Gulf of Mexico are presented first. Although we will not use these properties directly since the depth of the soil samples are too shallow and we don't have corresponding formation fracture pressure (FFP) data. However, the range and trend of the properties could give us concepts about the region.

LOT plots are major reference of interpretation and therefore of drilling decision. Shallow leak-off test plots from different areas are collected and analyzed in the chapter. Compared with those in deep wells, the characteristics of shallow LOTs will be summarized.

Also analyzed is LOT data from different countries and operators. The LOT data are generally plotted as leak-off pressure (LOP) versus depth. The data, especially the trend, of FFP will be discussed. Data from deep wells are also presented to compare the relation or difference with those in shallow. Although on shore LOT data are collected, I will focus my analysis on LOT results from shallow marine sediments.

#### **3.1 Soil Properties in Green Canyon of Gulf of Mexico**

Soil mechanical properties are needed for stress and strain analyses. Unlike the properties of metals, soil properties vary not only with depths but also locations. During 1982 to 1986, Conoco Inc. had conducted geotechnical investigation in Green Canyon region of the Gulf of Mexico. The locations of the tested borings are shown in Fig. 3.1. The water depth of the interested area is in 1739 ft to 1767 ft.

Conoco Inc. had investigated many blocks. However, only a few blocks are collected and analyzed here since most of the tested results couldn't provide enough

data for stress-strain analysis. What the tested data from boring samples are not mechanical properties. Formulas used to calculate mechanical properties from data source are presented.

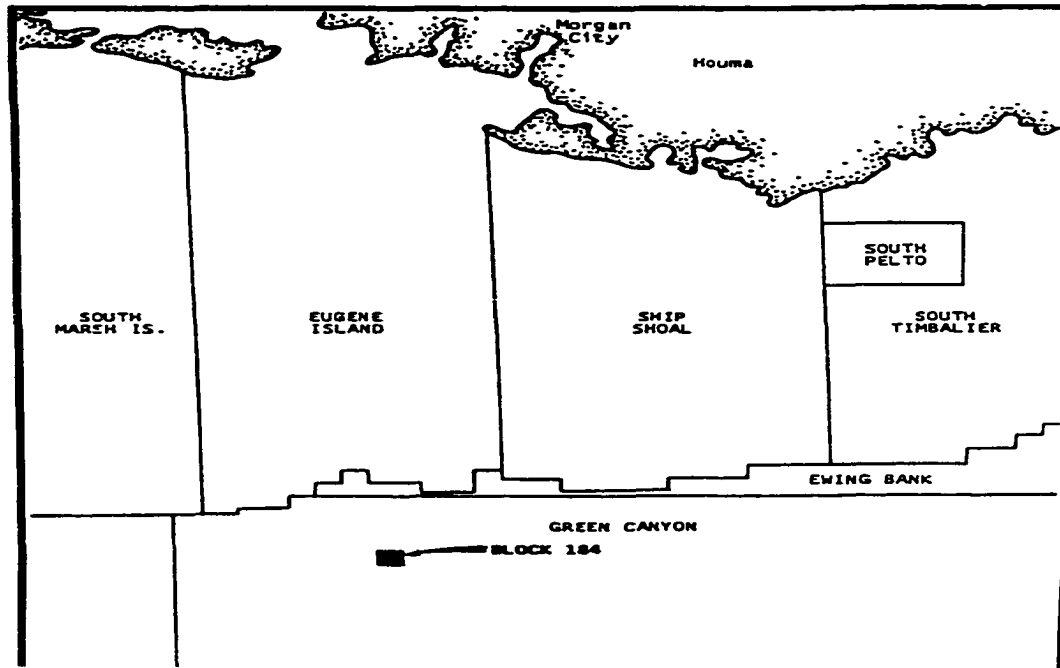


**Figure 3.1 Borings location map (Block 184, Green Canyon in the Gulf of Mexico).**

The borings were collected in upper marine sediments (less than 500 ft below sea floor for all places). Their tested soil properties are liquid limit, plastic limit, water content in percent, and unit wet weight in lb/cu ft. Shear strengths were measured (in kips/sq ft) with torvane and miniature vane. Compression tests were conducted to measure water content in percent, unit dry weight in lb/cu ft, shear strength in kips/sq ft, strain in percent, lateral pressure in kips/sq ft, and failure strain in percent.

Table 3.1 gives an example of analyzed data. The deepest tested place is at 376.5 ft below sea floor. Collected data are in-situ vertical effective stress, friction angle, un-drained shear strength and shear strength with depth.

**Table 3.1 Summary of deformation-controlled simple shear test results, boring 1, Block 184, Green Canyon Area.**

Depth, ft	In-situ Vertical Effective Stress		Friction Angle	Unstrain Shear Strength		Shear Strength	
	KSF	in PSI		KSF	in PSI	KSF	in PSI
49	1.4	9.72	24.2	1.14	7.92	0.14	0.97
85.5	2.65	18.40	27.0	2.17	15.07	0.19	1.32
116.5	3.9	27.08	20.8	2.51	17.43	0.13	0.90
195.5	7.3	50.69	26.1	3.35	23.26	0.4	2.78
226.5	8.6	59.72	20.7	5.59	38.82	0.44	3.06
256.5	9.9	68.75	20.1	5.45	37.85	0.75	5.21
316.5	12.55	87.15	18.7	6.15	42.71	1.35	9.38
346.5	13.85	96.18	21.9	7.77	53.96	1.52	10.56
376.5	15.2	105.56	17.7	7.88	54.72	1.4	9.72

According to the measured data, the major soil strata could be classified and tabulated as Table 3.2.

**Table 3.2 Major soil strata in Green Canyon.**

Stratum	Penetration, ft		Description
	From	To	
I	0	50	Very soft to firm clay
II	51	58	Silty fine sand
III	58	124	Firm to stiff clay
IV	124	134	Silty fine sand to clayey fine sand
V	134	300+	Stiff to very stiff clay

The needed properties for stress-strain analysis are Young's modulus ( $E$ ), Poisson's ratio ( $\mu$ ), cohesion strength ( $\tau_0$ ), friction angle ( $\phi$ ), and effective vertical stress ( $\sigma_v$ ).

Vertical effective stress profile could be calculated from the submerged unit weight and the depth. It is the difference of overburden pressure with the formation pore pressure. Calculated vertical stresses with depth plots are summarized in Fig. 3.2. The maximum depth is 460 ft.

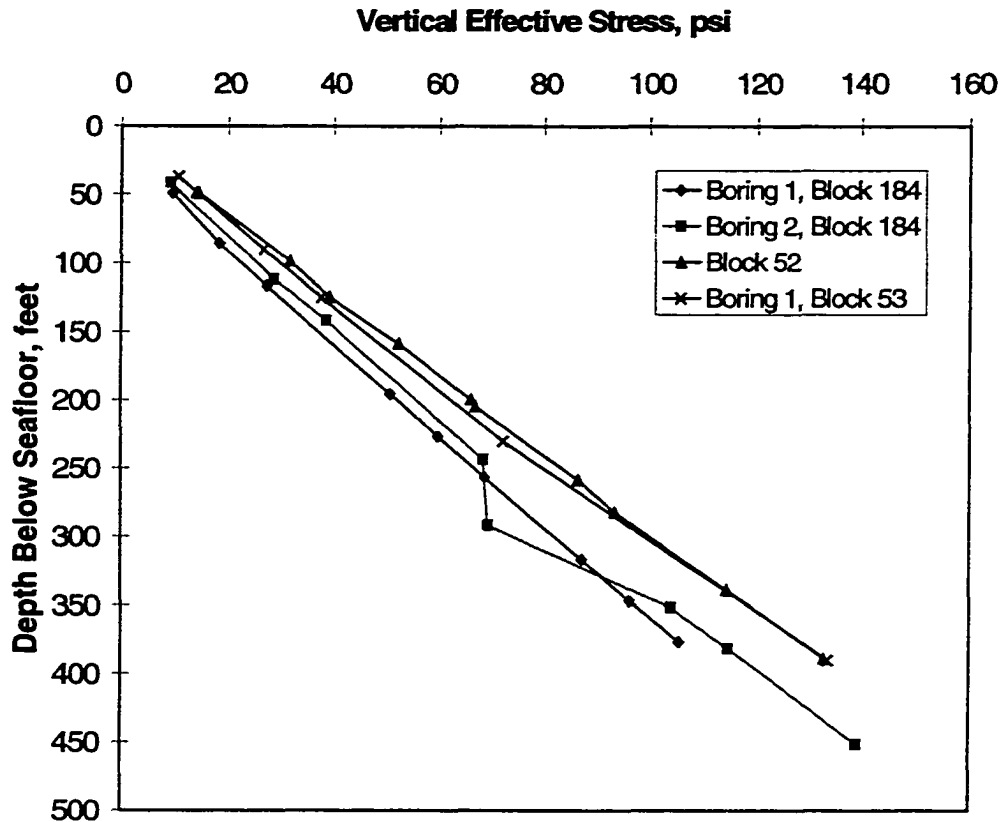


**Figure 3.2 Effective vertical stress vs. depth below sea floor.**

Overburden pressure can be calculated from the wet boring density and sea water density in the region (Bourgoyne et al., 1991).

$$p_{over} = \int_0^{D_w} g \rho_w dD + \int_{D_w}^D g \rho_b dD \quad (3.1)$$

Poisson's Ratio  $\mu$  is defined as the ratio of lateral strain to axial strain. It can be calculated based on the confined tested results by the following formula.

$$\mu = k / (1 + k) \quad (3.2)$$

Where  $k$  is the confined-vertical stress ratio tested from the borings. The variation of Poisson's ratio versus depth is plotted in Figure 3.3.

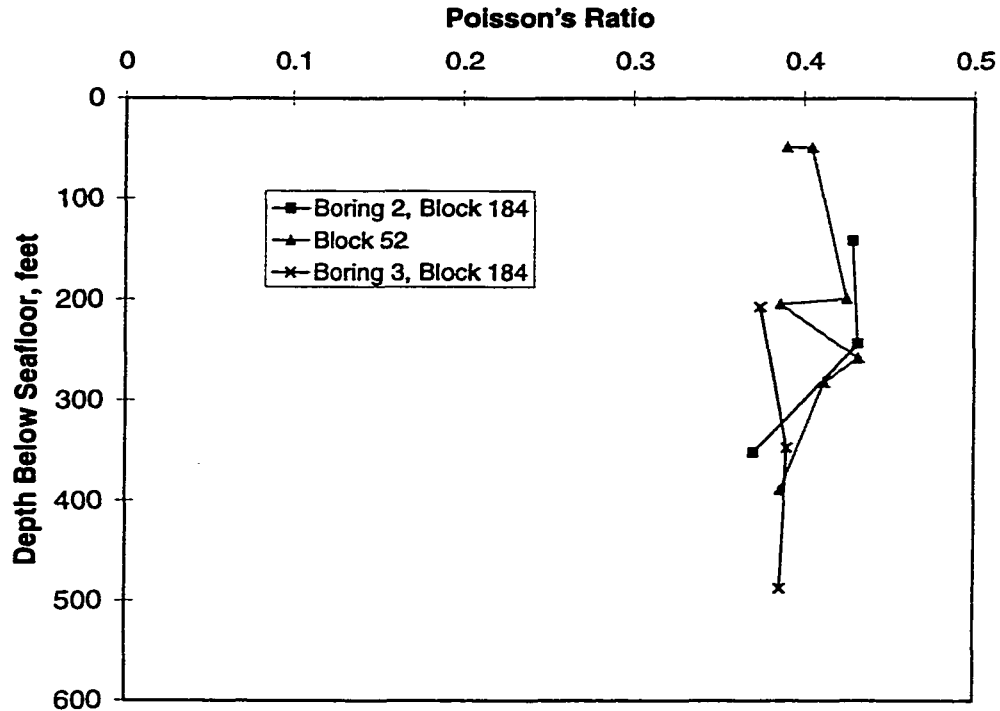


**Figure 3.3 Poisson's ratio vs. depth below sea floor.**

Young's Modulus,  $E$ , can be derived from the tested shear modulus  $G$  following Equation 3.3. Shear modulus is 1/3 of 2 times of the slope in the consolidated undrained triaxial tested curves according to their units and definition. Figure 3.4 gives the plot of shear modulus with depth.

$$E = 2G(1 + \mu) \quad (3.3)$$

Cohesion strength,  $\tau_0$ , is defined as the shear strength when no friction angle exists. It equals the tested unconsolidated undrained shear strength. Figure 3.5 shows cohesion strength variation.

Friction angle,  $\phi$ , could be calculated from its definition of Equation 3.4.

$$\phi = \arctan \frac{\tau - \tau_0}{\sigma_n} \quad (3.4)$$

The formula comes from Mohr's circle.

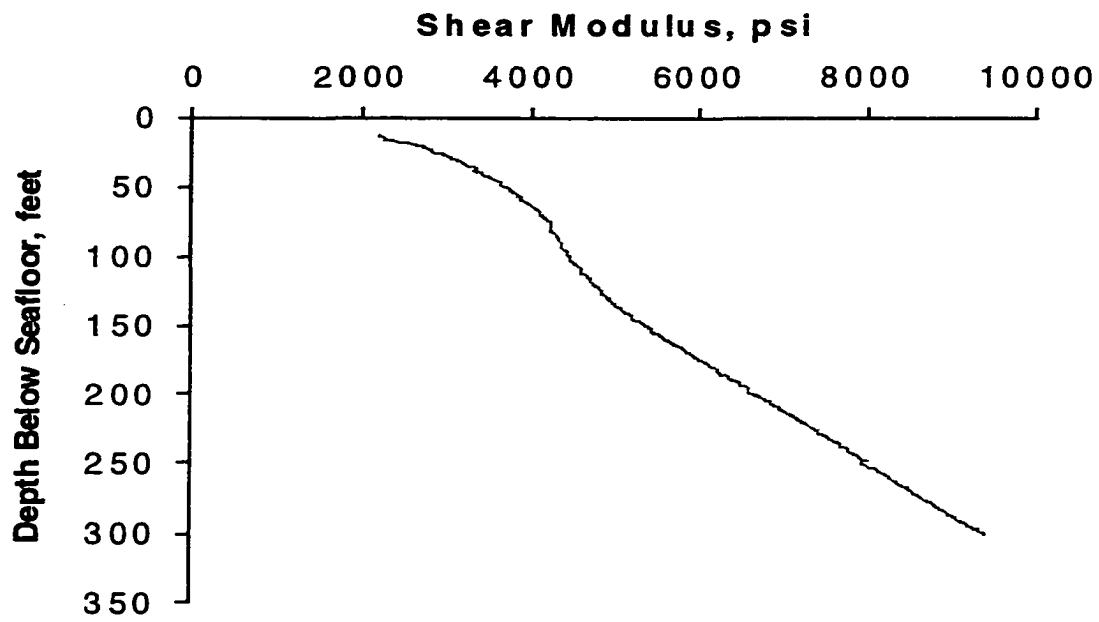


**Figure 3.4** Shear modulus vs. depth below sea floor.

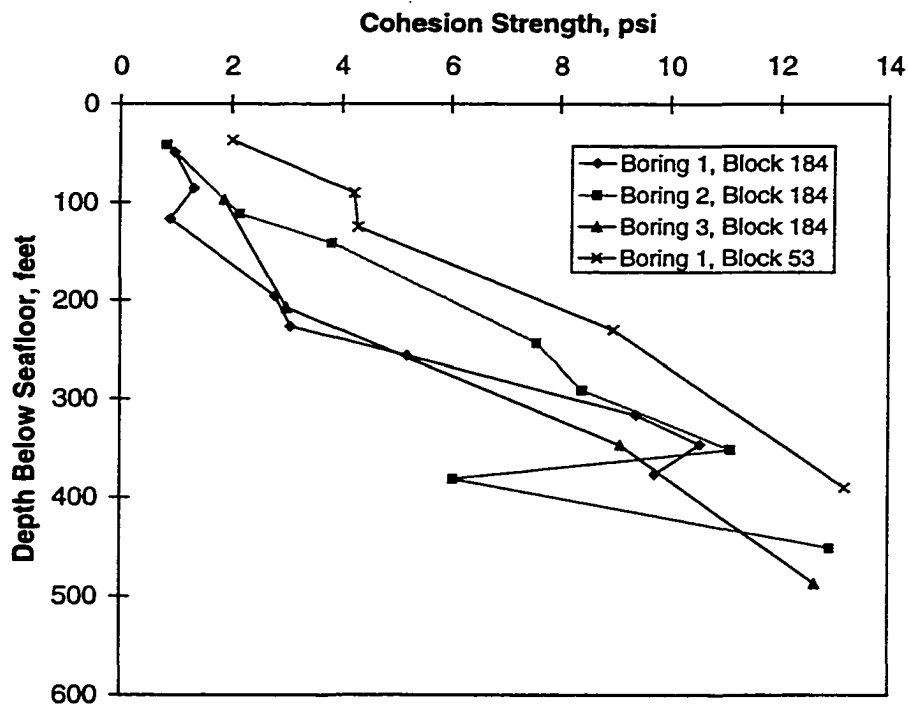


**Figure 3.5** Cohesion strength vs. depth below sea floor.

According to the formula Equation 3.4, friction angles are calculated and shown in Fig. 3.6. variation with depth.

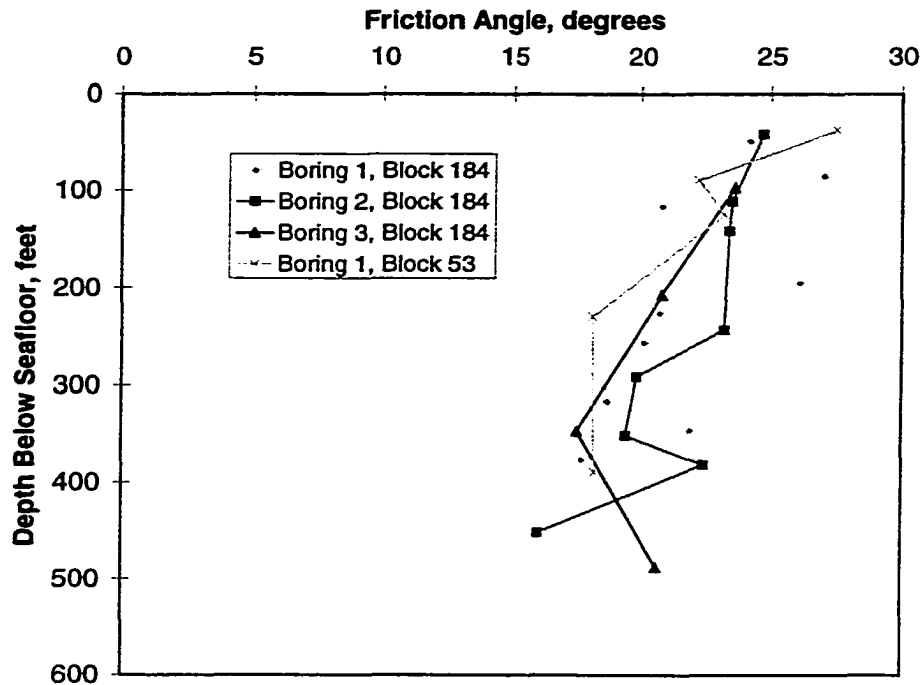


**Figure 3.6 Friction angle vs. depth below sea floor.**

Figures 3.2 to 3.6 summarize the properties needed for extensive stress-strain analyses. Effective vertical stress is about 0.33 psi/ft which is rather light comparing to heavy deep rock. The average Poisson's ratio is round 0.4 from Fig. 3.3. The value means the rock in shallow is rather soft and trend to plastic. Young's modulus is very small from Fig. 3.4 and Eq. 3.3 in shallow marine sediments which is about  $3 \times 10^4$  psi at 300 ft. Recall metal's young's model is  $3 \times 10^6$  psi and that of deep rock with the same order as metal. Fig. 3.5 shows the cohesive strength is very small and the assumption of negligible rock strength in shallow works. The friction angle decreases with depth and 20 degree could be used at 500 ft.

### 3.2 Leak-off Test Plots

Fig. 3.7 gives a typical deep-well LOT. A distinct straight line in pressure build-up section is the basic guidance for interpretation. The point deviated from the straight line is the leak-off point and the pressure there is the leak-off pressure (LOP). After leaking off, a rapidly developing curvature indicates the start of elastic failure. This type of pressure response can be fully explained by elastic rock model with linear stress-strain relation and the maximum value of tangential stress at the wellbore wall to be overcome in order to initiate the fracture.

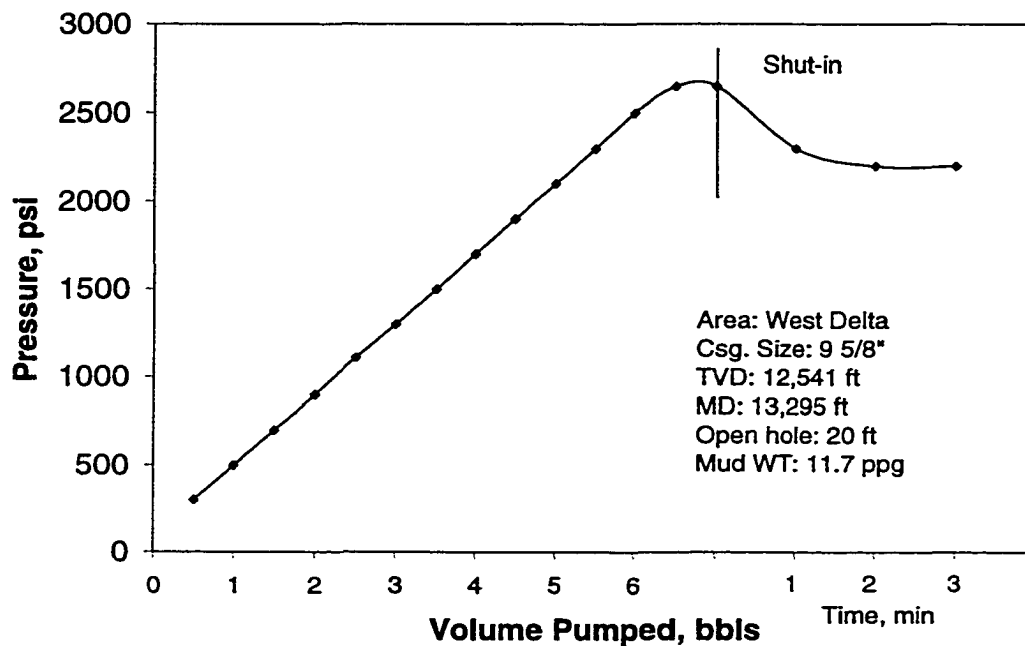


**Figure 3.7** Typical LOT in deep formation.

Leak-off test (LOT) in shallow marine sediments (SMS) is performed for the same reason as for deeper formations; to estimate how much pressure can be applied to the rock just below the casing shoe before the shoe/rock system fails. Also, the LOT procedures for both situations are conceptually the same; to stress out the shoe/rock

system until the first sign of failure appears. The problem is that in deep rocks the beginning of failure (fracture) is well supported by theory and relatively easy to recognize; which is not the case for shallow and soft rocks (as shown in Fig. 3.8).

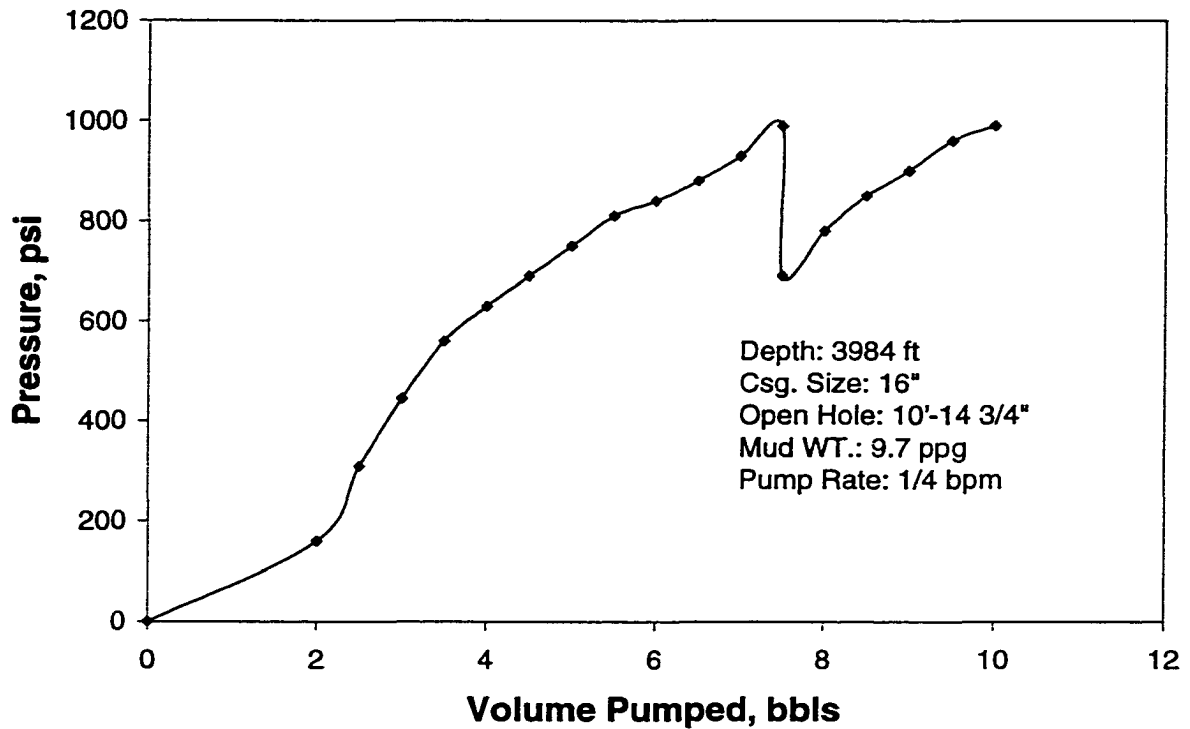


**Figure 3.8 Non-linear LOT in shallow marine sediments.**

In shallow formations, particularly upper marine sediments (UMS), recorded LOTs give various plots with no clear indication of the beginning of failure. Moreover, as the elastic theory cannot explain non-linearity of those plots other factors must be hypothesized upon such as mud filtration, micro-fracturing or equipment malfunction. Shown in Fig. 3.8 is a LOT record with nonlinear trend. The trend was confirmed by bleeding back 4.5 bbls of mud followed by pumping additional 3 bbls.

Operators have long realized that because the onset of formation breakdown is not clear in soft rocks a rock failure may be underway during the test. The failure may

result in permanent damage to the annular seal. To avoid the damage some operators have eliminated LOTs in UMS while others put an arbitrary limit (with safety margin) on the maximum pressure during the test. The result of such test with limiting pressure 990 psi is shown in Fig. 3.8. Also, some other operators perform LOTs as a series of slow pumping periods intermittent with the stop-pump/hold-pressure periods. Typically, such test is terminated when the system does not hold pressure any more.

Fig. 3.9 is another example of LOT result in SMS.

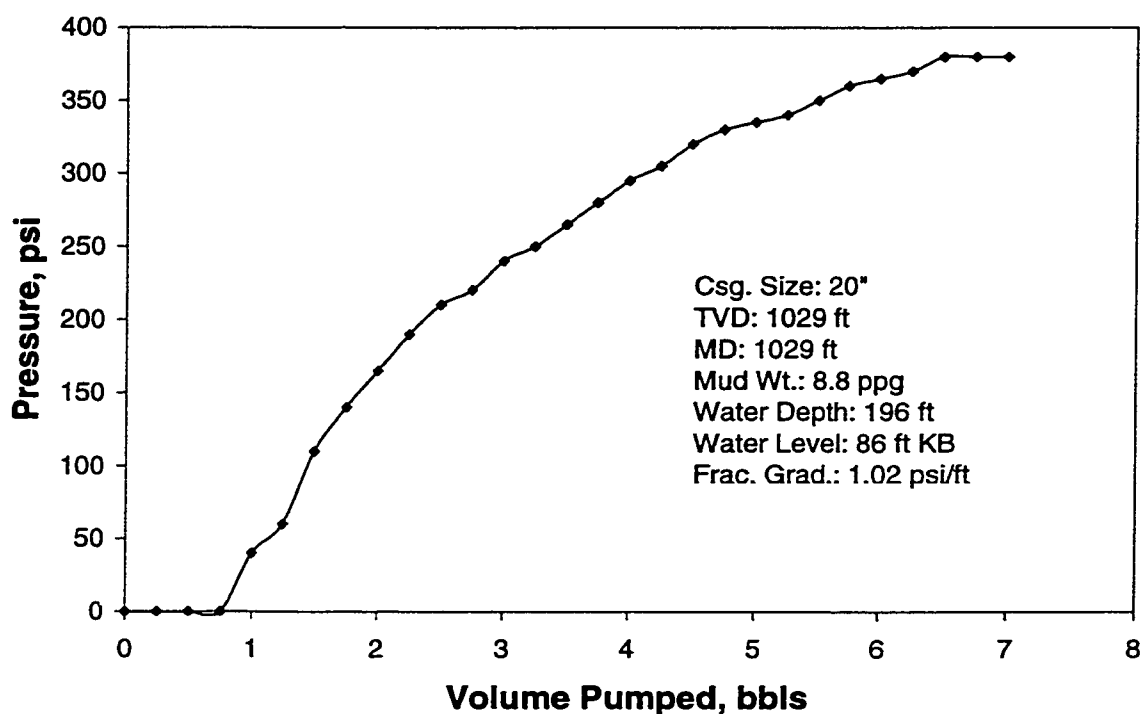


**Figure 3.9 Nonlinear LOT in UMS with “yield” pressure.**

The LOT in Fig. 3.9 was performed in UMS at 747 ft BML with 196 ft of water depth. Non-linearity of the plot is evident with no pressure peak indicating concentration of stresses around the wellbore. Instead, pressure stabilized at a constant value of 370 psi at which the system “yielded”. This response bears some resemblance to the stress-strain behavior of elasto-plastic materials.

The pressure response depicted in Fig. 3.9 is typical for LOTs in UMS. The plots may be different in the way of their “yield” pressure behaves; instead of remaining constant the yield pressure may slowly drop in a linear manner. Also, it has been observed by many operators that the typical values of the yield pressure gradients are high, ranging from 0.75 psi/ft to over 1.0 psi/ft, as documented by data from five LOTs in UMS, shown in Table 3.3.

**Table 3.3 Values of yield pressure gradients from LOTs in UMS.**

<b>PROPERTY</b>	<b>UNIT</b>	<b>LOT 1</b>	<b>LOT 2</b>	<b>LOT 3</b>	<b>LOT 4</b>	<b>LOT 5</b>
<b>Water depth</b>	ft	195	195	196	102	103
<b>Shoe depth, BML</b>	ft	218	534	747	583	582
<b>Pressure @ yield</b>	psi	185	170	380	155	220
<b>Pump rate</b>	bbbl/min	5.00	5.00	0.25	0.25	0.25
<b>Mud weight</b>	lb/gal	8.65	8.5	8.8	9.0	8.9
<b>Water gradient</b>	psi/ft	0.44	0.44	0.45	0.44	0.44
<b>Pressure gradient @ yield</b>	psi/ft	1.49	0.84	1.02	0.829	0.94

High pressure gradients indicate that UMS are much “stronger” than it has been previously believed. It was reported that for some shallow sediments fracturing gradients can become two-fold greater than those for deeper sediments (Arifun and Wahyu H. Sumpennpo, 1994).

One way of predicting high strength of shallow sediments is to use equations from the theory of fracturing deep sediments, and make empirical correlation between the ratio of vertical-to-horizontal stresses versus depth using data from LOTs. Though the approach may work in practical applications it is theoretically incorrect because it is based upon an implicit assumption that elasto-plastic behavior can be modeled as pseudo-elastic one. The approach may generate values of the stress ratio greater than

one which are difficult to explain without considering the effects of some external factors such as tectonic stresses.

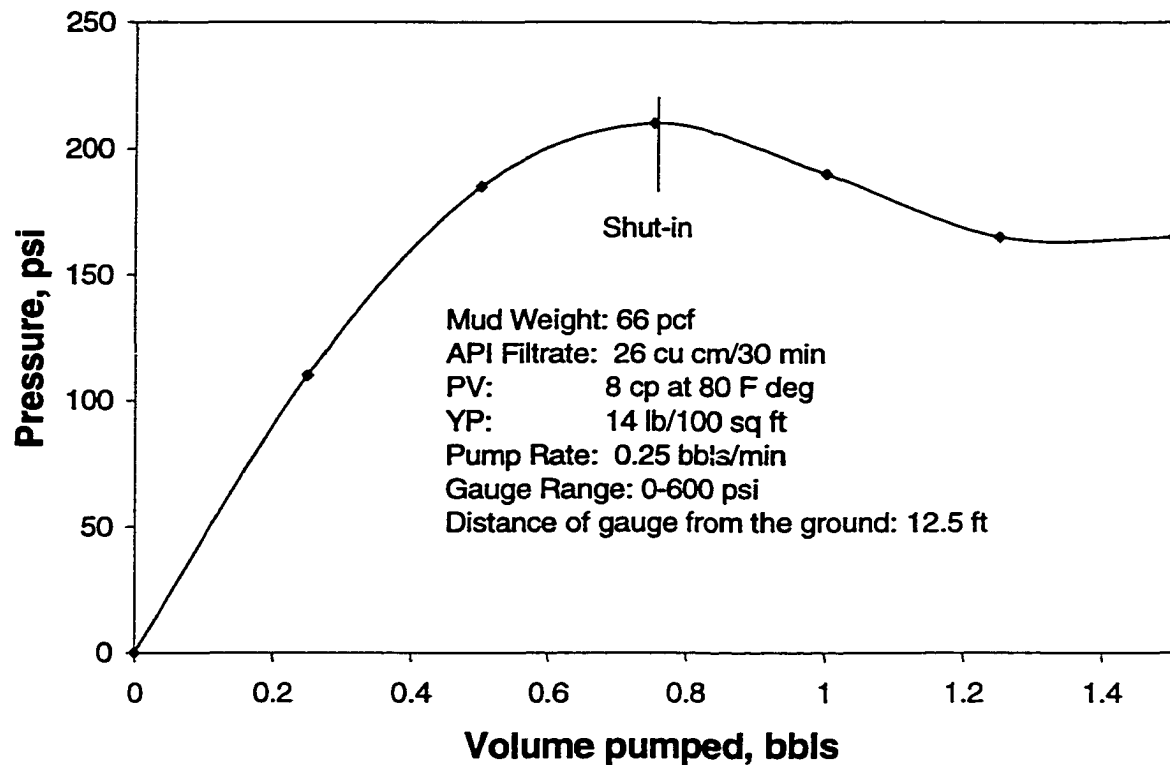


**Figure 3.10** Fewer tested points to maximum pressure.

Generally, upper marine sediments are weaker and have higher stress ratios than deep sediments. They are also most likely to exhibit plastic rather than elastic behavior under stress loads applied by LOTs. Therefore, the conventional fracturing theory based on elastic analysis cannot fully explain either the behavior of UMS during LOTs or potential damage resulting from these tests.

Besides non-linear behavior of LOT plots in UMS, fewer tested points are another feature. Figure 3.10 shows this characteristics. Only 3 tested points get the maximum pressure that makes interpretation difficult.

Unlike LOT results in deep wells where pressure drops sharply after breakdown pressure if keep pumping, the pressure keeps almost constant once it gets maximum value during further pumping period. Figure 3.11 is an example.

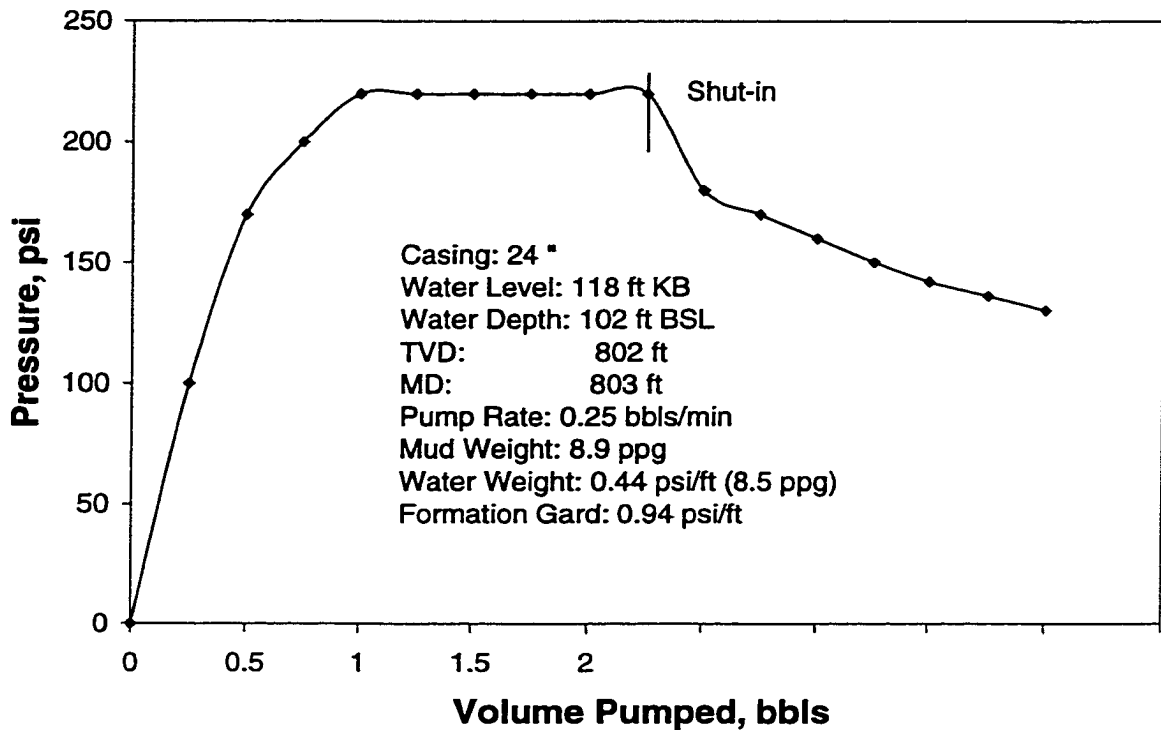
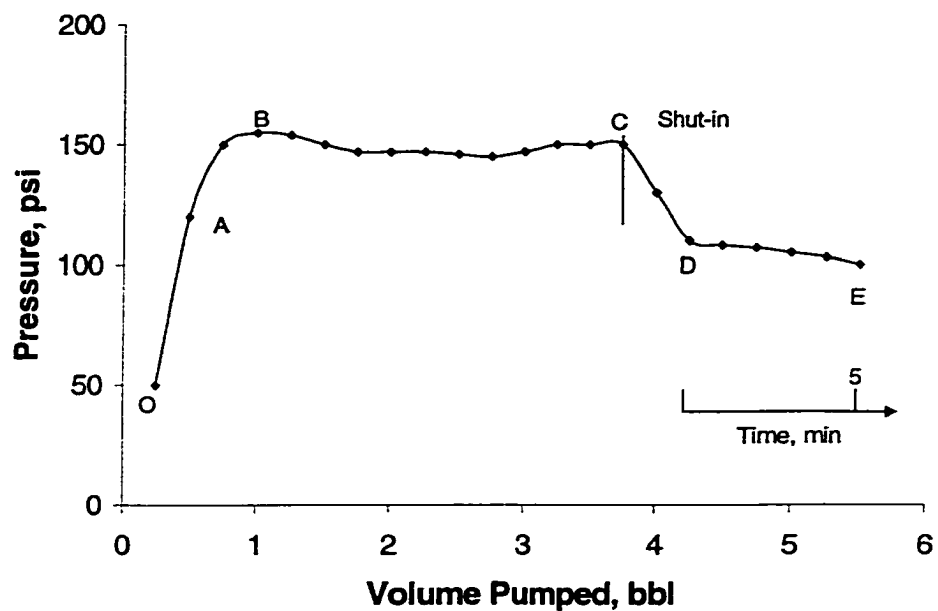


**Figure 3.11 Almost no pressure drop of maximum pressure.**

From Figure 3.11, the maximum pressure is 220 psi and LOP gets the value after pumping into 1 bbl mud. However, the LOP keeps 220 psi with further pumping of 1.25 bbls until shut-in.

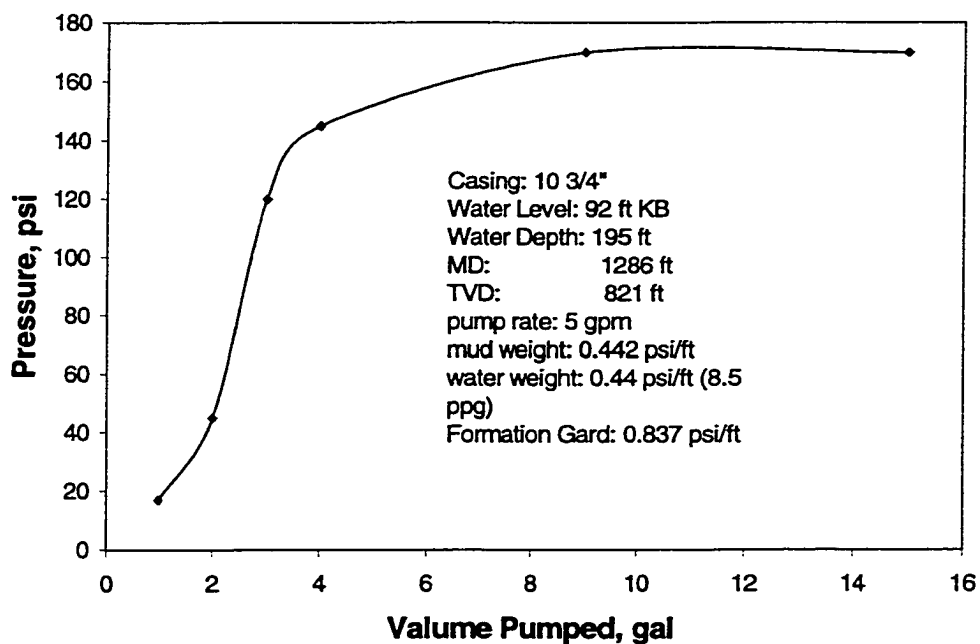
Same as that in deep wells, shallow LOT pressure drops after shut-in. This is because both suffer loss of mud frictional stress after stopping pump. Also pressure will be recorded after shut-in for a few minutes (Fig. 3.11). The pressure versus time relation is called level-off section which is useful for LOT plot interpretation.

Figure 3.12 shows a LOT plot with the basic characteristics of LOT curves in shallow marine sediments: non-linear, fewer points, and no break-down pressure drop.



**Figure 3.12 Pressure drop after shut-in and level-off.**

The interpretation technique based on straight line couldn't be used for LOT in SMS. As shown in Figure 3.13, 120 psi were the LOP if used traditional method.



**Figure 3.13 Traditional method based on straight line fails.**

More LOT results are shown in Figures 3.14 and 3.15.

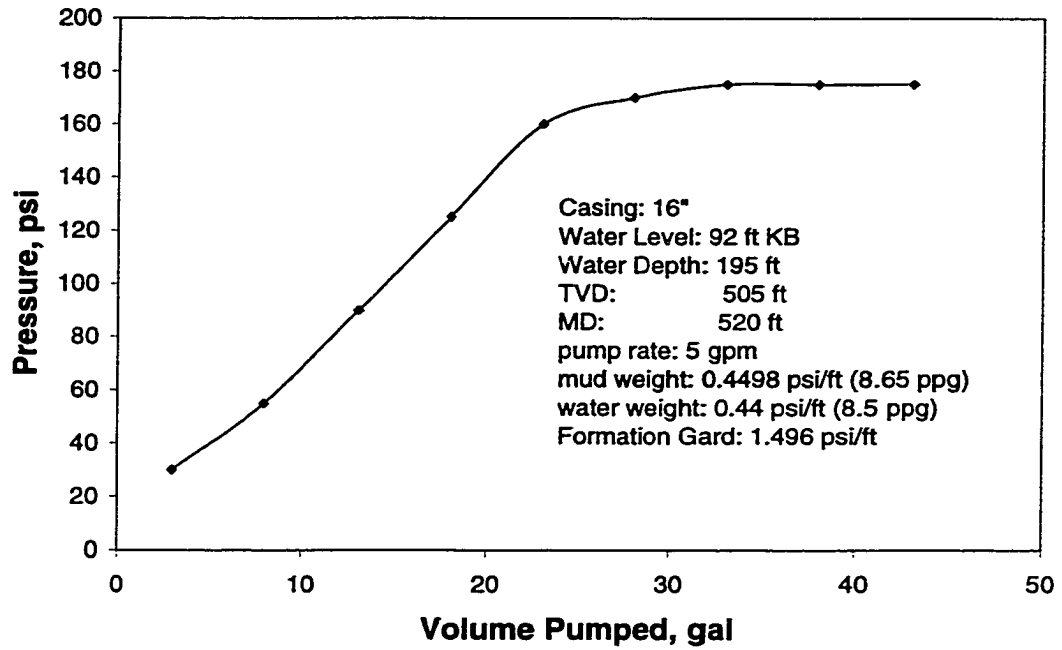


Figure 3.14 Leak-off test result in UMS.

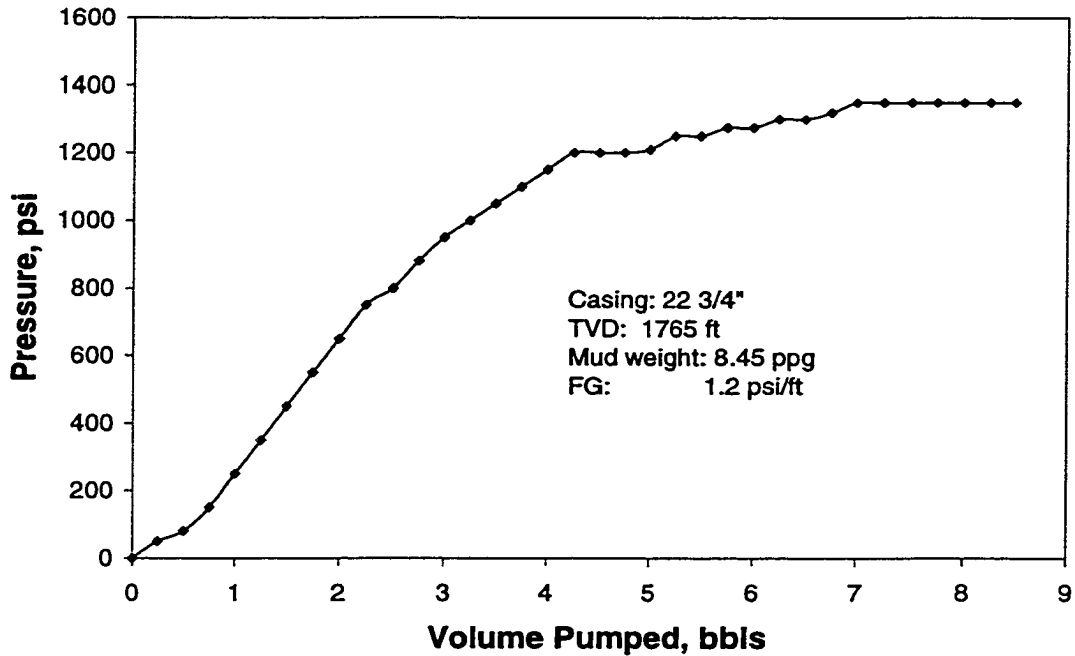
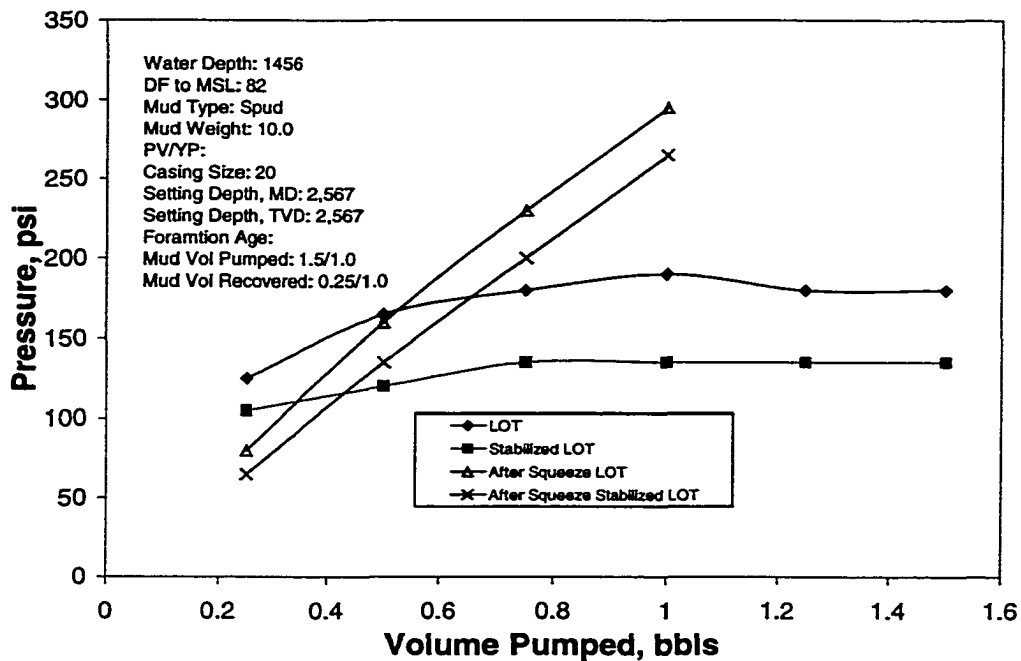


Figure 3.15 Non-linear LOT.

Leak-off pressure is reading dynamically. A pressure will be read and recorded for every pumped ¼ bbl mud. However, the recorded pressure is not stable and will decrease if stop pump. A reason for pressure dropping is frictional pressure loss. Logically, the pressure drop due to frictional pressure loss could be assumed as constant and therefore results in another LOT plot that is almost parallel to usual LOT plot (dynamic). Figure 3.16 shows a LOT in SMS with dynamic and stabilized LOT plots.



**Figure 3.16 LOT and stabilized LOT.**

The propose of pump-and-wait LOT procedure is not only used to find how many pressure drops due to mud frictional pressure loss. The propose is try to find leaking as early as possible. As shown in Fig. 3.17, mud leaking occurred around 700 psi if comparing the usual LOT plot (casing shoe test) and the stabilized LOT result. The leaking could not be recognized if only use casing shoe test plot.

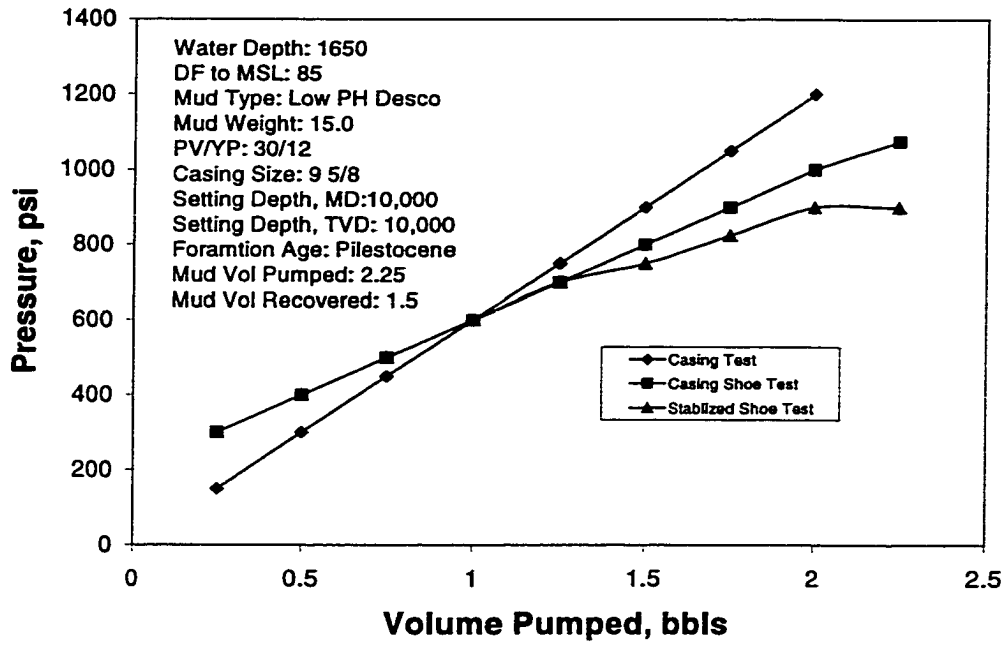


Figure 3.17 LOT and stabilized LOT.

Figure 3.18 gives an example of the stabilized leak-off test in SMS.

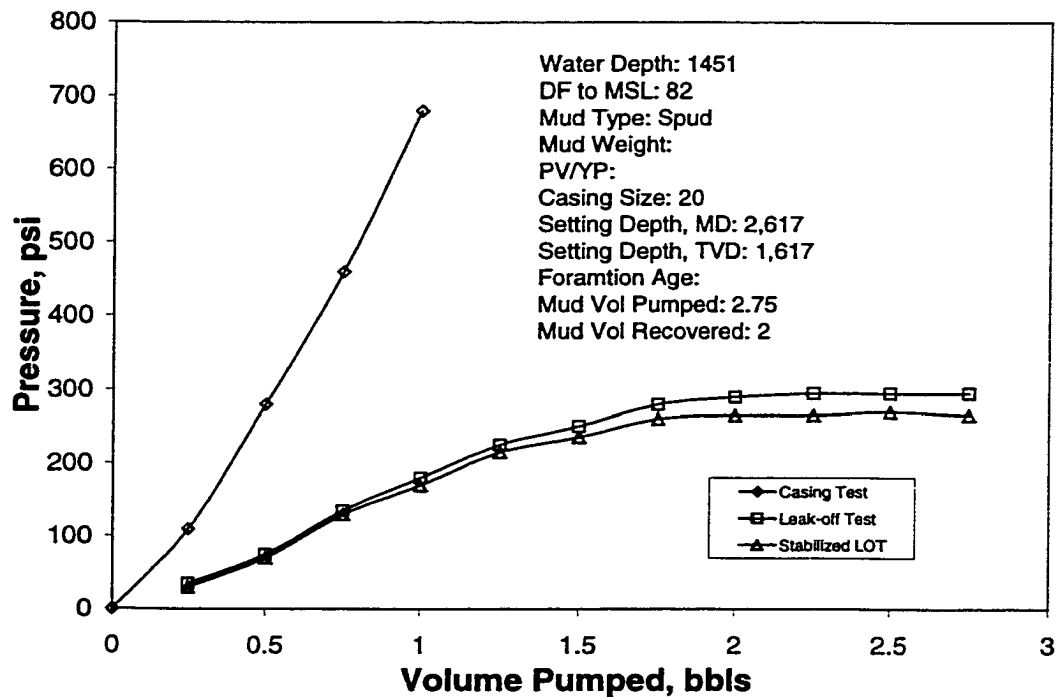
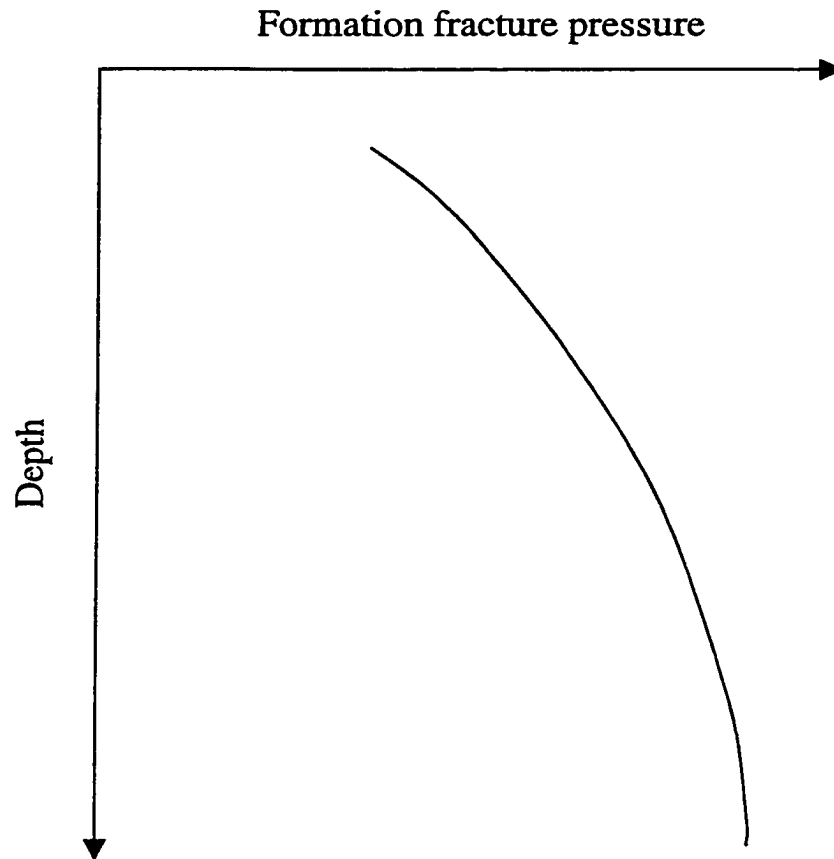


Figure 3.18 LOT and stabilized LOT in SMS.

### 3.3 Leak-off Pressure (Formation Fracture Pressure) Analysis

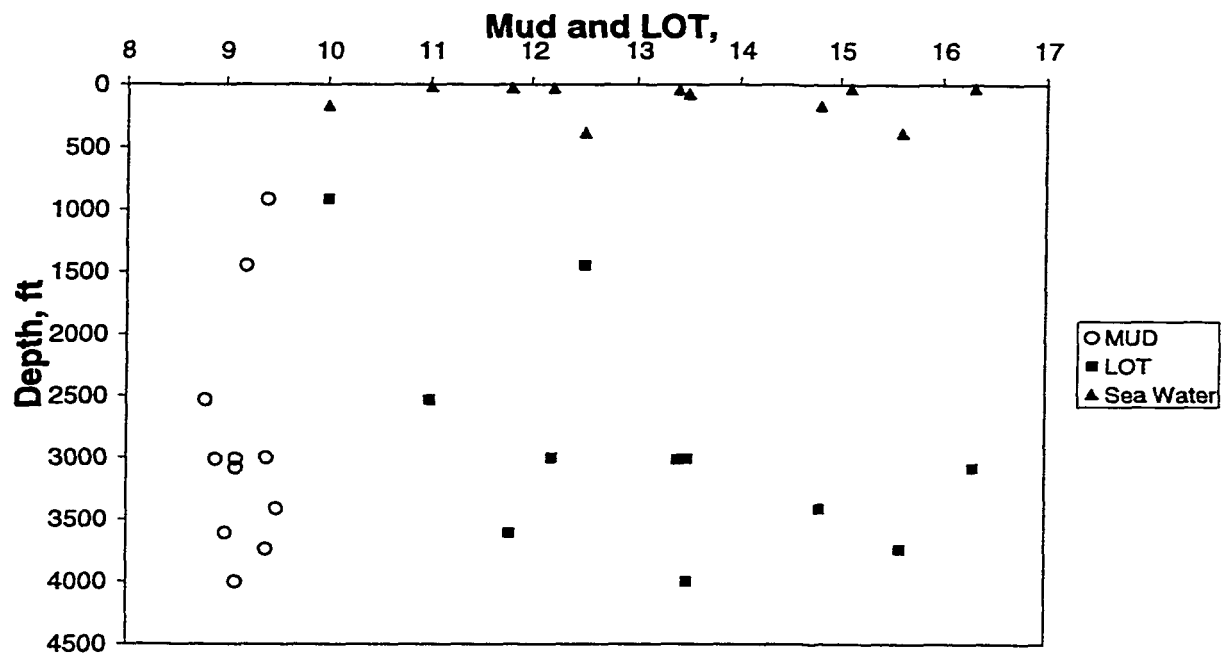
Leak-off test data are the original source of formation fracture prediction models and are used directly for well planning by some engineers. The tested data are generally used as formation fracture pressure (FFP) data for well plan. Typically, formation fracture data are plotted with depth (Bourgoyne et al, 1991) as shown in Fig. 3.19.



**Figure 3.19** Typical formation fracture pressure curve for deep wells.

From Fig. 3.19, the variation of FFP with depth is represented by a curve. The curve comes from the least-square regression or some curve fitting from source LOT data. The actual data distribute around the curve. FFP increases with depth.

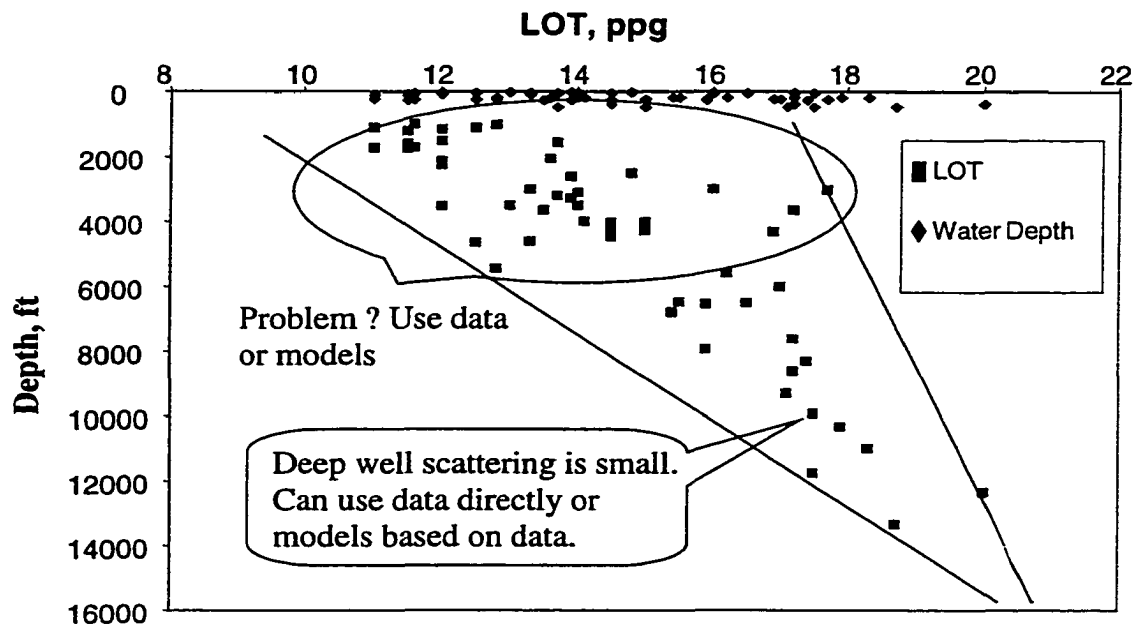
Our data analysis focuses on shallow marine sediments. The collected LOTs data were grouped based on drilling areas and operators to eliminate geological variation and the bias resulting from different operators. The analyzed data included US Gulf of Mexico (High Island, Eugene Island, West Cameron, Vermillion, South Timbalier, and Main Pass), UK North Sea, and Brazil SES. Figure 3.20 shows the data from West Cameron.



**Figure 3.20 Shallow scatter LOT data from West Cameron.**

As shown in Fig. 3.20, LOPs are expressed as equivalent mud weight in pounds per gallon (ppg) and depth in feet (ft). For comparison, mud densities are put on the same plot. As shown in the figure, mud density is about 9.2 ppg and LOP is about 12.4 ppg at the depth of 1500 ft. The mud weight is the mud used during leak-off test. Also, sea water depths of corresponding wells are plotted. For example, the sea water depth is about 450 ft for the well with mud density of 9.2 ppg and LOP of 12.4 ppg. It is hard to get a correlation form the data since they scatter so much.

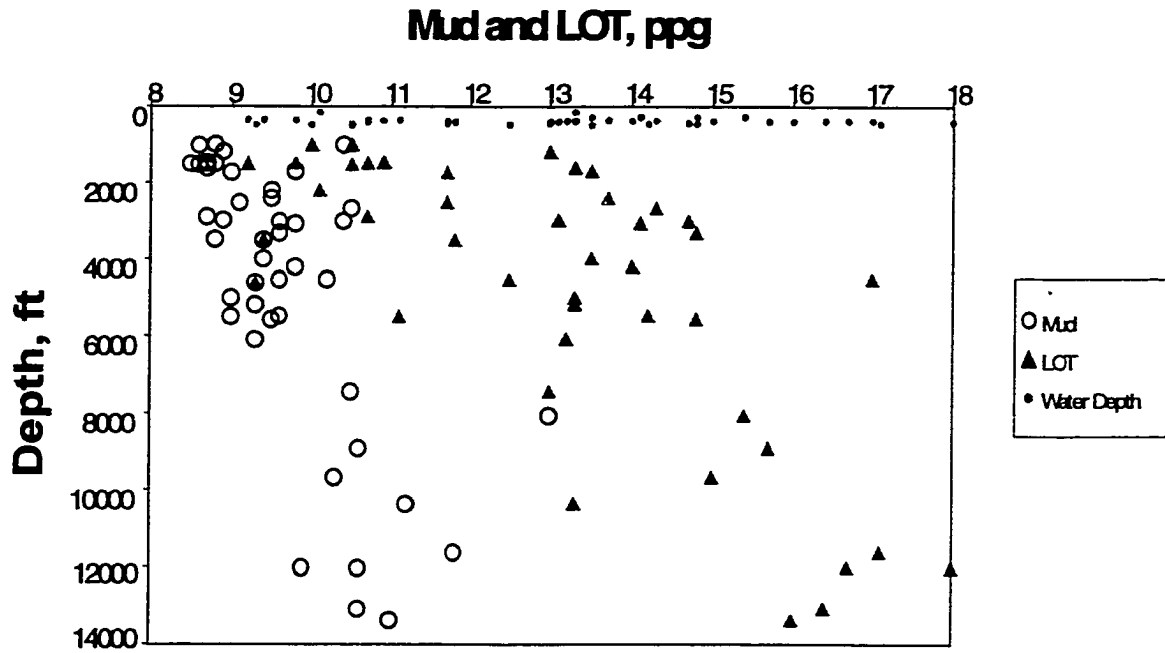
The analysis of LOT data vs. depth showed similar trends in all drilling areas considered. At deep depths there is fairly good correlation between leak-off pressure and depth, while no correlation exists at shallow depths (Fig. 3.21).



**Figure 3.21** Narrower scatter of LOT data with depth from High Island.

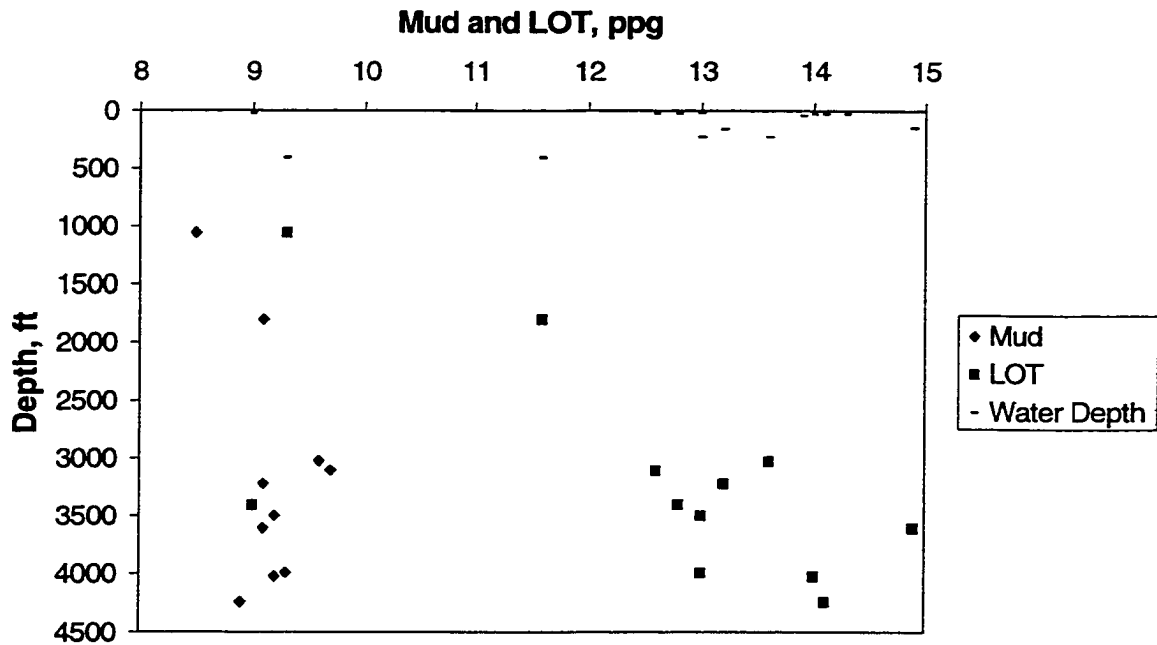
In Fig. 3.21, leak-off test data in deep and shallow are plotted together. A trend with small standard deviation could be drawn for the deeper part below 6,000 ft. However, the data in shallower part scatter so large that no correction or trend could be made based on the data. Traditional models or correlations are based on deep well data and therefore no problem used as a guide for well planning and control. However, traditional models could not be used for shallow sediments since it is hard to say there is correlation.

Figure 3.22 shows leak-off test pressure at North Sea. Again, all the predicted models lose their meaning since large dispersion of the LOT data in the shallow marine sediment.



**Figure 3.22** No correlation, impossible to use minimum data, and average data at depth having high risk (North Sea, UK).

Figure 3.23 gives an example of very low leak-off pressure.



**Figure 3.23** Scatter in shallow with one almost equals mud density (Eugene Island).



data at a depth has 50% risk since almost half of the LOT data are less than planned value. High standard deviation from large scatter in SMS makes the average method unworkable either. Fig. 3.26 gives an other example.

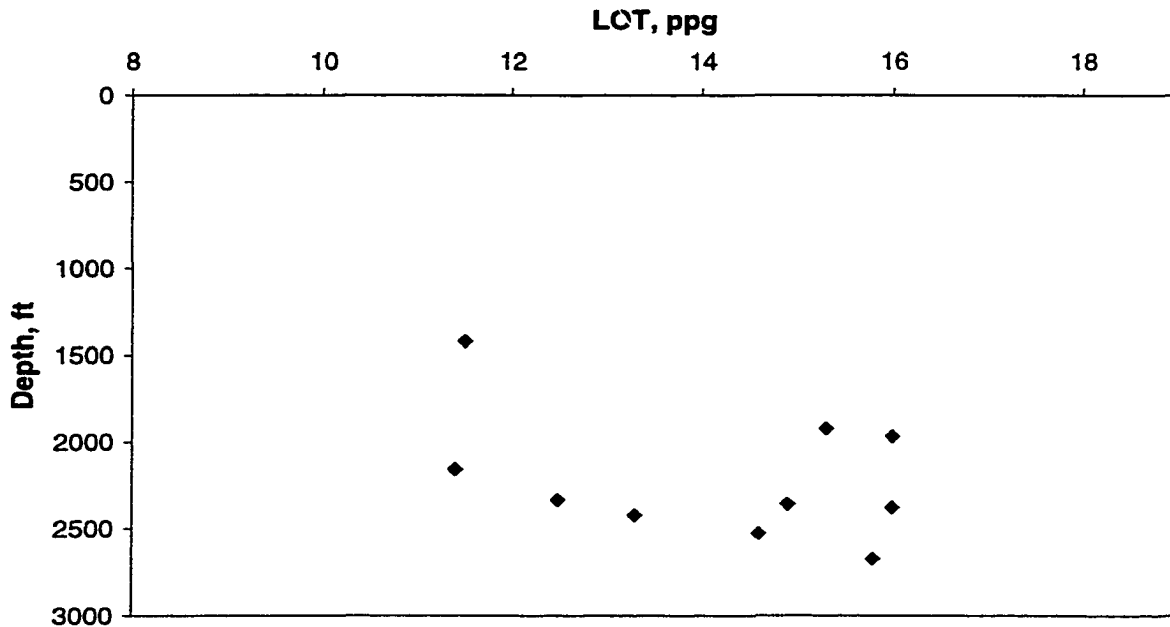


**Figure 3.25** Minimum LOP is too conservative and average LOP has high risk (SES, Brazil).

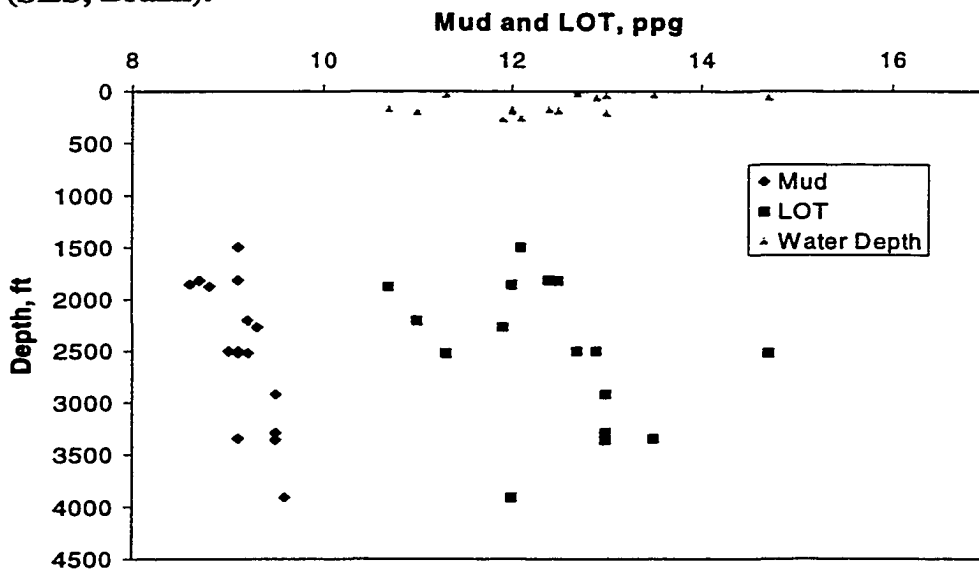


**Figure 3.26** No trend for shallow marine sediments (Main Pass).

### 3.4 Leak-off Test Database

Two Leak-off test databases are analyzed. One is LOTs from offshore. 677 offshore LOTs are analyzed. The other is LOTs onshore which contains 10,000 tested results. Table 3.4 is an example of the offshore LOT file. Every record (row) represents a LOT and its associated information. They are well name, water depth, hole size, casing size, casing depth, mud weight, LOT, field, country, operator, DBSF, result, air gap and count.

**Table 3.4 Offshore LOT data file record example.**

Well Name	Water Depth	Hole Size	Casing Size	Casing Depth	Mud Weight	LOT
M1	1307	17.5	13.38	6775	9.9	13.3
M1	1307	12.25	9.63	9445	12	13.3
M1	1307	26	20	2637	8.5	10.4
	25	26	20	1020	8.7	11
	25	17.5	13.38	4623	9.3	13.6
	230	17.5	13.38	1637	9.1	12.7
	118	17.5	13.38	1306	9.1	16.3
	186	9.88	7.63	4212	9.2	12
	186	13.5	10.75	1883	9.1	12
	186	13.5	10.75	1668	8.7	12
	78	17.5	13.33	5014	9.3	15.2
	78	26	20	1257	9.1	12
	96	20	16	5062	9.1	14.5
	96	10.63	9.63	12300	16	17

Continue of Table 3.4.

LOT	Field	Country	Operator	DBSF	Result	Air Gap	Count
13.3	LOBM-1	ANGOLA	ELF AQUITAIN	5468			3
13.3	LOBM-1	ANGOLA	ELF AQUITAIN	8138			4
10.4	LOBM-1	ANGOLA	ELF AQUITAIN	1330			5
11	INDA-4	NIGERIA	CHEVRON	995			6
13.6	INDA-4	NIGERIA	CHEVRON	4598			7
12.7	MARINE VIII	CONGO	AMOCO	1407			8
16.3	MARINE VIII	CONGO	AMOCO	1188			9
12	MATA GORDA	USA	HALL HOUSTON	4026			10
12	MATA GORDA	USA	HALL HOUSTON	1697			11
12	MATA GORDA	USA	HALL HOUSTON	1482			12
15.2	MATA GORDA ISLAND	USA	SANTA FE MINERALS	4936			13
12	MATA GORDA ISLAND	USA	SANTA FE MINERALS	1179			14
14.5	MATAGORDA ISLAND	USA	ARCO	4966			15
17	MATAGORDA ISLAND	USA	ARCO	12204			16

Table 3.5 is an example of the onshore LOT database. Table 3.6 gives the detail information of the fields (columns).

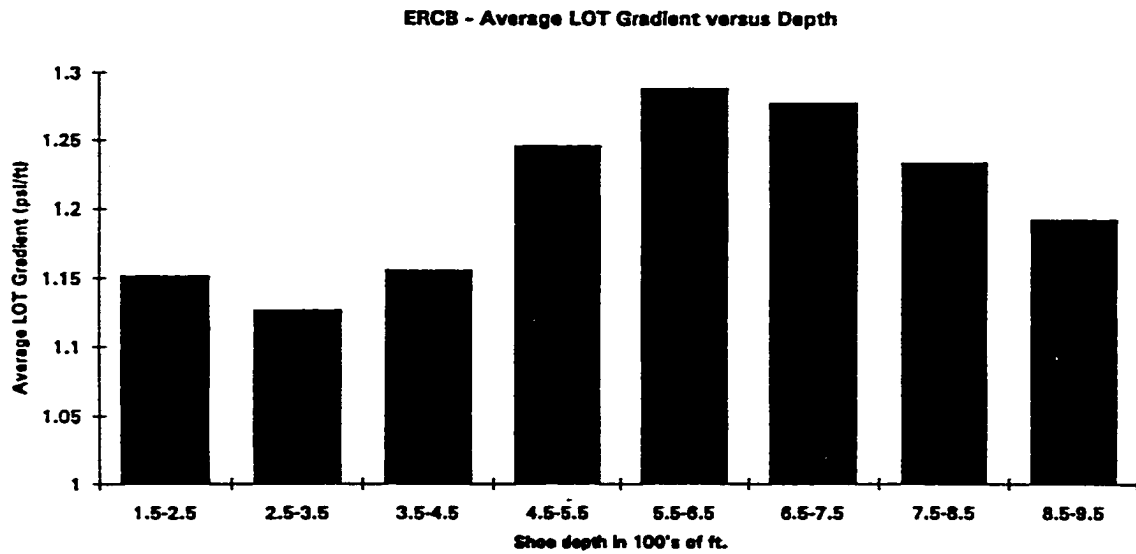
**Table 3.5 Onshore LOT data file record example.**

LE	LS	SE	TWN	RG	M	SFC_DEPTH	PRESSURE	GRADIENT	QUAL_FACT	FORMATION	TD
00	06	06	001	01	4	184.4	4275	32.9	1	SAW/LIV	1189
00	06	17	001	01	4	219.0	5654	35.5	1	SA/BISD	1189
00	06	31	001	01	4	216.0	3516	26.0	1	SAW	1158
00	07	04	001	02	4	189.0	5654	39.7	1	SA/BSLC/BIS	1158
00	07	05	001	02	4	180.0	2750	25.1	1	SWTH	1195
00	06	06	001	02	4	215.0	4068	28.7	1	SAW	1128
00	06	10	001	02	4	189.0	4100	31.5	1	LIV/SAW	1195
00	10	12	001	02	4	181.0	2250	22.2	1	SWTH	1172
00	06	19	001	02	4	219.0	5240	33.7	1	MANN	1188
00	07	29	001	02	4	189.0	4685	33.5	1	SAW/BI	1180
00	06	33	001	02	4	189.0	5378	38.2	1	MANN	1128
00	06	02	001	03	4	193.0	5792	39.7	1	SAW	1158
00	10	03	001	03	4	180.0	1725	19.4	1	SAW/LIV	1182
00	11	05	001	03	4	192.5	3722	29.0	1	SAW/MANN	1170

**Table 3.6 Symbols of fields of Table 3.5.**

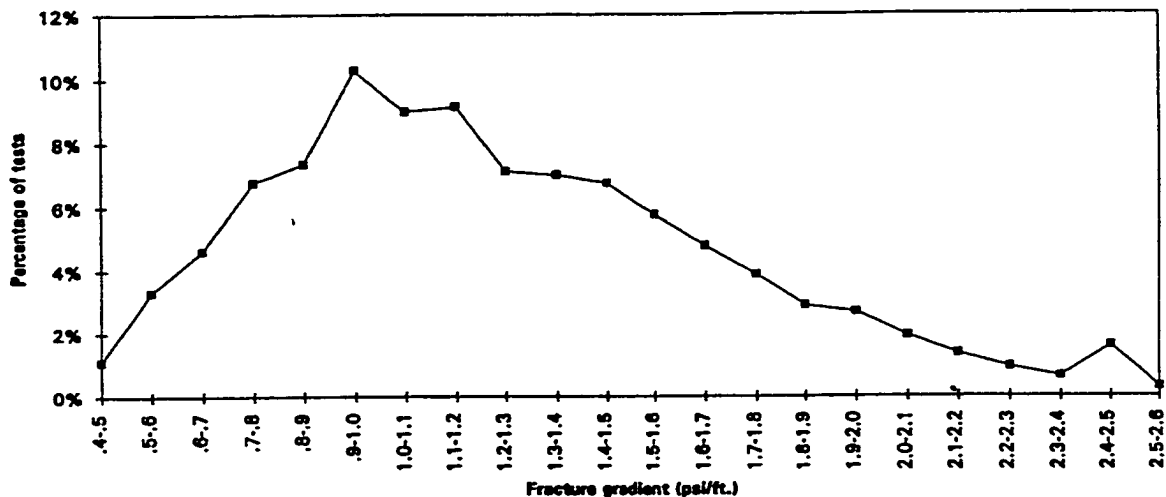
LE	=	The well's location exception
LS	=	The well's legal subdivision
SE	=	The well's section
TWN	=	The well's township
RG	=	The well's range
M	=	The well's meridian
SFC_DEPTH	=	The setting depth in meters of the well's surface casing
PRESSURE	=	The surface leak-off pressure in KPa
GRADIENT	=	The leak-off gradient in Kpa per meter
QUAL_FACT	=	A number (1 to 5) based on the following leak-off gradient criteria
		1. 17.0 to 40.0 Kpa/m
		2. LOT not run to leak-off
		3. 0 to 16.9 KPa/m
		4. 40.1 to 50.0 Kpa/m
		5. 50.1 and greater
FORMATION	=	The projected formation (abbreviation) the well will be terminating
TD	=	The projected total depth of the well in meters

Figure 3.27 gives the average LOT gradient versus depth.



**Figure 3.27 LOT gradient versus depth.**

Figure 3.28 is a statistical result of 7658 shallow LOTs (less than 1000 ft). As shown in Fig. 3.28 77% of the LOTs result with fracture gradients greater than 1.0 psi/ft. The data were from Rocky Mountains and would be a little stronger than those in the GOM.



**Figure 3.28 Fracture gradient distribution from 7658 shallow LOTs.**

## **CHAPTER 4**

### **ANALYTICAL MODEL IN SHALLOW MARINE SEDIMENTS**

As reviewed in Chapter 2, a major characteristic of shallow marine sediment (SMS) is its soft property comparing with rocks in deep. In this chapter, analyses will focus on the effect of “soft” formation properties on the stress distribution around a wellbore and the variations of the distribution during leak-off test (LOT). Models related with the forming of the plastic zone during drilling and re-deforming of the plastic zone during leak-off test are presented. The theoretical analyses not only clarify or explain some concepts in SMS, but also found the basis of the analysis and interpretation of LOTs in SMS.

Compressive stress is assumed as positive and tensile stress negative in the analytical part in the dissertation. Also, the stresses are all effective stresses (Terzaghi, 1967)-in-situ stresses subtract pore pressure there. The hydraulic pressure in a well is also changed to effective wellbore pressure by subtracting the pore pressure at the same depth. Other pressures are actual total pressures. For example, wellbore pressure is the hydraulic pressure in a well and its effective pressure is the subtraction of formation pore pressure from the wellbore pressure; overburden pressure is the summation of overburden stress (vertical matrix stress) and pore pressure.

To study fracture pressures by leak-off test, the stress distribution around a wellbore should be analyzed. Three principle in-situ stresses (one in vertical, two in horizontal) are balanced during sedimentation. Drilling action breaks the balance and cause the in-situ stresses re-distributed around the wellbore wall. The re-distributed stresses are the basis of analyses of wellbore stability, formation fracture and leak-off

test (Harrison et al., 1954, Hubbert and Willis, 1957, Matthews and Kelly, 1967). However, more specifically, leak-off test produces further stress variation due to wellbore pressure increase. The re-distributed stresses due to drilling action will be changed and thus re-redistributed the in-situ stress for leak-off test. Therefore, the loading process of a wellbore for leak off test is two steps: drilling action; leak-off test. There is no problem for leak-off test analysis if not distinguishing the two process when the wellbore wall is in elastic state since elastic deformation does not depends on loading history (Timoshenko and Goodier, 1951). However, plastic deformation depends on its loading history (Chen and Han, 1988). In the chapter, the stress analysis for leak-off test will be discussed according to the loading history: drilling action and leak-off test.

#### **4.1 In-Situ Stress Model for Shallow Marine Sediments**

In-situ stresses are the basis for the stress analysis underground. There are three principle stresses at any underground point. For normal fault sediments, the three in-situ principle stresses are vertical stress and two equal horizontal stresses. The in-situ stress was be derived from basic stress-strain model and shown in Appendix A.

##### **4.1.1 In-Situ Elastic Stresses**

In-situ vertical stress can be calculated from overburden pressure and formation pore pressure that may be estimated from well log information. To get the horizontal stresses, a horizontal to vertical stress ratio is introduced. Generally, the stress ratio is given from the back-calculation from the known old wells. Theoretical estimation was proposed by Eaton (1969) based on elastic theory. The only variable associated with the stress ratio is formation Poisson's ratio according to elastic theory.

For elastic state of stress and laterally infinite sediment, the ratio is:

$$F_{\sigma} = \frac{\sigma_h}{\sigma_v} = \frac{\mu}{1-\mu} \quad (4.1)$$

However, since the above relation comes from elastic theory, it is not suitable for sediments in plastic state which typically show high in situ values of stress ratio. To solve this problem one may assume a 0.5 value of Poisson's ratio for upper marine sediments (UMS) which results in a hydrostatic state of stress. However, since by its definition Poisson's ratio is purely elastic constant it does not pertain to sediment in plastic state. Generally speaking, in plastic sediments Poisson's ratio calculated from the above equation (or called equivalent or effective "Poisson's ratio") will be greater than its actual value for the sediment.

#### **4.1.2 In-Situ Plastic Stress Model**

Many agree that upper marine sediments are soft and ductile comparing with sediments at depth. Also, many mentioned that "soft shales and unconsolidated sands frequently found in the Texas and Louisiana Gulf Coast can be considered to exist in a plastic state of stress (Harrison et al., 1954)", "soft, clay-rich materials like shale often act as plastic (Warpinski and Smith, 1989)", or "shallow marine sediment behaves plastic (Rocha, 1993).

There is no correlation of in-situ stress in UMS where rocks are soft and may be in plastic state similar to those for deeper formations (below 3,000 ft). Therefore, the problem is open to speculations.

For an elasto-plastic sediment that is continuous, isotropic, homogeneous and obeys the linear Mohr-Coulomb criterion of perfectly plastic yield, stress ratio in plastic state is (from Appendix A):

$$F_{\sigma} = 1 - \frac{2(\sin \varphi + \frac{\tau_0}{\sigma_{zo}} \cos \varphi)}{1 + \sin \varphi} \quad (\sigma_{zo} \geq (\sigma_{zo})_{\text{lim}}) \quad (4.2)$$

Where:

$$(\sigma_{zo})_{\text{lim}} = \frac{2(1 - \mu)\tau_0 \cos \varphi}{1 - 2\mu - \sin \varphi} \quad (4.3)$$

Compared with the in-situ stress in elastic rocks (Eq. 4.1), Equation 4.2 indicates that the in-situ stress of plastic formations depends on not only Poisson's ratio but also cohesion strength, friction angle, and the vertical stress at the interested depth. Also, Equation 4.2 gives values of stress ratio different that one. The only situation when the ratio may become unity is for frictionless sediment for which the Tresca's yield criterion applies and the stress ratio is:

$$F_{\sigma} = 1 - 2\tau_0 / \sigma_{zo} \quad \text{for, } \sigma_{zo} > 2\tau_0(1 - \mu) / (1 - 2\mu) \quad (4.4)$$

In deep wells, when the vertical stress becomes much greater than cohesive strength, the stress ratio also approaches unity and the state of stress becomes seemingly "hydrostatic" for very deep wells.

It should be emphasized that the derived in-situ stress relations are valid only for sediments in geostatic state (that is horizontal stress is induced only by overburden stress). According to the derived formulas, whether or not sediments in UMS will turn into plasticity depends on their sediment properties. Therefore, it is not a rule that sediments are always in plastic state while elastic state in deep wells.

#### 4.1.3 In-Situ Stresses of Green Canyon in Gulf of Mexico

The state and in-situ stress of Green Canyon region could be determined from the above formulas by substituting the properties summarized in Chapter 3.

As shown in Fig. 3.3, Poisson's ratio is in the range of 3.7 to 4.25 in the upper 500 ft sediment. The trend of the ratio decreases with depth and the average decrease is about 0.08/100 ft.

Cohesive strength increases with depth from 0.8 psi at 40 ft to 13 psi at 500 ft with a rate of about 2.6 psi/100 ft from Figure 3.5. Friction angle decreases with depth with an average rate of about 2.4 deg/100 ft with a lowest value of 16 degree around 450 ft and a highest value of 27.5 degree around 30 ft.

Substitution the Poisson's ratio, cohesive strength and friction angle into Eq. (4.3) yields all the sediments in the section of up to 500 ft are in plastic state. The closer the sediments near the sea floor, the more plastic they are. The point around 450 ft with a lowest friction almost hits the elastic-plastic boundary. It is reasonable that the sediments below 500 ft (such as 600 ft or 700 ft) may turn into elastic state according to the trends of Poisson's ratio and friction angle and vertical stress in Fig. 3.2.

#### **4.2 Stress Distribution around A Wellbore due to Drilling Operation**

The LOT in the Gulf of Mexico are usually down below 1000 ft. The sediments should be in elastic state according to the trends of Poisson's ratio and friction angle. All the work done researcher up to now is also based on the assumption of elastic in-situ state of formation. The following research is also based on elastic in-situ state.

For soft formation, such as shallow marine sediment, although sediments are in elastic state, a plastic zone is general formed due to drilling operation. The condition of forming such a plastic zone will be discussed first.

#### 4.2.1 Condition of Forming Plastic Annular

The elastic stress distribution around a hollow cylinder can be found in usual books of rock mechanics (Jaeger and Cook, 1976). For plastic stress analysis, the same cylinder geometry will be used as shown in Fig. 4.1. The hollow part simulates wellbore and the outside diameter should be infinite for actual drilling situation.

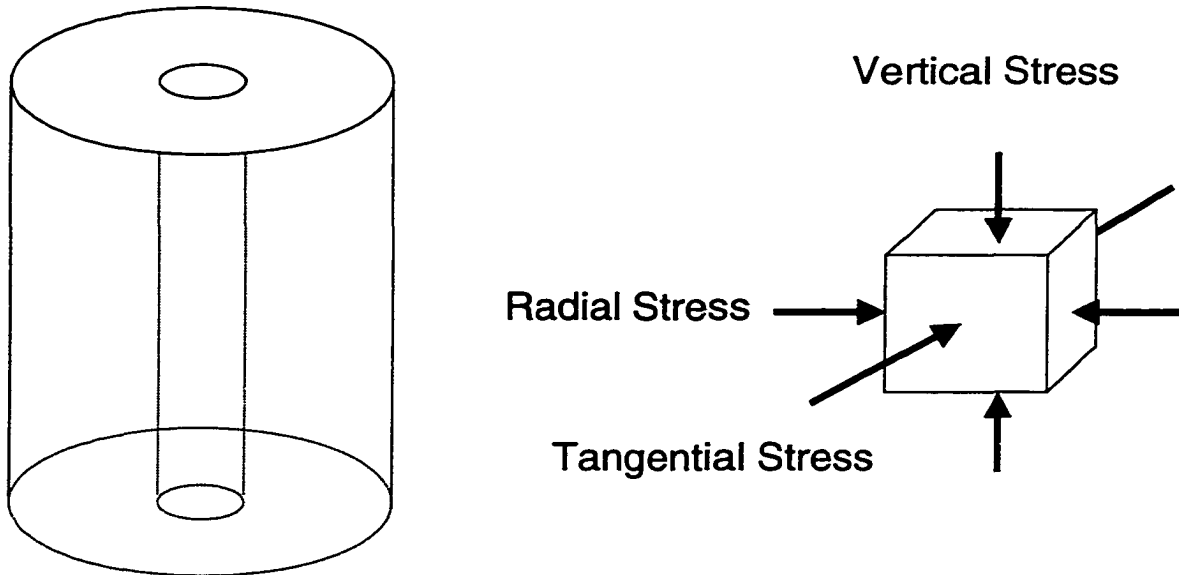


**Figure 4.1** Stresses around a wellbore.

Three principal stresses exist at any point in rock. In a cylinder's coordinates, the three stresses are radial stress in horizontal plane in the direction of well cylinder radius. Tangential stress is hoop stress in the plane which determines formation fracture. Vertical stress is in the direction paralleling to well center axis. When the cylindrical outer radius tends to infinite, the stress relations are

$$\begin{aligned}
 \sigma_r &= \sigma_h - (\sigma_h - p_w) \frac{r_w^2}{r^2} \\
 \sigma_\theta &= \sigma_h + (\sigma_h - p_w) \frac{r_w^2}{r^2} \\
 \sigma_z &= \sigma_{z0}
 \end{aligned}
 \tag{4.5}$$

At the wall of the wellbore,  $r=r_w$ , the difference between the maximum and minimum stresses increases to maximum according to the stress distribution.

$$\begin{aligned}\sigma_{rw} &= p_w \\ \sigma_{\theta w} &= 2\sigma_h - p_w \\ \sigma_{zw} &= \sigma_{z0}\end{aligned}\tag{4.6}$$

Figure 4.2 is a plot illustration of the stress distribution around a wellbore. Contrasting Fig. 4.2 to Fig. 2.5, the effective wellbore pressure affects the stress concentration a lot.

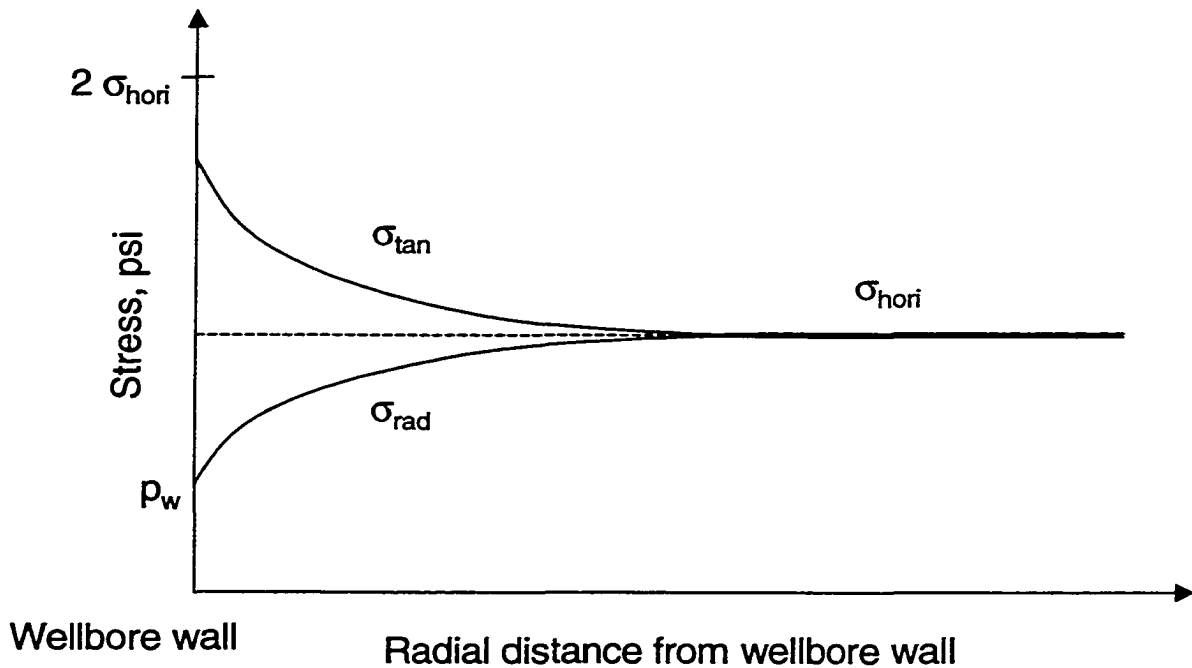


**Figure 4.2 Stress distribution around an elastic wellbore.**

Equation 4.6 and Fig. 4.2 clearly indicates that at wellbore wall the radial stress is equal to the effective wellbore pressure (mud hydraulic pressure subtracts pore pressure) and the tangential stress is the subtraction of effective wellbore pressure from 2 times far-away in-situ horizontal stress. Interestingly, the statement, tangential

stress at wellbore wall is 2 times of in-situ horizontal stress, is only a special case of actual wells (zero balance situation) although it is widely accepted and addressed by many papers and books.

In principle stresses, Mohr-Coulomb yield criterion can be written as (Jaeger and Cook, 1976)

$$\sigma_1 - N\sigma_3 = \sigma_0 \quad (4.7)$$

Where  $N = \frac{1 + \sin \phi}{1 - \sin \phi}$ .  $\sigma_0$  is the uniaxial compressive strength of this sedimental

sample, and  $\sigma_0 = \tau_0 \frac{2 \cos \phi}{1 - \sin \phi}$ .

Under normal conditions, the radial stress  $\sigma_{rw}$  around a wellbore is the smallest stress (Eq. 4.5). Substitution the larger stress of  $\sigma_{\theta w}$  and  $\sigma_{zw}$  into Eq. 4.7, the condition to form a plastic annular around a wellbore is obtained. Since shallow marine sediment has lower friction angle and uniaxial compressive strength, it can be proved that a plastic annular is usually formed around the wellbore for most shallow marine sediments.

If the tangential stress  $\sigma_{\theta}$  is the largest stress, substitution the first two relations of Eq. 4.6 into Eq. 4.7 yields

$$p'_w = \frac{2\sigma_h - \sigma_0}{1 + N} \quad (4.8)$$

The condition of forming a plastic annular around a wellbore is the pure wellbore pressure  $p_w$  less than the critical value  $p'_w$ . Compared with usual drilling case, Eq. 4.8 indicates a plastic annular around a wellbore will be formed for many kinds of sediments especially for soft SMS.

If the vertical stress is the largest stress, the critical value of pure wellbore pressure is the form of Eq. 4.9. It may also make the wellbore wall of wells in SMS turn into plastic state.

$$p'_w = (\sigma_{z0} - \sigma_0) / N \quad (4.9)$$

The stresses at the plastic-elastic boundary are

$$\begin{aligned} \sigma_{rc} &= \sigma_{rc} \\ \sigma_{\alpha c} &= \frac{2\mu}{1-\mu} \sigma_{z0} - \sigma_{rc} \\ \sigma_{zc} &= \sigma_{z0} \end{aligned} \quad (4.10)$$

The condition of  $\sigma_{\alpha c} \geq \sigma_{zc}$  is  $\sigma_{rc} \leq \frac{3\mu-1}{1-\mu} \sigma_{z0}$ . At the boundary, the

maximum stress  $\sigma_{\alpha c}$  and the minimum stress  $\sigma_{rc}$  must satisfy Eq. 4.8, therefore

$$\mu \geq \frac{(1+N)\sigma_{z0} - \sigma_0}{(1+3N)\sigma_{z0} - \sigma_0} \quad (4.11)$$

Equation 4.11 is the critical condition for  $\sigma_{\alpha c} \geq \sigma_{zc}$ . Once it is satisfied, tangential stress is the largest stress. On the other hand, if Eq. 4.11 is not satisfied,  $\sigma_{zc}$  is the largest stress of the three principal stresses at the boundary.

#### 4.2.2 Stress Distribution in Plastic Zone

Mohr-Coulomb criterion (Eq. 4.7) needs distinguish the minimum and maximum stresses. As stated in Chapter 4.1.1, the radial stress is the minimum stress around a wellbore, and either the tangential stress or the vertical stress may be the maximum stress depends on rock properties. Only the larger stress of tangential and vertical should be used in Eq. 4.8. The following will discuss the stress distribution in plastic zone for combinations of tangential-radial and vertical-radial.

#### 4.2.2.1 Maximum Tangential Stress

When  $\sigma_{\alpha} \geq \sigma_{\alpha}$ , the method to derive stresses is similar to that of plane problem. The equilibrium equation in elastic and plastic zone is

$$\frac{\partial \sigma_r}{\partial r} = \frac{\sigma_{\theta} - \sigma_r}{r} \quad (4.12)$$

Substitution Eqs. 4.5 and 4.7 into Eq. 4.12 gets the radial and tangential stress distribution in the plastic zone

$$\begin{aligned} \sigma_r &= (p_w + \frac{\sigma_0}{N-1}) (\frac{r}{r_w})^{N-1} - \frac{\sigma_0}{N-1} \\ \sigma_{\theta} &= N(p_w + \frac{\sigma_0}{N-1}) (\frac{r}{r_w})^{N-1} - \frac{\sigma_0}{N-1} \end{aligned} \quad (4.13)$$

Vertical stress can be derived from Hooke' law by assuming only radial displacement. Vertical strain in far-field can also be obtained assuming no horizontal strain. Combining the two relations together, one can get the vertical stress around a wellbore

$$\sigma_z = \frac{E}{\lambda + G} \sigma_{z0} + \mu(\sigma_r + \sigma_{\theta}) \quad (4.14)$$

In the region of elasticity, the stress distribution is could be expressed as Eq. 4.15 (Jaeger and Cook, 1976):

$$\begin{aligned} \sigma_r &= A + \frac{B}{r^2} \\ \sigma_{\theta} &= A - \frac{B}{r^2} \end{aligned} \quad (4.15)$$

Where  $A = \sigma_h$  from the equation since tangential and radial stresses trend in-situ horizontal stress,  $\sigma_p$ , when radial distance,  $r$ , trends to infinite. At the plastic and

elastic boundary, the radial and tangential stresses should keep continuous. Combining Eqs. 4.13 and 4.14 with Eq. 4.15, at  $r=r_p$ , we get

$$\begin{aligned}\sigma_h + \frac{B}{r_c} &= (p_w + \frac{\sigma_0}{N-1}) \left(\frac{r_c}{r_w}\right)^{N-1} - \frac{\sigma_0}{N-1} \\ \sigma_h - \frac{B}{r_c} &= N(p_w + \frac{\sigma_0}{N-1}) \left(\frac{r_c}{r_w}\right)^{N-1} - \frac{\sigma_0}{N-1}\end{aligned}\quad (4.16)$$

The radius of the boundary between plastic and elastic zones,  $r_p$ , can be derived from the continuity of the radial and tangential stresses at the boundary. Solving Eq. 4.16, the radius between elastic and plastic zones is

$$\begin{aligned}r_c &= r_w \left( \frac{\frac{N-1}{N+1}(2\sigma_h - \sigma_0) + \sigma_0}{(N-1)p_w + \sigma_0} \right)^{\frac{1}{N-1}} \\ B &= \left( \frac{((N-1)p_w + \sigma_0) \left(\frac{r_c}{r_a}\right)^{N-1} - \sigma_0}{N-1} - \sigma_h \right) r_c^2\end{aligned}\quad (4.17)$$

Figure 4.3 is a graphic representation of the above derived formulas. In-situ vertical stress is greater than two equal horizontal stresses. However, the tangential stress becomes the largest stress near the wellbore due to stress concentration.

According to Mohr-Coulomb yield criterion, the tangential and radial stress determines the rock elastic-plastic state near a wellbore. Once the rock around the wellbore turns into plastic state, the tangential and vertical stresses drop sharply in the plastic zone. The stress dropping releases the heavy stress concentration around the wellbore.

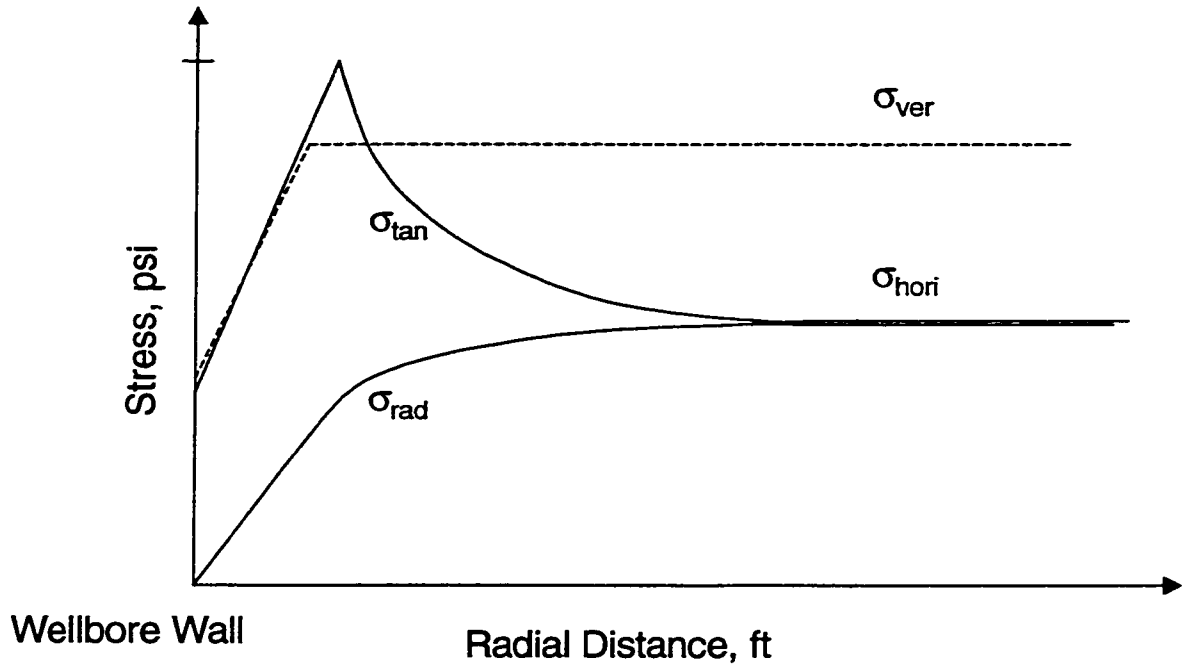


**Figure 4.3** Stress distribution around a wellbore with largest tangential stress.

#### 4.2.2.2 Maximum Vertical Stress

For the case of  $\sigma_{\theta} < \sigma_z$ , the two principal stresses used in Mohr-Coulomb yield criterion should be the radial stress and the vertical stress. The stress relations under the condition can be derived as the case of maximum tangential stress stated above except the vertical stress will be used to instead of tangential stress.

Vertical stress decreases in the plastic boundary. Tangential stress increases in the plastic region first and then decreases unlike it in elastic situation. The radius at which the tangential stress turns to decrease is expressed  $r_p$  which is given by Rinses et al. (1982).

Figure 4.4 is a plot of stress distribution around a wellbore when vertical stress is the largest stress. From the plot, the tangential and vertical stresses drops a lot in the plastic zone and they are almost the same in the inner plastic zone.

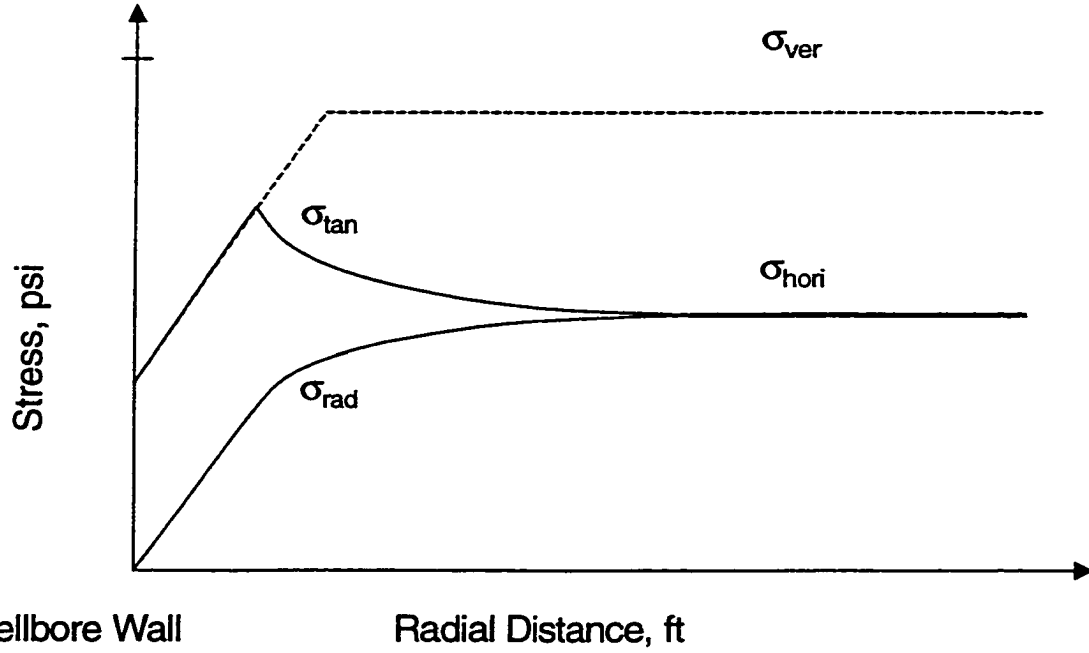


**Figure 4.4** Stress distribution around a wellbore with largest vertical stress.

Under the situation of maximum vertical stress, each stress has different forms beside a radius  $r_i$  in the plastic zone. For  $r_w < r < r_p$ :

$$\begin{aligned}
 \sigma_r &= (p_w + \frac{\sigma_0}{N-1}) \left(\frac{r}{r_w}\right)^{N-1} - \frac{\sigma_0}{N-1} \\
 \sigma_\theta &= N(p_w + \frac{\sigma_0}{N-1}) \left(\frac{r}{r_w}\right)^{N-1} - \frac{\sigma_0}{N-1} \\
 \sigma_z &= N(p_w + \frac{\sigma_0}{N-1}) \left(\frac{r}{r_w}\right)^{N-1} - \frac{\sigma_0}{N-1}
 \end{aligned} \tag{4.18}$$

For  $r_i < r < r_c$

$$\begin{aligned}
 \sigma_\theta &= p_w \left(\frac{r}{r_w}\right)^{N-1} + \frac{\sigma_0}{N-1} \left[ \left(\frac{\gamma+N}{2}\right) \left(\frac{r_b}{r_w}\right)^{N-1} - \frac{\gamma+1}{2} \right] \left(\frac{r}{r_b}\right)^{y-1} \\
 &\quad - \frac{\sigma_0}{N-1} \left[ \left(\frac{\gamma-N}{2}\right) \left(\frac{r_b}{r_w}\right)^{N-1} - \frac{\gamma-1}{2} \right] \left(\frac{r}{r_b}\right)^{-y-1} \\
 &\quad - \frac{1}{N-2\mu} \left[ \sigma_0 - \frac{(1+\mu)(1-2\mu)}{1-\mu} \sigma_{z0} \right] \left[ 1 - \left(\frac{\gamma+1}{2}\right) \left(\frac{r}{r_b}\right)^{\gamma-1} + \left(\frac{\gamma-1}{2}\right) \left(\frac{r}{r_b}\right)^{-\gamma-1} \right]
 \end{aligned}$$

$$\begin{aligned}
\sigma_r &= p_w \left( \frac{r}{r_w} \right)^{N-1} + \frac{\sigma_0}{N-1} \left[ \left( \frac{\gamma+N}{2\gamma} \right) \left( \frac{r_b}{r_w} \right)^{N-1} - \frac{\gamma+1}{2\gamma} \right] \left( \frac{r}{r_b} \right)^{\gamma-1} \\
&+ \frac{\sigma_0}{N-1} \left[ \left( \frac{\gamma-N}{2\gamma} \right) \left( \frac{r_b}{r_w} \right)^{N-1} - \frac{\gamma-1}{2\gamma} \right] \left( \frac{r}{r_b} \right)^{-\gamma-1} \\
&- \frac{1}{N-2\mu} \left[ \sigma_0 - \frac{(1+\mu)(1-2\mu)}{1-\mu} \sigma_{z0} \right] \left[ 1 - \left( \frac{\gamma+1}{2\gamma} \right) \left( \frac{r}{r_b} \right)^{\gamma-1} - \left( \frac{\gamma-1}{2\gamma} \right) \left( \frac{r}{r_b} \right)^{-\gamma-1} \right] \\
\sigma_z &= p_w \left( \frac{r}{r_w} \right)^{N-1} + \sigma_0 - \frac{N\sigma_0}{N-1} \left[ \left( \frac{\gamma+N}{2\gamma} \right) \left( \frac{r_b}{r_w} \right)^{N-1} - \frac{\gamma+1}{2\gamma} \right] \left( \frac{r}{r_b} \right)^{\gamma-1} \\
&- \frac{N\sigma_0}{N-1} \left[ \left( \frac{\gamma-N}{2\gamma} \right) \left( \frac{r_b}{r_w} \right)^{N-1} - \frac{\gamma-1}{2\gamma} \right] \left( \frac{r}{r_b} \right)^{-\gamma-1} \\
&- \frac{N}{N-2\mu} \left[ \sigma_0 - \frac{(1+\mu)(1-2\mu)}{1-\mu} \sigma_{z0} \right] \left[ 1 - \left( \frac{\gamma+1}{2\gamma} \right) \left( \frac{r}{r_b} \right)^{\gamma-1} + \left( \frac{\gamma-1}{2\gamma} \right) \left( \frac{r}{r_b} \right)^{-\gamma-1} \right]
\end{aligned} \tag{4.19}$$

From Eq. 4.18, the stresses at the wellbore are

$$\begin{aligned}
\sigma_r &= p_w \\
\sigma_\theta &= Np_w + \sigma_0 \\
\sigma_z &= Np_w + \sigma_0
\end{aligned} \tag{4.20}$$

Compared with the wellbore stresses of an elastic well (Eq. 4.6), radial stress is the same and equal to effective wellbore pressure at the wellbore wall. The tangential and vertical stresses change to almost the same but much lower than those when the wellbore is in an elastic state. The tangential and vertical stresses at a plastic wellbore wall are determined by rock's uni-axial compressive strength, friction angle and effective wellbore pressure (overbalance pressure). They are not dependent on in-situ stresses anymore.

### 4.3 Stress Distribution around A Wellbore due to Leak-Off Test

As stated above, a plastic annular around a wellbore will be formed by drilling operation for soft formation. According to the yield criterion of Mohr-Coulomb, the left hand value of Eq. 4.7 equals the value of that on the right hand in plastic region. This balance will be broken if the minimum stress increases, that is radial stress increases. Radial stress will increase as the wellbore pressure increases during leak-off test.

Since the increase of wellbore pressure will increase the radial stress and decrease the tangential stress, the left hand value of Eq. 4.7 will less than the value of the right hand value. Therefore, the further deformation of this plastic annulus will be elastic deformation during leak-off test. The whole deformation process of this annular is from elastic state before drilling to plastic state after drilling operation, and then back to elastic state by the leak-off test. Certainly, the annulus may turn into plastic state again when the leak-off pressure is increased much high. Since this process includes plastic deformation, linear superposition as elastic theory is not valid. The resultant stress depends on the loading history (Chen and Han, 1988). Two steps is adopted to simulate this process here: the first is the formation of the plastic annular by drilling; the second step is to analyze the stress re-distribution on the basis of the first step by leak-off test.

In step one, stress distribution in plastic zone is shown in Eqs. 4.18 and 4.19. During leak-off test this plastic zone will turn into elastic deformation as stated above. As shown in Eq. 4.5, when the effective wellbore pressure  $p_w$  increases to  $p_{w\Delta} = p_w + \Delta p_w$  the stress relation changes to

$$\begin{aligned}
\sigma_r + \Delta\sigma_r &= \sigma_h - (\sigma_h - p_w - \Delta p_w) \frac{r_w^2}{r^2} \\
\sigma_\theta + \Delta\sigma_\theta &= \sigma_h + (\sigma_h - p_w - \Delta p_w) \frac{r_w^2}{r^2} \\
\sigma_z + \Delta\sigma_z &= \sigma_{z0}
\end{aligned} \tag{4.21}$$

Subtracting Eq. 4.5 from Eq. 4.21 gives the stress increase due to wellbore pressure change  $\Delta p_w$

$$\begin{aligned}
\Delta\sigma_r &= \Delta p_w \frac{r_w^2}{r^2} \\
\Delta\sigma_\theta &= -\Delta p_w \frac{r_w^2}{r^2} \\
\Delta\sigma_z &= 0
\end{aligned} \tag{4.22}$$

The resultant stresses around the wellbore are calculated by superposing the existing stresses before leak-off test and the new incremental stresses. The stress in plastic zone depends on which is the largest principle stress as discussed in Chapter 4.1. For simplification, the stress distribution of maximum tangential stress situation will be used no matter which stress is the largest. The simplification gets rid of the complex form of math calculation of Eq. 4.19 since what we interested in is the stress around the wellbore. Combing Eq. 4.13 and Eq. 4.22 yields the stress distribution during leak-off test.

$$\begin{aligned}
\sigma_r &= (p_w + \frac{\sigma_0}{N-1}) (\frac{r}{r_w})^{N-1} - \frac{\sigma_0}{N-1} + \Delta p_w \frac{r_w^2}{r^2} \\
\sigma_\theta &= N(p_w + \frac{\sigma_0}{N-1}) (\frac{r}{r_w})^{N-1} - \frac{\sigma_0}{N-1} - \Delta p_w \frac{r_w^2}{r^2} \\
\sigma_z &= \frac{E}{\lambda + G} \sigma_{z0} + \mu(\sigma_r + \sigma_\theta)
\end{aligned} \tag{4.23}$$

The vertical stress does not change by leak-off test according to the correlation. However, after a fracture is formed and it is large enough to allow drilling fluid flow into, the vertical stress will affect the fracturing process.

#### 4.4 Fracture Pressure

If a wellbore was initially in elastic state and its well pressure reduced below a critical value,  $p_w < p'_w$ , the wellbore wall would yield and result in the formation of a plastic zone around the wellbore. An expression for the critical pressure is derived by writing Eq. 4.5 for the wellbore wall and substituting the larger of the two stresses at the wall,  $\sigma_{\theta w}$  or  $\sigma_{zw}$ , into the Mohr-Coulomb yield criterion in Eq. 4.7, which is summarized as:

The critical condition of elastic wellbore is shown in Eq. 4.24. Once it is satisfied, the wellbore is in elastic. Otherwise, a plastic zone occurs.

$$p_w \geq p'_w \quad (4.24)$$

Where

$$p'_w = \frac{2\sigma_h - \sigma_0}{1 + N} \quad (4.8)$$

for,  $\sigma_{\theta w} > \sigma_{zw}$  ; or,  $p_w < \frac{3\mu - 1}{\mu} \sigma_h$ .

$$p'_w = (\sigma_{z0} - \sigma_0) / N \quad (4.25)$$

for,  $\sigma_{\theta w} < \sigma_{zw}$  ; or,  $p_w > \frac{3\mu - 1}{\mu} \sigma_h$ .

Wellbore wall fracture occurs when its stress turns into tensile stress and exceeds its tensile strength. Following we will exam the fracture condition for elastic and plastic wall respectively.

#### 4.4.1 Vertical Fracture of Elastic Wellbore

As wellbore pressure increases, the radial stress around the wall will increase and tangential stress will decrease as indicated by Eq. 4.22 for elastic deformation. The tangential stress may be reduced to tensile stress as wellbore pressure increases to some value (fracture pressure) as shown in Fig. 4.5.

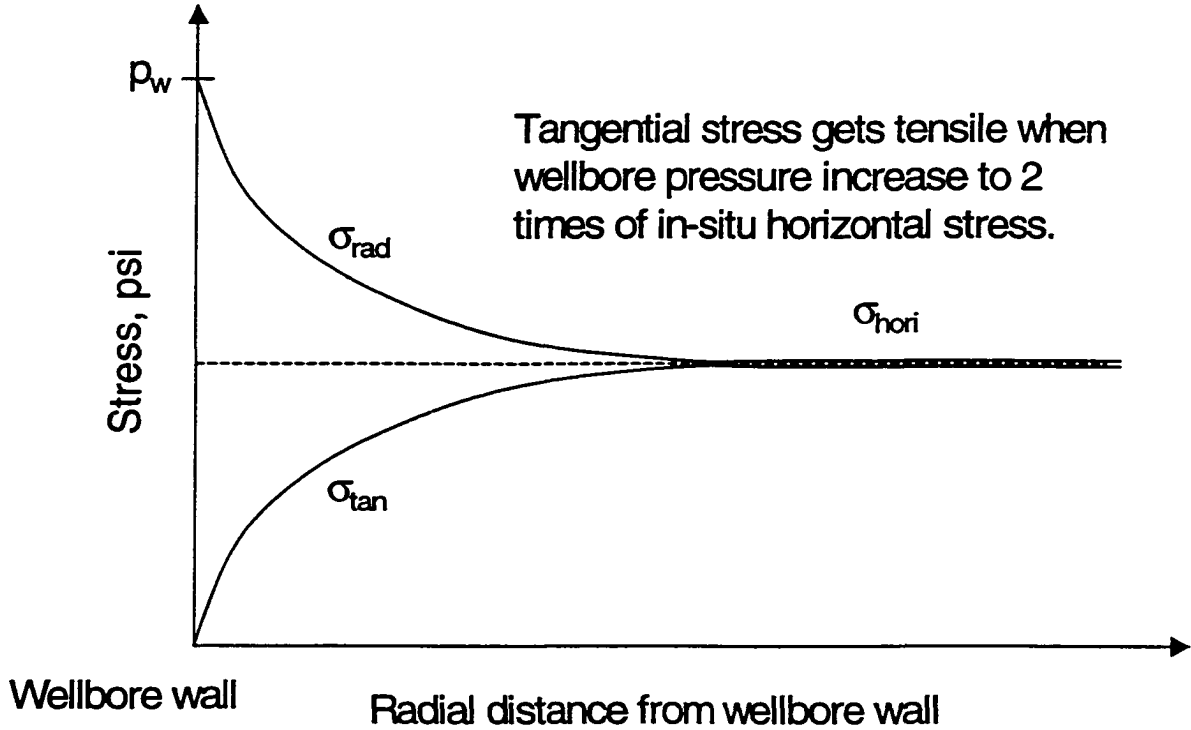


**Figure 4.5** Formation fracturing when tangential stress gets tensile (negative).

The fracture direction is perpendicular to tangential stress, and thus is vertical. This is the reason of wellbore fracture is in vertical direction. Combining the stress change (Eq. 4. 22) with the stress (Eq. 4.5) for elastic situation yields

$$\sigma_r = \sigma_h - (\sigma_h - p_w) \frac{r_w^2}{r^2} + \Delta p_w \frac{r_w^2}{r^2}$$

$$\sigma_\theta = \sigma_h + (\sigma_h - p_w) \frac{r_w^2}{r^2} - \Delta p_w \frac{r_w^2}{r^2} \quad (4.26)$$

The minimum tangential stress is at the wellbore wall. Fracture occurs from the wall. At wellbore wall,  $r=r_w$ , Eq. 4.26 reduces to

$$\begin{aligned}\sigma_{rw} &= p_w + \Delta p_w \\ \sigma_{\theta w} &= 2\sigma_h - p_w - \Delta p_w\end{aligned}\tag{4.27}$$

It should be pointed out that Eq. 4.26 describes the stress distribution during leak-off test but Eq. 4.6 is the distribution before leak-off test although both are correct for elastic deformation. Eq. 4.6 is also used to explain fracture widely. However, strictly speaking, Eq. 4.26 should be used.

Fracture occurs when tensile stress overcomes tensile strength. That is tangential stress reduces to negative (tensile stress) and less than the tensile strength ( $S_{ten}$ ):  $\sigma_{\theta} < -S_{ten}$ . Substitution the critical condition into Eq. 4.27 gives the pressure increase needed to initialize a vertical fracture.

$$\Delta p_w > 2\sigma_h + S_{ten} - p_w\tag{4.28}$$

When overbalance pressure  $p_w$  and tensile strength  $S_{ten}$  are zero, the condition becomes what we usually say: fracture pressure is 2 times of horizontal stress.

#### 4.4.2 Vertical Fracture of Plastic Wellbore

When wellbore is in elastic state. Eq. 4.27 specifies the condition of vertically fracturing. Obviously,  $p_w \geq p'_w$  to satisfy an elastic wellbore. If  $p_w < p'_w$ , a plastic annulus will appear around the wellbore and its size depends on the difference of  $p_w$  and  $p'_w$ .

The stress distribution for a wellbore with a plastic zone has already been given in Eq. 4.23. The tangential stress decreases as leak-off pressure increase. The tangential stress drops heavily around the wellbore wall. The initial position should be

the wall if a vertical fracture may appear. For a long open well the vertical stress keeps constant during leak-off test. It is not given in the following part. From Eq. 4.23, the stresses at the wall are

$$\begin{aligned}\sigma_r &= p_w + \Delta p_w \\ \sigma_\theta &= Np_w + \sigma_0 - \Delta p_w\end{aligned}\tag{4.29}$$

As we know, vertical fracture occurs as the tangential stress becomes less than the tensile strength,  $\sigma_\theta < -S_{ten}$ . It looks like a vertical fracture may be initialized as  $\Delta p_w$  increases to a big value according to Eq. 4.29. However, the difference of radial stress and tangential stress may be meet the plastic criteria before tangential stress reduces to satisfy fracture criteria.

The radial stress and tangential stress during leak-off test will meet Mohr-Coulomb yield criterion (Eq. 4.7) the tangential stress is reduced to initial wellbore pressure,  $\sigma_\theta = p_w$ . The radial stress will be  $Np_w + \sigma_0$  at the plastic bound. The plastic region will increase as wellbore pressure increases further. We call the newly formed plastic zone as re-plastic state since the wellbore is in plastic state before leak-off test. The wellbore pressure for the appearance of re-plastic state is

$$p_w + \Delta p_w = Np_w + \sigma_0\tag{4.30}$$

Eq. 4.30 is derived by substituting  $\sigma_r = \sigma_1$  and  $\sigma_\theta = \sigma_3$  into Eq. 4.7 which gives:

$$\Delta p_w = (N - 1)p_w + \sigma_0.$$

After re-plastic, tangential compressive stress at (and close to) the wall starts to increase with increasing LOT pressure according to Eq. 4.7. Analysis of the condition,  $\sigma_\theta = p_w$ , shows that wellbore in shallow marine sediment (SMS) cannot be in

tensile state during LOT unless the initial well pressure,  $p_w$ , is negative. Therefore, we conclude that except for under-balance drilling, LOT cannot induce vertical fractures in wells that have a plastic zone around a wellbore prior to LOT. Generally, shallow marine sediments have plastic zones, therefore no vertical fracture.

Similar reasoning can be applied to SMS well in the elastic state prior to LOT, i.e. when  $p_w > p'_w$ . An increase of well pressure to the critical value,  $p_w''$ , induces plastic yield in the initially elastic wellbore. Also, tangential stress at the wall reduces to  $\sigma_\theta = p'_w$  when  $\sigma_r = p_w''$ . (Further increase of well pressure would result in the increasing tangential stress.) The critical pressure,  $p_w''$ , is determined from combining Eqs. 4.5, 4.7 and Eq. 4.22, as

$$p_w'' = \frac{2N\sigma_h + \sigma_0}{1 + N} \quad (4.31a)$$

for,  $\sigma_{\theta w} > \sigma_{zw}$ ; or,  $p_w < \frac{3\mu - 1}{\mu} \sigma_h$

$$p_w'' = 2\sigma_h - \frac{\sigma_{z0} - \sigma_0}{N} \quad (4.31b)$$

for,  $\sigma_{\theta w} < \sigma_{zw}$ ; or,  $p_w > \frac{3\mu - 1}{\mu} \sigma_h$

Since the minimum value of tangential stress is  $p'_w$ , an initiation of vertical fracture requires that  $p'_w < 0$ . It follows from Eq. 4.8 that,  $p'_w < 0$ ; only if,  $2\sigma_h < \sigma_0$ ; or,  $\sigma_{z0} < \sigma_0$ . However, the values of  $2\sigma_h$  and  $\sigma_{z0}$  are generally greater than  $\sigma_0$  below the depth of two hundred feet in SMS due to its low strength. Hence, unlike for deep wells, an SMS well can not be fractured vertically even if its wall is in elastic state prior to LOT.

Figure 4.6 shows the stress distribution around a wellbore during leak-off test. Instead of going to tension, the tangential stress turns back before decreasing to zero and increases with further LOT pressure. It can never be reduced to tension for the effect of plastic zone.

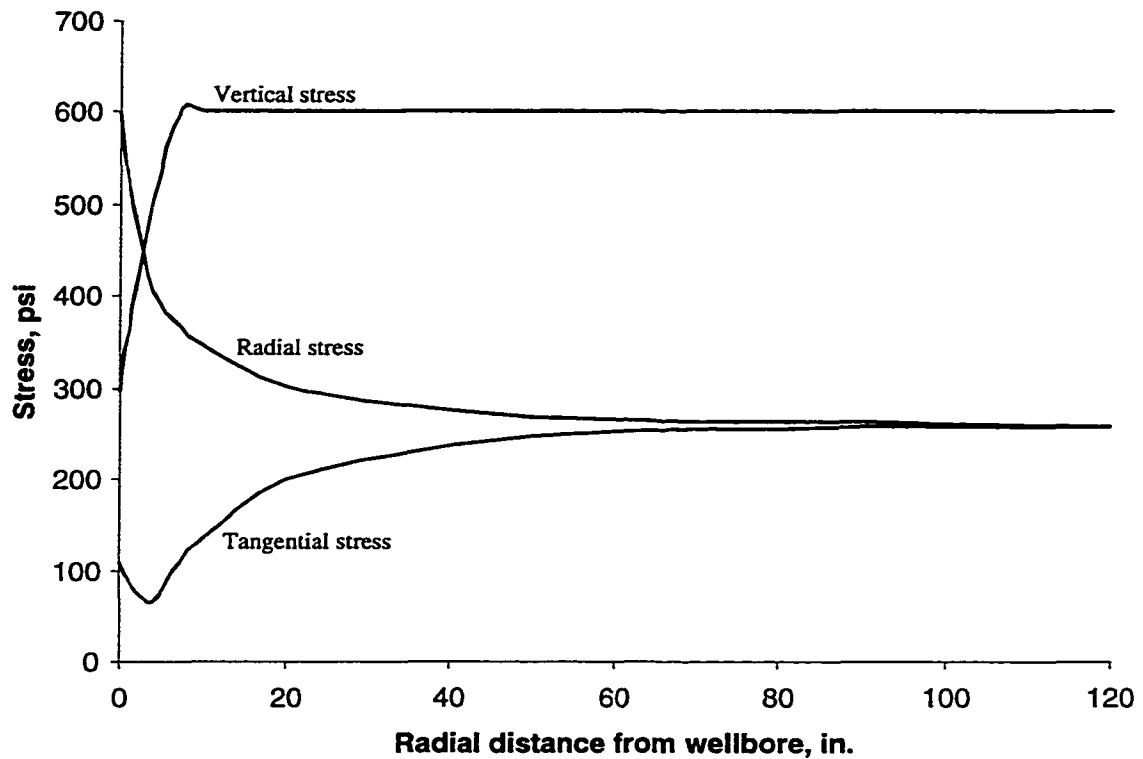


**Figure 4.6** Tangential stress cannot be reduced to tensile and formation re-yield.

## **CHAPTER 5**

### **FINITE ELEMENT ANALYSES OF LEAK-OFF TEST**

Stress distribution around a wellbore is the basis of interpreting the result of leak-off test (LOT). Possible fractures during LOT are formation fracture and cement parting (cement fracture). In the analysis of formation fracture as in Chapter 4, stress distribution around a wellbore is derived using plane strain problem method. Although vertical stress is used in the formulas, it is based on plane strain assumption and therefore the stress analysis in Chapter 4 is not real three dimensional solution.

The two dimensional assumption is suitable for a long uncased well. However, in the case of leak-off test, the uncased part of a wellbore is relatively short and the open hole section (generally less than 15 ft) is constrained by casing and cement at its top and bottom hole at bottom. Although vertical stress is also discussed in the analysis, its not a real three dimensional problem. Three dimensional analysis considering the upper and lower bounds is too complex to solve analytically. A numerical way (finite element analysis) should be used.

For the cement parting analysis, the area around casing shoe includes casing string, cement and rock. Theoretical solution is very difficult. Finite element analysis is a good method to solve such a complex problem.

Sediments discussed in this paper are regarded as continuous, homogeneous, and isotropic. The wellbore is a smooth cylinder and its bottom hole is in a horizontal plane. Wellbore center line is vertical and the vertical axis OZ of a coordinate system coincides with it. The other two axes are in horizontal plane. Vertical force is caused by the overlying mass. Two horizontal in-situ stresses are assumed as equal to each other. Only effective stresses are used in this chapter.

## 5.1 Mechanical Models

Finite element analysis is based on mechanical and mathematical relation of every element. In an element, stress must be of equilibrium. Deformation should satisfy geometrical relation. Constitutive equation controls the elastic to plastic state. Loading, unloading or neutral unloading is the key to determine further deformation in a plastic state.

### 5.1.1 Basic Relation

The equation of equilibrium of stresses and geometrical equation are basic mechanical models in elastic analysis. Although they are set up in elastic analysis, they are suitable in plastic analysis also.

#### (1). Equilibrium equation

The equation of equilibrium is inferred from the condition of force equilibrium of an infinitesimal part in a physical body. It has the form in terms of stresses.

$$\begin{cases} \frac{\partial \sigma_x}{\partial x} + \frac{\partial \tau_{xy}}{\partial y} + \frac{\partial \tau_{xz}}{\partial z} = -F_x \\ \frac{\partial \tau_{yx}}{\partial x} + \frac{\partial \sigma_y}{\partial y} + \frac{\partial \tau_{yz}}{\partial z} = -F_y \\ \frac{\partial \tau_{zx}}{\partial x} + \frac{\partial \tau_{zy}}{\partial y} + \frac{\partial \sigma_z}{\partial z} = -F_z \end{cases} \quad (5.1)$$

Where,  $\sigma_x, \sigma_y, \sigma_z$  are the normal stresses in the directions of three coordinate axes.

$\tau_{xy}, \tau_{xz}, \tau_{yz}$  are the three shear stresses in planes of xy, xz, and yz respectively.

$F_x, F_y, F_z$  are the body forces in three axial directions.

#### (2). Geometrical equation

Geometrical equation is obtained from the geometrical deformation relation of an infinitesimal unit. Variables determining size are strains and displacements in

elastic and plastic theory. Therefore, geometrical equation is the relation of strains and displacements in a deformation body, and it is also called strain-displacement equation sometimes.

$$\varepsilon_r = \frac{\bar{\partial}u}{\partial r}, \varepsilon_\theta = \frac{u}{r}, \varepsilon_z = \frac{\bar{\partial}w}{\partial z}, \gamma_{rz} = \frac{\bar{\partial}u}{\partial z} + \frac{\bar{\partial}w}{\partial r} \quad (5.2)$$

$\varepsilon_r, \varepsilon_\theta, \varepsilon_z$  are the normal strains in three axial directions.  $\gamma_{rz}$  is the shear strain which describes the variation of a right angle in a body. It represents the change of the shape of the body.  $u, v, w$  are the displacements in X, Y, Z directions respectively.

### 5.1.2 Constitutive Equation

#### (1). Yield criterion and flow rule

As discussed in Chapter 2.2.1, Mohr-Coulomb criterion is the most popular method used in petroleum engineering. However, its edges in principal stress space result in mathematical problem for numerical solution. Drucker-Prager criterion overcomes the shortcoming and will be used in our finite element analysis. Drucker Prager yield criterion is:

$$g = \alpha I_1 + J_2^{1/2} - H \quad (5.3)$$

Where,  $I_1$  is the first invariant of stress tensor,  $I_1 = \sigma_1 + \sigma_2 + \sigma_3$ .  $J_2$  is the second invariant of the deviatoric stress tensor.  $J_2 = -(S_1 S_2 + S_2 S_3 + S_1 S_3) = \frac{3}{2} \tau_{oc}^2$ ,  $S_1, S_2, S_3$ , and  $\tau_{oc}$  are the principle deviatoric stresses and octohedral sheer stress.

Flow rule is used to describe further deformation of a body when it is in plastic state. There are three cases for a plastic body: The first is the body will turn back to elastic state if the load acted upon it decreases. The second is the loading makes the body keep its original plastic state. The third is a further plastic deformation.

Further plastic deformation depends on its plastic potential function. Proposing a postulation and associating it with yield function, Drucker (1956) proposed an associated flow rule. The associated flow rule will make the body volume over-dilatency. Non-associated flow rule will be used in the analysis.

Flow rule can be expressed as:

$$\frac{\partial f}{\partial \sigma_{pq}} D_{pqkl} d\varepsilon_{kl} \begin{matrix} > 0 & \text{loading} \\ = 0 & \text{neutra unloading} \\ < 0 & \text{unloading} \end{matrix} \quad (5.4)$$

Where  $f$  is plastic potential function.

(2). Constitutive equation of elasto-plastic material

Plastic deformation depends on not only the state of strains but also the history of loading and deforming, so the constitutive equation of an elasto-plastic material is usually expressed as the form of increment. By binding the Drucker-Prager criterion and the non-associated flow rule, the constitutive equation is:

(a). For plastic potential function  $f < 0$ , the body is in elastic state. Stress and strain relation is

$$d\sigma_{ij} = D_{ijkl} d\varepsilon_{kl} \quad (5.5)$$

(b). For  $f=0$  and  $\frac{\partial f}{\partial \sigma_{pq}} D_{pqkl} d\varepsilon_{kl} > 0$ , the body is under loading. Constitution equation is

$$d\sigma_{ij} = D_{ijkl} d\varepsilon_{kl} - \frac{1}{B} D_{ijmn} \frac{\partial f}{\partial \sigma_{mn}} \frac{\partial f}{\partial \sigma_{pq}} D_{pqkl} d\varepsilon_{kl} \quad (5.6)$$

(c). For  $f=0$  and  $\frac{\partial f}{\partial \sigma_{pq}} D_{pqkl} d\varepsilon_{kl} \leq 0$ , the body is in unloading or neutral unloading.

The stress and strain relation is the same as that of elastic state for unloading and neutral unloading as:

$$d\sigma_{ij} = D_{ijkl} d\varepsilon_{kl} \quad (5.7)$$

## 5.2 Finite Element Method

Finite element method is a popular numerical method used to solve complex problem especially with complex shape, loading and boundary. The main idea of finite element analysis is dividing the body into small elements so that a solution could be got for every element.

### 5.2.1 Finite Element Models

(1). Displacement model of an element

$$\{\delta\} = \{N\}\{U_e\} \quad (5.7)$$

Where,  $\{\delta\}^T = \{u, v, w\}$  is the displacement matrix of points in an element.  $u, v, w$  are the displacement of a point in the element.  $\{U_e\}$  is the nodal displacement matrix of the element.  $\{N\}$  is a transfer matrix.

(2). Geometrical equation

In a cylindrical coordinate system, strains are expressed by displacements  $u$  and  $w$  in the direction of radial and tangential respectively.

$$\{\varepsilon\} = \begin{Bmatrix} \varepsilon_r \\ \varepsilon_z \\ \varepsilon_\theta \\ \gamma_{rz} \end{Bmatrix} = \begin{Bmatrix} \frac{\partial u}{\partial r} \\ \frac{\partial w}{\partial z} \\ \frac{u}{r} \\ \frac{\partial u}{\partial z} + \frac{\partial w}{\partial r} \end{Bmatrix} \quad (5.8)$$

Equation 5.8 in matrix expression is

$$\{\varepsilon\} = [B]\{U_e\} \quad (5.9)$$

(3). Constitutive equation in matrix expression

$$\{d\sigma\} = ([D_e] - [D_p])d\varepsilon \quad (5.10)$$

(4). Stiffness matrix

Based on the minimum potential principle or the principle of virtual work, the stiffness matrix of an element is derived as:

$$K_e = \iiint_A ([B]^T [D_e] [B]) r dr dz \quad (5.11)$$

$$[K_e]\{U\} = \{P\} + \{P'\} \quad (5.12)$$

Where  $\{P'\}$  is the matrix of equivalent nodal force matrix by  $[D_p]\{d\varepsilon\}$ ,  $[K_e]$  is the global stiffness matrix, and  $\{U\}$  is the nodal displacement matrix.

### 5.2.2 Procedures

(1). Divide load into a few increments  $\{P'\}$ . Solve the stiffness equation stated above in each loading increment at the initial condition  $\{P'\}=0$ . Iterate the calculation procedure in every increment until equilibrium.

(2). Calculate corresponding stress increments and stresses in every element.

$$\begin{aligned} \{\Delta\varepsilon_i\}_j &= [B]\{\Delta U_i\}_j \\ \{\Delta\sigma_i\}_j &= [D_e]\{\Delta\varepsilon_i\}_j \\ \{\sigma_i\}_j &= \{\sigma_i\}_{j-i} - \{\Delta\sigma_i\}_j \end{aligned} \quad (5.13)$$

(3). Calculate plastic stresses

$$\{\Delta\sigma_p\}_j = [D_p]\{\Delta\varepsilon_i\}_j \quad (5.14)$$

(4). Calculate equivalent nodal force as

$$\{\Delta P_i\}_j = \sum_A \iint [B]^T \{\Delta \sigma_p\}_j r dr dz \quad (5.15)$$

(5). Using new  $\{P_i\}_j$  to repeat the cycle until all plastic elements are convergent.

$$[K]\{\Delta U_i\}_j = \{\Delta P_i\}_j \quad (5.16)$$

### 5.3 Using ABAQUS/Standard-A Finite Element Software

ABAQUS/Standard is a finite element software for general propose having ability to solve linear and nonlinear problems. It is useful for problems associating with metal and granular material (rock). I use this kind of software since it is more convenient for problems of rock than other software. Like other finite element software, ABAQUS has its own language and subprograms designed in FOTRTRAN or C programming languages can be combined for special proposes.

ABAQUS procedure is consist of instructions. Each instruction in ABAQUS contains a keyword and some data if necessary. A set of instructions consists a model describing some physical feature, such as elements, nodes, properties, loading, boundary and so on.

#### 5.3.1 ABAQUS Functions

##### (1). Static Stress/Displacement Analysis

Many stress analysis problems can be solved with this software. Problem can be divided into static and dynamic response according to the consideration of inertia effect. Linear and nonlinear response is another problem during design. For a linear problem, loads are applied to models and model's response is obtained directly. Many nonlinear problems need to consider history dependent response, so that its solution is

usually obtained as a series of increments, with iteration within each increment to obtain equilibrium. Newton's integration method of nonlinear solution is used. To assure correct modeling of history dependent effects and computational efficiency, the increment should be chosen reasonably. An automatic increment scheme is provided by ABAQUS.

#### (2). Dynamic Stress/Displacement Analysis

ABAQUS offers several methods for dynamic analysis. Dynamic studies of linear problems are generally performed by using the eigenmodes of the system as a basis for calculating the response. Direct integration of a system must be used when nonlinear dynamic response is being studied. ABAQUS offers three approaches for direct integration.

#### (3). Heat transfer and thermal stress analysis

Heat transfer problems including conduction, cavity radiation, force conversion, boundary radiation and convection can be solved with ABAQUS. The problems can be transient or steady-state and linear or nonlinear.

#### (4). Coupled pore fluid diffusion and stress analysis

The software provides capabilities for modeling coupled pore fluid diffusion/stress analysis problems involving partially and/or fully saturated fluid flow which are useful for reservoir analysis.

#### (5). Mass diffusion analysis

ABAQUS provides modeling of the transient or steady-state diffusion of one material through another, such as the diffusion of hydrogen through a metal. The governing equations are an extension of Fick's equations, to allow for non-uniform solubility of the diffusing substance in the base material.

(6). Acoustic and coupled acoustic-structure analysis

A set of elements are provided for modeling an acoustic medium undergoing small displacements, and interface elements to couple these acoustic elements to a structural model.

(7). Piezoelectric analysis

Fully coupled piezoelectric analysis may be performed for continuum problems in one, two and three dimensions.

(8). Fracture mechanics

ABAQUS offers the evaluation of two contour integrals, J-integral and G-integral for fracturing studies. Crack propagation on a pre-determined surface is simulated by defining a slave surface and a master surface that are initially bonded and may de-bond during the process of analysis.

### 5.3.2 Parameters of Drucker-Prager Criterion

Rock properties, such as Young's modulus and Poisson's ratio, are measured from laboratory on rock sample. Common tests are designed for the use of Mohr-Coulomb yield criterion. Some way should be figured out to obtain properties for Drucker-Prager yield criterion from those of Mohr-Coulomb model.

Drucker-Prager criterion uses uni-axial compression strength,  $\sigma_0$ , which can be calculated from the friction angle  $\phi$  and cohesion strength  $\tau_0$  in Mohr-Coulomb model.

$$\sigma_0 = 2\tau_0 \frac{\cos \phi}{1 - \sin \phi} \quad (5.17)$$

Another parameter used by Drucker-Prager criterion is the friction angle  $\beta$  of the material in the ( $t$ - $p$ ) stress plane. The Drucker-Prager friction angle can be

calculated from the friction angle  $\phi$  in Mohr-Coulomb criterion as Eq. 5.18. The friction angle  $\phi$  is what we usually say.

$$\beta = \arctan \frac{6 \sin \phi}{3 - \sin \phi} \quad (5.18)$$

#### 5.4 Finite Element Model for Leak-off Test

To do a finite element analysis, a geometry model should be constructed. After those, boundary condition should be considered.

##### 5.4.1 Geometry

Since the wellbore, casing and cement are axisymmetric about the wellbore center line. We choose the geometry as axisymmetric problem and thus simplify the solution (as shown in Fig. 5.1).

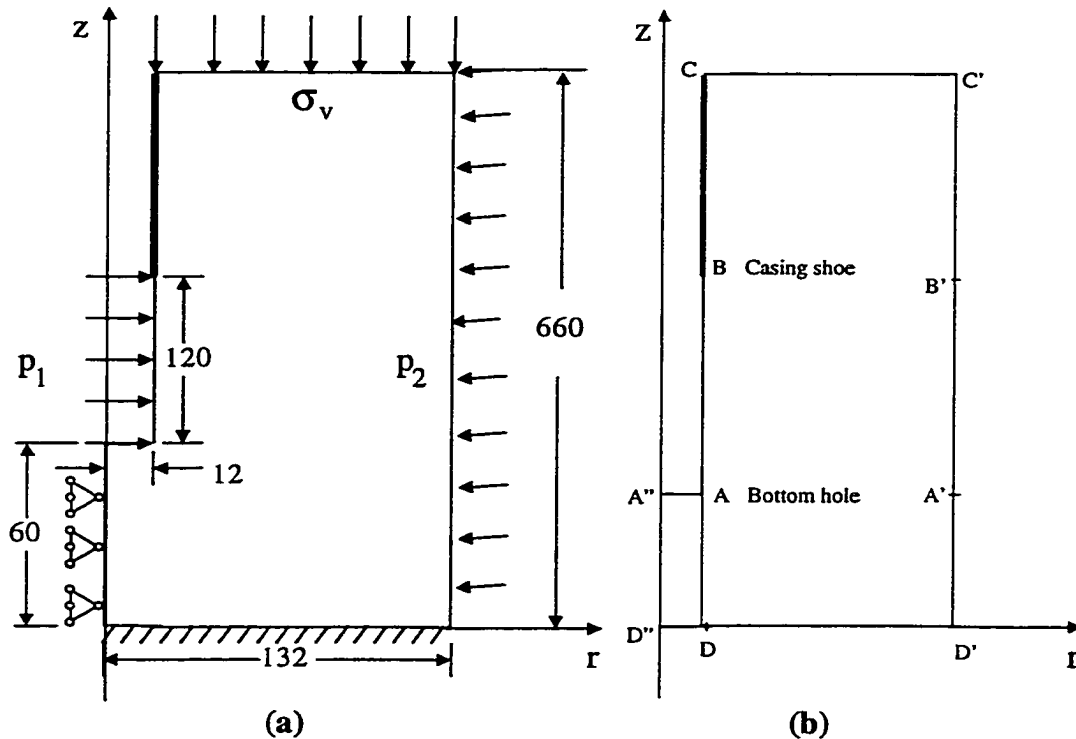


**Figure 5.1** Calculation part geometry: (a). Geometry; (b). Division.

Figure 5.1(a) shows the analysis geometry. From theoretical analysis as shown in Chapter 4, the effect range due to leak-off test and drilling operation is around the wellbore, and is within 5 times of the radius of a wellbore. A larger range is used in the analysis to reveal the detail information of leak-off test effect on stress distribution.

A cylinder is used with internal diameter of 24 inches, external radius of 132 inches, and a height of 600 inches. The bottom of the cylinder represents the bottom hole and a height of 60 inches below the bottom hole as shown in Figure 5.1(a). The height of uncased section in the wellbore is 120 inches.

#### **5.4.2 Divided Nodes and Elements**

Stress concentration will be formed around the bottom hole and the wall of the wellbore under the action of external pressure and/or internal pressure. The variation magnitudes of stresses are greater near the wall and the bottom hole, and smaller or even no variation away from the wellbore and bottom hole. To describe this variation and save running time at the same time, the distance between adjacent nodes. The more a position near the wellbore, the more the nodes are used. 3137 nodes in 17 node sets are designed in our analysis model. As shown in Figure 5.1(b), in the vertical direction: line AB is divided equally by 59 nodes. The interval between any two adjacent nodes is the same, which is 1 inch. Line AD is divided by 9 nodes. The spacing of the nodes is not equal, and concentrated toward the point A. The ratio of adjacent distances between nodes along DA is 1.1, as the nodes go from point D to point A. Line BC has the same unequal distance. There are 59 nodes between point B and point C. The ratio of adjacent distances is 0.97 from B to C. In the horizontal direction: 5 Nodes are distributed uniformly on line AA" and 29 nodes are placed

between A and A' with a distance ratio of 0.95 from A to A'. As shown in Figure 5.1(b), a series of horizontal lines are drawn through all the nodes on line DC, and vertical lines through nodes on line A'A".

8-node biquadratic, reduced integration axisymmetric elements are used in this model to provide more accurate results and reduce running time (Figure 5.2). This kind of element has 4 sides and 4 nodes are chosen in the middle of each side. Since such an element is determined by per adjacent 8 nodes, there are 3, 15 and 65 elements along line AA", line AA' and line DC respectively. There are total of 990 elements in 9 element sets in the whole area as shown in Figure 5.2.

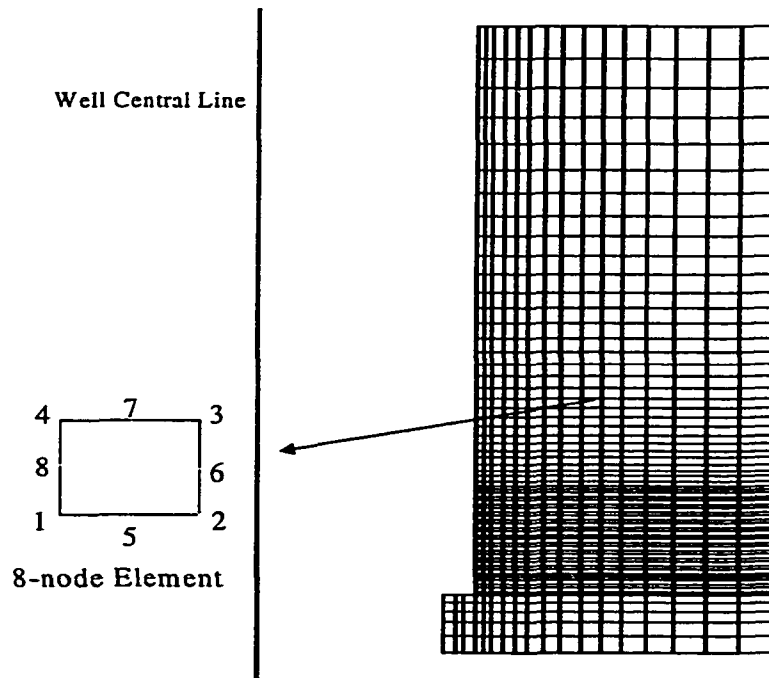


**Figure 5.2** Finite element analytical nodes and elements.

### 5.4.3 Boundary Conditions

It is not difficult to determine the boundary of this chosen area. As shown in Figure 5.1(b), D''D' is the radius of the bottom plane of this area. The bottom plane is

considered as fixed in the vertical direction. This means that there is no vertical displacement for any point on the plane during deforming. A"D" represents the center line of the cylinder. There is no displacement in horizontal direction for any point on this line due to the cylinder is axisymmetric about this line. The planes determined by line CC' and A"A are loaded by the overlying weight of rock and internal fluid pressure downwards. The surface of the cylinder shown by CD' is loaded by the lateral horizontal stress. Wellbore surface is represented by line AB, and loaded by internal fluid pressure.

The boundary condition of the cased surface (BC line) is assumed as fixed in horizontal. That is the casing and cement prevent the expansion or contraction of the wellbore during leak-off test. Our similar ABAQUS procedure shows that the radial distance is almost zero because of the existence of casing and cement.

The weight of overlying rock can be obtained by integrating the density of the rock with depth. External loading is calculated from Eq. 4.5 if it is unknown.

Internal fluid pressure is designed as an increasing variable to simulate the process of leak-off test and obtain the stress distribution and displacements in the area at different pressure.

#### **5.4.4 Sample Rocks**

Three kinds of rocks are used to study possible cases of rock effect on leak-off test. The three cases are: elastic wellbore, wellbore with a plastic zone, and a well is in a plastic formation.

##### **(1). Case 1-elastic wellbore**

If the rock in the chosen area is in elastic state before leak-off test, it is called elastic wellbore. Most deep wells should be in this kind of state.

Rock properties used in this study are: Young's modulus- $1.04 \times 10^5$  psi; Poisson's ratio-0.25; cohesive strength-94.8 psi; the angle of internal friction-25.4 degrees; plastic flow is assumed as non-dilatant.

(2). Case 2-plastic wellbore

Plastic wellbore indicated here is that an annulus around the wellbore is in plastic state but the farther part outside the plastic annulus is still in elastic state before leak-off test.

Rock properties are: Young's modulus- $1.04 \times 10^5$  psi; Poisson's ratio-0.3; cohesive strength-31.6 psi; the angle of internal friction-25.4 degrees; non-dilatant flow.

(3). Case 3-plastic formation

If all the rock is in plastic state before leak-off test, this case is called plastic formation here. The study is to check what will happen for such plastic formation under the action of leak-off pressure.

The properties of this formation are: Young's modulus- $1.04 \times 10^5$  psi; Poisson's ratio-0.25; cohesive strength-40.1 psi; the angle of internal friction-12.5 degrees; non-dilatant flow.

## **5.5 Results from Finite Element Analysis**

As stated above, the deforming process of the wellbore has some relation with plasticity. Plastic deformation depends not only on plastic strains but also loading history. The actual stress is not a simple addition of the stresses before or during leak-off test. To model plastic deformation process, two steps are adapted. The first is the calculation of the stresses around wellbore before leak-off test. The second is the

stress/displacement analysis under leak-off test pressure while the wellbore is in pre-stressed state.

Finite element result gives information of every element. As shown in Figure 5.3, some special lines are chosen to see the stress distribution.

In Fig. 5.3, Lines 1 to 4 are horizontal, which are used to describe the variations of stresses along axial direction at different depth. Line 1 and Line 2 are lines at the place just above and below the casing shoe. Line 3 is in the middle of leak-off test open hole. Line 4 is at the place of bottom hole. Line 5 is a vertical line that is used to describe the stresses and displacement at the wellbore.

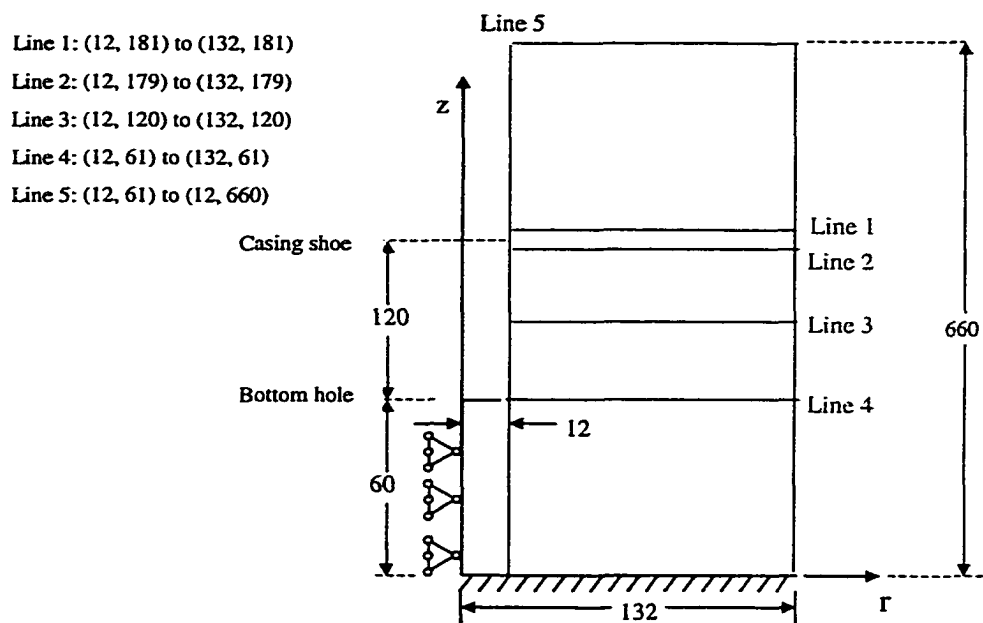


**Figure 5.3 Special analytical places.**

Finite element results are stored in finite element output files. For our plastic analysis, stresses, strains and displacements are available for every node and at any time. In the next few sections, results from finite element analysis are provided and discussed. They are only a very small part of our finite element outputs.

Figure 5.4 shows a finite element analysis graph for Case 2 during LOT.

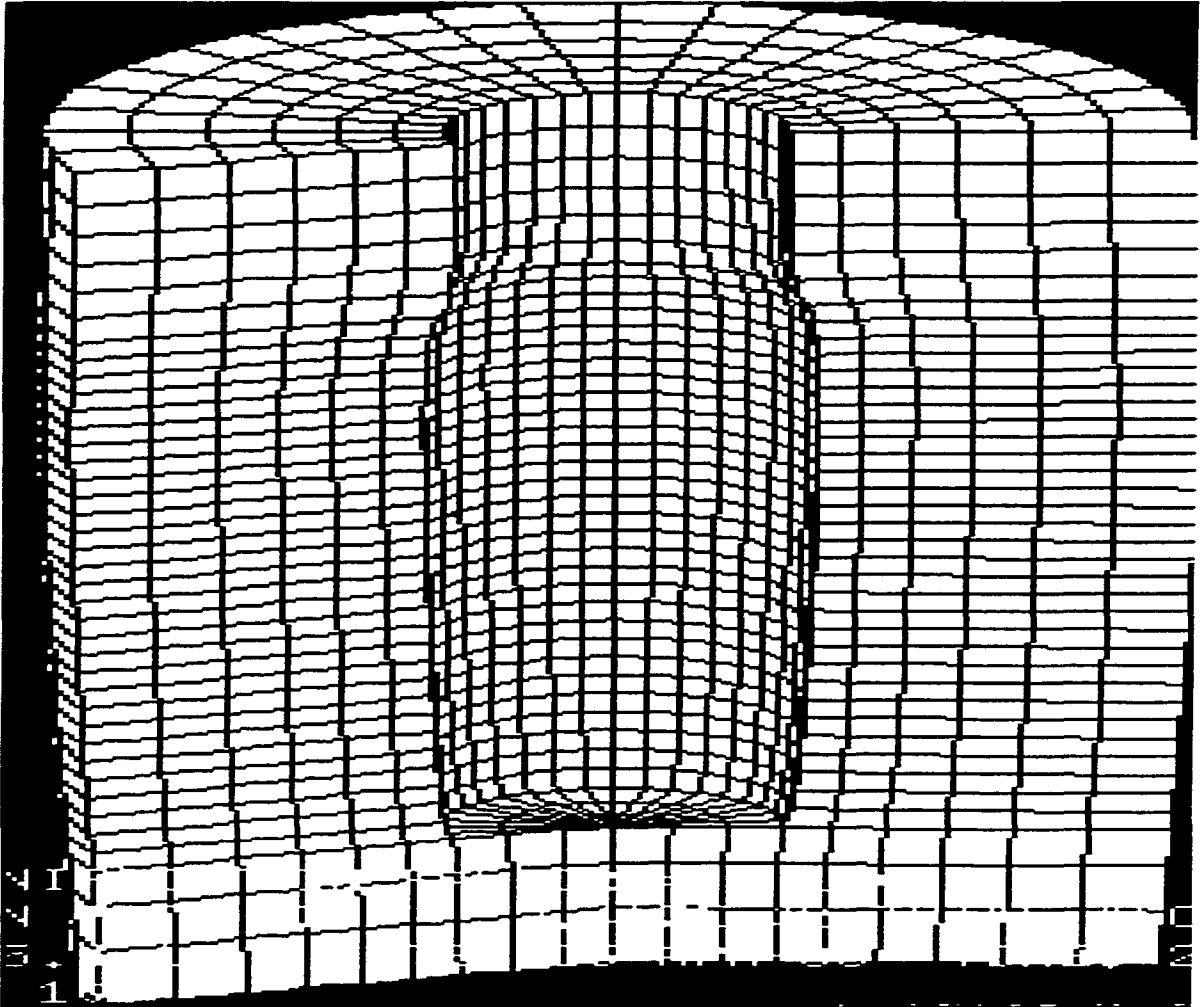


**Figure 5.4** Finite element results for Case 2 during LOT.

### **5.5.1 Case 1-Elastic Wellbore**

Fig. C.1 to Fig. C.6 are figures calculated from Case 1. Fig. C.1 to Fig. C.3 are the results before leak-off test. That is the state of stresses caused by drilling. Note that compression stresses reported in finite element analysis are negative, and tensile stresses are positive.

Fig. C.1 gives the distribution of stresses around wellbore along radial direction in the middle of the uncased section (Line 3). It is exactly the same as the results of many plane strain analyses. In-situ tangential stress is equal to in-situ horizontal stress and two times at the wall of the wellbore. Vertical stress keeps constant from wellbore to outside boundary. Radial stress decreases from in-situ stress to zero. This result proves that plane strain analysis can be used in the middle of the uncased section, even though in such a short section as LOT (5-15 feet).

Fig. C.2 shows the stresses along the wall of the wellbore. Radial, tangential and vertical stresses vary largely in the position of bottom hole. Shear stress occurs around the bottom hole as shown in Fig. C.3.

Shear stresses are not only concentrated around the bottom hole, but also around casing shoe as shown in Fig. C.4. Fig. C.5 shows a plastic zone is formed around the wellbore.

Fig. C.6 gives the displacement of the wellbore during LOT. The rock is parted from the cement at the casing shoe. The figure proves that cement parting is possible. This is main reason for the formed shear stress around there since drilling fluid is not allowed to go into this newly produced channel.

### **5.5.2 Case 2-Plastic Wellbore**

Calculated results for Case 2 are shown in Fig. C.7 to Fig. C.16 for a wellbore with a plastic annular around it. Since generally wells in shallow marine sediments have this kind of plastic annulus, Case 2 is discussed more detail here. From Chapter 4, the plastic annulus could be prevented in drilling by increasing mud weight. However, this plastic annular is assumed as stable and yield is only considered when stresses get the yield/failure criterion.

Figs. C.7 and C.8 are the results before leak-off test. As discussed in Chapter 4, tangential stress will drop sharply near the wellbore when there is a plastic annulus. Fig. C.7 clearly shows this result. In the case of plane strain analysis, vertical stress is generally regarded as constant, however, it also drops sharply according to Fig. C.7.

Fig. C.8 shows the stress distribution at the bottom hole. Shear stress appears around the wellbore.

Fig. C.9 shows the tangential stress firstly decreases with the increase of wellbore pressure in the middle of the open hole. This phenomenon look like the same as that in deep wells. However, as shown in Fig. C.10, instead of decrease to tensile, tangential stress comes back before getting zero and increasing with the further increase of wellbore pressure. That is tangential stress can never become tensile as that in deep well. Therefore, vertical fracture is impossible in shallow marine sediments. Theoretically, tangential stress comes back because of the occurrence of re-yield. The mechanism was discussed in detail in Chapter 4.

Fig. C.11 gives the stress distribution at the bottom hole during LOT. Shear stress appears instead of fracturing.

Fig. C.12 and Fig. C.13 show the stress distribution just below and above casing shoe (Line 2 and Line 1 in Figure 5.3) respectively. Shear stress is also produced around casing shoe. No fracture will occur below casing shoe as shown in Fig. C.12. However, the element above casing shoe looks free of stresses (all stresses goes to zero) and radial stress gets tensile above casing shoe as shown in Fig. C.13. Again, cement parting occurred.

The thickness of the plastic zone is almost the same at different wellbore pressures as shown in Fig. C.14. Plastic strains produced by drilling operation could

not be eliminated during LOT. Fig. C.15 gives the values of the different wellbore pressures during LOT. The pressure increase at wellbore wall is continuous. The selected pressures are used for understanding wellbore displacements in Fig. C.16. Wellbore wall expanded as wellbore pressure increases as shown in Fig. C.16. However, the wellbore enlargement is very small. The idea of large balloon for wells with plastic annulus is not right. Again, cement parting will be formed. It was called channeling by Wojtanowicz and Zhou (1998).

### **5.5.3 Case 3-Plastic Formation**

The wellbore retracts largely before leak-off test in this case. This formation is so soft that it is easy to "flow" into wellbore. More heavy mud should be used in real drilling process. It is studied here for comparison.

Finite element analysis results for Case 3 are shown in Fig. C.17 to E.23 in Appendix C. Fig. C.17 shows the stress distribution along radial direction at the uncased middle (Line 3 in Figure 5.3) before leak-off test. The turning point of tangential stress is moved right comparing to that in Fig. C.7. The stresses around wellbore become small and stress concentration occurs in the sediment. It should be pointed out that all the sediment is in plastic state. Fig. C.18 is the case during leak-off test. The same as Case 2, tangential stress does not go up to zero but turn down with further increase of wellbore pressure. Vertical fracture could not be formed.

Fig. C.19 and Fig. C.20 represent the stress distributions just above and below the casing shoe. That all the stresses trend to zero means cement parting occurred. Tensile radial stress clearly proves this conclusion. Also, a horizontal fracture would occur if an upward fluid pressure were added on the small horizontal displacement of the uncased section. The fact is hydraulic pressure is in all directions.

Therefore, casing shoe is the most possible place for horizontal fracturing. The place below casing shoe is safe based on Fig. C.20. Also, bottom hole is safe from the Fig. C. 21.

Fig. C.22 and Fig. C.23 summary the distributions of tangential stress and radial stress at different places respectively.

## 5.6 Horizontal Fracture

In the above analysis, the pressure is acted on the wellbore wall directly. In the following, the pressure is acted in any direction including upward to study the horizontal fracture. The model's schematic is shown in Fig. 5.5.

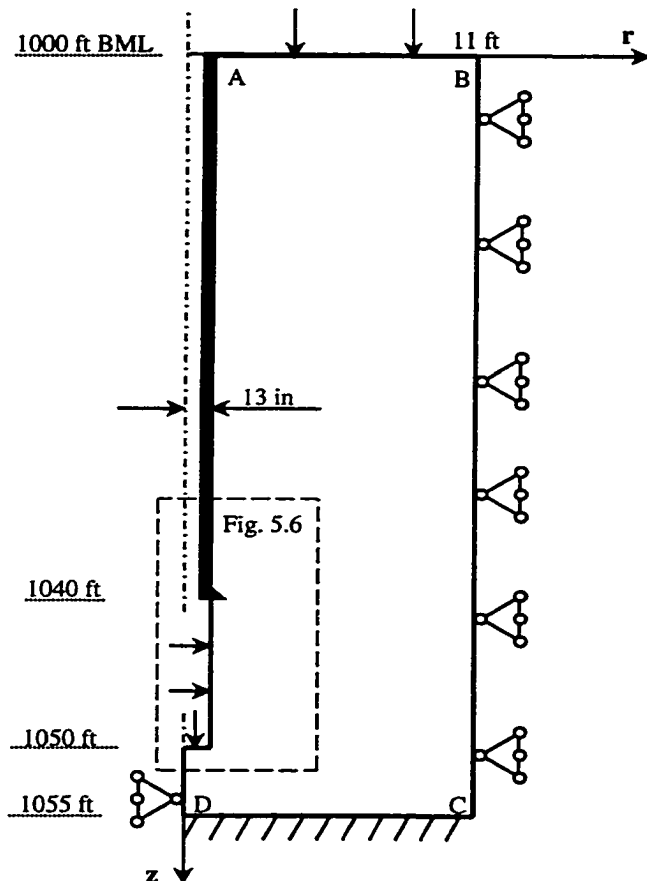


**Figure 5.5 Model of vertical fracture initialization during LOT.**

In Fig. 5.5, the dash rectangular area will be used for detail analysis. Outside surface BC is set as simple support (no displacement in radial but free move in vertical direction). The bottom DC is fixed since pre-analysis proved no displacement below bottom hole. The center of the rock (along axis Z) below bottom hole is also simply supported.

No contact stress is assumed at the inner boundary (i.e. the surface between the well's cement and rock) at the beginning analysis. Also, defines a cylindrical outer boundary of the rock-well system having an 11-foot radius around the 26- inch well. Deformations at the outer boundary are laterally constrained. (Preliminary finite element calculations indicated that at the radial distance from a well exceeding five well diameters stresses were almost equal to in-situ stress).

An example calculations, presented here, considered the following UMS properties: Young's modulus =  $1.1 \times 10^5$  psi; Poisson's ratio = 0.3; cohesion strength = 31.6 psi; and angle of internal friction = 25.4 degrees. The yield criterion is Drucker-Prager criterion with non-associated flow. It has already been proved that this kind of yield criterion is appropriate for modeling yielding of shale (Steiger and Leung, 1988). Also, in this example we consider a 600-psi vertical stress and initial wellbore pressure (prior to LOT) equal to zero.

The plot of tangential stress in Fig. 5.6 demonstrates stress conditions resulting from the second plastic failure (re-yielding). This wellbore failed before the decreasing tangential stress became negative, which means that the wellbore wall had never been in tension during this LOT. Consequently, no LOT - induced vertical fracture is possible in this well which agrees entirely with conclusion from the study above.

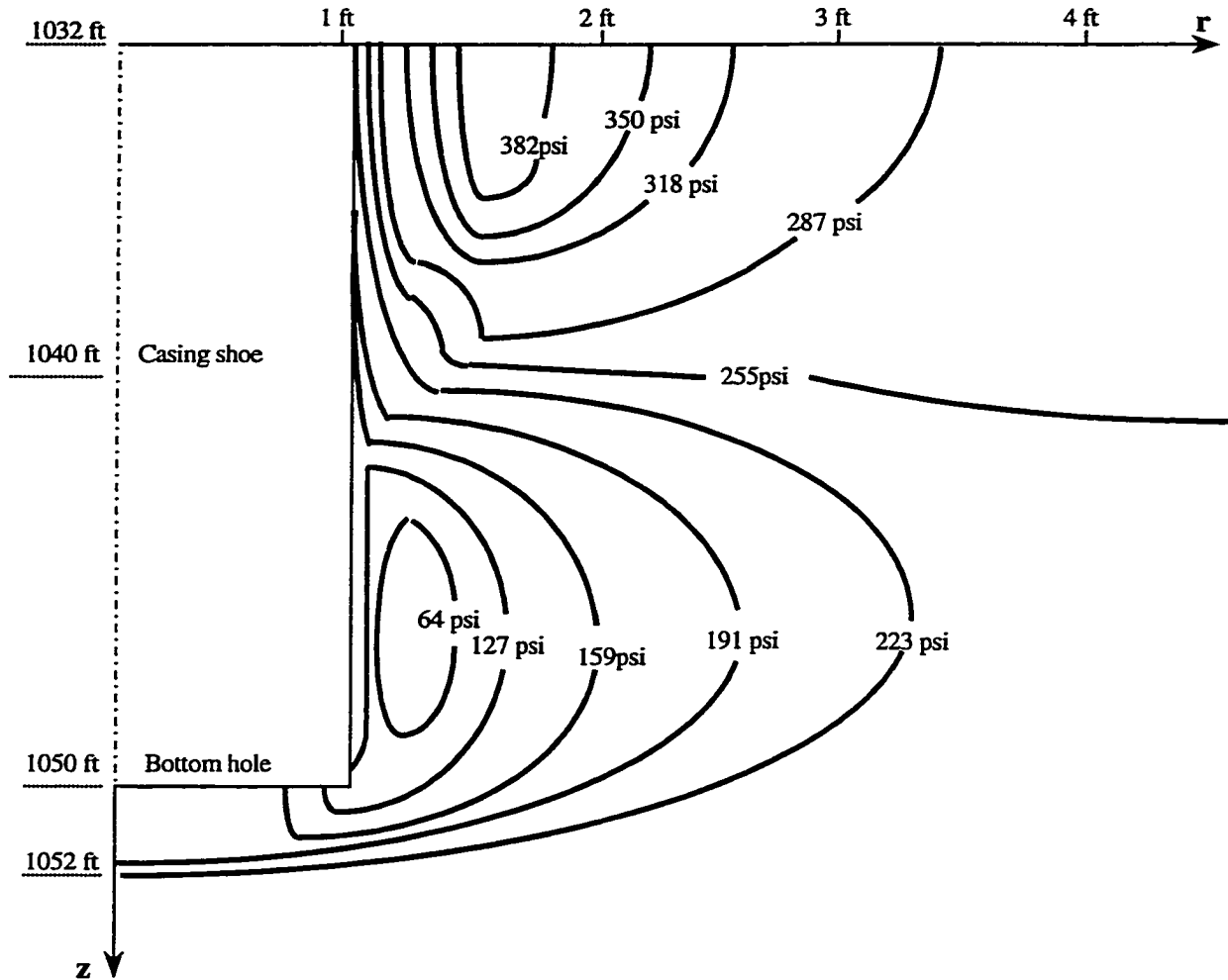


**Figure 5.6 Concentration of tangential stress at top/bottom of open hole shows no tension during LOT.**

We also checked values of tangential stresses at the top and bottom of the open hole section where complex geometry precluded an analytical analysis. In spite of stress concentration at these points - shown in Fig. 5.6 - tangential stress remains positive for  $p_w = 700$  psi thus indicating that no tension exists around the casing shoe. This result further supported our conclusion.

We also checked a possibility of vertical fracture for the elastic borehole when the wellbore pressure before LOT was 150 psi. Again, the finite element simulation

showed that the increasing LOT pressure would inflict plastic yield without bringing the wellbore wall to tension.

Mechanism of horizontal fracture involves fracture initiation and propagation. The latter is well described by balancing effective wellbore pressure with overburden matrix pressure (or actual well pressure with overburden pressure). On the other hand, mechanism of horizontal fracture initiation is typically addressed by assuming that wellbore liquid somehow invades the rock through pre-existing fractures or discontinuities and without addressing the invasion mechanism. Our assumption regarding non-penetrating fluid precludes such hypothetical speculations and requires some quantitative description of the mechanism of fluid invasion into the rock at the casing shoe.

One such mechanism would be an uplift of the wellhead at sea bottom caused by LOT pressure increase. During LOT the well is shut-in around the drill pipe and pressure pushes the wellhead upwards. As the casing is attached to the wellhead the uplifting of the wellhead may reduce vertical compression at the casing shoe which, in turn, may be transferred to the rock. If the reduction of compressive stress was large enough it would reduce vertical stress at the wellbore wall from compression to tension which would cause horizontal fracture.

Unfortunately, our finite element analysis showed that this uplifting mechanism can only reduce part of vertical compressive stress at the shoe even for a rigid column of casing and cement. Moreover, our numerical calculations showed that vertical compressive stress at the borehole wall would not be reduced to tension even for bottomhole pressure several-fold greater than overburden pressure!



The rock properties are: Young's modulus =  $1.1 \times 10^4$  psi; Poisson's ratio = 0.35; cohesion strength = 9.2 psi; and, internal friction angle = 23 degrees. The cemented casing string has Young's modulus =  $30 \times 10^6$  psi and Poisson's ratio of 0.3. The value of contact stress is assumed as zero. Effective overburden pressure was calculated using average submerged unit weight, 8.345 lb/gal, which represents UMS having a porosity of 61% and wet bulk density, 13.9 lb/gal. Casing shoe was set at 400 ft below mud line. Effective wellbore pressure is zero before LOT and increased to 145 psi during LOT.

Shown in Fig. 5.8 is an effective vertical stress distribution at the borehole wall from the mud line (sea bottom) to the open hole bottom.

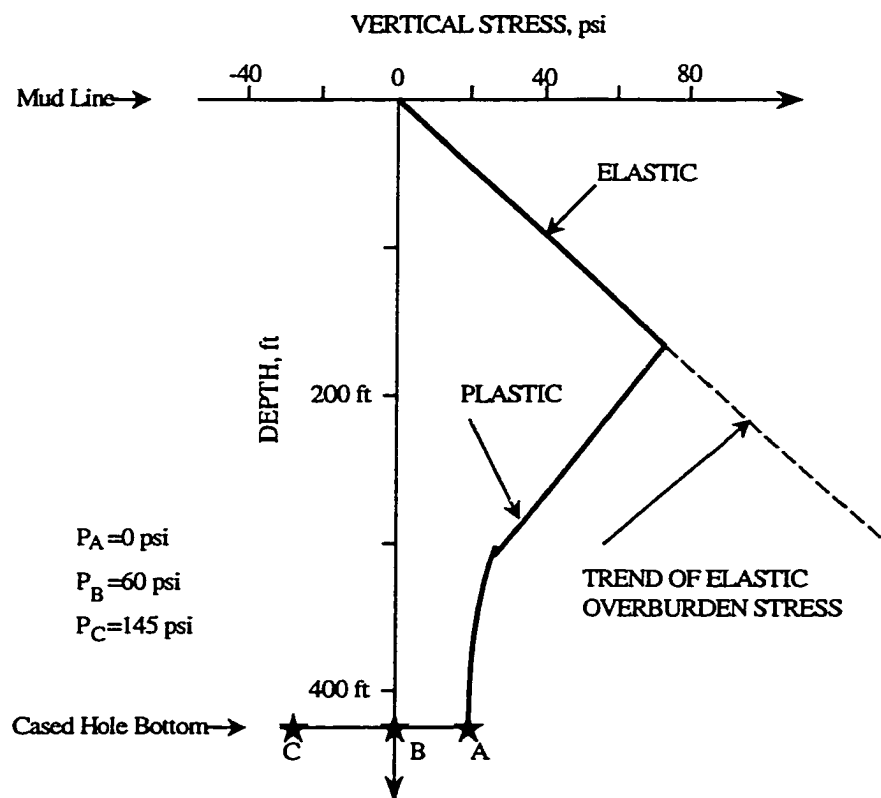


**Figure 5.8** Vertical stress change shows initiation of horizontal fracture at casing shoe during LOT.

The finite element results are summarized in Appendix C. In Fig. 5.8, there is a linear increase of vertical stress with depth in the upper section of the well indicating that the well's wall is in elastic state from surface to the depth at which plastic failure occurs. Below this depth vertical stress steadily decreases indicating an expansion of the plastic zone with increasing depth.

The vertical stress at casing shoe turns from compression into tension by increasing LOT pressure to 145 psi (points A-B-C). Horizontal fracture will be initiated since tensile strength is very small for most SMS. This mechanism has been verified with ABAQUS in several simulation runs for various SMS properties and wellbore conditions, shown in Table 5.1. FEA results are shown in Fig. C.24 to Fig. C.33 in Appendix C. Although the effective wellbore pressure is 145 psi for all the figures, all the vertical stress turns into tension showing the initiation of horizontal fractures.

**Table 5.1 Data for horizontal fracture simulation study.**

CASE	$2 r_w$ (in)	E (psi)	$\mu$	$\varphi$ (deg)	$\tau_0$ (psi)	$\gamma$ (lb/gal)	$E_{cc}$ (psi)	D (ft)	$d_{cc}$ (in)
1	26	1.1E4	0.4	12.5	11.6	8.35	3E7	400	30
2	26	1.1E4	0.4	12.5	11.6	8.35	3E7	564	30
3	20	1.1E4	0.4	12.5	11.6	8.35	3E7	400	24
4	26	1.1E4	0.4	12.5	11.6	16.7	3E7	400	30
5	26	1.1E6	0.4	12.5	11.6	8.35	3E7	400	30
6	26	1.1E4	0.4	12.5	11.6	8.35	3E8	400	30
7	26	1.1E4	0.4	15.3	11.6	8.35	3E7	400	30
8	26	1.1E4	0.4	12.5	16.6	8.35	3E7	400	30
9	26	1.1E4	0.35	12.5	11.6	8.35	3E7	400	30

Once a horizontal fracture is formed at the wall of a well, the drilling fluid will penetrate into it and try to propagate the fracture. As shown above, however, the

vertical stress increases in the plastic zone around wellbore with increasing distance from the well to the plastic - elastic boundary where it becomes stress in-situ. Hence, horizontal fracture will not propagate beyond the plastic zone until the actual wellbore pressure is greater than in-situ overburden pressure.

## **5.7 Cement Parting**

The occurrence of an upward propagating annular channel around the cemented casing is another potential failure resulting from LOT in UMS. In our recent study, we investigated plastic deformations of the open hole during LOT and concluded that drilling fluid may invade the contact surface between cement and rock at the casing shoe (Wojtanowicz and Zhou, 1996). We also found that the opening gap size might be of the order of 0.01 in. which was within the critical range (0.01-0.015 in.) for drilling fluid's inflow, as determined by other researchers (Morita, 1990). We reached these conclusions from the finite element simulations assuming no bond and no contact pressure existed between cement and rock. We did not, however, address the issue of critical pressure for initiation of the annular channel.

Critical pressure for induction of the annular channel during LOT is the minimum bottomhole pressure required to change contact stress at the casing shoe from compression to tension (In order to determine critical pressure one must assume that mechanical continuum exists between cemented casing and rock, which means assuming both a bonding and contact stress.). As critical pressure for channeling may be smaller than the one for horizontal fracture, both critical conditions should be included in the LOT analyses.

Our study of annular channeling involved a finite element analysis of the mechanical model of wellbore shown in Fig. 5.5. Conceptually, the model is identical

to the one for vertical fracture except for a constant non-zero value of contact stress between the cemented casing and rock. Also, geometry of the wellbore is different to that in Fig. 5.1 with wellbore diameter - 26 in., height (CB) - 60 ft, and radius (DC) - 17.5 ft. Rock properties are the same as those in Fig. 5.5. The initial value of the bottomhole effective pressure before LOT is assumed zero. Shown in Fig. 5.9 is the effect of LOT bottomhole pressure on contact stress at the casing shoe.

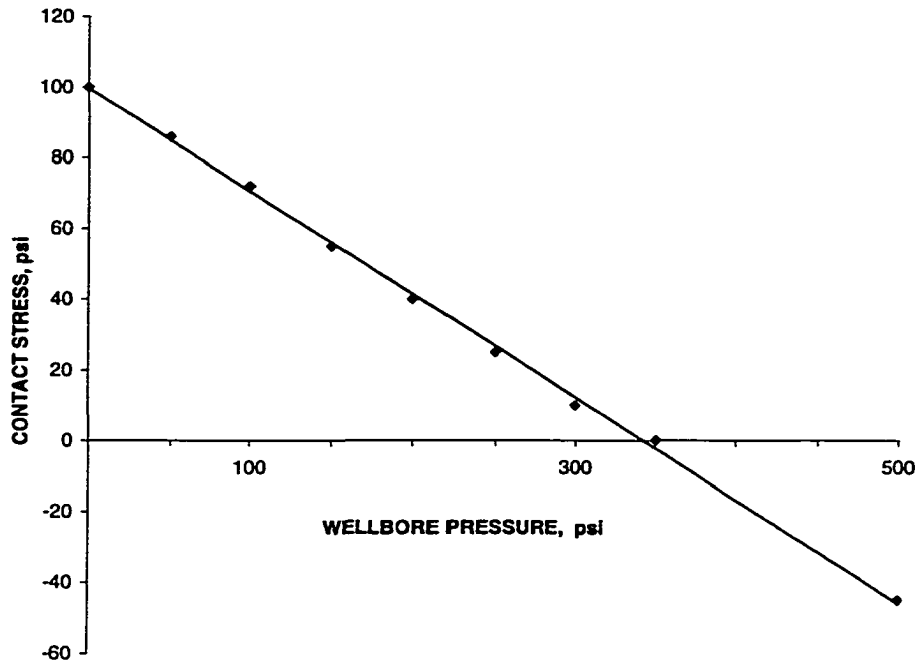


**Figure 5.9** Contact stress change shows initiation of channel at bottom of cemented casing during LOT.

As bottomhole pressure increases from zero to 350 psi contact stress reduces from 100 psi to zero. Thus at 350 psi annular channeling begins, which means that the critical value of bottomhole pressure is 3.5 - fold greater than the initial contact pressure.

Critical pressure for annular channeling strongly depends on contact stress. Intuitively, the larger the contact stress is, the higher the wellbore pressure is needed

to create a channel. We believe that the value of the contact stress depends upon time, formation properties, and to some extent properties of the cement slurry. Although determination of the contact pressure is beyond the scope of this study, we can estimate its range from zero (for compacted sediments) to horizontal stress in-situ - for very weak sediments. Thus, the maximum value of contact stress is,

$$\delta_c = \sigma_h = \frac{\mu}{1-\mu} \sigma_{z0} \quad (5.19)$$

The relationship between the contact stress and the critical pressure for annular channeling is shown in Table 5.2. As shown in Table 5.2, in all cases considered in the study, critical channeling pressure was about 3.5 - fold greater than the contact stress.

**Table 5.2 Data for annular channeling simulation study.**

CASE	E (psi)	$\mu$	$\varphi$ (deg)	$\tau_0$ (psi)	LOAD (psi)	D (ft)	$2r_w$ (in)	RATIO
1	1.1E5	0.3	25.4	31.6	600	1100	26	3.6
2	1.1E5	0.3	21.6	34	600	1100	26	3.5
3	1.1E5	0.3	25.4	78	600	1100	26	4.3
4	1.1E3	0.3	25.4	31.6	600	1100	26	3.5
5	1.1E5	0.2	25.4	31.6	600	1100	26	3.5
6	1.1E5	0.3	25.4	31.6	600	1100	20	3.5
7	1.1E5	0.3	25.4	31.6	700	1300	26	3.4

Moreover, with this 3.5 value, the pressure ratio was not affected by varying rock properties such as Young's modulus, Poisson's ratio, internal friction angle and cohesive strength. In addition, vertical stress and wellbore diameter did not affect the ratio, either.

Findings of this study are being used in our continuing research project aimed at an improvement in procedures and analyses of LOTs in UMS. There are two potential applications of these results; prediction and diagnosis. Prediction of the type

of formation failure; i.e. annular channeling or horizontal fracturing, requires prior knowledge of rock properties, contact pressure, and vertical stress. From this data one can decide if LOT may result in channeling which would potentially lead to the loss of the well's integrity or merely horizontal fracturing which brings about no serious environmental or technical risk.

If the only data available are LOT results, a diagnostic analysis can be performed to decide which type of damage resulted from the test. The analysis would require an estimation of overburden and pore pressure gradients, first. A simple method was proposed for calculating overburden pressure in UMS at depth using a constant representing exponential trend of sediment compaction trend with depth (Bourgoyne, et al, 1991). Also, another proposed method would use data from geotechnical borings offshore to estimate the change of the sediment's bulk density with depth subsea (Bender and Bourgoyne, 1995).

Secondly, a recorded LOT should be analyzed. According to this study we believe that the LOT plots for horizontal fracture and annular channel may have similar shapes showing a pressure increase until a maximum value,  $p_{max}$ , is reached and it stays constant. From this plot a failure pressure,  $p_f$ , is calculated as

$$p_f = 0.052\rho D_T + p_{max} \quad (5.20)$$

Where,  $D_T$  (ft) is the TVD;

$\rho$  is mud density (ppg).

If overburden pressure,  $\sigma_{over}$ , is known, the diagnostic procedure may be as follows: Compare  $p_f$  to  $\sigma_{over}$ ; a channel is formed if,  $p_f < \sigma_{over}$ ; Otherwise, horizontal fracture occurs.

For example, there is a LOT for a 24" casing shoe at 803 ft TVD and TMD, mud weight is 9.0 ppg, RKB is 118 ft above sea level, mud line is 102-ft below sea level, LOT pressure is 155 psi. The fracture pressure is  $P_f = (0.052)(9)(803) + 155 = 530$  psi. Bulk density is 11.7 ppg to 16.7 ppg in UMS. The possible minimum overburden pressure is  $(102)(.44) + (0.052)(803 - 102 - 108)(11.7) = 405$  psi. The possible maximum overburden pressure is  $(102)(.44) + (0.052)(803 - 102 - 108)(16.7) = 560$  psi. The average overburden pressure is  $(102)(.44) + (0.052)(803 - 102 - 108)(14.2) = 483$  psi. Because the fracture pressure is greater than the average overburden pressure, we can conclude that the maximum strength at the shoe represents an overburden pressure in this area and there is no risk of an upward migration of fluids along the well.

If LOT results indicate annular channeling, preventive or remedial action can be considered. For prevention, a key point is to increase the contact stress between cement and rock by using non-shrinking or expanding cements, for example. Using results from this study an increase of contact stress above 29 percent of overburden pressure should prevent annular channeling. (This safe value of contact stress is smaller than horizontal stress in-situ.)

For this example, to prevent annular channeling, the contact stress should be greater than 153 psi (using 3.5 value of the stress ratio) at the casing shoe with overburden pressure 1000 psi and pore pressure 465 psi. That gives the required value of hydrostatic pressure of a non-shrinking cementing slurry at the casing shoe greater than 618 psi.

## **5.8 Finite Element Validation of In-situ Stress Model**

A confined triaxial compressive test is simulated in finite element analysis. Samples are dry rocks for effective stress analysis. The variation of the stress, the

strain, and the displacement of the sample during the simulated experiments are simulated.

Rock specimen is an axi-symmetric cylinder (container) with a radius of 24 inches and axial height 98 inches. The cylinder is confined by an enclosing structure and is squeezed only axially on the top of the sample. The confining structure is perfectly smooth and rigid, and there are no friction and displacement between the specimen and the confining container.

### **5.8.1 Analytical Results**

(1). The rock has Poisson's ratio of 0.3, Young's modulus of  $1.04 \times 10^5$  psi, friction angle of 25.4 degrees and the cohesive strength of 6.32 psi. This sample is used to test the stress ratio when the rock is in elastic state.

According to Chapter 4.1.2, the inclination of the rock's Mohr's circle is 23.6 degrees. Therefore, since the angle of internal friction greater than the inclination, this rock is in elastic state under the action of a vertical load. The stress ratio is about 0.429 in elastic state.

(2). The rock has Poisson's ratio 0.3, Young's modulus  $1.04 \times 10^5$  psi, friction angle of 7.36 degrees and cohesive strength of 8.79 psi. This sample is used to test the in-situ stresses in plastic state.

Theoretical analysis from Chapter 4.1.2 points out the inclination angle of its Mohr's circle is 23.6 degrees. Since the friction angle is less than the inclination and the cohesive strength is not zero, the rock will be in elastic state in first, and then turn into plastic state. The threshold value of this turning point should be 44.89 psi. The threshold value is relatively small comparing to our loading, so the rock will be in plastic state for most of the loading levels.

(3). The third rock has Poisson's ratio of 0.25, Young's modulus of  $1.04 \times 10^5$  psi, friction angle of 12.49 degree, and cohesive strength of 40.14 psi. This sample is used to test the stress ratio of elastic and plastic states and the turning threshold value from elasticity to plasticity.

The inclination angle of the Mohr's circle of this sample is 30 degrees. Its threshold value of turning is 207.17 psi. The sample is in elastic state before the loading is less or equal to 207.17 psi, then it will be in plastic state once the threshold is passed.

### **5.8.2 Finite Element Model**

Nodes are the intersection points on the one square inch web. There are 25 nodes on horizontal axis, 99 nodes on vertical axis. There are totally  $25 \times 99$  nodes on a half axisymmetric plane.

8-node biquadratic, reduced integration axisymmetric elements are used in this model to provide more accurate results and decrease program running time. There are 12 elements in OR direction and 49 elements in OZ direction. The total number of the elements of the discussed plane are  $12 \times 49$ .

Rock samples are regarded as homogeneous and isotropic. For the convenience of mathematical calculation in the finite element method, Drucker-Prager yield model is used in this simulation, which is proved to be effectively suitable to granular materials, such as soils and rocks. For avoiding too much volumetric expansion of the yield material predicted by associated flow, nonassociated flow rule is adopted. Now, the plastic flow is assumed to be normal to the yield surface in the  $\pi$ -plane (Chen and Han, 1988). The parameters of this yield model are got by matching the Mohr-Coulomb parameters to compare with the theoretical results.

The sample is confined on the outside surface and the bottom. Since the sample is axisymmetric about the its vertical axis, there is no horizontal displacement along the vertical axis. A uniform distributed force is loaded on the sample top. 1000 psi, 2000 psi, and 1000 psi are used for the three different rocks stated above.

### 5.8.3 Simulated Results

Simulated results are summarized in the following three tables (Tables 5.3 to 5.5). The process of loading is divided into a series of steps in each case to compare the coincidence with the theoretical results at the same load.

**Table 5.3 Stress Ratio in Elastic State.**

Load(vertical stress)(psi)	Horizontal stress(psi)	Stress ratio	Elastic or plastic state(E/P)	Theoretical stress ratio
25	10.71	.429	E	.429
50	21.49	.429	E	.429
87.5	37.5	.429	E	.429
144	61.71	.429	E	.429
228	97.71	.429	E	.429
328	140.57	.429	E	.429
428	183.43	.429	E	.429
528	226.29	.429	E	.429
628	269.14	.429	E	.429
728	312	.429	E	.429
828	354.86	.429	E	.429
928	397.71	.429	E	.429
1000	428.57	.429	E	.429

In Table 5.3, more steps are used to simulate the detail process around the elastic to plastic turning value to verify the calculated threshold. The status of

elasticity or plasticity of those samples is determined by checking the occurrence of plastic strain in the samples.

Letter *E* in Table 5.3 is used to indicate elastic state and *P* is used for plastic state in following tables. Stress ratio is the stress ratio calculated from finite element analysis. Theoretical stress ratio is the stress ratio from Eq. 4.1 for elastic state or Eq. 4.2 for plastic state.

There is no threshold value of turning from elasticity to plasticity for case 1, as in Table 5.3. The rock is still in elastic state even the load gets to 1000 psi. The stress ratio is the same as that from the formula of Eq. 4.1. Table 5.4 shows that the sample is in plastic state for all the steps.

As given above, the threshold value for this sample is 40.14 psi. The load is 50 psi in the first step, which is greater than the threshold value calculated from Eq. 4.2, therefore no elastic states.

**Table 5.4 Stress Ratio in Plastic State.**

Load(vertical stress)(psi)	Horizontal stress(psi)	Stress ratio	Elastic or plastic state(E/P)	Theoretical stress ratio
50	23.2	.464	P	.464
175	120	.686	P	.685
287.5	206.8	.719	P	.719
456	337	.739	P	.739
855	645	.754	P	.755
1055	800	.758	P	.758
1255	955	.761	P	.761
1455	1110	.763	P	.762
1655	1264	.764	P	.764
1855	1420	.765	P	.765

The calculated result (Table 5.4) shows that all is plastic state and confirms the theoretical result. The stress ratio is the same as the result from plastic ratio Eq. 4.2 which proves the formula is workable in plastic formation.

Table 5.5 shows that the state of variation from elastic state into plastic state. The threshold is estimated between 188.5 psi and 218.5 psi. The threshold value of this sample is 207.17 psi according to Eq. 4.3. The stress ratios in elastic and plastic states prove the Eq. 4.1 and Eq. 4.2.

**Table 5.5 Stress Ratio From Elastic To Plastic State.**

Load(vertical stress)(psi)	Horizontal stress(psi)	Stress ratio	Elastic or plastic state(E/P)	Theoretical stress ratio
25	8.33	.333	E	.333
50	16.65	.333	E	.333
87.5	29.15	.333	E	.333
128.5	42.8	.333	E	.333
144	47.9	.333	E	.333
158.5	52.8	.333	E	.333
188.5	62.8	.333	E	.333
218.5	76.4	.349	P	.349
248.5	95.7	.385	P	.385
278	114.7	.413	P	.413
300	129	.43	P	.430
527.5	275.5	.522	P	.522
627.5	340	.542	P	.542
727.5	404.5	.556	P	.556
1000	580	.58	P	.580

From Tables 5.3, 5.4, and 5.5, the horizontal to vertical effective stress ratios of the theoretical value (Eqs. 4.1 and 4.2) and the simulated value from finite element

analysis are almost the same. The result proves that the theoretical method is correct under its assumption. The small differences of some items in tables are caused by the numerical approximation.

## **CHAPTER 6**

### **CEMENT PARTING**

As presented in Chapter 4 and Chapter 5, two kinds of fractures may occur around a casing shoe: formation fracture and cement parting (cement fracture). Formation fracture has two kinds of forms: vertical formation fracture and horizontal formation fracture. Vertical formation fracture is impossible due to the appearance of a plastic annular for soft formation such as shallow marine sediments (SMS). Horizontal formation fracture and cement parting are the possible fractures around a casing shoe in SMS. Leak-off test (LOT) result may come from either of them.

Unfortunately, only cement pre-existed channels have been addressed in the analysis of casing shoe integrity up to now. No method is proposed to distinguish cement parting and formation fracture. All the formation fracture predictive methods are based minimum principle stress theory (using overburden pressure, formation pore pressure, stress ratio as their parameters) and therefore predict formation fracture pressure. That is all the models are geological specific. All the predictive methods use leak-off test results to obtain their parameters. It is reasonable that a big mistake might occur if LOT results contain cement partings.

In the chapter, the mechanism of cement parting is studied. Factors affecting cement parting will be discussed, and model to predict the factors will be presented.

#### **6.1 Contact Stress Model**

Cement parting is a possible way around a casing shoe. What factor determines this kind of fracture. This kind of study is rather new since cement leak is generally regarded as through pre-existed channels in cement annulus.

### **6.1.1 Contact Stress Concept**

To seal the annulus between casing string and rock, cement slurry is pumped into the annulus. The quality of the cement seal depends on the cement cohesive strength to casing string and rock, and the compressive stress between cement and casing string as well as cement and rock. The cement cohesive strength is a property of the cementing slurry. The compression stress, or contact stress defined by Wojtanowicz and Zhou (1998), results from the cement setting process.

It is the compressive stress that seals the annulus between casing and formation. The idea is the same as most the seals in our daily life. A pressure is usually applied on a seal to make the seal better. The higher the pressure on the seal, the better the seal is. The pressure applied on a seal is simple for most of mechanical sealing part. However, to handle the contact stress between cement and casing or cement and rock is much difficult since it is not only dependent on the hydraulic pressure of cement slurry before cement setting but the setting process.

Formation creep can also increase the contact stress with time. However, the increase by creep is ignored here since leak-off test is generally conducted shortly after cementing.

### **6.1.2 Cement Slurry Pressure Reduction**

The pressure at casing shoe gets its maximum value at the time of setting cement top plug. The hydraulic pressure will decrease during cement setting due to cement volume reduction, filtration and gelation. Sutton et al. (1984) proposed the first model to estimate the pressure reduction by assuming uniform distribution of shear stress along casing string and rock surface and using static gel strength (SGS) instead of

shear stress. Chenevert and Jin (1989) developed a more detailed model by giving a differential form of force balance. Prohaska et al. (1993) improved the previous work by considering the influence of shearing, temperature and pressure on the development of SGS. Zhou and Wojtanowicz (2000) presented a new model using compressibility model and including the effect of slurry expansion by geothermal heating, casing expansion by annular pressure reduction and temperature increase, and wellbore contraction due to annular pressure decrease.

### **6.1.3 Mathematical Model**

During cement setting, cement matrix develops. It is the developed matrix that supports the casing and wellbore, and seal the annular, since physically the pore pressure in the set cement should fall and get the pore pressure of the formation at the same place of interesting by the communication through pores. The cement slurry still behaves like liquid until developed cement compressive strength exceeds same value. At the value (500 lbf/100ft<sup>2</sup> for most researcher), the matrix becomes strong enough to support further pressure change. Once the matrix is formed, the further pressure reduction mainly comes from its internal pore pressure.

Appleby and Wilson (1996) proved this concept in their experimental tests. Therefore, the final contact stress between the developed matrix and the rock surface is the effective hydraulic pressure when the cement strength has developed to the critical value.

Unlike the pressure reduction in upper annular column, cement volume reduction could be partly compensated by the elastic elongation of casing string. Appendix D gives the derivation of the final pressure reduction at casing shoe by

considering cement compressibility, wellbore contraction, filtration and casing elastic elongation.

$$\Delta p_{de} = \frac{1}{\frac{A_{ww}(D_{cas} - 0.5D_t) + A_{oc}(D_{cas} + 0.5D_t)}{2A_{cs}E_{cas}\Delta h} + C_{cem} + \left(\frac{3}{E_{form}}\left(1 + \frac{d_{ww}}{48\Delta h}\right)\right)} K_{loss} \quad (6.1)$$

Where  $\Delta p_{de}$  = pressure reduction at cement critical strength;  $K_{loss}$  = cement slurry volumetric loss rate;  $C_{cem}$  = average cement slurry compressibility;  $E_{cs}$  and  $E_{form}$  = Young's modulus of casing string and rock at bottom hole;  $\Delta h$  = the open hole height below casing shoe for cementing;  $D_{cas}$  and  $D_t$  = heights of casing string and tail cement slurry.  $A_{ww}$ ,  $A_{cs}$  and  $A_{oc}$  = areas of wellbore, cross-section of casing string and outer casing string.

During displacement of cement slurry, the bottom hole pressure increases. It reaches the maximum value when top plug is bumped. The pressure on the top plug will decrease after stopping. The bottom hole pressure will make the casing string move up a little bit for the pressure difference between the plugs. Since the elasticity of casing string is so strong that the displacement is negligible. Initial pressure at casing shoe,  $P_{max\ cs}$ , is the pressure at casing shoe when cement has been just placed. It's value can be estimated from the fluid column in casing annular (Bourgoyne et al, 1990).

$$p_{max\ cs} = p_o + 0.052 \sum_{i=1}^n \rho_i (D_i - D_{i-1}) \quad (6.2)$$

Where  $p_{max\ cs}$  = hydrostatic pressure at casing shoe;  $p_o$  = formation pore pressure at casing shoe;  $D$  = height of slurry;  $i = i^{th}$  slurry section.

This maximum annular pressure will decrease during cement initial setting. As shown in the derivation of Eq. (6.1), compressive pressure in the cement and the cement-formation contact pressure are equal and expressed as

$$p_c = p_{\max cs} - \Delta p_{de} \quad (6.3)$$

Where  $p_c$  = contact pressure.

## 6.2 Cement Parting Pressure

The compressive stress between cement and rock is the major issue to be discussed here, since it dominates the seal in shallow marine sediment. As shown in Fig. 6.1, face CD is the contact surface of cement and formation. The bond along CD

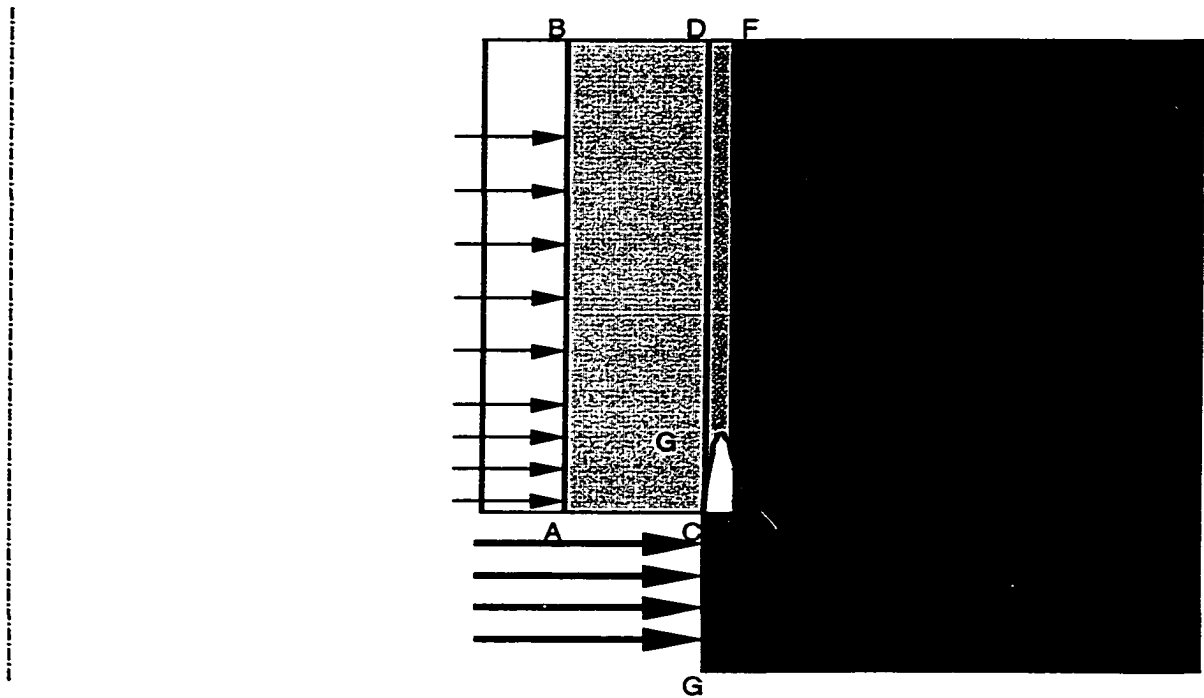


**Figure 6.1** Cement parting.

depends on the properties of cement. CDEF is a thin layer of formation stuck to the cement. EF is the boundary between the stuck thin layer and formation whose

connection strength is determined by the cohesive strength of the formation. When wellbore pressure acts on face CG, the contact stresses along CD and EF are reduced first and may go to zero for increasing wellbore pressure. The contact stress reduces to tension as wellbore pressure increases further, but fracture does not occur until the tension overcomes the tensile strength of the rock. The tensile strength in shallow sediment (shale and clay) is small. It is about a few *psi* for most shallow soft sediments. As the result, an annular fracture will be formed along EF no matter how strong the bond between cement and formation is. Therefore, in shallow marine sediment the initiation of cement fracture depends on the value of compressive stress (contact stress) between the rock and cement.

Cement fracture will be initiated when wellbore pressure at the casing shoe is larger than the sum of contact pressure and tensile strength. It should be stressed, however, that this fracturing mechanism implies that wellbore fluid could penetrate into the rock matrix around the cement at the casing shoe. Also, the penetration occurs without pressure drop across the fluid loss zone. This assumption holds only when there is a micro-fracture at the casing shoe, such as EG in Fig. 6.1. The condition of cement fracture,  $p_{cf}$ , is  $p_c + S_{ten}$ . Where  $S_{ten}$  is the smallest of the four values of tension strengths: cement, cement bond with casing, cement bond with formation and formation. Generally, the value of formation tensile strength is the smallest of the four in shallow marine sediment.

If there is no penetration of wellbore fluid into the rock matrix, pressure value greater than contact stress is needed to initiate cement fracture. Without penetration, wellbore pressure must first deform the open hole wall and transfer upwards to the

bond of cement and rock to reduce the contact stress there to zero. According to Wojtanowicz and Zhou (1998), wellbore pressure increases by 3.5 *psi* is needed to reduce the contact stress by one *psi* for non-penetration case.

In actual wellbores there is always some degree of wellbore fluid loss into the rock. Thus, cement fracture pressure should be in the range of

$$\begin{aligned}
 p_{\min cf} &\leq p_{cf} \leq p_{\max cf} \\
 p_{\min cf} &= p_c + S_{ten} \\
 p_{\max cf} &= n(p_c + S_{ten} - p_p) + p_p
 \end{aligned}
 \tag{6.4}$$

Where  $n$  is around 3.5. The sum of contact pressure and tensile strength is the minimum cement fracture pressure,  $p_{\min cf}$ , for complete penetration case. Wellbore pressure smaller than this value can not initiate a cement fracture. In all, critical condition for cement fracturing is

$$p_{cf} = m(p_c + S_{ten} - p_p) + p_p
 \tag{6.5}$$

Where:  $1 \leq m \leq 3.5$ , and the coefficient  $m$  depends upon the degree of fluid penetration.

### 6.3 Field Example

To illustrate the use of the proposed model, field examples are given. A well with sea water depth of 387 ft was drilled to 720 ft and casing string was set at 712 ft. Rotary table was 95 ft above sea water. The well size was 36" and casing size 30". As shown in Fig. 6.2, the tail cement slurry got the depth of 634 ft and lead cement slurry was pumped the sea floor. No leak-off test was conducted after setting casing.

Figure 6.3 is the same well but was drilled to 3468 ft. Wellbore size was 26" and casing string of 20" was set at 3439 ft. The open hole height below casing shoe was 29 ft. Tail slurry was pumped to 492 ft above the casing shoe.

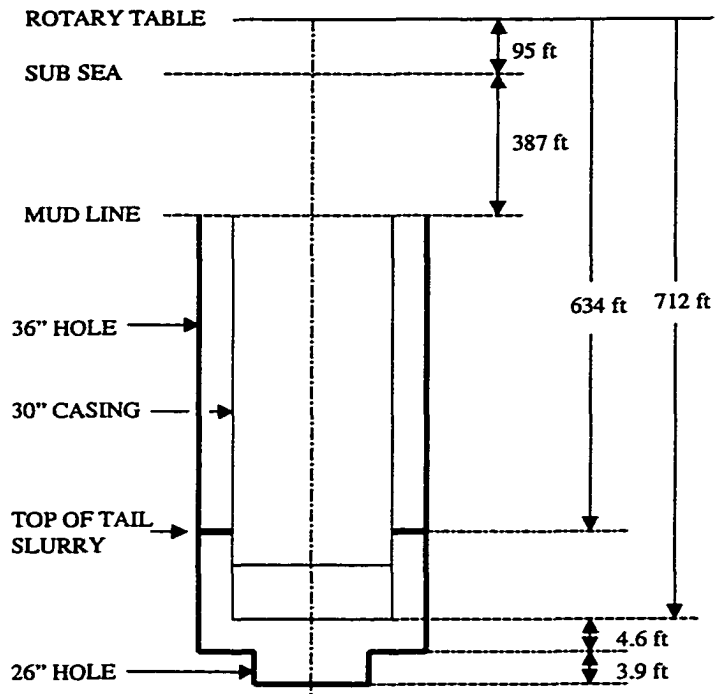


**Figure 6.2 Case 1 (30") well configuration.**

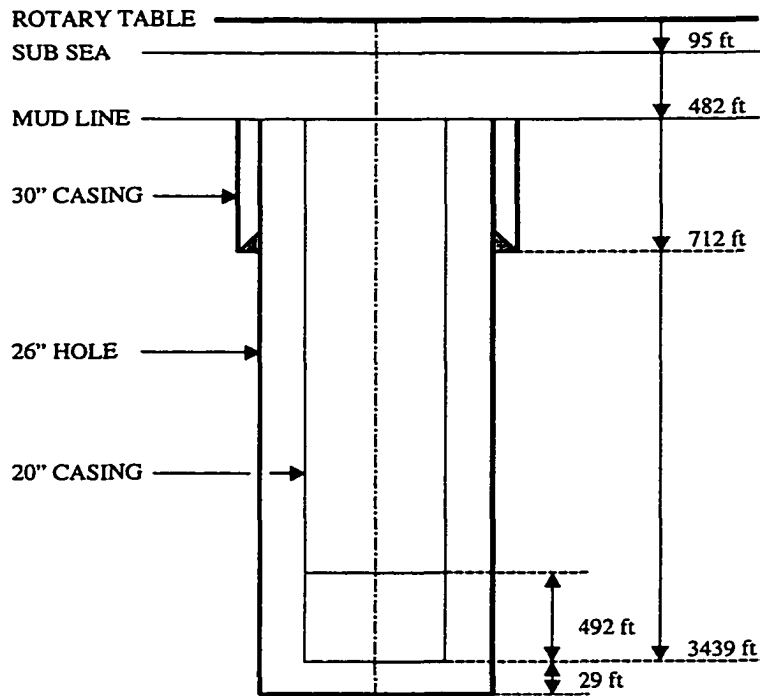


**Figure 6.3 Case 2 (20") well configuration.**

Tables 6.1 gives the properties of 30” casing string case and 20” casing string case needed for calculation.

**Table 6.1 Example data.**

Parameters	Case 1 (Fig. 6.2)	Case 2 (Fig. 6.3)
Casing OD, inches	30	20
Casing ID, inches	29	18.73
Well Diameter, inches	36	26
Lead Slurry Density, ppg	13.2	15.8
Tail Slurry Density, ppg	13.2	15.8
Mud Density, ppg	9.8	10
Sea Water Density, ppg	8.6	8.6
KB Over Sea Level, ft	95	95
Sea Water Height, ft	387	387
Annular Mud Height, ft	0	0
Lead Slurry Height, ft	160	2469
Tail Slurry Height, ft	70	492
Effective Open Hole, ft	6.6	28.6
E <sub>c</sub> , psi	30E6	30E6
E <sub>f</sub> , psi	1E4	2E5
C <sub>c</sub> , 1/psi	3E-5	3E-5
Volume Loss, %	1	3

The effective open hole is a vertical distance from the casing shoe to the hole bottom with the same borehole size. For an open hole with two borehole sizes (Fig. 6.2) the effective open hole is the total volume divided by the area of the borehole outside casing shoe.

$$\Delta h = \Delta h_1 + \frac{d_2^2}{d_1^2} \Delta h_2 \quad (6.6)$$

The effective open hole in Fig. 6.2 is:  $\Delta h = 4.6 + (26*26/(36*36))*3.9 = 6.6$  ft.

Volume loss during forming cement matrix is relatively small in shale. Here, 1% volume loss has been used for Case 1, i.e. casing set in shale, and a 3% volume loss for Case 2, i.e. casing set in sand. Eq. 6.2 was used to calculate pressure at casing

shoe after cement placement. Equation 6.1 was used to calculate bottomhole pressure reduction. The calculated results are listed in Table 6.2.

**Table 6.2 Cement fracture calculations: Case 1 (shale) and Case 2 (sand).**

Parameter	30" casing Case 1 (Fig. 6.2)	20" casing Case 2 (Fig. 6.3)
$P_{max\ cs}$ , psi	413	2350
$P_{mcs}$ , psi	363	1788
$\rho_{e\ max}$ , ppg	11.2	13.1
$P_{de}$ , psi	27	142
$P_c$ , psi	386	2208
$\rho_{ec}$ , ppg	10.4	11.0

Table 6.2 shows that, for leaching casing shoe (complete penetration case), cement fracture may occur if mud pressure is greater than 10.4 ppg when drilling from 712 ft to 3439 ft. There was no leak-off test conducted for the casing shoe at 712 ft. However, density of mud used for drilling this well section was 10 ppg which was less than the minimum cement fracture pressure. Actually, cement fracture initiation pressure should be higher than the estimated 10.4 ppg since the formation was shale, i.e. non-penetration rock.

For Case 2, according to the designer, the casing shoe should sustain 12 ppg mud pressure. It was required that the leak-off test pressure there should be at least 350 psi at the casing shoe by 10.0 ppg mud to prevent gas kick while drilling the next well section. From Table 6.2, the estimated cement fracture pressure for Case 2 is 11.0 ppg. This may be the actual cement fracture pressure since the casing shoe was set in a sand which is a penetrated rock. Since the estimated value of cement fracture pressure is lesser than 12 ppg, a cement squeez job may be needed to increase contact stress,  $p_c$ , and make the cement fracture pressure higher than 12 ppg.

The leak-off test plot for the 20" casing (Case 2) is given in Fig. 6.4. Three leak-off tests were conducted and the leak-off pressures were 210 psi, 185 psi and 190 psi respectively with 10 ppg mud. Fracture pressure at casing shoe was calculated from Eq. 6.7 and equivalent mud density from Eq. 6.8.

$$p_f = 0.052\rho_m(D_K + D_w + D_f) + p_{LOT} \quad (6.7)$$

$$\rho_{em} = \rho_m + p_{LOT} / (0.052(D_K + D_w + D_f)) \quad (6.8)$$

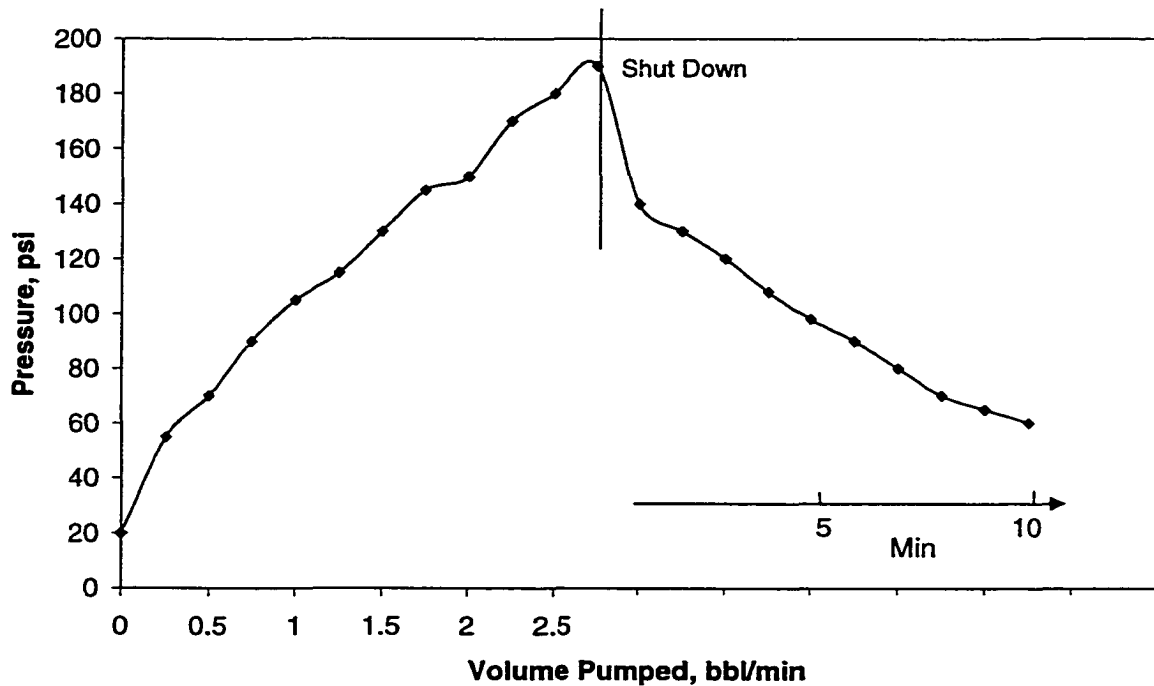


**Figure 6.4** LOT at 20'' casing shoe.

The tested fracture pressures in ppg were 11.2 ppg, 11 ppg and 11.1 ppg respectively which are in a good agreement with the calculated pressure of 11 ppg as shown in Table 6.2. Note that the only assumption taken for these calculations was that of the volumetric loss of volume during cement slurry setting.

The required leak-off pressure was 350 psi with 10.0 ppg mud to get a critical mud weight of 12 ppg. Squeezing cement was used to increase the leak-off pressure to

above 12 ppg. However, according to Eq. 6.1 the pressure reduction could be increased if a appropriate planning were used. The leak-off pressure at the casing shoe will increase if increase casing shoe maximum pressure, control cement slurry fluid loss, minimize the open hole section below casing shoe and so on.

As example, if we change the open hole height to 10 ft and keep all the other parameters constants (Table 6.1), using the same formulas and procedures as those used for Table 6.2, the calculated contact pressure is 12.0 ppg. Actual leak-off pressure should be greater than the value according to Eq. 6.4. Therefore, if the casing shoe open hole height were planned as 10 ft instead of 28.6 ft, one leak-off test would be enough and squeezing cement job could be saved.

Cement parting under wellbore pressure was explained theoretically and formulated in equation as stated previously. The phenomenon was proved by Upchurch (1999) and called “halo” instead of cement parting here. After cement had cured, an ultrasonic imager cement bond mapping tool was used to map the cement bond and ensure no channels exist in the cement sheath between the casing and formation. The author found cement channels occurred after stimulation for soft and unconsolidated formation.

#### **6.4 Sensitivity Analysis**

From Eq. 6.1, pressure reduction at the casing shoe during the transition of cement slurry from liquid to solid depends on many factors. These are height of casing shoe off bottom, slurry volumetric loss and compressibility, wellbore size and Young’s modulus, length, size and Young’s modulus of casing string.

Major factors affecting pressure reduction are fluid loss (slurry volumetric loss) and pressure compensation effect of the casing string (elongation, borehole wall

inside moving, cement slurry compressibility, and hole bottom upward moving. The four compensations are listed as follows (derived in Appendix D).

1. Casing string compensation:  $K_{csg} = \frac{A_w(D - 0.5D_t) + A_{oc}(D + 0.5D_t)}{2A_c E_c \Delta h} \Delta p_{de}$ .
2. Borehole wall compensation:  $K_w = \frac{3\Delta p_{de}}{E_f}$ .
3. Borehole bottom compensation:  $K_B = \frac{3\Delta p_{de} d_w}{4E_f \Delta h}$ .
4. Slurry compressibility compensation:  $K_c = C_c \Delta p_{de}$ .

Analyzing the above formulas indicates that the casing string compensation effect depends on casing size and tail slurry height. The longer and thinner the casing string is, the bigger the compensation effect becomes. Hence, casing string will dominate the effect in deep well. Wall compensation comes from the elastic deformation of the formation at the casing shoe. The larger the Young's modulus, the lesser the compensation. The hole bottom compensation effect is  $d_w/(4\Delta h)$ -times small than that of the borehole wall. Thus, it can be ignored for general effective open hole height. In all, wall compensation should be a major factor in very shallow depth since Young's modulus is generally smaller at shallow depth.

Table 6.3 lists the compensation of for the examples of case 1 and case 2.

**Table 6.3 Compensation sensitivity in 30" and 20" examples.**

	$K_{csg} / K, \%$	$K_w / K, \%$	$K_B / K, \%$	$K_c / K, \%$
30" Casing Shoe	5.5	77.9	8.9	7.8
20" Casing Shoe	44.9	18.3	0.4	36.5

## **CHAPTER 7**

### **MODELING LEAK-OFF TEST IN SHALLOW MARINE SEDIMENTS**

Chapters 4 studied the fractures around a wellbore analytically. Chapter 5 analyzed numerically the deformation and fractures of a wellbore including the effect of casing string, cement and bottomhole. Drilling fluid may leak through the bonds of cement and rock. The kind of fluid loss is called fracturing since it is produced by higher hydraulic pressure to distinguish the fluid loss through nature existed channels in or around cement. The previous analyses improve the knowledge of fracture in shallow marine sediment (SMS).

As discussed in Chapter 2, Chenevert and McClure (1978) presented the first model of leak-off test. Their model considered the whole mud in a well during LOT. A linear relation of pressure versus pumped volume was given proved by most of the LOTs. Almeida (1986) studied systematically leak-off test and presented the whole compressibility concept including mud compressibility, wellbore expansion, uncased casing expansion, filtration. Similar model was proposed by Hazov and Hushudov (1993). All the models give a linear relation between pressure and pumped volume which reflects the regular LOT results. Using Darcy's law to pre-existed channels, Altun (1999) modeled the non-linear behavior occurred sometimes in deep wells.

The above models were proposed to model LOTs in deep wells where linear relation of pressure versus pumped volume is the regular cases. However, as shown in Chapter 3, LOT curves in SMS are much more complex with a general non-linear behavior. The non-linear behavior in SMS could not explained as pre-existed channels or cracks since no one believe bad cementing always occurs in shallow. Based on our

analytical and numerical results, the model of LOT in SMS will be presented in the chapter.

### 7.1 Wellbore Expanded Volume

Elastic wellbore expansion has been discussed by some of the above authors. It is presented here since the wellbore in shallow generally has a plastic annular around it, as shown in Fig. 7.1. The deformation of such a wellbore with a plastic zone should be studied. Also, the models of elastic wellbore expansion are not satisfied.

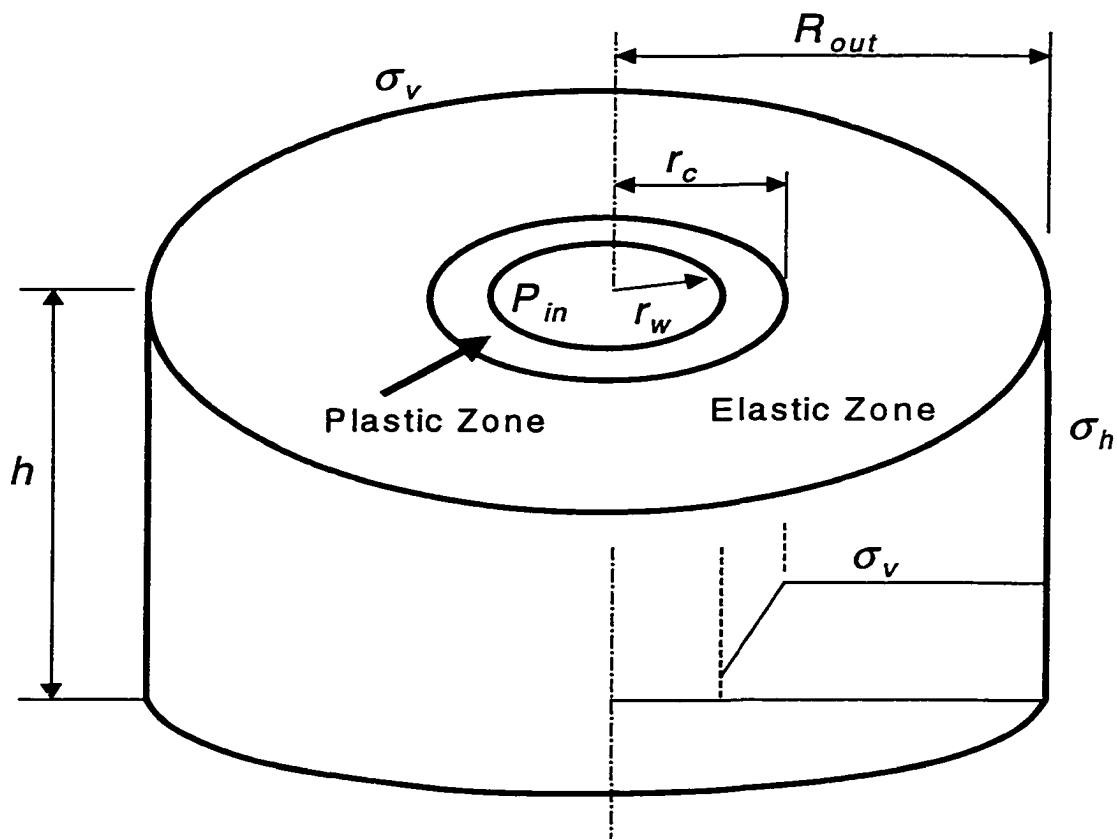


**Figure 7.1** Expansion of wellbore with plastic zone is controlled by outer elastic zone.

In SMS, a plastic zone is generally formed around the wellbore due to drilling operation. In the plastic zone, vertical stress  $\sigma_v$  reduces significantly from its in-situ value to a small value at wellbore wall (Risnes et al., 1982, Wojtanowicz and Zhou,

1998). Some operators believe that the deformation of a wellbore wall with a plastic zone is large enough to explain everything: the non-linear pressure-volume relation, the large volume pumped, and the volume returned. However, theoretical calculations based upon finite element analysis shows this is a wrong concept.

An example of a wellbore with a plastic zone is shown in Fig. 7.1. The rock has Young's modulus of  $1.04 \times 10^5$  psi, Poisson's ratio of 0.3, cohesion strength of 31.6 psi, and internal friction angle of 25.4 degree. The rock cylinder in Fig. 7.1 has an internal radius of  $r_w=12$  inches, external diameter of  $R_{out}=132$  inches, and a height of  $h=60$  inches. The overburden stress (vertical stress)  $\sigma_{z0}$  is 600 psi, in-situ horizontal pressure,  $\sigma_h=257$  psi, and effective wellbore pressure (the difference wellbore pressure and formation pore pressure),  $p_w=0$ . Based upon Drucker-Prager yield criterion and associated flow rule (Chen and Han, 1988), the calculated radial size of the plastic zone around the wellbore is  $r_c=21$  inches.

During a simulated LOT, the wellbore wall expanded linearly with increasing wellbore pressure, and the radial displacement of the wall was about 0.109 inches when the wellbore pressure was 600 psi. To compare with purely elastic well deformation (no plastic and no formation fracture), the same rock cylinder was considered with the same values of Young's modulus using the same wellbore size and pressure loads as those for the plastic wellbore. The deformation of a pure elastic wellbore showed a displacement of 0.104 inches.

The displacement of a well with a plastic zone was calculated by finite element method, and the elastic displacement was calculated from Eq. (7.1) derived in Appendix E, as

$$u_w = \frac{3\Delta p_w r_w}{2E} \quad (7.1)$$

Since the elastic and plastic wellbore deformations are almost the same, we conclude that the effect of plastic zone deformation on wellbore expansion is negligible. Actually, the phenomenon is not too hard to see. Physically, plasticity means a body can deform easily while its volume is almost constant (Obert and Duvall, 1967, Chen and Han, 1988). That is no radial displacement if fixing the outside boundary of the plastic annulus. The expansion depends on the deformation of the elastic zone outside the plastic zone. Therefore, the displacement of a well with a plastic zone could not be large different from that of a elastic well. In conclusion, the volume of wellbore expansion ( $\Delta V_w$  in gallon) can be estimated from Eq. 7.2 by using elastic displacement  $u_w$  from Eq. 7.1 as,

$$\begin{aligned} \Delta V_w &= 2\pi r_w u_w H * 12 / 231 \\ &= 0.49 r_w^2 H \Delta p_w / E \end{aligned} \quad (7.2)$$

## 7.2 Loss into Rock

Drilling fluid losses into rock pores through rock/mud interface due to filtration. Filtration mechanism and formulas are well addressed such as by Roodhart (1985) and Settari (1985). In words, static model and dynamic models are widely accepted models dealing with filtration into porous media.

The thickness of mud cake will increase with time during the process of filtration. However, drilling fluid flow will erode the cakes and decrease the cake thickness. Once a steady state is reached that is characterized by constant filtration velocity, a dynamic filtration is set up. Darcy's law is the best formula to describe

dynamic filtration. That is the filtration loss is proportional to the pressure difference between drilling mud and formation pressures ( $p_w = p_{wo} - p_p$ ), i.e. wellbore effective pressure. Flow rate through a wellbore with wall area of  $A_{fil}$  and open wall height of  $\Delta h$  and wellbore diameter of  $d_w$  is

$$q_{fil} = CA_{fil} p_w \nu / k_c \quad (7.3)$$

Where  $\nu$  = mud apparent viscosity;  $k_c$  = permeability through mud cake. The pressure difference  $p_w$  increases with time as leak-off pressure increases.  $C$  is the coefficient of the relation. It should be a function of mud thickness.

Haberman et al. (1992) measured in-situ filtration rate. Their overall average rate was about 2.0 gal/min (range of 0.8 to 3.2 gal/min). The fluid loss was estimated to be about 5 to 10 times lower than the drilling mud API tests, 100 to 200 lower than the API cement fluid loss from the slurries with fluid-loss additives, and more than 1,000 times lower than the slurries without fluid-loss control. The rate of 0.0002 gal/ft<sup>2</sup>/min was the average value. The initial hydrostatic pressure of the slurry column was  $0.82 \times 8754 = 7178$  psi and the pore pressure at 8754 ft is about 3790 psi. An average coefficient of  $D = 5.9 \times 10^{-8}$  gal/ft<sup>2</sup>/min/psi is calculated and used in the following simplified formula

$$q_{fil} = DA_{fil} p_w \quad (7.4)$$

Another filtration is so called static filtration. Filtration volume is a function of square root of the time for this kind of static filtration.

$$V_w = V_{spt} + 2C_w \sqrt{t} \quad (7.5)$$

Where  $V_w$  is the filtration volume per unit area,  $V_{spt}$  represents spurt loss,  $C_w$  is well filtration coefficient.

$$C_w = \sqrt{\frac{k_c \alpha p_w}{2v}} \quad (7.6)$$

Where  $\alpha$  = mud cake deposition constant.

Differentiating Eq. 7.5 and writing it as filtration rate by multiplying filtration area yields

$$q_{fil} = C_w A_{fil} / \sqrt{t} \quad (7.7)$$

### 7.3 Plastic Fracture in Plastic Zone

Gidley et al. (1989) found out that shallow formation fractures are horizontal. Wojtanowicz and Zhou (1998) proved analytically the fact. A horizontal fracture is shown as Fig. 7.2.

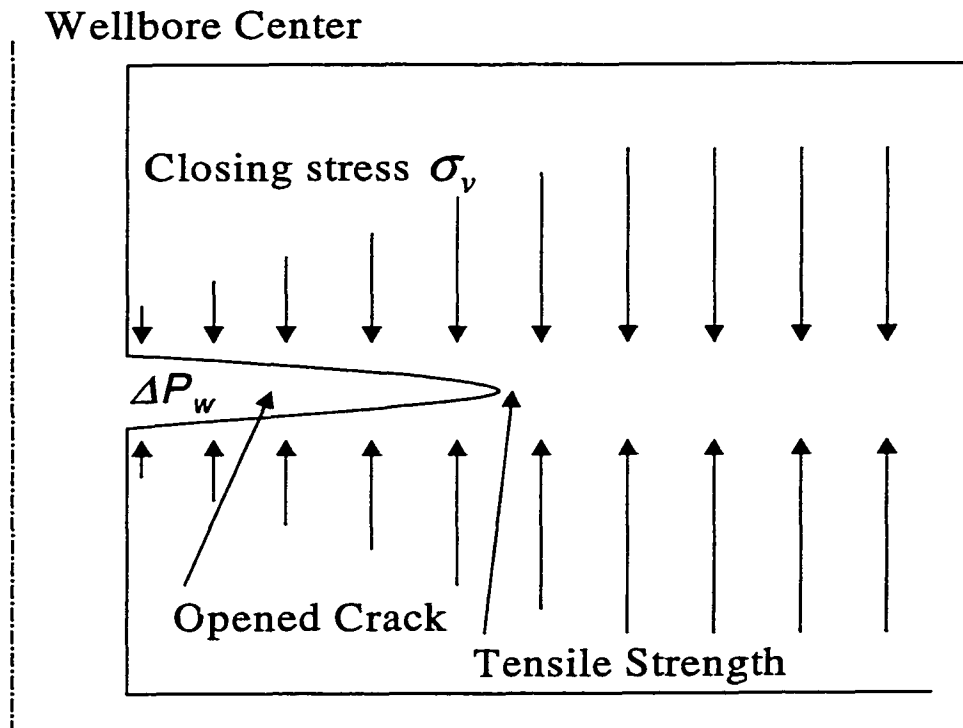


**Figure 7.2 Horizontal (plastic, non-penetrating) fracture in plastic zone around wellbore.**

It is a common assumption that micro-cracks exist around a wellbore. As shown in Fig. 7.2, the opening of a crack depends on the closing stress on the crack and the tensile strength around the tip of the crack. The larger the closing stress, the higher the fluid pressure needed to part it. The width of the opened crack depends on the displacements of the crack's two sides which are controlled by the rock's Young's modulus for infinite rock (Sneddon and Lowengrub, 1969).

For horizontal fractures, vertical stress  $\sigma_v$  is the closing stress. Since the vertical stress increases from small value at the wellbore wall to the overburden stress at the outer (elasto-plastic) boundary of the plastic zone (Fig. 7.1), low wellbore pressures may initiate the fracture but the fracture will not propagate. To make the fracture propagate, wellbore pressure must be equal to the in-situ overburden pressure. For the value of wellbore pressure smaller than overburden, the fracture in a plastic zone is called plastic (or non-propagating) fracture (Wojtanowicz and Zhou, 1998).

The horizontal fracture will be extended and widened with increasing wellbore pressure. Eq. 7.8 gives the relation of the effective wellbore pressure with the space volume in the opened fracture. The equation is derived in Appendix F.

$$\Delta V_{ff}(R) = \frac{1}{110}(R^2 + r_w R - 2r_w^2)w(r_w, R) \quad (7.8)$$

Where,  $R$  = radial distance of the fracture tip from the wellbore center;  $R \leq r_c$ ,  $r_c$  = radial size of plastic zone (Eq. B.7 in Appendix B);  $w(r_w, R)$  = half of the crack width at the wellbore wall given by Eq. F.8 for  $r=r_w$  in Appendix F.

The crack width formula has been derived from the model of a penny-shaped crack (Sneddon and Lowengrub, 1969). The tensile strength of rock was considered as

small and was ignored in the penny-shaped crack model - an assumption particularly suitable for SMS. The distribution of a fracture width along a horizontal fracture is calculated from Eq. B.8 and shown in Figure 7.3.

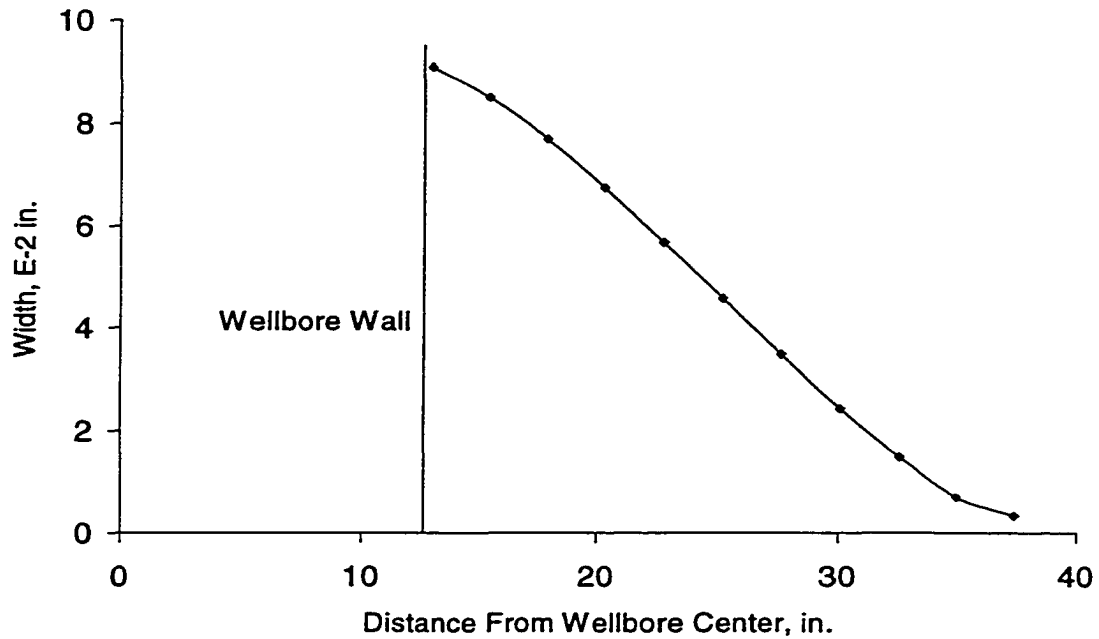


**Figure 7.3** Width of plastic fracture vs. radial distance.

As an example, a rock from the Gulf of Mexico at a depth of 389 ft subsea has properties as: Young's modulus - 32,915 psi; Poisson's ratio - 0.39; internal friction angle - 17.8; cohesion strength - 10.2; effective overburden stress - 133 psi; wellbore diameter - 26 inches; and initial wellbore effective pressure - 0. From Eq. B.7, the size of plastic zone is 37.4 inches away from the wellbore center. The maximum width of a plastic fracture is measured at the wellbore wall when the fracture tip reaches elasto-plastic boundary and the effective wellbore pressure equals the overburden stress. A computer program has been written for the width calculations. The calculations is as follows:

1. Calculate the tip position ( $R$ ) of the plastic fracture from Eq. F.5 for a given effective wellbore pressure;
2. Calculate the half width of the fracture at the wellbore wall from Eq. F.8 for  $r=r_w$ ;
3. Calculate fracture volume from Eq. 7.8.

A plot of the effective wellbore pressure versus fracture volume is shown in Figure 7.4. The maximum fracture width is 0.18 inches, and the maximum fluid volume in the fracture is 1.3 gallons. Also, the fracture initiating pressure is 28 psi from Eq. F.3.

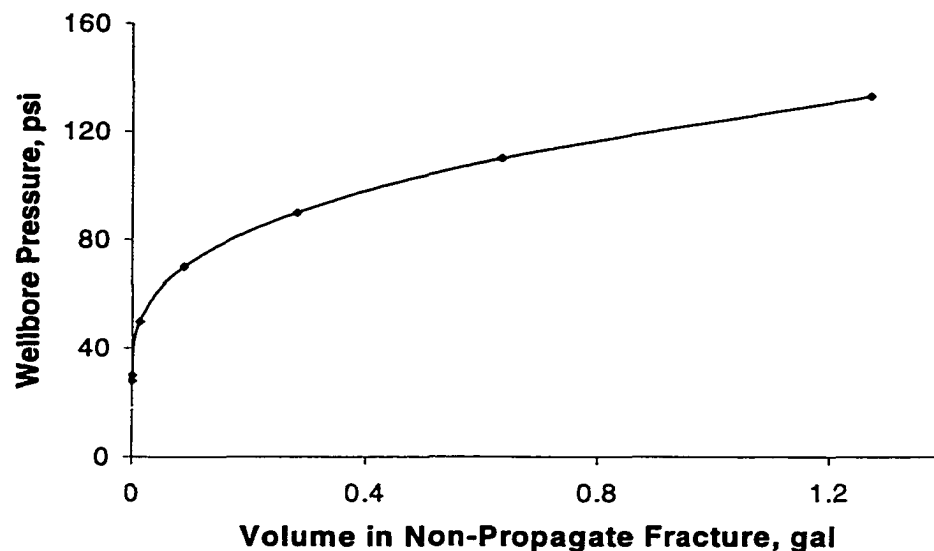


**Figure 7.4** Volume taken by rock fracture in plastic zone.

It is obviously from Figure 7.4 that the pressure build-up section of pressure versus volume is non-linear for a plastic fracture. However, the fracture volume is small. Plastic fracture will take larger volume of fluid only for very small value of the Young's modulus ( $E$ ) and/or large size of plastic zone ( $R$ ) as shown in Eq. F.8. The non-linear behavior may become severe when mud leaks off through the newly formed fracture surfaces to a permeable formation.

#### **7.4 Cement Parting between Cement and Rock**

To date, non-linearity of LOTs has been explained by assuming a pre-existed “cement channels” with certain size and length. Generally, the pre-existed channels in cement may result from bad cementing, excessive temperature change, or excessive pressure change inside the casing string (Nelson, 1990). For LOT, however, no high temperature change occurs in casing string and formation. Also, excessive pressure variation is eliminated by releasing surface pressure right after setting top plug during displacing cement. Therefore, bad cementing may be the major reason for the pre-existed channels for LOTs.

Pre-existed cement channels work as a conduit for drilling fluid. Drilling fluid would flow or “leak” through the channel to a shallow permeable formation (Poster, 1997, Altun et al., 1999).

Wojtanowicz and Zhou (1998) eliminated the “pre-existence” assumption and proved that cement fracture may be initiated by LOT even for perfect cement body (no pre-existed channels). The difference between pre-existed cement channel and annular cement parting is that the cement channel works as a fixed conduit while cement parting must be opened and propagated. Cement parting was proved by Upchurch (1999) from field test data.

The mechanism of cement parting is the same as that of rock fracturing, as shown in (Figure 7.2), with the closing stress equals the contact stress,  $\sigma_c$ , (Figure 7.5). As stated in Chapter 6, contact stress is developed during cement setting. Its value is the difference of cement slurry pressure before setting and the pressure loss during cement setting. The contact stress can be considered constant across the cement

sheath at the same depth. However, tensile strength around a crack tip could depend on the position of the crack within the sheath as explained below.

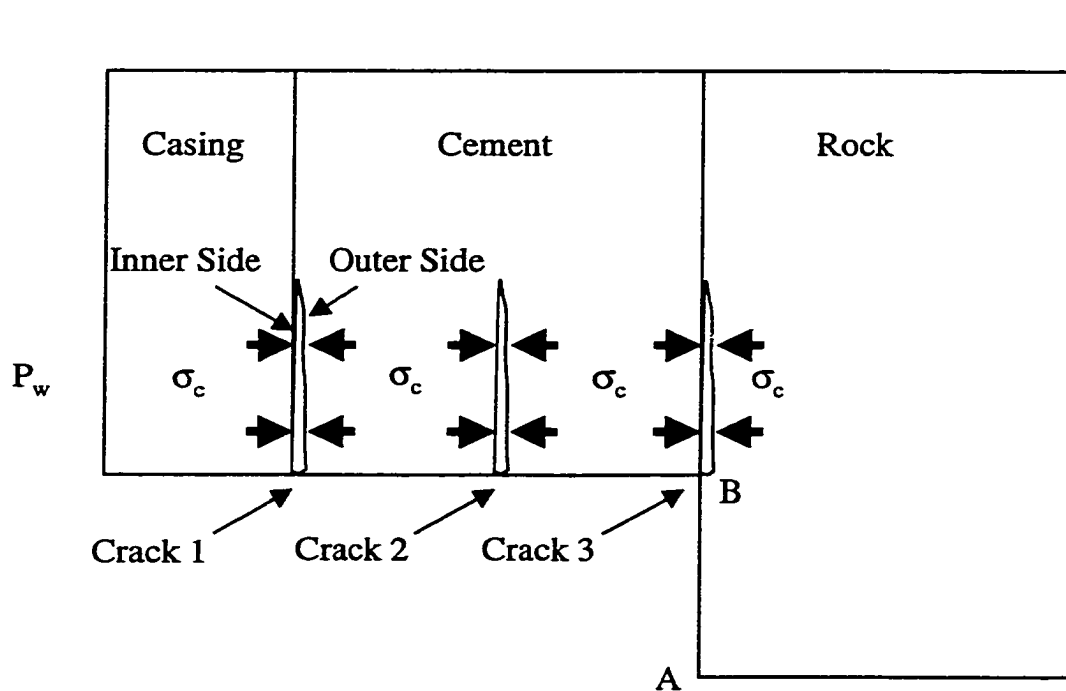


**Figure 7.5** Annular cement parting between cement and rock is opened by increasing LOT pressure.

Micro-cracks exist everywhere. As shown in Figure 7.5, Crack 1 is the micro-crack between the casing and the cement. Its tensile strength depends on the bond between the cement and the casing. Crack 2 a micro-crack is in the cement, and its tensile strength is the tensile strength of the cement. Crack 3 is a micro-crack between the cement and rock, and its tensile strength is the tensile strength of the rock and almost zero for SMS. Therefore, the connection between the cement and the rock is most likely the weakest of the three. Cement parting will be initialized and propagates along this surface between the cement and the rock.

Drilling fluid pressure will decrease along the cement parting due to friction pressure loss. Based on the equation of fluid flow in annular (Bourgoyne et al, 1991),

a relation between wellbore pressure and volume of the annular crack was derived as Eq. 7.9 as shown in Appendix G.

$$\Delta V_{cem} = \frac{r_w^4 (P_{LOT} - \sigma_c)^3}{E^2} \left( \frac{1}{\frac{\mu_p q E^2}{8262 (P_{LOT} - \sigma_c)^2 r_w^2} + \frac{\tau_y r_w}{75}} \right) \quad (7.9)$$

For example, a mud with plastic viscosity of 40 cp and yield point of 15 lbf/100 sq. ft is pumped into a 26" well during LOT at a rate of ¼ bbl/min. Also, Young's modulus of the rock is 32,915 psi, total compressibility is 52 psi/gal, and initial effective wellbore pressure and contact stress are zero. The calculated results are shown in Figure 7.6.

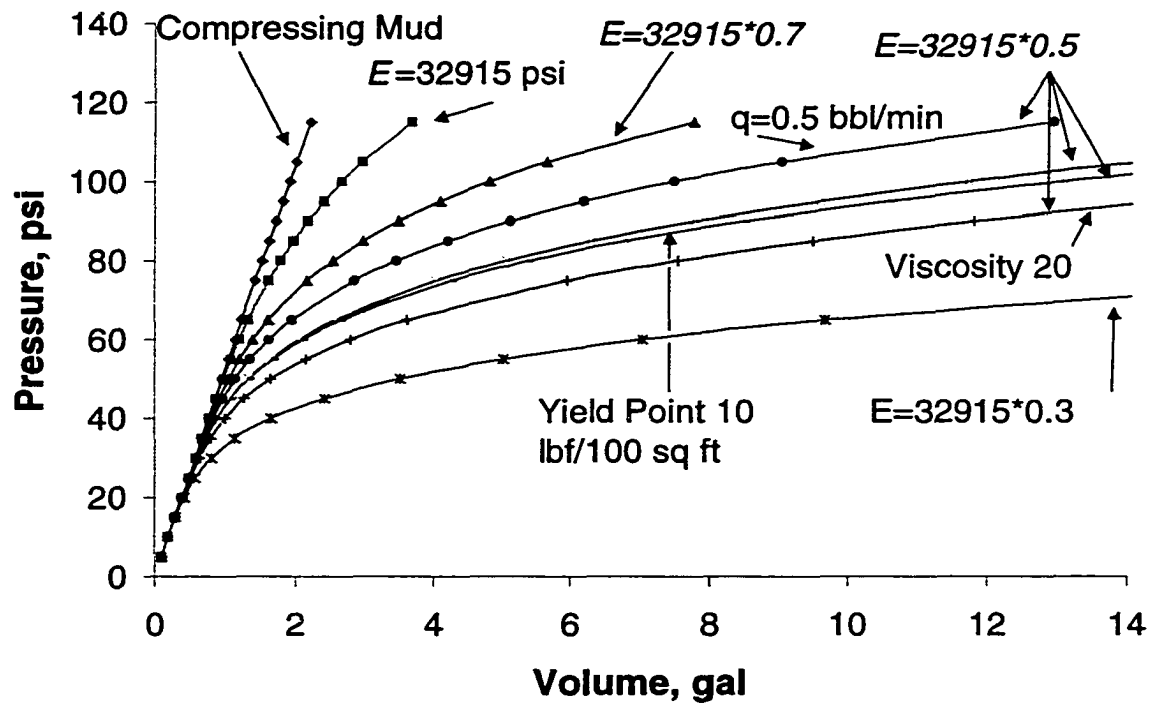


**Figure 7.6 Non-linear behavior of annular crack.**

It is obviously that cement parting makes the pressure-volume relation non-linear. The Young's modulus of the rock heavily affects the non-linear behavior. The

smaller the Young's modulus, the more curvature of the pressure-volume plot. Furthermore, pumping rate, plastic viscosity, and yield point of the mud also affects the curvilinear behavior of the pressure-volume plot.

The contact stress in Figure 7.6 is zero. However, the effect of the contact stress can be estimated by shifting the curves in Figure 7.6 upward by the contact stress value along the "compressing mud" line for penetrating drilling fluid.

### 7.5 Modeling Leak-off Test

Leak-off test monitors pressure versus pumped drilling fluid volume. The model of leak-off test is to set up a correlation between the pressure and the volume.

For any mud element  $V_i$ , the relation of its volume reduction  $\Delta V_i$  and the increased pressure  $\Delta p_i$  can be expressed by basic fluid compressibility equation:

$$C_{mi} = \frac{1}{V_i} \frac{\Delta V_i}{\Delta p_i} \quad (7.10)$$

Where  $C_{mi}$  = compressibility (1/psi) of the mud in element  $V_i$ .

The whole mud in a well  $V_0$  is the sum of all the elements in the well.

$$V_0 = \sum_{i=1}^n V_i = \sum_{i=1}^n \frac{\Delta V_i}{C_{mi} \Delta p_i} \quad (7.11)$$

Where  $n$  is the total number of elements.

If the pressure change  $\Delta p_i$  is the same  $\Delta p$  on every element in the well, Eq. 7.11 can be expressed as Eq. 7.12 provided that the mud compressibility is constant for all the mud elements in the well (no air effect, constant mud density) and mud friction in the well is negligible.

$$V_0 = \frac{\Delta V_p}{C_m \Delta p} \quad (7.12)$$

Where,  $\Delta V_p$  is the sum of all the compressed volume of every element. For leak-off test, it is the volume pumped into the well provided the well is rigid and no leak. Rewrite Eq. (7.12) gets

$$\Delta p = \frac{\Delta V_p}{C_m V_0} \quad (7.13)$$

Equation (7.13) states that pressure change of a well is proportional to pumped volume and inversely to total mud and mud compressibility. It is the basic equation used by Chenevert and McClure (1978) to model leak-off test. However, for an actual well, not all the pumped mud is used to compress the whole mud system. Some part of the pumped volume is lost through leak, some part flows into opened fracture, and some part takes the volume from wellbore expansion. Therefore, the pumped volume is divided into two parts: One is the lost volume including loss through penetration, wellbore and casing expansion, loss into fractures et al., and is called dumb volume ( $\Delta V_{dumb}$ ). Another is the volume used to compress the mud system which is called effective volume ( $\Delta V_{effe}$ ) in the dissertation.

Dumb volume consists of the volumes of casing expansion- $\Delta V_{cas}$ , open hole expansion- $\Delta V_w$ , leak through filtration-  $\Delta V_f$  (Almeida, 1986, Hazov and Hurshudov, 1993, Altun et al., 1999), and also the volume of cement parting- $\Delta V_{cem}$  and formation fracture- $\Delta V_{ff}$  as discussed in previous Chapters. Both cement parting and plastic fracture create new surfaces to drilling fluid, so drilling fluid will filtrate through the newly created surfaces. Two new filtration terms as expressed are  $\Delta V_{cemf}$  for the filtration volume through parted cement surface and  $\Delta V_{fff}$  for the leak through the surfaces of horizontal plastic fracture.

Filtration through parted cement surface and created horizontal fracture surfaces can be calculated as the formulas of Eqs. 7.3, 7.4 or 7.7 with the areas of  $A_{cemf}=2\pi r_w L$  for parted cement surface and  $A_{fff}=2\pi(R^2-r_w^2)$  for plastic fracture surfaces. Where  $L$  and  $R$  are the length of fracture for cement parting and plastic fracture respectively and are given in Eq. G.4b in Appendix G and Eq. F.5 in Appendix F.

$$\Delta V_p = \Delta V_{effe} + \Delta V_{dumb}$$

$$\Delta V_{dumb} = \Delta V_{cas} + \Delta V_w + \Delta V_f + \Delta V_{cem} + \Delta V_{cemf} + \Delta V_{ff} + \Delta V_{fff} \quad (7.14)$$

Substituting  $\Delta V_p$  of Eq. 7.13 by  $\Delta V_{effe}$  of Eq. 7.14 yields the pressure-volume relation (pressure build-up section of LOT curve).

$$\Delta p = \frac{\Delta V_p}{C_m V_0} - \frac{\Delta V_{dumb}}{C_m V_0}$$

$$\Delta p = \frac{\Delta V_p}{C_m V_0} - \frac{\Delta V_{cas}}{C_m V_0} - \frac{\Delta V_w}{C_m V_0} - \frac{\Delta V_f}{C_m V_0} - \frac{\Delta V_{cem}}{C_m V_0} - \frac{\Delta V_{cemf}}{C_m V_0} - \frac{\Delta V_{ff}}{C_m V_0} - \frac{\Delta V_{fff}}{C_m V_0} \quad (7.15)$$

In Eq. 7.15, the first term represents the compression of the whole mud by the pumped mud volume. The term gives a linear relation between the increased pressure and the pumped volume. The second term can be neglected for cemented casing string since casing expansion is constrained by cement and formation and thus the expansion volume is almost zero. The third term represents the effect of the expansion of the open-hole section below casing shoe. The pressure-volume relation of the term is also linear according to Eq. 7.2.

Terms of the fourth, the sixth, and the eighth in Eq. 7.15 represent mud filtration effect. Term four may give a smooth curving relation based on Darcy's law

(Altun et al., 1999) and a linear relation if the effect of mud cake is considered (Almeida, 1986). The fifth term represents the effect of the parting cement crack and gives a smooth curving pressure-volume relation starting from some lower wellbore pressure as shown in Fig. 7.6. The last term also gives a smooth curving relation reflecting the effect of non-propagation formation fracture (Fig. 7.4). It is also initiated when wellbore pressure gets some lower value.

## 7.6 Model Analysis

The leak-off test model presented in Eq. 7.15 considers the mud system compressibility, wellbore and casing expansion, and leak to rock through rock pores, cracks and pre-existed channels in cement. Also, two kinds of possible fractures (cement parting and horizontal fracturing) are included for shallow marine sediments. The model gives different pressure-volume relation under different situation since some items may dominate the volume change.

Pressure-volume relationship for LOT is,

$$\Delta P = \frac{\Delta V_p - \Delta V_{cas} - \Delta V_w - \Delta V_f - \Delta V_{cem} - \Delta V_{cemf} - \Delta V_{ff} - \Delta V_{fff}}{C_m V_0} \quad (7.15)$$

The first three terms in Eq. 7.15 gives a linear relation as discussed above. Term  $\Delta V_f$  represents the filtration into rock, pre-existed cracks in rock or channels in cement. The filtration into rock and loss into pre-existed rock cracks are generally small since the exposed rock section for leak-off test is short (in 15 ft) and mud cake is always there. Pre-existed cement channels may be the major reason for the term.

$\Delta V_{cem}$  is the space volume of cement parting and  $\Delta V_{cemf}$  is the filtration volume through the newly exposed wellbore wall in the cement parting.  $\Delta V_{ff}$  is the space

volume in the horizontal fracture and  $\Delta V_{ff}$  is the filtration through the newly formed fracture walls. The two fracture terms occur at some pressure threshold values. Therefore, the initial section of leak-off test plots may be

$$\text{Linear relation } \Delta p = \frac{\Delta V_p - \Delta V_{cas} - \Delta V_w}{C_m V_0} \text{ if no pre-existed channels;}$$

$$\text{Non-linear } \Delta p = \frac{\Delta V_p - \Delta V_{cas} - \Delta V_w - \Delta V_f}{C_m V_0} \text{ if there is large fluid loss through filtration.}$$

It should be pointed out that free gas in mud would affect the pressure-volume relation especially the initial part of LOT plot. Gas effect is ignored here since fewer gas zones exist in shallow. It is easier to de-gas in shallow section, and mud circulation for de-gasing before LOT is a required operation.

Cement parting or formation fracturing may occur once LOT pressure is increased to some value. The added fracture term makes the linear relation turn to curve or non-linear become severe non-linear.

Linear to curve:

$$\Delta p = \frac{\Delta V_p - \Delta V_{cas} - \Delta V_w - (\Delta V_{cem} + \Delta V_{cemf} \text{ or } \Delta V_{ff} + \Delta V_{fff})}{C_m V_0}$$

Non-linear to more severe curving:

$$\Delta p = \frac{\Delta V_p - \Delta V_{cas} - \Delta V_w - \Delta V_f - (\Delta V_{cem} + \Delta V_{cemf} \text{ or } \Delta V_{ff} + \Delta V_{fff})}{C_m V_0}$$

## 7.7 Developed Software\_LOTUMS

Software LOTUMS, leak-off test in upper marine sediments, is developed with MS Visual Basic 6.0 to simulate leak-off test in shallow marine sediments. The

theoretical background of the software is the mechanism of formation fracture and cement parting presented in the chapter. Basic equation used is Eq. 7.15. Formulas needed to calculate some parameters in the equations have all been addressed in previous Chapters.

Installation and usage of the software is presented in Appendix H. Users need to know the operation of MS Windows. Since LOTUMS is a software for leak-off test analysis, users are assumed understanding basic drilling engineering. Figure 7.7 shows the main interface of the software.

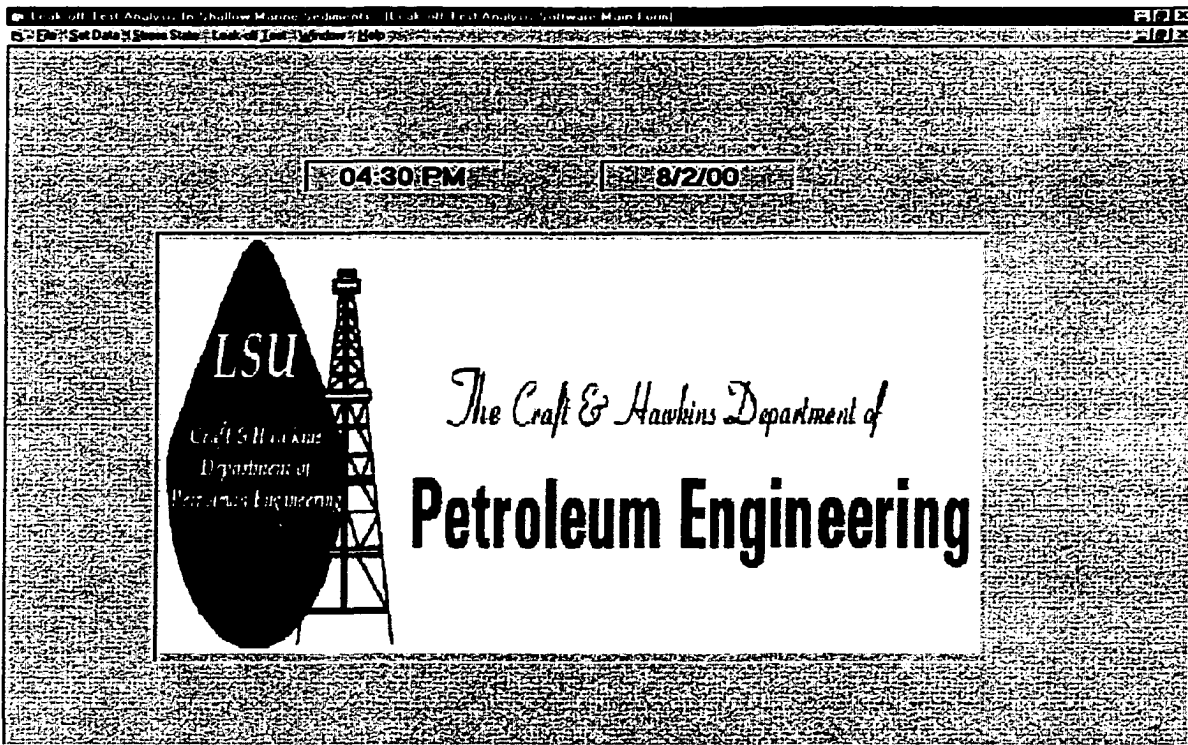


**Figure 7.7** Leak-off test software main interface.

Functions of the software are provided in the menus on the top of the window. To start analysis, users should input data. The software provides a set of default data for users. Users may use the default data to complete analysis during learning period.

Users may also input all the needed data one by one or change some data based on the default data. To observe detail effect of some factors, users may only change one or a group data and analyze the results. Data are organized in four forms: Well and Casing, Mud and LOT, Cement Slurry, and Rock. For example, Fig. 7.8 is the form of Mud and LOT.

Parameter	Value
Density (ppg)	
Compressibility (1/psi)	0.0000019
Viscosity (cp)	10
Yield point (lb/100 sq ft)	15
Mud cake permeability (md)	0.0001
Mud Cake Thickness (in)	0.04
Contact stress coefficient (1 to 3.5)	1.5
Pump rate (bb/min)	0.25
Open hole length (ft)	10
Mud loss coefficient (gal/min:psi:sq ft)	0.0001

**Figure 7.8 Data input form.**

The most important thing we need know before doing LOT analysis is the stress status of the formation, wellbore pressure, and formation pore pressure. Figure 7.9 is the form provided by the software for stress analysis. The command button “In-Situ Stress” on the form calculates the in-situ stress of the formation and put the results on the right hand of the button. On the right corner, pore and wellbore pressures at the bottom hole are also calculated. A function of “Plastic Analysis” is

provided. The software will do elastic and plastic analysis of the well based on the input data once users click the button. Results are outputted on the right side of the plastic analysis button. A graph is also drawn based on the analysis. Another important analysis is provided through the button of “Find Contact Stress”. As a response of clicking the button, the software will do cement slurry analysis and calculate the contact stress between cement and rock.

**Figure 7.9 Stress analysis form.**

The “Clear” button provided on the form (Fig. 7.9) clears all the results and plots on the form for further analysis. “Print” button is used to print out the results on a printer. If no printer is connected with the user’s computer or the user likes to print it on another printer, user could use the menu function “Set Printer” to select his printer as shown in Fig. 7.10. Figure 7.11 shows the form for fracture analysis.

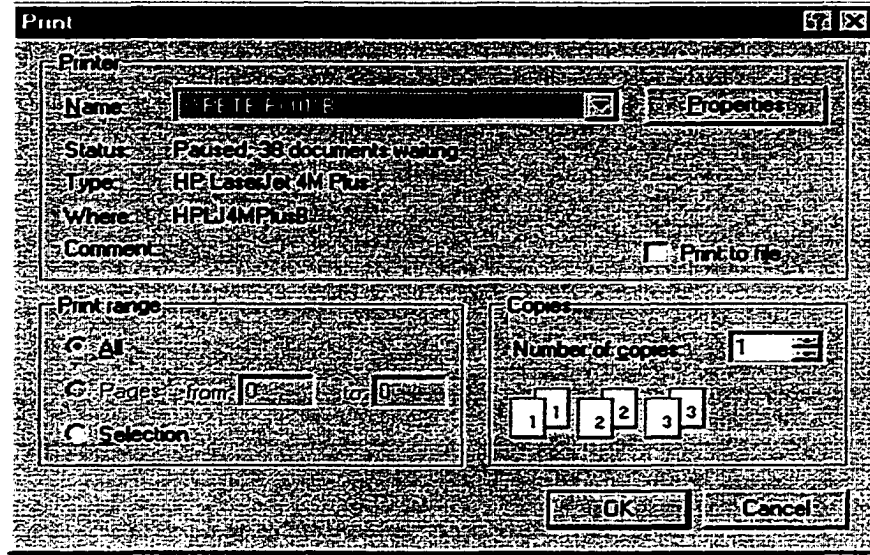


Figure 7.10 Set printer.

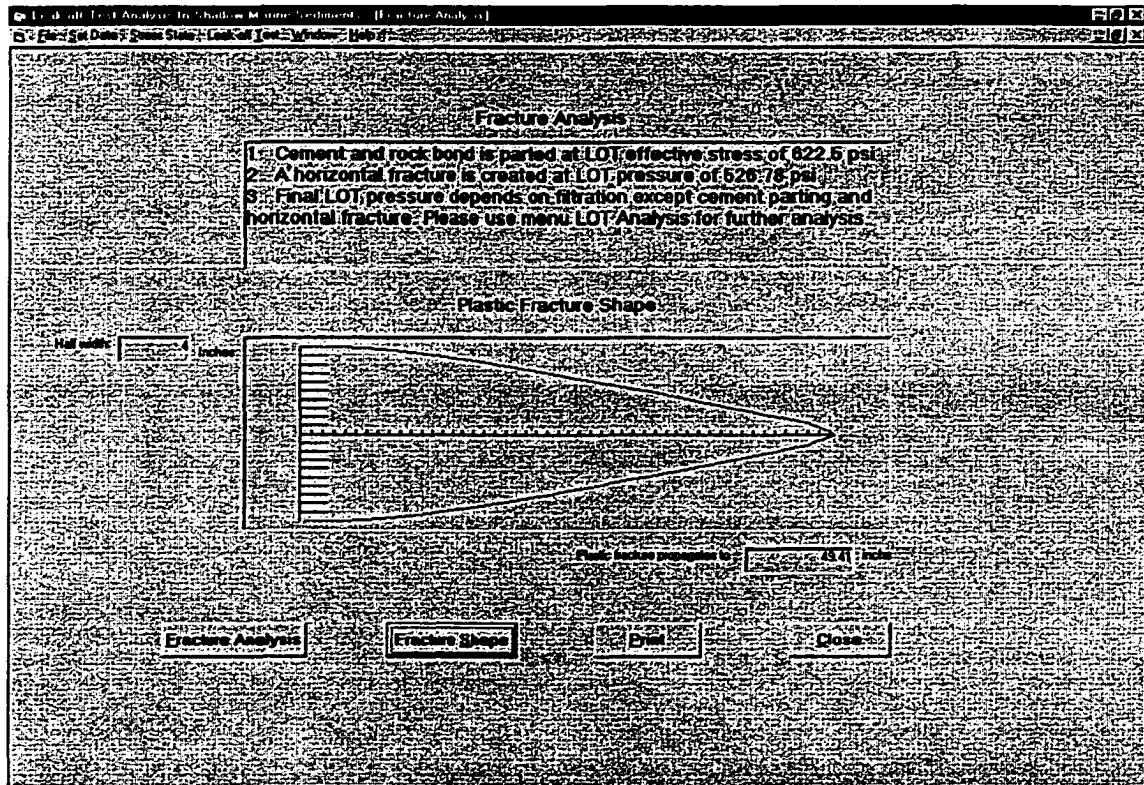


Figure 7.11 Fracture analysis form.

On the fracture analysis form (Fig. 7.11), “Fracture Analysis” and “Fracture Shape” buttons are used to do the analysis and show the result of fractures and the shape and size of the horizontal fracture.

Leak-off test analysis form provides a process for simulating LOTs (Fig. 7.12). Two groups of checks are provided. LOT component group allows user exam the LOT result for each component or some combination of components. Color group provides a few colors used to draw the LOT for each analysis. “View LOT” button completes all the analysis work and gives the simulated result in the form of plot as field engineer does.

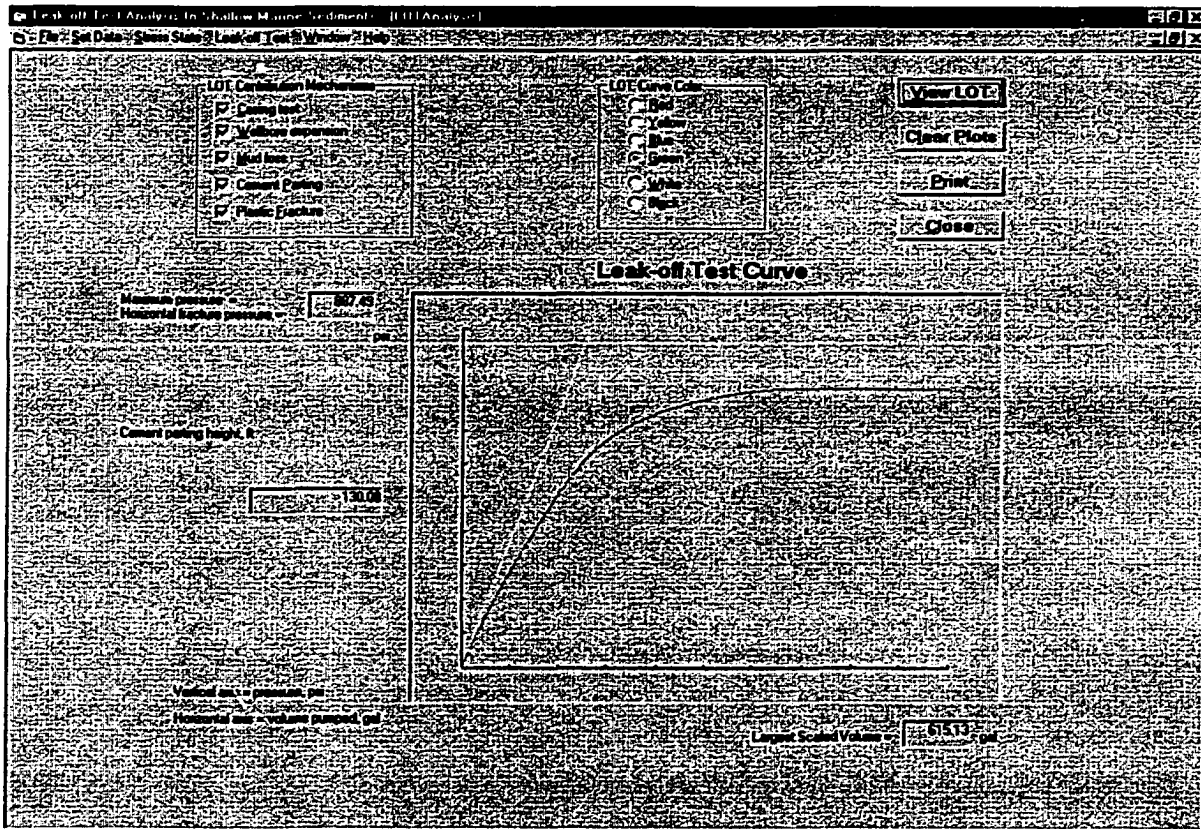


Figure 7.12 Leak-off test analysis.

## **CHAPTER 8**

### **INTERPRETATION OF LEAK-OFF TEST IN SHALLOW MARINE SEDIMENTS**

The analysis of a typical linear leak-off test (LOT) record involves finding the leak-off point at which the data deviated from the straight line. However, in shallow marine sediment LOTs do not give such linear relation as summarized in Chapter 3.

#### **8.1 Leak-off Test Plot in Shallow Marine Sediments**

In shallow marine sediments (SMS), LOT procedure is conceptually the same as that in deep wells. The only difference is the decision on stopping the pump. In deep wells, there is an obvious sign of the casing shoe failure and pumping is stopped after two consecutive test points deflect from the linear trend. In SMS, however, pumping should be stopped when pressure no longer increases with the pumped volume.

Figure 8.1 shows a conceptual LOT plot in SMS used for interpretation. Two horizontal lines are drawn for reference. One represents the overburden pressure line at the casing shoe. Its value is the difference of overburden pressure and mud hydrostatic pressure at the casing shoe. The second line is the maximum pressure line at the casing shoe. Again, its value is the difference of the maximum hydrostatic pressure during cementing and the hydrostatic mud pressure before LOT.

As shown in Fig. 8.1, segment OB is called pressure build-up section. In the section, pressure increases with further pumping. Point A is the point deviated from the early straight line. Point B is the maximum pressure after which pressure no longer increases with pumping and is called leak-off pressure.

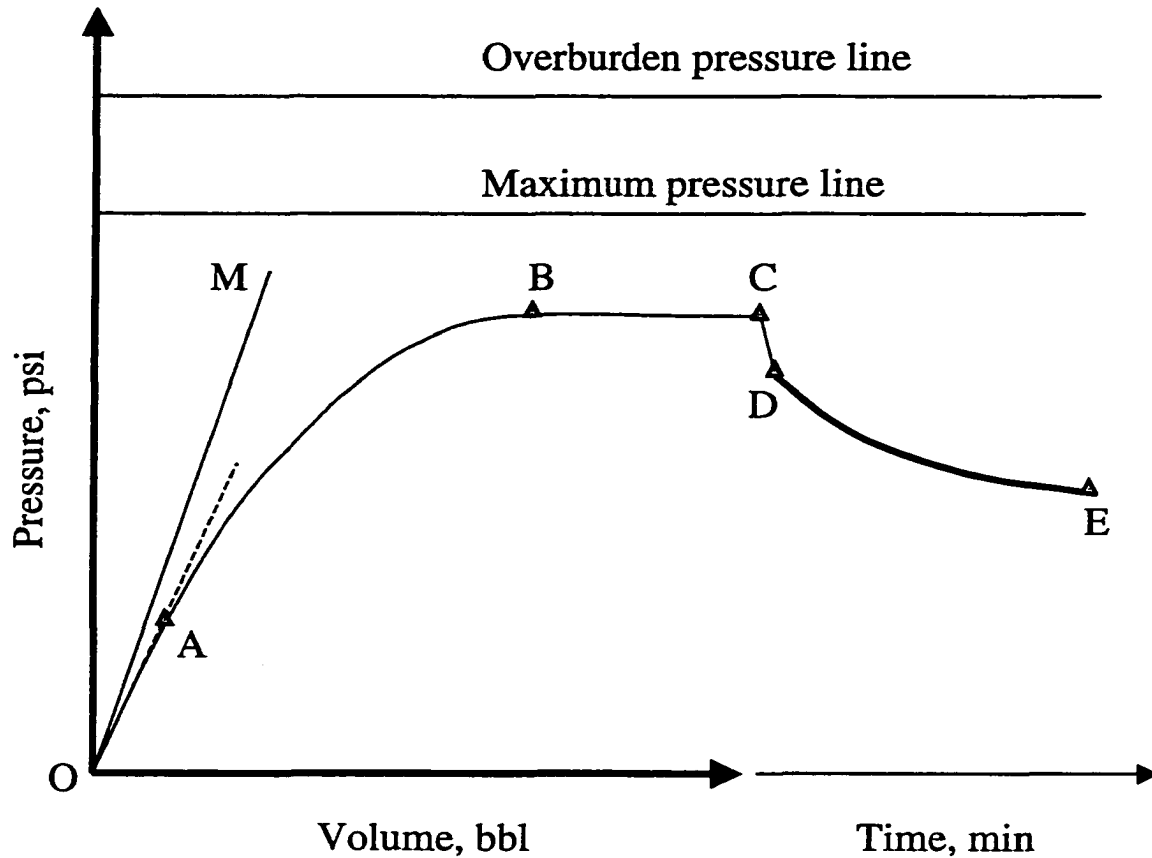


**Figure 8.1** Conceptual/typical leak-off test result in shallow marine sediment for interpretation.

In segment BC, pressure almost keeps constant with pumping and is called stable pressure section. The pressure in the section gets the maximum pressure of the test. There is no limitation for the length of the section, but two more minutes are needed to observe no pressure increase with pumping any more. The well is shut-in at Point C. Section CD represents the sharp pressure drop due to the loss of frictional pressure after shut-in the well.

In Fig. 8.1, section DE records the relation of pressure versus time after shut-in. Generally, the pressure will decrease with time since mud filtrates no matter the well is shut-in or not.

As summarized in Chapter 3, leak-off pressure in SMS is generally very low and it takes only one or two barrels of pumped mud to get the breakdown pressure. In the result of small volume there will be only few points in the LOT plot-each point corresponds to  $\frac{1}{4}$  barrels pumped. Fewer points make the interpretation difficult. Furthermore, the pumped volumes are not exact values since they are just approximate readings. The computer-recorded plot during LOT should be used for reference. The plot represents detail variation of pressure vs. volume. Both the computer-generated and the manual recorded plots should be used for LOT interpretation.

## **8.2 Analysis of Leak-off Test with Rock Fracturing**

The horizontal plastic fracture can only be propagated when wellbore pressure equals overburden pressure. Therefore, rock fracture occurred when the maximum leak-off test pressure greater than overburden pressure, and cement parting or leaking occurred when the maximum pressure is less than overburden. Interpretation procedure is:

1. Drawn horizontal lines of overburden and maximum hydrostatic pressures on the LOT plot;
2. If the tested maximum LOT pressure is greater than overburden pressure line, horizontal plastic fracture occurred.
3. If the tested maximum LOT pressure is less than overburden pressure line, cement parting or leaking occurred around casing shoe.
4. If no overburden pressure available, using maximum hydrostatic pressure line. Smaller tested LOT maximum pressure than the maximum hydrostatic pressure indicated cement parting or leaking.

### 8.2.1 Overburden and Maximum Hydrostatic Pressure Lines

To determine the leak-off test plot gets the rock fracturing, overburden pressure line ( $p_{overLOT}$ ) and maximum pressure line ( $p_{maxLOT}$ ) should be drawn on the plot. Equation 8.1 gives the values to draw the two lines.

$$\begin{aligned} P_{overLOT} &= P_{over} - P_w \\ P_{maxLOT} &= P_{max} - P_w \end{aligned} \quad (8.1)$$

Where  $p_{over}$  = overburden pressure at casing shoe;

$p_w$  = mud pressure the casing shoe;

$p_{max}$  = maximum pressure at casing shoe during cementing.

Maximum pressure,  $p_{max}$ , is the pressure at casing shoe when cement has just been placed. Its value can be estimated from the fluid columns in casing annular.

$$P_{max} = p_o + 0.052 \sum_{i=1}^n \rho_i (D_i - D_{i-1}) \quad (8.2)$$

Where  $p_o$  = pressure at casing head;  $\rho_i$  and  $D_i$  = density and height of the  $i$  liquid column in the annulus.

Mud pressure at casing shoe is

$$P_w = 0.052 \rho_m D_{shoe} \quad (8.3)$$

Overburden pressure can be calculated from rock density data available from well logs. If the bulk density ( $\rho_b$ ) is known as a function of depth, the overburden pressure for each depth interval is calculated by integrating the bulk density for each depth interval as Eq. 8.4.

$$P_{over} = \int_o^{D_w} g \rho_w dD + \int_{D_w}^D g \rho_b dD \quad (8.4)$$

Where  $D_w$  and  $\rho_w$  are water depth and density,  $D$  and  $\rho_b$  are the vertical depth and formation density which is function of depth.

If rock density is unknown, overburden pressure can be estimated as Bourgoyne et al (1991) method.

$$p_{over} = g\rho_w D_w + g\rho_g D_s - \frac{(\rho_g - \rho_f)g\phi_0}{K} (1 - e^{-KD_s}) \quad (8.5)$$

Where constants  $\phi_0$  and  $K$  are surface porosity and porosity decline constant.

Overburden pressure from Eq. 8.5 is not satisfied for shallow marine sediments. Appendix I presents a new model for the overburden pressure in shallow marine sediment based on measured sample boring data. For only clay sediments, the formula is

$$\begin{aligned} p_{over} &= g\rho_w D_w + 1.2D_s - 240(1 - e^{-D_s/400}) : & 0 \leq D_s < 100 \\ p_{over} &= g\rho_w D_w + 66.9 + 3929.5e^{-D_s/5500} + 1.4289D_s - 4001.56 : & 100 \leq D_s < 650 \\ p_{over} &= g\rho_w D_w + 485.6 + 5888.8e^{-D_s/8000} + 1.4722D_s - 6386.19 : & 650 \leq D_s < 3000 \end{aligned} \quad (8.5a)$$

Where overburden pressure  $p_{over}$  is in psi.  $D_s$  is the depth of interesting in feet. The first item  $g\rho_w D_w$  is the pressure of sea water in psi.

From Appendix I, for shallow sediments with sand layers the overburden pressure can be estimated as

$$p_{over} = p_{over-clay} + 0.86D_{sand} \quad (8.5b)$$

Where  $p_{over-clay}$  = overburden pressure from Eq. 8.5a with a depth of  $(D_s - D_{sand})$ .  $D_s$  and  $D_{sand}$  are the total depth of the sediment and the depth of sand respectively.

Overburden pressure can also be assumed to be 1.0 psi/ft according to Harrison et al, 1954; Hubbert and Willis 1957 if nothing is known.

### 8.2.2 Examples

A well was drilled to 1029 ft (TVD). The water depth below sea level was 196 ft. Water level below kelly bushings was 86 ft. The mud weight before LOT was 8.8 ppg and sea water density is about 8.8 ppg. Leak-off test plot is drawn as Fig. 8.2.

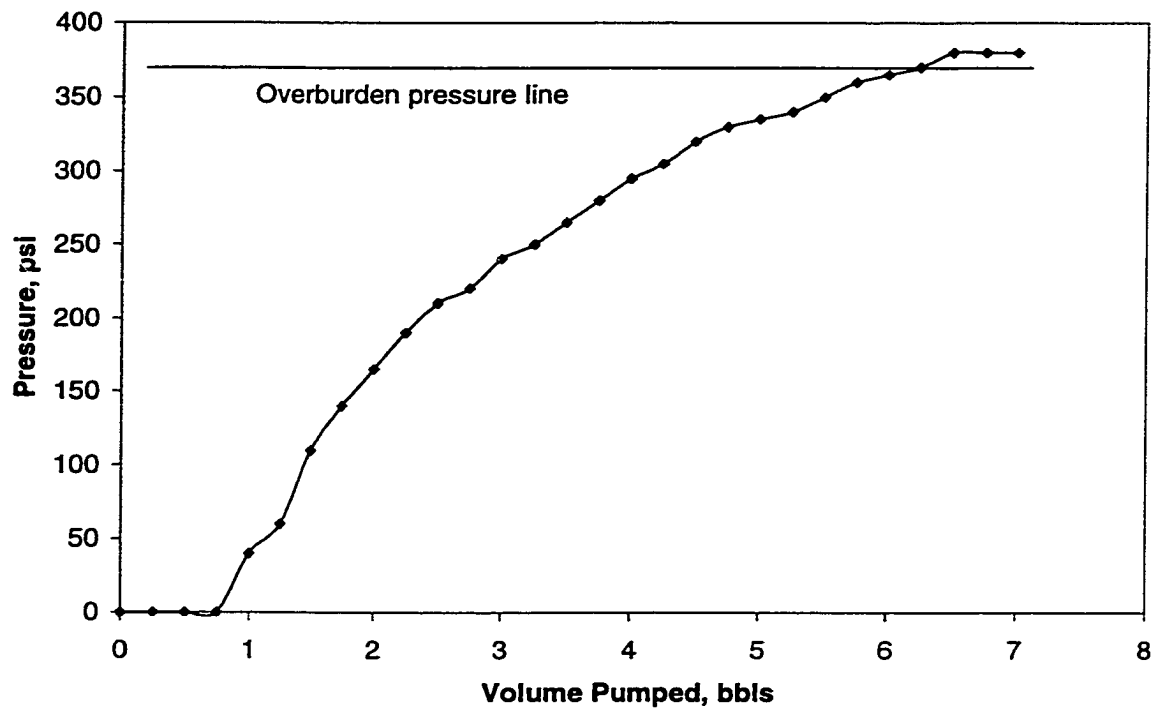


Figure 8.2 Rock fracture.

No detail rock density information and cementing data are available for the well. It is known that the average overburden pressure is 1 psi/ft. We calculate the overburden pressure line based on the average overburden pressure.

Rock depth is  $1029 - 196 - 86 = 747$  ft. The overburden pressure at the casing shoe by the rock is  $747 \text{ ft} \times 1 \text{ psi/ft} = 747$  psi. Overburden pressure from sea water is  $0.052 \times 8.8 \times 196 = 90$  psi. Total overburden pressure at the casing shoe is  $747 + 90 = 837$  psi. Mud pressure at the casing shoe is  $0.052 \times 8.8 \times 1029 = 471$  psi. The

overburden pressure line is  $837 - 471 = 366$  psi. The line is drawn on the LOT plot as shown in Fig. 8.2.

The maximum pressure from LOT was 380 psi which is higher than the overburden pressure line. Therefore, horizontal fracture should be formed.

Shown in Fig. 8.3 is another example which was drilled to 821 ft. Water level below kelly bushings to sea water level was 95 ft and mudline below sea level was 195 ft. Mud weight was 0.442 psi/ft and sea water weight was 0.44 psi/ft.

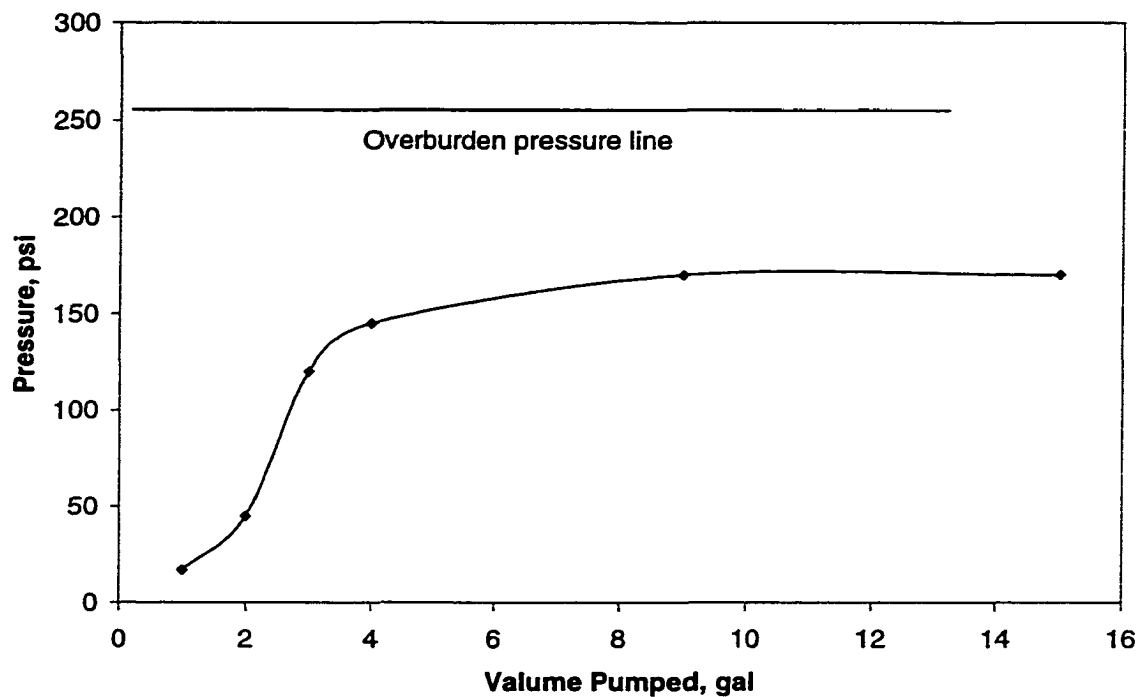


**Figure 8.3 Cement parting or leaking.**

The rock depth to casing shoe is  $821 - 195 - 92 = 534$  ft. With an average overburden pressure is 1 psi/ft, the overburden pressure from rock is 534 psi. Overburden pressure from sea water is  $0.44 \times 195 = 86$  psi. Total overburden pressure at the casing shoe is  $534 + 86 = 620$  psi. The mud pressure at the casing shoe is  $0.442 \times 821 = 363$  psi. Therefore, the overburden pressure line is at  $620 - 363 = 257$  psi.

As shown in Fig. 8.3, the maximum tested LOT pressure was 170 psi which is less than the overburden pressure line. Therefore, cement parting or leaking might occur at the casing shoe.

### 8.3 Pressure Level-off Section Analysis

Pressure level-off section is the section from shut-in to release pressure. Section DE in Fig. 8.1 represents the level-off section. The level-off section is the most important for the interpretation of leak-off test result for both shallow and deep wells since this section is required “level-off” for a good casing shoe integrity by all operators. However, the meaning of level-off depends on operators and the time unit scale. The same level-off section data may be interpreted as level-off or not level-off if different time scales are used.

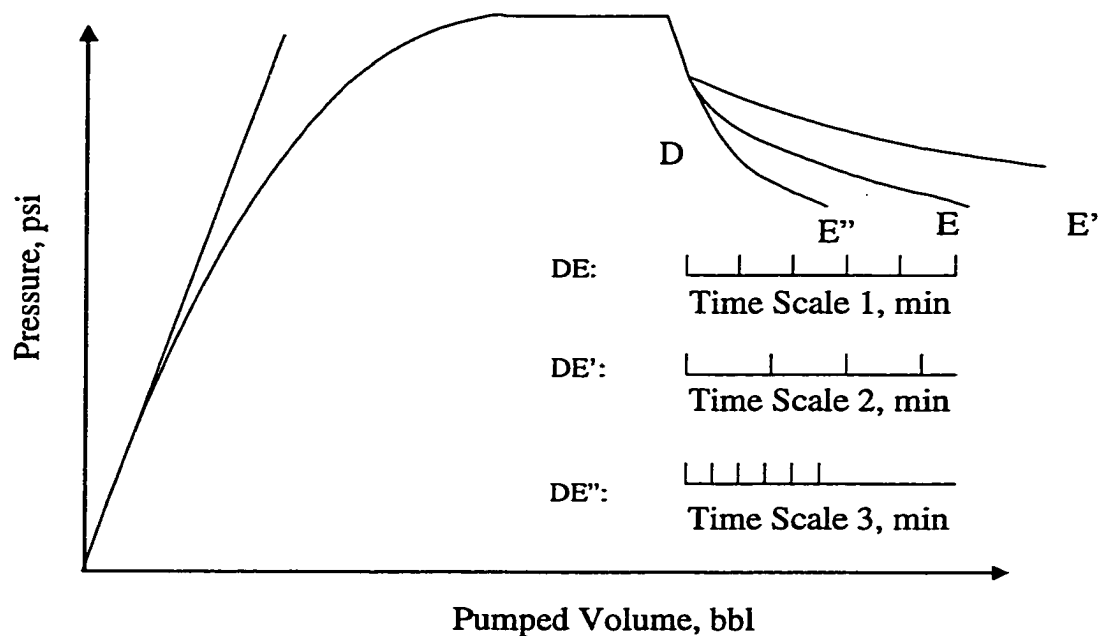


**Figure 8.4** Level-off section DE level-off ?

As shown in Fig. 8.4, same data give three level-off sections (DE, DE', and DE''). Does the level-off section should be horizontal to be interpreted as level-off?

What kind of decline slope is acceptable as level-off ? Is there a technique to follow so that the interpretation no longer depends on experience and operators? We will answer the questions in the following sections. Note that although the technique provided here is mainly for leak-off test in shallow marine sediment, it does work for LOT results of deep wells.

### 8.3.1 Normalizing Time Unit Scale

Whether the level-off section looks like level off or not depends on the scales and units on the two coordinates. The scale on vertical axis is generally 10 or 100 psi depending on recorded maximum pressure. Two units are on horizontal axis (X axis): bbls and min. The problem comes from the scale of the two units. The length of a barrel and the length of a minute on X axis have been drawn randomly by operators. Therefore, same standard should be set up. As shown in Fig. 8.5, the time axis and pumped volume axis have the same length scale per minutes. That is the scale of  $q$  bbl on the pumped volume axis equals the scale of one minute on the time axis.

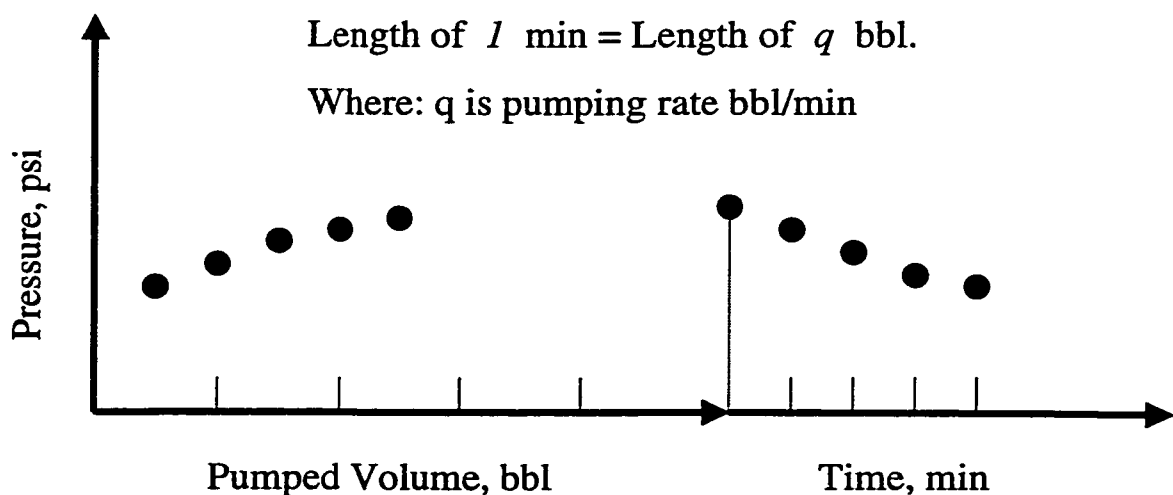


**Figure 8.5** Normalizing time and volume scale by making the length of per minute equal to the length of a pumping rate value.

### 8.3.2 Construction of Level-off Section

To distinguish leaking from fracturing, pressure build-up section is used to compare with the level-off section. The technique presented here is to construct a level-off section based on pressure build-up section and compare the two level-off sections.

#### 8.3.2.1 Pressure Build-up Section Analysis

Divide the pressure build-up section into a series of small segments. The relation of pressure increase ( $\Delta p$ ) versus the pumped volume ( $\Delta V_p$ ) in any segment for a casing test is

$$\Delta p = \Delta V_p / (C_c V_o) \quad (8.6)$$

The relation of pressure increment and pumped volume for leak-off test should be

$$\Delta p = (\Delta V_p - \Delta V_{loss}) / (C_c V_o) \quad (8.7)$$

Where  $\Delta V_{loss}$  = volume loss due to leaking or taken by new opened fracture;

$C_c$  = well system compressibility and approximately equals the slope of casing integrity test plot;

$V_o$  = total mud in the well.

AE in Fig. 8.6(a) is a small segment in the pressure build-up section. Fig. 8.6(b) is the zoomed section of AE for graphic analysis. As shown in Fig. 8.6(b), for a given pumped volume AC, the pressure increase should be CF according to Eq. 8.6 if all the mud were used to increase wellbore pressure. However, the actual pressure increase is CE because some mud has been lost. To get the pressure increase of CE, the effective volume should be AB according to Eq. 8.6. Therefore, the lost volume

for the pumped volume AC is BC. The dash line AF parallels to the casing test line and is used as a reference to find the Point D. Line DE parallels to line AC.

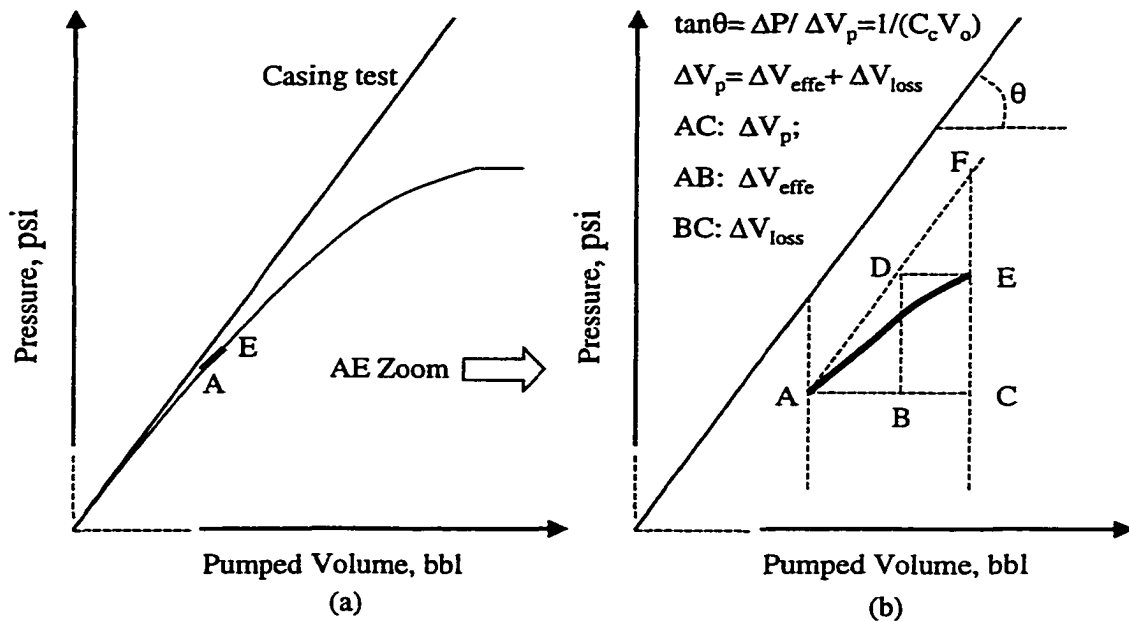


**Figure 8.6** Graphic expression of pressure build-up.

### 8.3.2.2 Constructing Ideal Leaking Level-off Section

A level-off section could be constructed graphically using the tested data on pressure build-up section of a leak-off test (shown in Fig. 8.7). The basic formula to construct the level-off section is Eq. 8.8 providing the same loss rate as that of pressure build-up section at a pressure.

$$\Delta p = (-\Delta V_{loss}) / (C_c V_o) \quad (8.8)$$

The procedure of constructing the level-off section is (as shown in Fig. 8.7):

1. For any increment on pressure build-up section AE, find the corresponding point of point E as A' at the same pressure. Draw a compressibility line as A'F' with a negative angle;
2. On the normalized time scale axis, draw a segment A'C' = AC;

3. Find the volume lost in the time as  $A'B' = BC$ ;
4. Find the intersection point  $D'$  with compressibility line  $A'F'$  by drawing a vertical line through  $B'$ ;
5. Find the intersection point of  $E'$  by drawing a horizontal line through point  $D'$  and a vertical line through point  $C'$ ;
6. Segment  $A'E'$  is the constructed level-off increment corresponding to the build-up increment  $AE$ ;
7. Repeat the process downward to construct the whole level-off section starting from point  $E'$ .

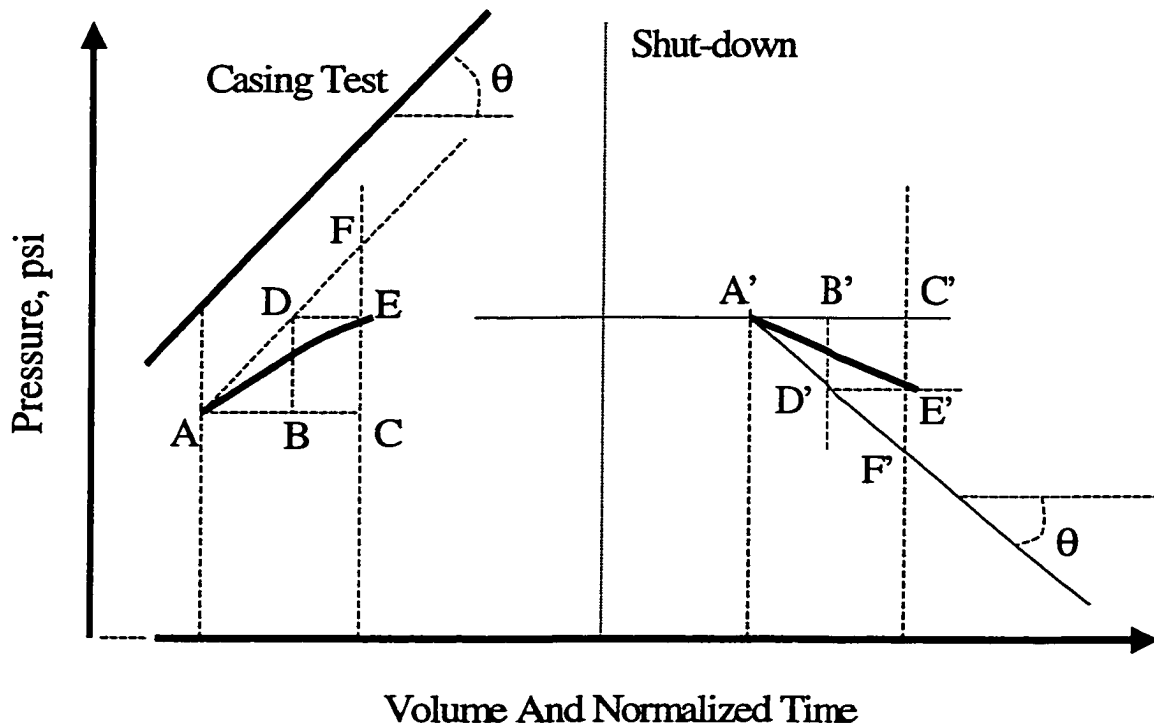


**Figure 8.7 Construction of level-off section.**

The assumption here is that pressure build-up section and level-off section has the same volume losses at the same period of time and average pressure. The

assumption is true when there is no fracture (cement parting and horizontal fracture) in pressure build-up section and leaking rate only depends on pressure. The latter condition could be explained as dynamic filtration (Darcy's law). If the tested level-off section stays above the constructed section the first condition is wrong that means fracture occurred during pressure build-up.

For most actual LOT plots, sharp pressure drops follow well shut-in. The pressure drop comes from frictional pressure loss. Due to the frictional pressure loss, the pressure build-up section records higher pressures, but the pressure level-off section records lower pressures. The pressures in build-up section should be adjusted to lower value and the pressures in level-off section should be moved to higher values according to the pressure loss. The effect of the frictional pressure loss during pumping and leaking after shut-in depends on mud and well properties and its study is not discussed in the dissertation.

If there were no pressure loss after shut-in, the whole level-off section should move up a distance. The period to the first point after shut-in is skipped to avoid the analysis of the pressure loss. The left pressure level-off section A'E' can be got by making an angle of C'A'E' equal the angle FAE where A'C' is a horizontal line and A'E' points downward.

#### **8.4 Interpretation Using Graphic Technique**

The techniques of using overburden pressure or maximum cementing pressure and constructing level-off section are useful for the interpretation of leak-off test results in shallow marine sediments. Two examples are provided to show the application of the technique.

### 8.4.1 Cement Parting

Figure 8.8 is a LOT from a well with TVD= 803 ft, water depth = 102 ft, kelly bushing to sea level=118. The well was drilled by 9.0 ppg mud and sea water density here is 0.442 psi/ft. Casing test line is MN.

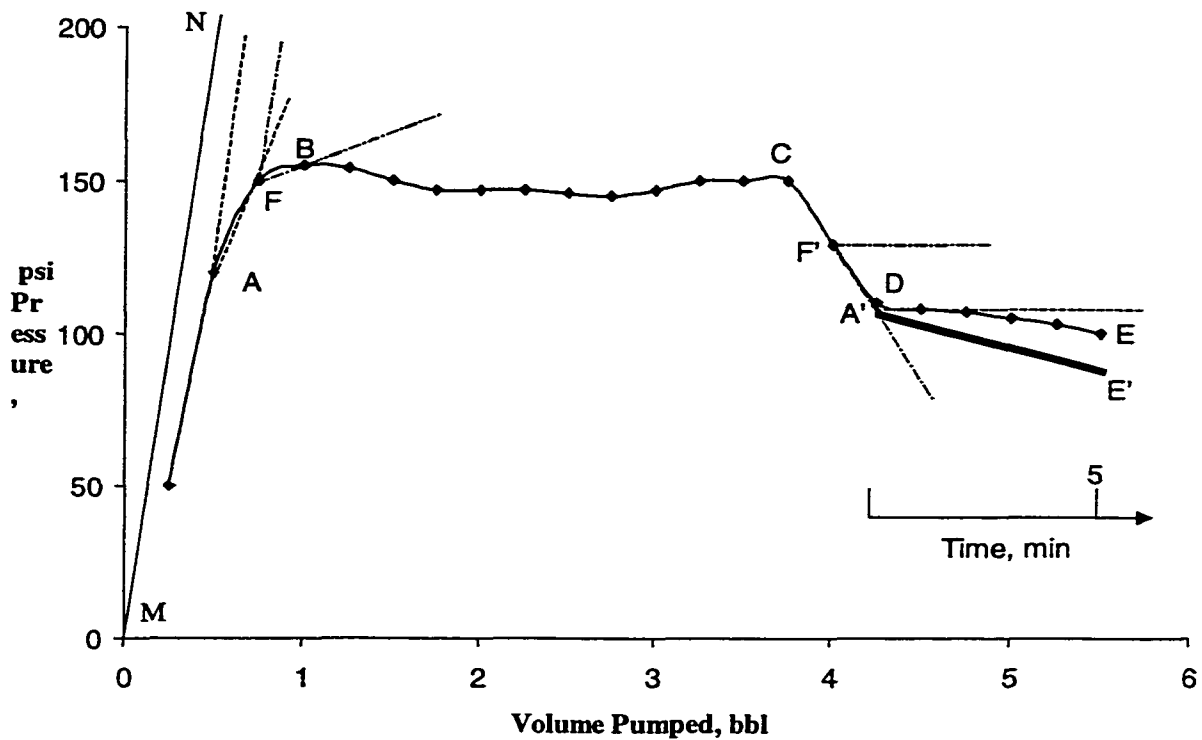


**Figure 8.8 Interpretation Example I.**

The overburden pressure from rock is  $(802-118-102) \times 1.0 = 583$  psi. Sea water causes  $0.442 \times 102 = 45$  psi. Total overburden pressure at casing shoe is  $583 + 45 = 628$  psi. Mud pressure at the casing shoe is  $0.052 \times 9.0 \times 803 = 372$  psi. Therefore the overburden pressure line on the LOT plot is at  $628 - 372 = 256$  psi. The maximum tested pressure was 155 psi lower than the overburden pressure line. Cement parting or leaking may be occurred at the casing shoe.

The well was shut-in at point C. The first tested section CF' after shut-in was affected mainly by the shut-in action and the analysis starts from the point F'. The procedure to construct level-off section is

1. Normalize time scale.
2. In pressure build-up section, draw an angle  $F$  with line FB as one side and the other parallels to the casing test line.
3. In pressure level-off section, draw an angle  $F' = F$  with one side horizontal and the other side downwards.
4. Find the point A' at the time of point D.
5. Repeat the process find angle A in build-up section. Draw angle  $A' = A$  in level-off section and find point E' corresponding point E providing pressure change in  $A'E' \leq$  pressure change in AF.
6. Compare the constructed level-off section F'A'E' with the tested level-off section F'DE. If the constructed F'A'E' is above tested F'DE, cement parting occurred. Otherwise, leaking occurred.

Since F'A' and F'D are almost the same and difference appears between A'E' and DE, the build-up section can be interpreted as: cement parting started at point A, propagated to point F, and FB was dominated by leaking.

#### **8.4.2 Leaking**

Figure 8.9 is a LOT from a well with TVD= 802 ft, water depth = 102 ft, kelly bushing to sea level=118. The well was drilled by 8.9 ppg mud and sea water density here is 0.442 psi/ft.

The overburden pressure from rock is  $(802-118-102) \times 1.0=582$  psi. Sea water causes  $0.442 \times 102=45$  psi. Total overburden pressure at casing shoe is  $582+45=627$

psi. Mud pressure at the casing shoe is  $0.052 \times 8.9 \times 802 = 371$  psi. Therefore the overburden pressure line on the LOT plot is at  $627 - 371 = 256$  psi. The maximum tested pressure was 220 psi lower than the overburden pressure line. Cement parting or leaking may be occurred at the casing shoe.

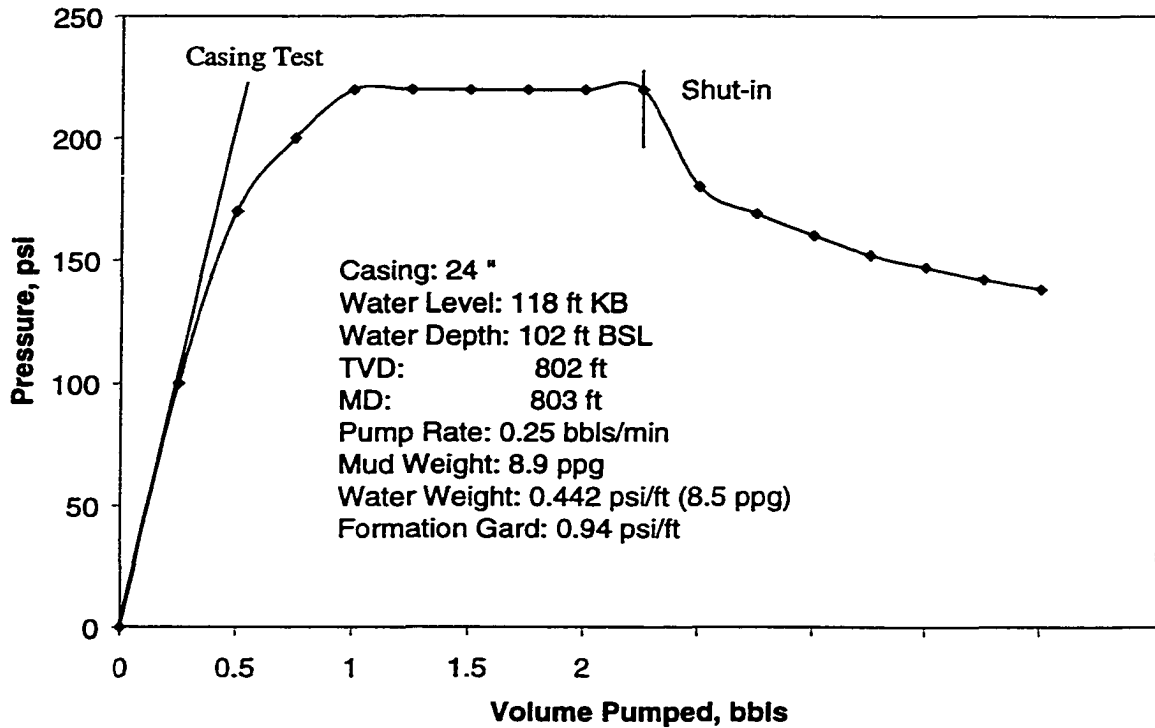


**Figure 8.9 Interpretation Example II.**

To decide whether cement parting or leaking occurred at the casing shoe, follow the same procedure as Section 8.4.1. As shown in Fig. 8.10, find angles of A, B, C and their corresponding angles of A', B', and C'. The constructed section is A'B'C'E'. Angle C is estimated since the section has a large pressure drop of point B to the next tested point below point B in build-up section.

The constructed level-off section A'B'C'D'E' is almost the same as the tested level-off section. Therefore, the casing shoe suffered a leaking from the LOT plot.

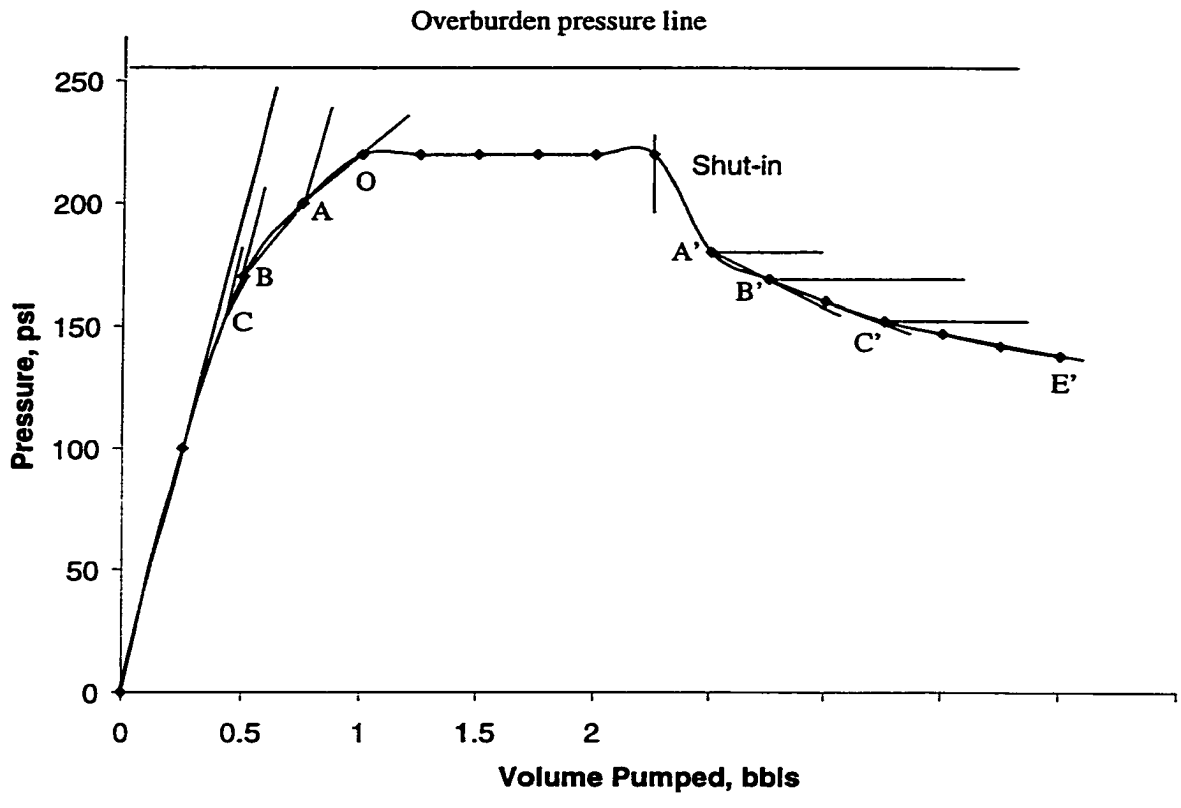


**Figure 8.10** Constructing level-off section for Example II.

## CHAPTER 9

### SUMMARY AND CONCLUSIONS

Shallow marine sediments (SMSs) were analyzed in this study. The shallow soil is rather soft with Poisson's ratio around 0.4, Young's modulus about  $3 \times 10^4$  psi at 300 ft, and low density with vertical gradient around 0.33 psi/ft. A plastic zone will appear around a well drilled in shallow marine sediments. Compared with leak-off tests (LOTs) in deep wells, shallow leak-off results have characteristics of high fracture pressure gradients, non-linearity, fewer tested points, and near constant pressure after breakdown.

For some shallow marine sediments, soil is so soft that it is in plastic state. Traditional method of in-situ stress analysis is based on elastic theory and is not applicable for such formations. An analytic, mathematical model based on elasto-plastic theory was presented in the study. A finite element program was also set up and used to simulate the transition process from elasticity to plasticity. The analytical model is supported by finite element analysis result.

Stress re-distribution due to drilling operation was studied analytically. Based on elasto-plastic theory, formulas were set up to determine the critical condition for transition from an elastic to a plastic wellbore, the size of the possible plastic zone, and stress distribution around the wellbore. Stress variation during leak-off test was also analyzed.

The open hole section, bottom hole, casing shoe, and cement were also simulated using a finite element model. The detailed stresses, strains, and wellbore displacements, especially around the casing shoe and bottom hole, were analyzed using finite element method.

Three types of possible failures from LOTs were studied: vertical fracture, horizontal fracture, and cement parting. It is proved that vertical fracture is the most unlikely failure of the three. Although horizontal fractures are initiated at low pressure in the plastic zone around the wellbore, they cannot propagate beyond the plastic zone until wellbore pressures exceed overburden pressures. Cement parting, on the other hand, may propagate upwards at pressures lower than overburden pressure. Unlike a cement channel that occurs during cementing, cement parting represents the phenomenon that a fracture or separation may be initiated between cement and rock by high wellbore pressure where there were no pre-existed channels are assumed. The dissertation shows that these partings are initiated at pressures equal to the contact stress between cement and rock and their propagation pressures are, on average, 3.5 - fold greater than contact stress.

Study shows that contact stress is developed during the process of cement setting as a result of volumetric changes in cement annulus. A mathematical model of contact stress around casing shoe was set up based on cement volume reduction and compensation from casing string, and cement and wellbore compressibility. The study identified two factors, related directly to drilling technology, that control critical pressure of cement parting in shallow marine sediments: contact stress at casing shoe – resulting from cementing operations, and rock penetration by liquid – an invasion of drilling fluid into the rock around the casing shoe. It was shown in the study that changes in cementing and drilling practices may increase casing shoe integrity and reduce the need for cement squeeze treatments.

A general pressure-volume model of LOT was presented including volumetric effects of wellbore expansion, mud loss into the rock, and propagation of both cement

parting and plastic fracture. The proposed model describes possible leak-off situation and therefore explains possible linear, non-linear or combination behaviors. Software LOTSMS was developed to simulate LOTs in SMS. Also proposed is a technique to interpret LOT results.

From the study, the following conclusions can be drawn:

1. Analysis based on elasto-plastic properties of SMS shows that vertical fractures cannot be induced by LOTs in these type of sediments. Therefore, LOT analysis in SMS cannot be extrapolated from the theory developed for conventional LOTs in deep wells.
2. Very soft sediments may be in plastic state. Their in-situ stresses should be calculated from the presented formula based on elasto-plastic theory.
3. Leak-off test pressure may represent either formation fracture or cement fracture (cement parting). The formation fracture is area specific; however, the cement fracture might be well- specific.
4. Cement fractures are more likely in shallow marine sediments. Cement fracture pressures could be predicted from calculated values of contact stress.
5. Casing shoe leak-off pressure can be increased by reducing early pressure loss after cementing, minimizing length of open hole below the shoe, and better control of mud penetration into the rock.
6. Shallow LOTs have the characteristics of high fracture pressure gradients, non-linear, fewer tested points, almost constant pressure after breakdown.
7. Continuous computer-recorded plots should be used for the analysis of LOTs in SMS. The plots would identify discontinuities that are instrumental in identifying the mechanism of leak-off and the need for remedial squeeze job.

8. Plastic zone appears generally in SMS. However, plastic deformation of the open hole does not result in non-linear pressure-volume behavior. Wellbore expansion during LOT can be calculated from elastic relationship no matter whether the well is in the elastic or plastic state.
9. Non-linear behavior of the LOT pressure build-up section results from fluid loss, annular cement cracking, and plastic (non-propagating) fracture in the plastic zone around a wellbore.
10. Linear behavior of the LOT pressure build-up section results from mud compression and wellbore expansion. The combination of the two linear and three non-linear factors give possible pressure build-up patterns of LOT in SMS. Theoretically, the three mechanisms could be recognized from the analysis of the LOT plot patterns.
11. Rock fracturing can be identified and distinguished from cement fracture and fluid loss into pre-existed channels by comparing the maximum recorded LOT pressures with overburden pressure and by repeating LOT. Moreover, the annular cement parting can be distinguished from the fluid loss mechanism by either finding discontinuity in the LOT pressure build-up section or a pressure plateau or level-off in the shut-in section at pressure value equal to the contact stress.
12. Cement fracture will be closed by contact stress after LOT. Squeeze job can improve its initiation pressure by increasing contact stress but is not necessary if further needed pressure gradient is less than the initiation pressure gradient.
13. Pressure level-off section should be normalized and plotted. A graphic technique was presented for interpretation in the study.

14. Unlike the determination of leak-off points of deep wells, maximum pressures of shallow LOTs should be used as leak-off points.

From the comprehensive literature review, the research presented new theoretical analysis of stress distribution before and during LOT, new models for non-propagation fracture and cement parting, new techniques for the interpretation of LOTs in SMS, and new concepts of “contact stress” and “area and well specific leak-off pressures”. The following works are recommended for further study.

1. Cement fracture depends on the contact stress and penetration coefficient. The coefficient value should be 1 to 3.5. Experimental works are suggested to measure and tabulate the coefficient for normal mud-cement-rock combination.
2. Contact stress is the result of cement slurry setting. Researches are suggested to find new cement slurry to get higher contact stress.

## REFERENCES

- Aadnoy, B. S., Soteland, T., Ellingsen, B., 1989, "Casing Point Selection at Shallow Depth", SPE 18718, SPE/IADC Drilling Conference, New Orleans, Louisiana, Feb. 28-Mar. 3, 1989, pp825-836.
- Addis, M. A., Last, N. C., Yassir, N. A., 1996, "Estimation of Horizontal Stresses at Depth in Faulted Regions and Their Relationship to Pore Pressure Variations", SPE Formation Evaluation, March 1996, pp. 11-18.
- Almeida, M. Aguiar., 1986, "Computer-Aided Analysis of Formation Pressure Integrity Tests Used in Oil Well Drilling", Ph.D. Dissertation, Louisiana State University, Baton Rouge, LA.
- Altun, G., 1999, "Analysis of Non-Linear Formation Fracture Resistance Tests Obtained During Oil Well Drilling Operations", Ph.D. Dissertation, Louisiana State University, Baton Rouge, LA.
- Appleby, S. and Wilson, A.: "Permeability and Suction in Setting Cement," *Chemical Engineering Science* (1996), Vol. 51, 251-267.
- Arifun and Sumpeno, W. H.: 1994 "A New Approach to Casing Setting Depth Selection in Unocal East Kalimantan Operations", IADC Well Control Conference of the Americas, Houston Texas, November 16-17.
- Bassiouni, Z., 1994, "*Theory, Measurement, and Interpretation of Well Logs*", SPE Textbook Series Volume 4, Richardson, Texas.
- Bell, F. C., 1983, "*Engineering Properties of Soils and Rocks*", Butterworths, 149p, London.
- Bender, C. V., Bourgoyne, A. T., Suheyda, J. N., 1995, "Use of Soil Borings Data for Estimating Break-Down Pressure of Upper Marine Sediments", LSU/MMS Well Control Workshop, May 23-24, 1995.
- Bourgoyne, Adam T., Chenevert, Martin E., Millheim, Keith K., Young, F.S., 1991, "*Applied Drilling Engineering*", SPE Textbook Series, Vol. 2., Richardson, Texas.
- Bradley, Howard B., 1992, "*Petroleum Engineering Handbook*", Third Printing, Society of Petroleum Engineering, Richardson, TX, U.S.A.
- Breckels, I. M., van Eekelen, H. A. M., 1982, "Relationship Between Horizontal Stress and Depth in Sedimentary Basins", JPT Sept. 1982, pp. 2191-2199.
- Burden, Richard L., Faires, J. Douglas, 1993: "*Numerical Analysis*", 5<sup>th</sup> Edition, PWS Publishing Company, Boston.

- Cheatham Jr., J. B.: 1984, "Wellbore Stability," *JPT*, June, 889-896.
- Chen, W. F. and Han, D. J.: *Plasticity for Structural Engineering*, Springer-Verlag New York Inc., 1988.
- Chenevert, M. E., Leo, J. M., 1978, "How to run casing and open-hole pressure tests", *Oil and Gas Journal*, Mar. 06, 1978, pp.66-70, 75, 76.
- Christman, S. A., 1973, " Offshore Fracture Gradients", *Journal of Petroleum Technology*, August 1973, pp. 910-914.
- Clark, P.E., Barkat, O., 1990, "Analysis of Fluid-Loss Data", *SPE Production Engineering*, August 1990, pp. 306-310.
- Constant, W. D., Bourgoyne, Adam T., 1988, "Fracture-Gradient Prediction for Offshore Wells", *SPE Drilling Engineering*, pp. 136-140.
- Cooke, C. E. et al: 1982, "Field Measurements of Annular Pressure and Temperature During Primary Cementing", *SPE 11206*.
- Craft, B. C., Hawkins, M., Terry, Ronald E., 1991, "*Applied Petroleum Reservoir Engineering*", Second Edition, Prentice Hall, Englewood Cliffs, NJ, U.S.A.
- Das M. Braja, 1994, "*Principles of Geotechnical Engineering*", 3<sup>rd</sup> edition, PWS Publishing Company, Boston, Massachusetts.
- Desai, C. S., Siriwardane, H. J., 1984, "*Constitutive Laws for Engineering Materials with Emphasis on Geologic Materials*" Prentice-Hall, Inc., Englewood Cliffs, New Jersey, USA.
- Detournay, E., Carbonell, R., 1997, "Fracture-Mechanics Analysis of the Breakdown Process in Minifracture or Leakoff Test", *SPE Production and Facilities*, Aug. 1997, pp. 195-199.
- Dusseault, M. B., Gray, K. E., 1992, "Mechanism of Stress-Induced Wellbore Damage", *SPE 23825*, Presented at the SPE international Symposium on Formation Damage Control held in Lafayette, Louisiana, Feb. 26-27, 1992.
- Eaton, B. A., 1969, "Fracture gradient prediction and its application in oilfield operations", *Journal of Petroleum Technology*, Oct. 1969, pp1353-1360.
- Eaton, Ben A., Eaton, Travis L., 1997 "Fracture gradient prediction for the new generation", *World Oil*, October 1997, pp. 93-100.
- Fjear, E., Holt, R. M., Horsrud, P., Raaen, A. M., Risnes, R., 1992, "*Petroleum Related Rock Mechanics*", Elsevier, New York, USA.

- Geertsma, J., and DeKlerk, F., 1969, "A Rapid Method of Predicting Width and Extent of Hydraulically Induced Fractures," *JPT*, Dec., 1571-1581
- Gidley, J. L., Holditch, S. A., Nierode, D. E., Veatch, R. W. Jr. 1989 "*Recent Advances in Hydraulic Fracturing*", SPE Monograph Volume 12, Richardson, Texas.
- Gnirk, P. F., 1972, "The Mechanical Behavior of Uncased Wellbores Situated in Elastic/Plastic Media under Hydrostatic Stress", SPEJ, Feb., pp. 49-59.
- Griggs, D. T., 1963, "Deformation of Rock Under High Confining Pressures", *Journal of Geology*, 1963, Vol. 44, pp. 541-577.
- Haimson, B., Fairhurst, C., 1967, "Initiation and Extension of Hydraulic Fractures in Rocks", SPE 1710, 9p.
- Harikrishan, R., Hareland, G., 1995, "Prediction of Minimum Principal In-Situ Stress by Comparison and Verification of Four Methods", SPE 29258, Proceedings of SPE Asia Pacific Oil and Gas Conference, Kuala Lumpur, Malaysia, Mar. 20-22, 1995, pp69-75.
- Harrison, E., Kieschnick, Jr., W. F., McGuire, W. J., 1954, "The Mechanics of Fracture Induction and Extension", AIME Petroleum Transactions, Vol. 201, 1954, pp. 252-263.
- Hazov, V. A., Hurshudov, V. A., 1993, "Leak-off tests help determine well bore compressibility", *Oil and Gas Journal*, Nov. 29, 1993, pp. 71-73.
- Hibbitt, Karlsson and Sorensen, Inc., 1994, ABAQUS/Standard user's Manual.
- Holbrook, P. W. and Maggiort D. A.: "Real-Time Pore Pressure and Fracture Gradient Evaluation in All Sedimentary Lithologies", Offshore European Conference, Set. 1993, SPE 26791
- Hubbert, M. K., Willis, D. G., 1957, "Mechanics of Hydraulic Fracturing", *Petroleum Transactions (AIME)*, Vol. 210, pp153-166.
- Jaeger, J. C., Cook, N. G. W., 1976, "*Fundamentals of Rock Mechanics*", Second Edition, John Wiley & Sons, Inc., New York, USA.
- Kreyszig, Erwin, 1993, "*Advanced Engineering Mathematics*", Seventh Edition, John Wiley & Sons, Inc. U.S.A.
- Mattews, W. R. and Kelly, J.: "How to Predict Formation Pressure and Fracture Gradient", *Oil and Gas Journal*, Feb. 20, 1967, pp. 39-43.

- Moria, N. and Black, A. D.: "Theory of Lost Circulation Pressure", 65th Annual Conference and Exhibition, Sept. 1990, SPE 20409.
- Morita, N., Fuh, G-F., Boyd, P. A., 1991, "Safety of Casing Shoe Test and Casing Shoe Integrity After Testing", SPE 22557, Proceedings of the 66<sup>th</sup> Annual Technical Conference and Exhibition of the Society of Petroleum Engineers, Dallas, Texas, Oct. 6-9, 1991.
- Nelson, E. B., 1990, *Well Cementing*, Schlumberger Educational Services.
- Obert, L., and Duvall, W. I., 1967, *Rock Mechanics and the Design of Structures in Rock*, John Wiley & Sons.
- Penny, G. S., Conway, M. W, Lee, W., 1985, "Control and Modeling of Fluid Leakoff During Hydraulic Fracturing", JPT, June 1985, pp. 1071- 1081.
- Postler, D. P., 1997, "Pressure Integrity Test Interpretation", Paper SPE 37589, presented at the 1997 SPE/IADC Drilling Conference, Amsterdam, The Netherlands, 4-6 March 1997.
- Prats, M., 1981, "Effect of Burial History on the Subsurface Horizontal Stresses of Formations Having Different Material Properties", Society of Petroleum Engineers Journal, Dec. 1981, pp658-662.
- Prohaska, M. et al: 1993, "Determining Wellbore Pressure in Cement Slurry Columns," SPE 26070.
- Risnes, R., Bratli, R. K., Horsrud, P., 1982, "Sand Stresses Around a Well", SPEJ, Dec. 1982, pp. 883-898.
- Rocha, L. A. S., 1993, "Mechanisms of Crater Formation While Drilling a Well", Dissertation, Louisiana State University, Baton Rouge, LA.
- Rocha, L. A. S., Bourgoyne, A. T., 1996, " A New Simple Method To Estimate Fracture Pressure Gradient", SPE Drilling and Completion, Sept. 1996, pp153-159.
- Roodhart, L.P., 1985, "Fracturing Fluids: Fluid-Loss Measurements Under Dynamic Conditions", SPEJ, Oct. 1985, pp. 629-636.
- Sabin, F. L. and Sutton, D. L.: 1991, "Interrelationship Between Critical Cement Properties and Volume Changes During Cement Setting", June, *SPEDE*.
- Schuh, F., 1979, "Conductor and Surface Casing Depth Requirements for Deep Water", SPE 8316, Proceeding of the 54<sup>th</sup> SPE Annual Fall Technical Conference and Exhibition, Las Vegas, Nevada, Sept. 23-26, 1979.

- Scot, P. P., Jr., Bearden, W. G. and Howard, G. C., 1953, "Rock Rupture as Affected by Fluid Properties," *Trans., AIME*, Vol. 198, pp. 111-124.
- Settari, A., 1985, "A New General Model of Fluid Loss in Hydraulic Fracturing", *SPEJ*, August 1985, pp. 491-501.
- Sneddon, I. N. and Lowengrub, M., 1969, "*Crack Problems in the Classical Theory of Elasticity*", John Wiley & Sons, Inc.
- Steiger, R. P., Leung, P. K., 1992, "Quantitative Determination of the Mechanical Properties of Shales", *SPE Drilling Engineering Journal*, Sept. 1992, pp. 181-185.
- Sutton, D. L. et al: 1984, "New evaluation for annular gas-flow potential", *Oil and Gas Journal*, Dec 17.
- Timoshenko, S. P. and Goodier, J. N., 1951, *Theory of Elasticity*, McGraw Hill Publishing Co., New York.
- Tinsley, J. M. et al: 1980, "Study of Factors Causing Annular Gas Flow Following Primary Cementing", Aug., *JPT*, 1427-1437.
- Terzaghi, K. and Peck, R. B., 1967, "*Soil Mechanics in Engineering Practice*", John Wiley & Sons, Inc.
- Upchurch, E. R., 1999, "Near-Wellbore Halo Resulting from Tip Screenout Fracturing: Its Direct Measurement and Implication for Sand Control", presented at the SPE Annual Technical Conference and Exhibition, Houston, TX, SPE 56589, pp. 389-397.
- Vuckovic, V., 1989, "Prediction of Fracture Gradients Offshore Australia", presented at the SPE Asia-Pacific Conference, Sydney, Australia, SPE 19468, pp27-34.
- Vardoulakis, I. et al: "Borehole Instabilities as Bifurcation Phenomena", *Int. J. Rock Mech. Min. Sci. & Geomech. Abstr.*, Vol. 25, No. 3, 1988, 159-170.
- Walters, J. V., 1991, "Internal Blowouts, Cratering, Casing Setting Depths, and Location of Subsurface Safety Valves", *SPE Drilling Engineering*, Dec. 1991, SPE 20909, pp285-292.
- Ward, C. D. et al." Brief: Pore- and Fracture-Pressure Determinations: Effective-Stress Approach," *JPT*, Feb. 1995, 123-124 and its discussion, *JPT*, Oct. 1995, 913-915.
- Wilcox, Terry C., 1982, "Mechanical Integrity Testing of Injection Wells", Thesis, Louisiana State University, Baton Rouge, LA.

- Wang, Y., Scott, J. D., Dusseault, M. B., (1994), "Borehole rupture from plastic yield to hydraulic fracture-A nonlinear model including elastoplasticity", *Journal of Petroleum Science and Engineering*, Dec. 1994, pp. 97-111.
- Wang, Y. and Dusseault, M. B.: "Borehole Yield and Hydraulic Fracture Initiation in Poorly Consolidated Rock Strata-Part I. Impermeable Media", *Int. J. Rock Mech. Min. Sci. & Geomech. Abstr.*, Vol. 28, No. 4, 1991, 235-246.
- Warpinski, N. R. and Smith, M. B.: "Rock Mechanics and Fracture Geometry, in Recent Advances in Hydraulic Fracturing", *SPE Monograph*, Vol. 12, 57-80.
- Wojtanowicz, A. K and Zhou, D.: 1998, "Borehole Failure Resulting From Formation Integrity (Leak-Off) Testing in Upper Marine Sediments Offshore", *Journal of Energy Resources Technology*, Vol. 120, 111-117.
- Yoshida, C., Ikeda, S., Eaton, B., 1996, "An Investigative Study of Recent Technologies Used for Prediction, Detection, and Evaluation of Abnormal Formation Pressure and Fracture Pressure in North and South America", *SPE 36381, Proceeding of IADC/SPE Asia Pacific Drilling Technology Conference, Kuala Lumpur, Malasia, Sept. 9-11, 1996.*
- Zienkiewicz, O. C., 1977, *The Finite Element Method*, 3rd edition. McGraw-Hill.

## **APPENDIX A**

### **IN-SITU STRESS IN PLASTIC FORMATION**

There are three principal stresses at any point underground: vertical stress, and two horizontal stresses that are perpendicular to each other. The stresses we are talking about are effective stresses that are the subtraction of in-situ pore pressure from the pressure there. Vertical stress can be easily calculated from the overlying rock density. The two horizontal stresses are equal to each other for a normal fault sediment. Horizontal stresses are generally calculated from vertical stress through a stress ratio. The stress ratio is defined as the ratio of horizontal stress to vertical stress.

It is very known that the stress ratio of sediment is determined by its Poisson's ratio. According to actual field test, the stress ratio has a great variability. Except for the influence of wellbore shape, mud, stress concentration, testing instrument, and any other testing condition and environment, this variability can be explained from a physical standpoint by the fact that in geological time the sediment experiences a complicated deformation history connected with complex loading and unloading cycles.

For the convenient of analysis, assumptions are given as following. Sediment is in geostatic state, that is the horizontal stress is produced only by the overburden pressure. The sediment is continuous, linear elastic, isotropic, homogeneous and obeys the linear Mohr-Coulomb criterion of perfectly plastic yield. There are no stresses of tectonic origin such as those accompanying folding, shrinkage, or other distortions of the earth's crust. The vertical stress is the largest principal stress, the two horizontal principal stresses, mutually perpendicular, are equal to one another.

### A.1 Mohr's Circle In Sediment

In elastic state, the Hooke's law at any point for isotropic material is of the form

$$\begin{aligned}\varepsilon_x &= \frac{1}{E}[\sigma_x - \mu(\sigma_y + \sigma_z)] \\ \varepsilon_y &= \frac{1}{E}[\sigma_y - \mu(\sigma_x + \sigma_z)] \\ \varepsilon_z &= \frac{1}{E}[\sigma_z - \mu(\sigma_x + \sigma_y)]\end{aligned}\tag{A.1}$$

Where  $\varepsilon_x, \varepsilon_y,$  and  $\varepsilon_z$  are the principal strains,  $\sigma_x, \sigma_y,$  and  $\sigma_z$  are the principal stresses,  $E$  is Young's modulus, and  $\mu$  is Poisson's ratio.

In the geostatic state, the horizontal plane is regarded as infinite which is axisymmetrical for any vertical axis. One of reference axes (Z axis) is chosen as perpendicular to the horizontal plane. The other two axes (X and Y axes) are in the horizontal plane. Using  $\sigma_v$  to instead of  $\sigma_z$ ,  $\sigma_h$  to replace  $\sigma_x$  and  $\sigma_y$ , since  $\varepsilon_x = \varepsilon_y = 0$ , from Eq. A.1

$$\begin{aligned}\sigma_h &= \frac{\mu}{1-\mu}\sigma_v \\ F_\sigma &= \frac{\sigma_h}{\sigma_v} = \frac{\mu}{1-\mu}\end{aligned}\tag{A.2}$$

Where  $F_\sigma$  is the horizontal to vertical stress ratio. This equation is derived on the basis of elastic theory, so it is not suitable for sediments in plastic state.

Mohr-Coulomb yield criterion is employed to judge the elastic and plastic state.

It can be expressed as:

$$|\tau| = C_0 \pm \sigma \tan \varphi \quad (\text{A.3})$$

In Eq. A.3,  $\tau$  is shear stress,  $C_0$  is cohesive strength,  $\sigma$  is normal stress, and  $\varphi$  is internal friction angle of any point of the sediment interested. This criterion means that when the Mohr's circle contacts with the yield line, this point of the sediment will change its state from elastic to plastic as shown in Fig. A.1(a). For the sake of convenience, only the above part of the normal stress axis is drawn, the other part is symmetric about the normal axis.

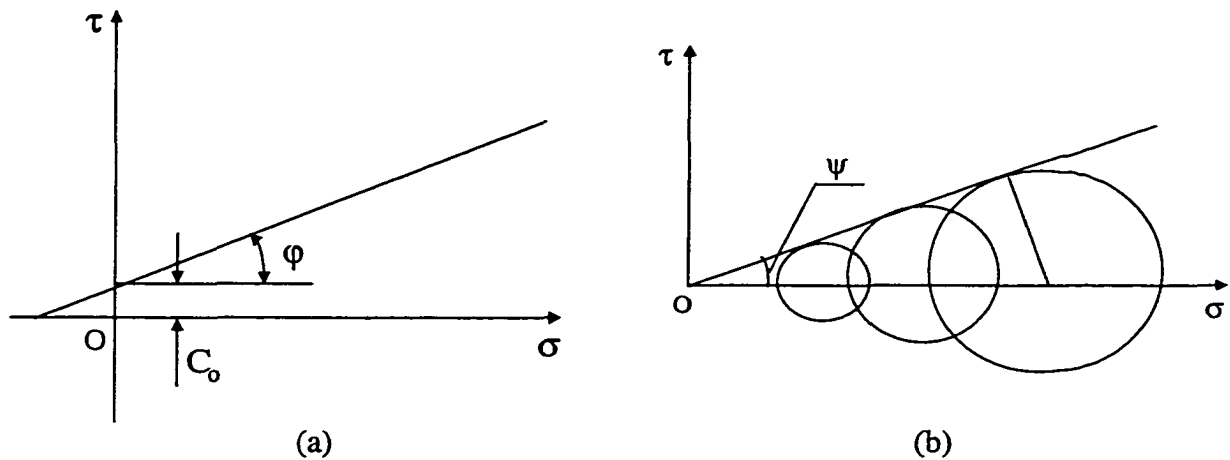


**Figure A.1 (a). Cohesive strength and friction angle. (b). Mohr's circles.**

When the Mohr's circle caused by overburden pressure  $\sigma_v$  does not contact with the yield line in Fig. A.1(a), the horizontal stress can be got from Eq. A.2. The radius  $R$  of the Mohr's circle of an arbitrary point of sediment under the action of  $\sigma_v$  can be deferred from

$$\sigma_v - \sigma_h = \frac{1-2\mu}{1-\mu} \sigma_v = 2R$$

$$R = \frac{1-2\mu}{2(1-\mu)} \sigma_v \quad (\text{A.4})$$

The coordinate of the center of the Mohr's circle on the normal stress axis is

$$\frac{\sigma_v + \sigma_h}{2} = \frac{1}{2(1-\mu)} \sigma_v \quad (\text{A.5})$$

From Eq. A.4 and A.5, there are a series of Mohr's circle as the overburden pressure increases. As shown in Fig. A.1(b), there are two common tangent lines for all circles: one is above normal stress axis, the other is below. Both tangent lines begin from the original point  $O$  to the right side of the shear stress axis, with inclination of

$$\psi = \arcsin(1-2\mu) \quad (\text{A.6})$$

## A.2 Condition of Elastic or Plastic State of Sediments

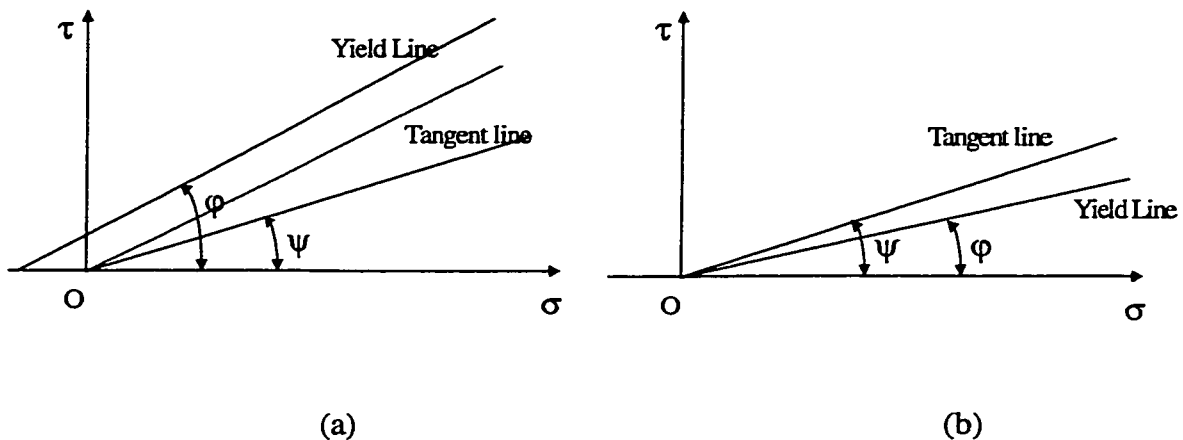


**Figure A.2** Tangent line and yield line.

As shown in Fig. A.2(a), for sediment with no-zero cohesive strength, if the internal friction angle  $\phi$  is greater than the tangent line inclination  $\psi$ , the yield line and the tangent line cannot intersect. This means that there is no possibility for any Mohr's circle by the overburden pressure can contact the yield line. It can be concluded that any sediment with such cohesive strength and internal friction angle

will not turn into plastic state under the action of overburden pressure, no matter how large the overburden pressure is.

If the cohesive strength is zero and  $\varphi > \psi$ , the yield line and tangent line will meet only at original point  $O$ . At this point, since  $\sigma = \tau = 0$ , there is no meaning in the analysis of stresses produced by overburden. This kind of sediment will not also come into plastic state.

In the case of Fig. A.2(b), where  $C_0=0$  and  $\varphi \leq \psi$ . This case represents that this kind of sediment will turn into the state of plastic once the overburden pressure acts on it.

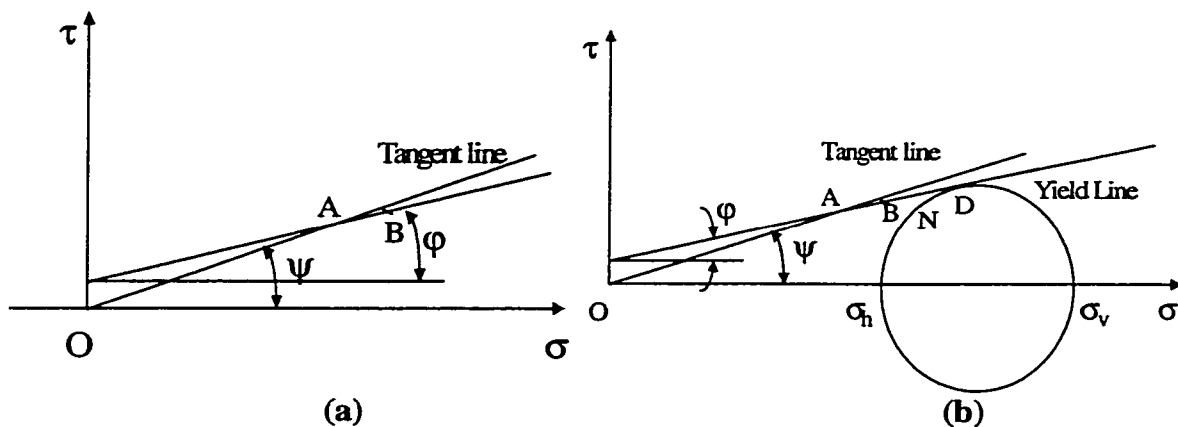


**Figure A.3 Elastic to plastic state.**

To some shallow marine sediment, the situation is  $C_0 \neq 0$  and  $\varphi < \psi$ . The yield line and tangent line intersect at point  $A$  in Fig. A.3(a). Therefore, in the first when the Mohr's circle is enough small, it will not contact with the yield line. The sediment is still in elastic state. Then Mohr's circle will contact with the yield line at point  $B$  and the sediment will change its state from elastic to plastic as the radius of Mohr's circle increase with the overburden pressure.

The coordinates of point  $B$  are:

$$\tau_B = \frac{1-2\mu}{2(1-\mu)} \sigma_v \cos \varphi \quad (\text{A.7})$$

$$\sigma_B = \frac{\sigma_v}{2(1-\mu)} - \frac{1-2\mu}{2(1-\mu)} \sigma_v \sin \varphi \quad (\text{A.8})$$

Substitution of Eqs. A.7, A.8 into Eq. A.3 yields

$$(\sigma_v)_{\text{lim}} = \frac{2(1-\mu)C_0 \cos \varphi}{1-2\mu - \sin \varphi} \quad (\text{A.9})$$

Therefore, sediment will be in elastic state when  $\sigma_v < (\sigma_v)_{\text{lim}}$  and in plastic state for  $\sigma_v \geq (\sigma_v)_{\text{lim}}$ .

In the case of frictionless sediment, as Trasca's criterion, the internal friction angle is zero, the yield line parallels to the normal stress axis. The limit vertical stress turning the sediment into plastic state is

$$(\sigma_v)_{\text{lim}} = \frac{2(1-\mu)}{1-2\mu} C_0 \quad (\text{A.10})$$

### A.3 Stress Ratio in Plastic State

As stated above, the horizontal to vertical stress ratio can be calculated from Eq. A.2 when the sediment interested is in the state of elasticity. Therefore, the stress ratio  $F_\sigma$  can be determined for all the elastic cases discussed above. In plastic state, however, the stress-strain relation (constitutive equation) used in elastic analysis is not suitable.

When  $C_0 = 0$  and  $\varphi \leq \psi$  or the overburden pressure  $\sigma_v$  is greater than the limit value  $(\sigma_v)_{\text{lim}}$  the sediment is in plastic state. If the plastic state of sediment is

perfectly plastic, the stress will keep the same with further plastic deformation. Thus, as the overburden pressure increases the corresponding Mohr's circle will always tangent to the yield line.

In plastic state, when a  $\sigma_v$  (greater than  $(\sigma_v)_{lim}$  for  $C_0 \neq 0$ ) is given, a Mohr's circle tangent to the yield line can be determined. Actually, there is only one Mohr's circle which passes point  $(\sigma_v, 0)$  and tangent to the yield line (under the condition of  $\sigma_v$  is the largest principal stress). Another intersection point of the Mohr's circle with the normal stress axis can be got graphically. If it is  $(\sigma_h, 0)$ , the horizontal to vertical stress ratio still is

$$F_\sigma = \frac{\sigma_h}{\sigma_v} \quad (\sigma_v \geq (\sigma_v)_{lim}) \quad (A.11)$$

Besides the method of geometry, the stress ratio can also be calculated mathematically. If Point  $D$  is the tangent point of the yield line to Mohr's circle (Fig. A.3(b)). The coordinates of point  $D$  are

$$\tau_D = R_D \cos \varphi \quad (A.12)$$

$$\sigma_D = \sigma_v - R_D(1 + \sin \varphi) \quad (A.13)$$

Where  $R_D$  = radius of the Mohr's circle. Eqs. A.12, A.13 into Eq. A.3 yields

$$R_D = \frac{C_0 + \sigma_v \tan \varphi}{\cos \varphi + (1 + \sin \varphi) \tan \varphi} \quad (A.14)$$

Substituting  $\sigma_h = \sigma_v - 2R_D$  into Eq. A.14 and simplifying

$$F_\sigma = 1 - \frac{2(\sin \varphi + \frac{C_0}{\sigma_v} \cos \varphi)}{1 + \sin \varphi} \quad (\sigma_v \geq (\sigma_v)_{lim}) \quad (A.15)$$

It can be seen from Eq. A.15, the horizontal to vertical stress ratio in plastic state depends on the properties of the sediment and the effective vertical stress, it is not a constant. In the condition of normal pore pressure, since the effective vertical stress increases with depth of overlying material, the stress ratio will increase with the depth for the same properties. Stress ratio is near to 1 only when sediment is frictionless or of smaller internal friction in plastic sediments.

## APPDEDEX B

### ELASTO-PLASTIC BOUNDARY

A plastic zone around a wellbore wall is generally formed by drilling operation in shallow marine sediments. The tangential stress and radial stress in the plastic zone is (Wojtanowicz and Zhou, 1998)

$$\begin{aligned}\sigma_r &= (P_w + \frac{\sigma_0}{N-1}) (\frac{r}{r_w})^{N-1} - \frac{\sigma_0}{N-1} \\ \sigma_\theta &= N(P_w + \frac{\sigma_0}{N-1}) (\frac{r}{r_w})^{N-1} - \frac{\sigma_0}{N-1}\end{aligned}\quad (\text{B.1})$$

Where Mohr -Coulomb yield criterion is used and it can be expressed as

$$\begin{aligned}\sigma_1 - N\sigma_3 &= \sigma_0 \\ \sigma_0 &= 2\tau_0 \cos \varphi / (1 - \sin \varphi) \\ N &= (1 + \sin \varphi) / (1 - \sin \varphi)\end{aligned}\quad (\text{B.2})$$

The radius of the boundary between the plastic and elastic zones,  $r_c$ , can be derived from the continuity of the radial and tangential stresses at the boundary when the tangential stress is the largest stress at the elasto-plastic boundary.

In the elastic region, the stress distribution is (Obert and Duvall, 1967)

$$\begin{aligned}\sigma_r &= A + \frac{B}{r^2} \\ \sigma_\theta &= A - \frac{B}{r^2}\end{aligned}\quad (\text{B.3})$$

Where  $A = \sigma_h$  when  $r$  goes to infinite. At the elasto-plastic boundary, the radial and tangential stresses should keep continuous. Combining Eq. (B.1) and Eq. (B.2) at  $r = r_c$  we get

$$\sigma_h + \frac{B}{r_c} = (P_w + \frac{\sigma_0}{N-1}) (\frac{r_c}{r_w})^{N-1} - \frac{\sigma_0}{N-1}$$

$$\sigma_h - \frac{B}{r_c} = N(P_w + \frac{\sigma_0}{N-1}) (\frac{r_c}{r_w})^{N-1} - \frac{\sigma_0}{N-1} \quad (\text{B.4})$$

Solving Eq. (B.4), the radius of the boundary at the elasto-plastic zone is

$$r_c = r_w \left( \frac{\frac{N-1}{N+1} (2\sigma_h - \sigma_0) + \sigma_0}{(N-1)P_w + \sigma_0} \right)^{\frac{1}{N-1}} \quad (\text{B.5})$$

If the vertical stress is the largest stress at the elasto-plastic boundary, the radius of the boundary can be calculated according to Rinses et al. (1982). Unfortunately, the equation had a very complex form. The radial stress in plastic zone approximates that in Eq. (B.1) for the case of vertical stress is the largest stress (Rinses et al., 1982, Wojtanowicz and Zhou, 1998). Therefore, the plastic radius is

$$r_c = r_w \left( \frac{(N-1)\sigma_{z0} + \sigma_0}{N((N-1)p_w + \sigma_0)} \right)^{\frac{1}{N-1}} \quad (\text{B.6})$$

Assuming  $N=2$  which corresponds to the friction angle of 20 degrees from Eq. (B.2), Eq. (B.6) reduces to Eq. (B.7). Shallow marine sediments in the Gulf of Mexico have 20 degrees of friction angle.

$$r_c = \frac{(\sigma_{z0} + \sigma_0)r_w}{2(p_w + \sigma_0)} \quad (\text{B.7})$$

## APPENDIX C

### PART OF FINITE ELEMENT ANALYSIS RESULTS

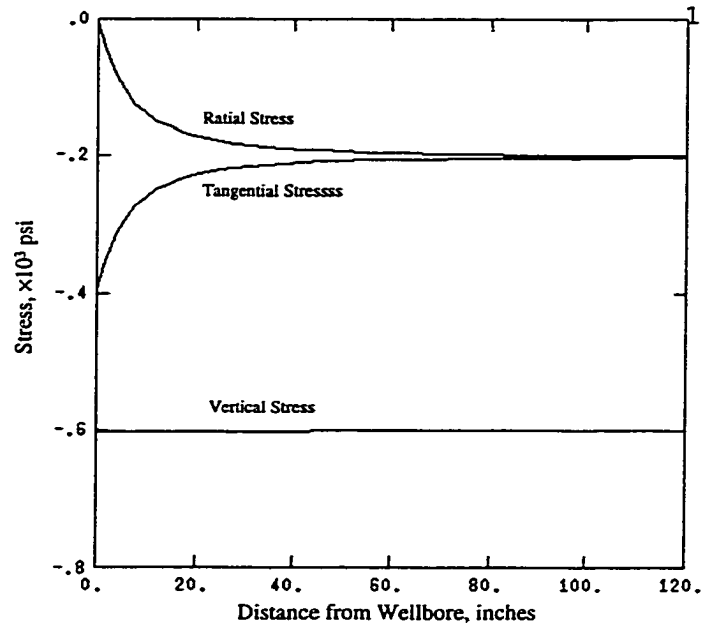


Figure C.1 Elastic wellbore before LOT of Line 3 in Figure 5.3 for Case 1.

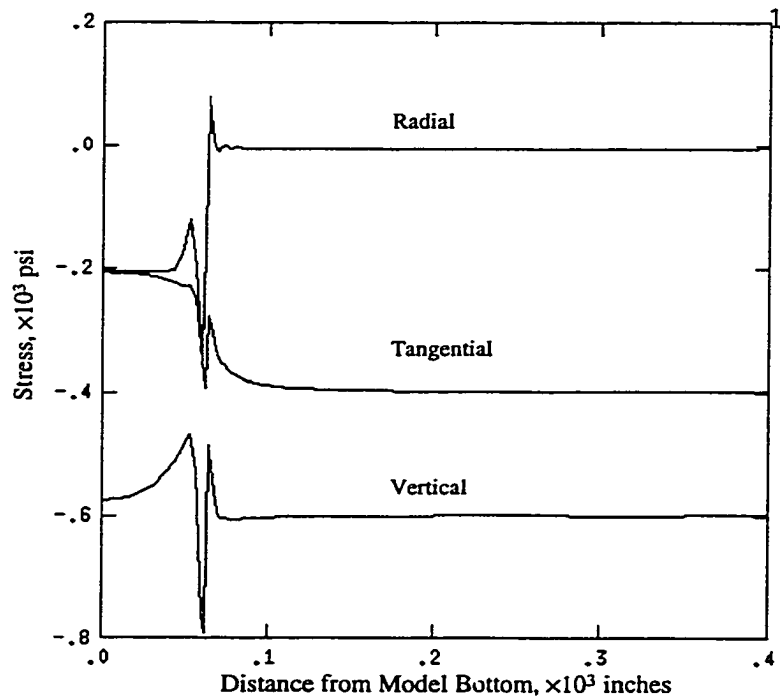
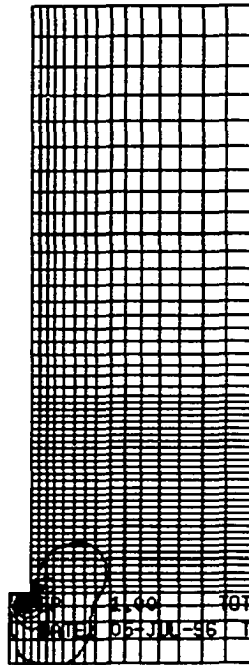
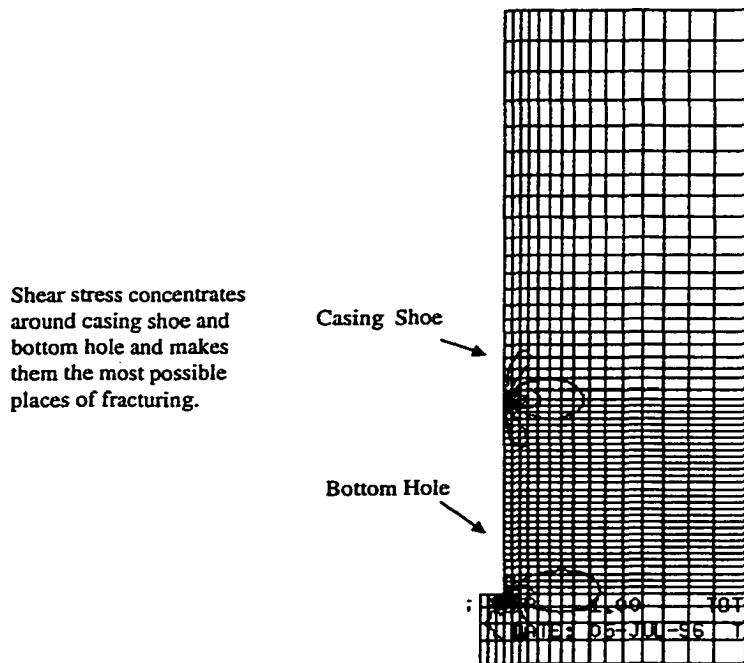


Figure C.2 Stress along Line 5 in Figure 5.3 for Case 1.



**Figure C.3 Shear stress contour around bottom hole for Case 1 before LOT.**



**Figure C.4 Shear stress contour for Case 1 during LOT.**

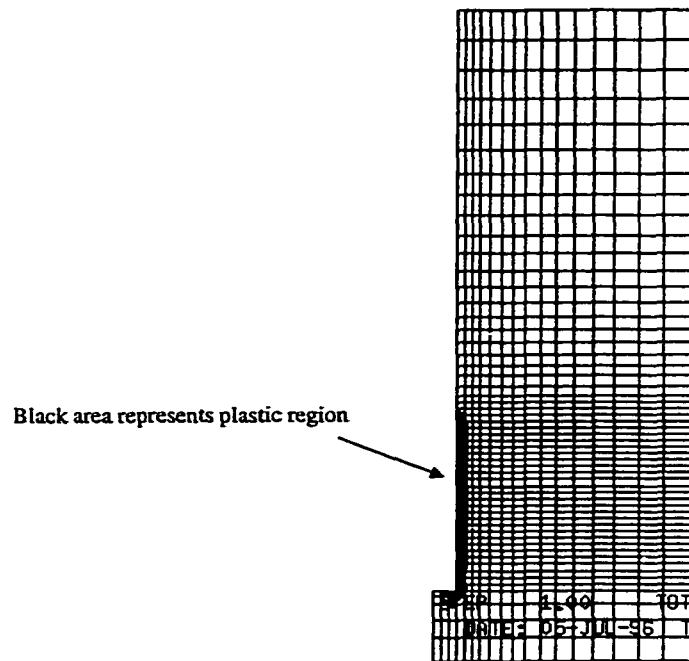


**Figure C.5** Plastic area appears for an elastic wellbore due to LOT (Case 1 in Figure 5.3).

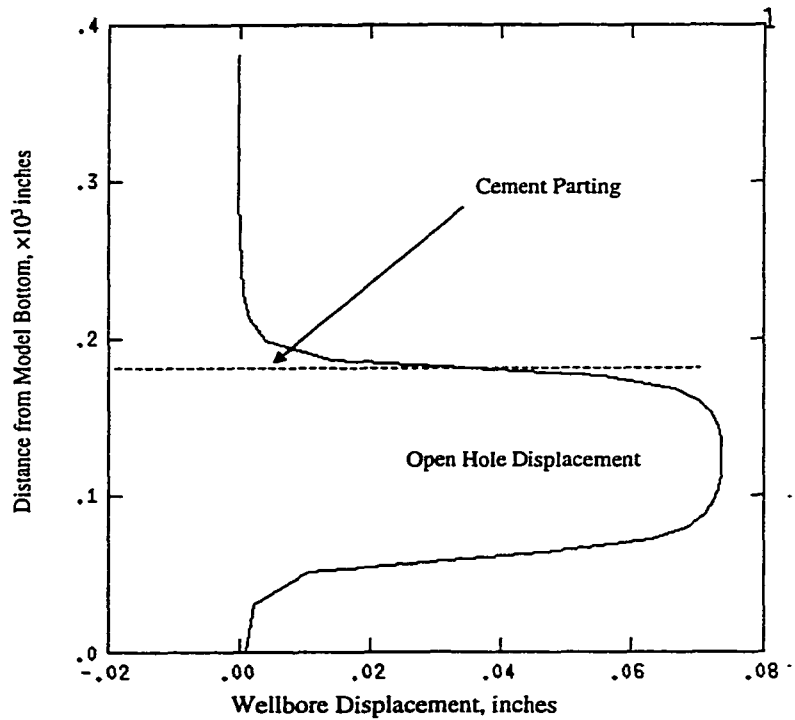


**Figure C.6** Cement parting by LOT (Case 1).

There was a pre-existing plastic zone around wellbore. Note a rapid drop of tangential and vertical stress at the wellbore

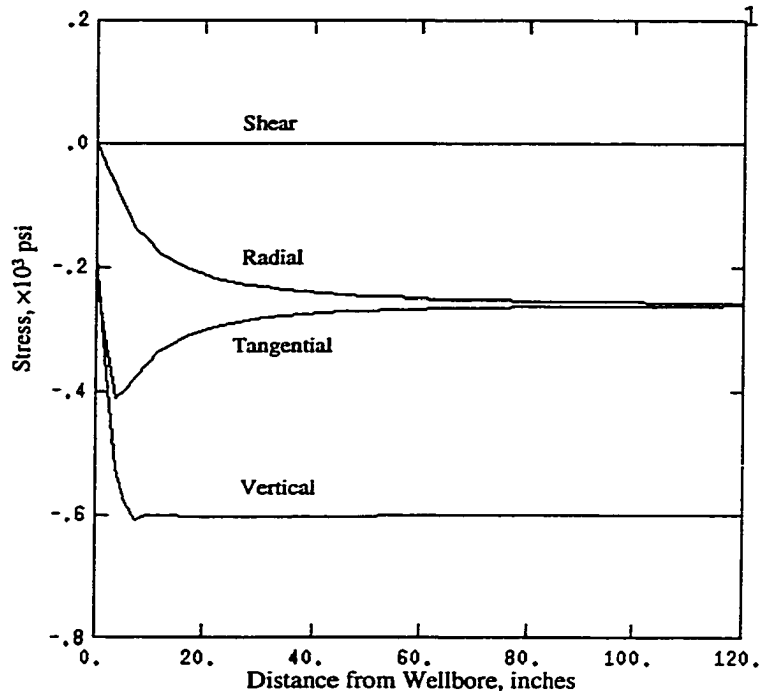


**Figure C.7 A plastic annulus existed before LOT (Case 2).**

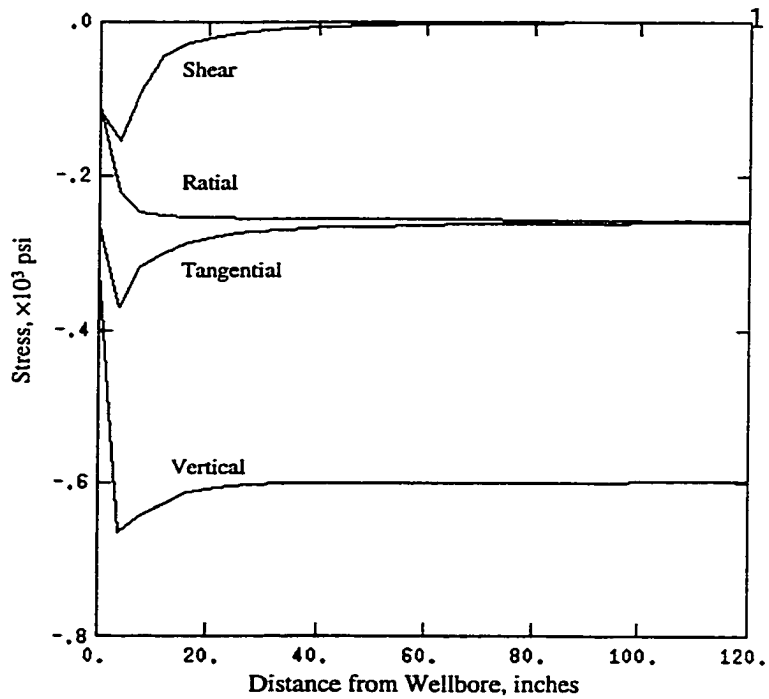


**Figure C.8 Stress distribution along Line 4 of Fig. 5.3 (Case 2, before LOT).**

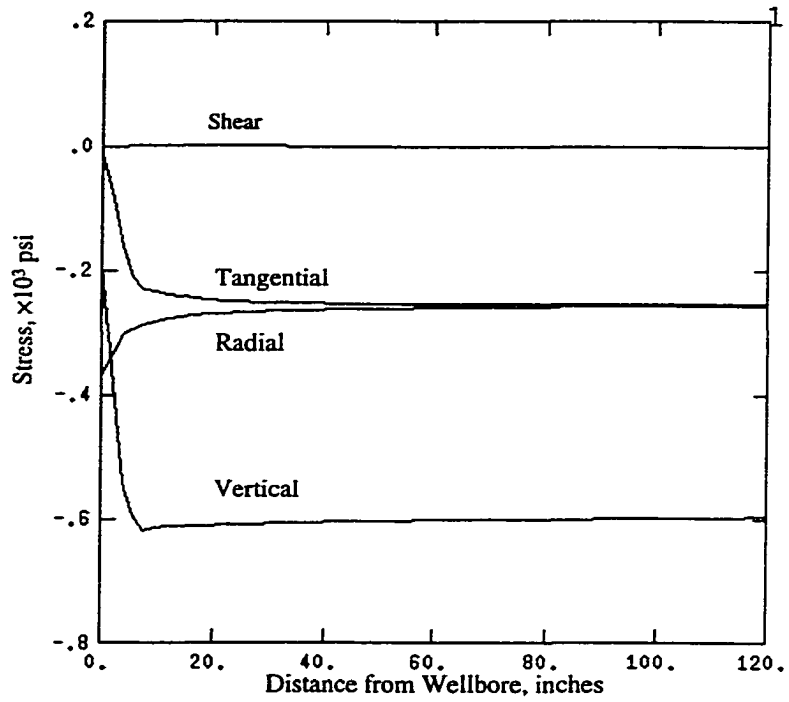


**Figure C.9** Tangential stress decreases and radial stress increases during LOT (Case 2).

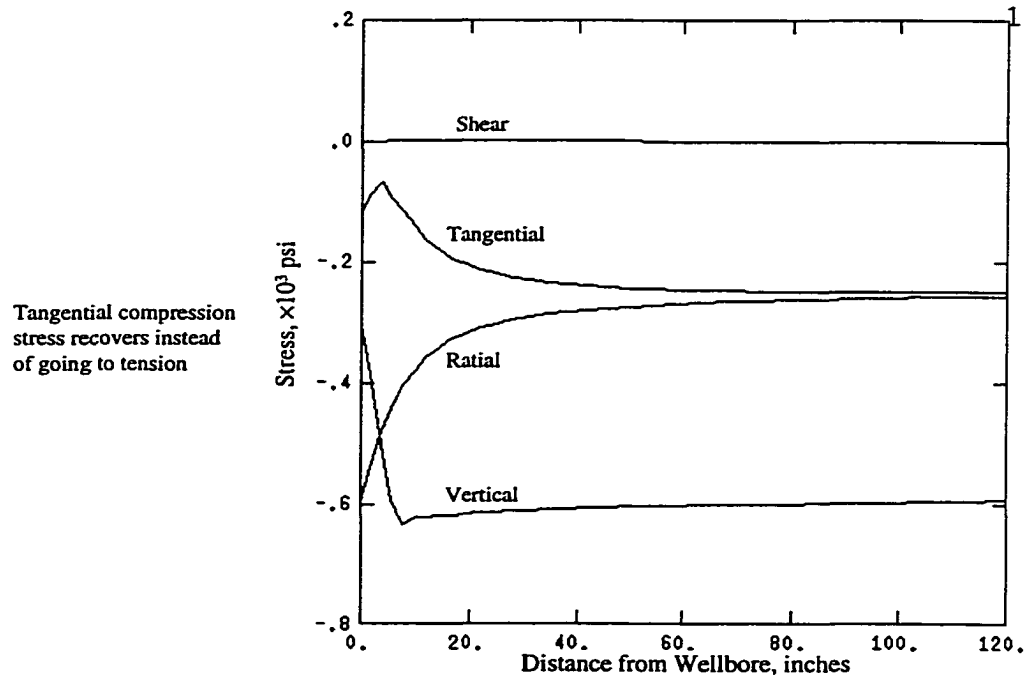


**Figure C.10** No vertical fracture even at high wellbore pressure (Case 2).

Plastic yield occurs instead of fracture at bottom of open hole

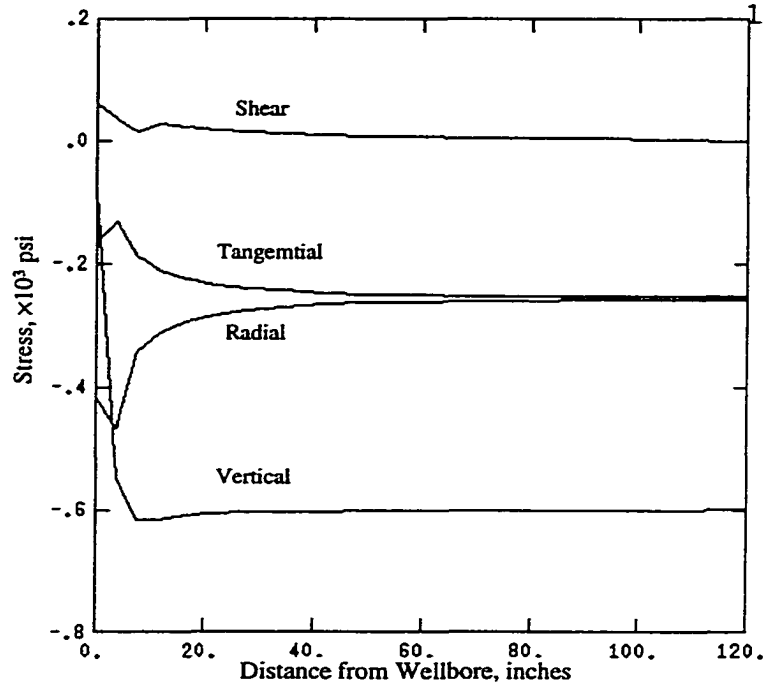


**Figure C.11** Stresses along Line 4 of Figure 5.3 During LOT (Case 2).

No vertical fracture below casing shoe

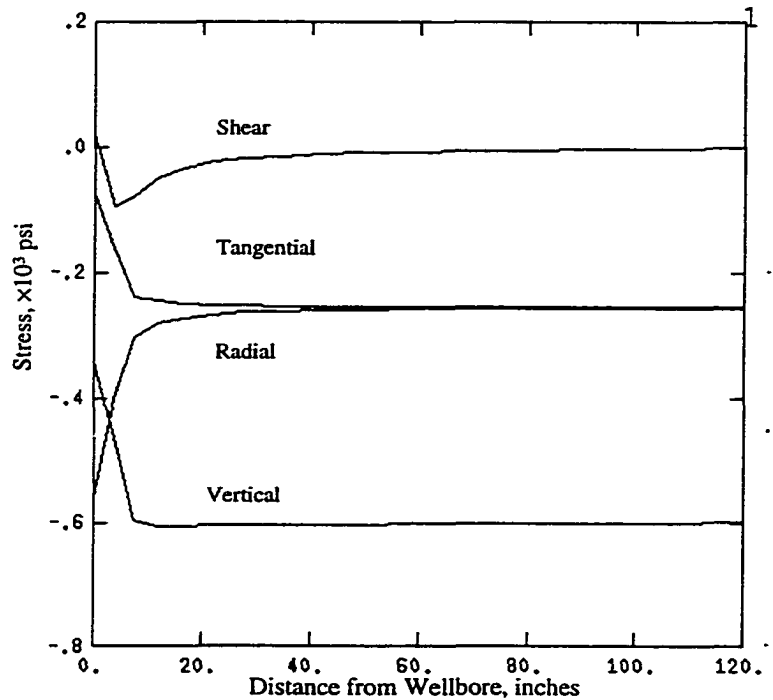


**Figure C.12** Stress distribution along Line 2 of Figure 5.3 for Case 2 during LOT.

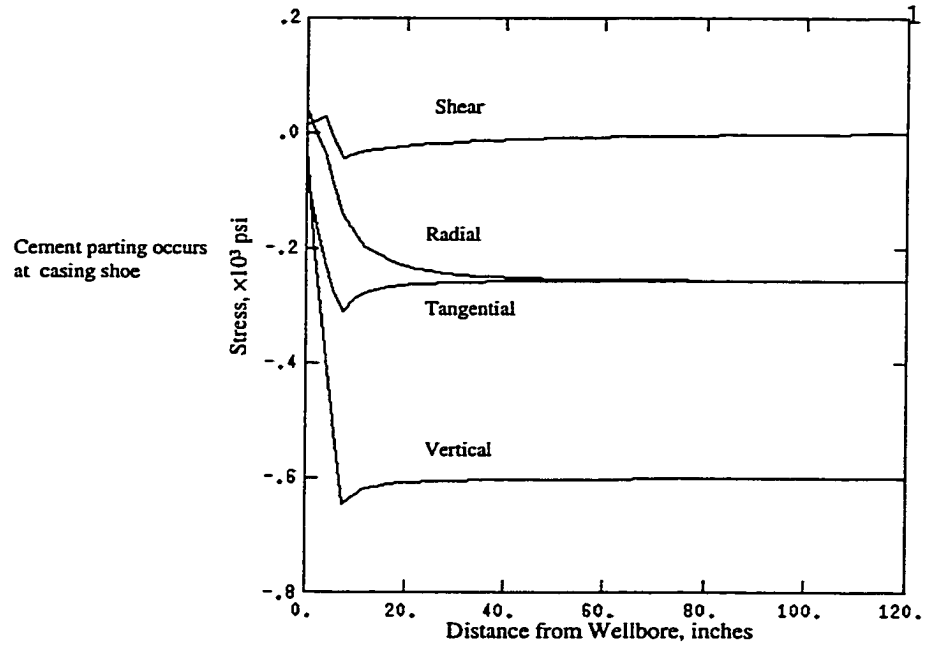


**Figure C.13** Stresses along Line 1 of Figure 5.3 for Case 2 during LOT.

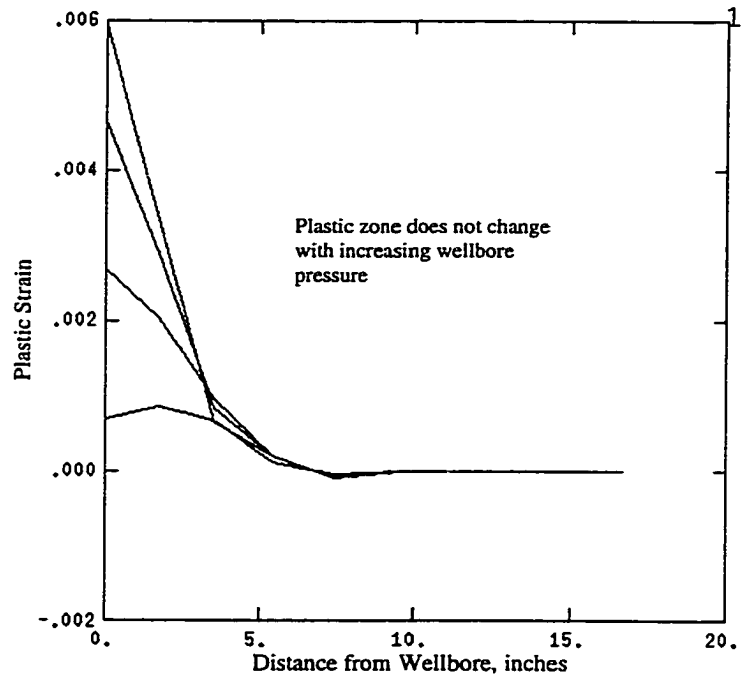


**Figure C.14** Plastic strains during LOT for Case 2.

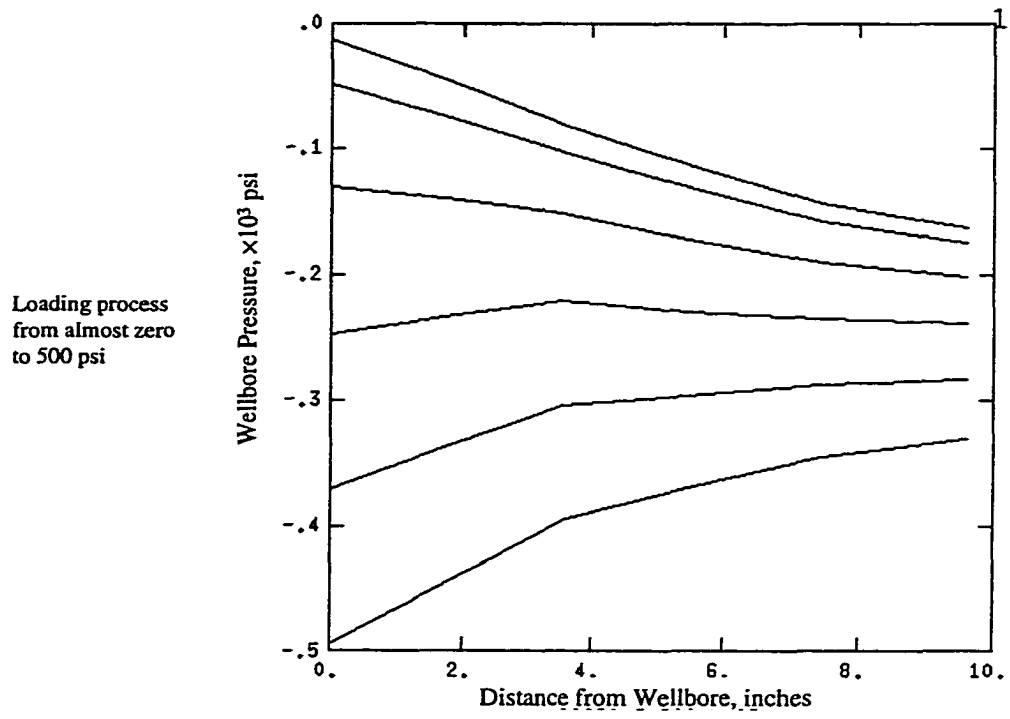


**Figure C.15 Selected LOT for further analysis.**

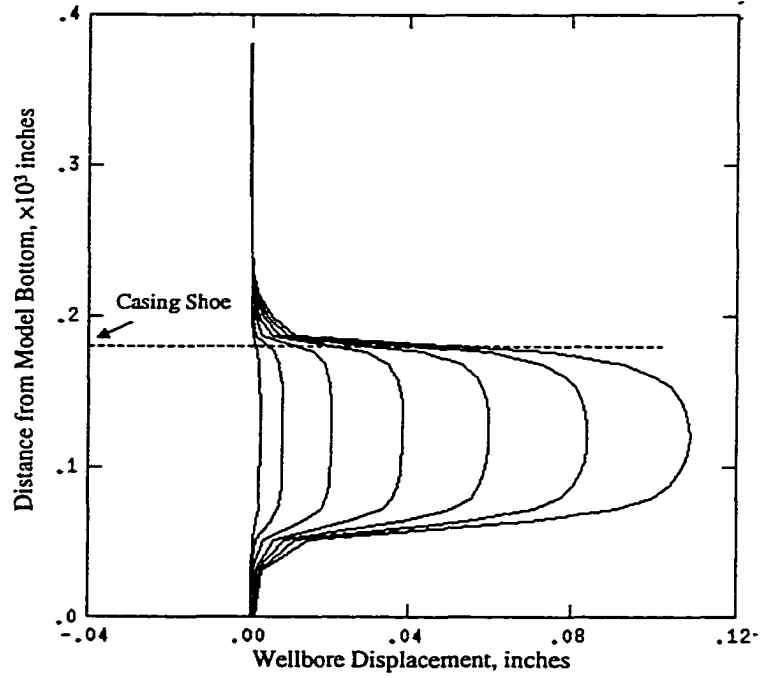


**Figure C.16 Radial displacements along Line 5 of Figure 5.3 for Case 2 at different LOT pressure. Cement parting is obvious.**

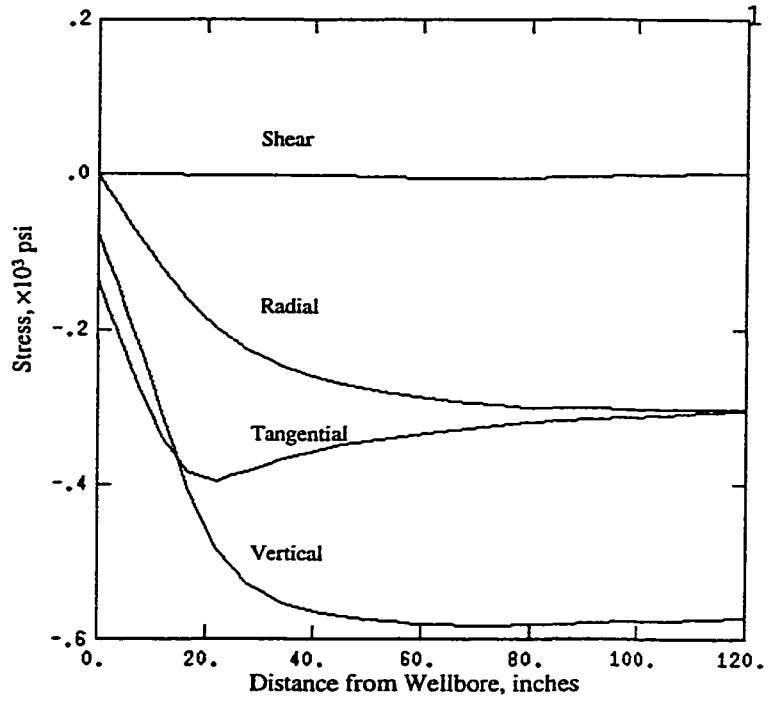


**Figure C.17** Stress distribution along Line 3 of Fig. 16 before LOT for Case 3.

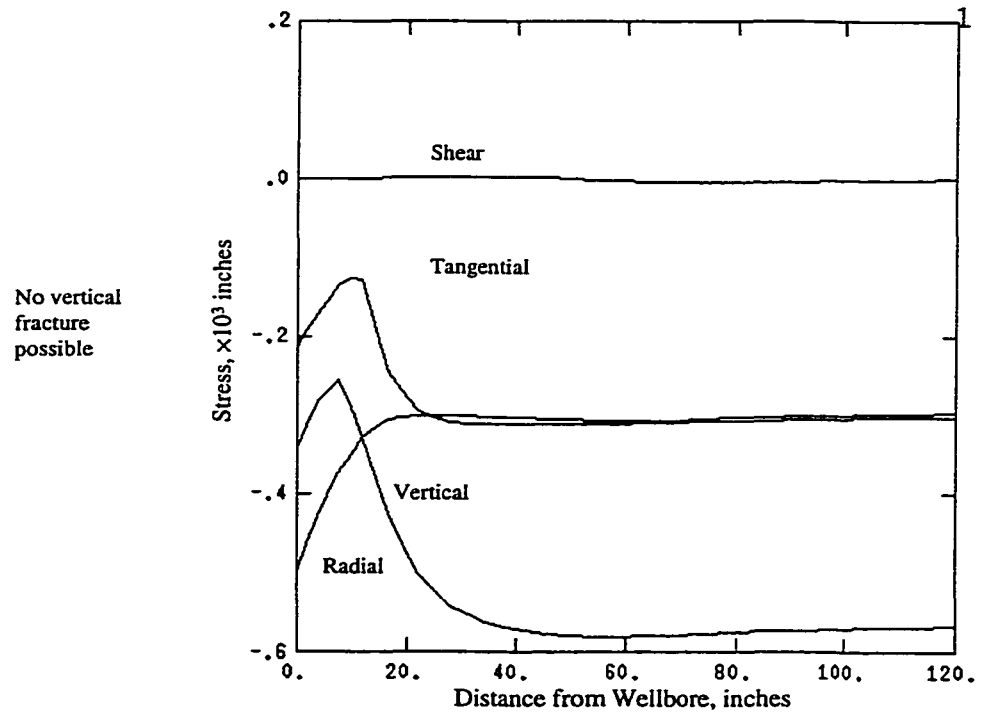


**Figure C.18** Stresses during LOT for Case 3.

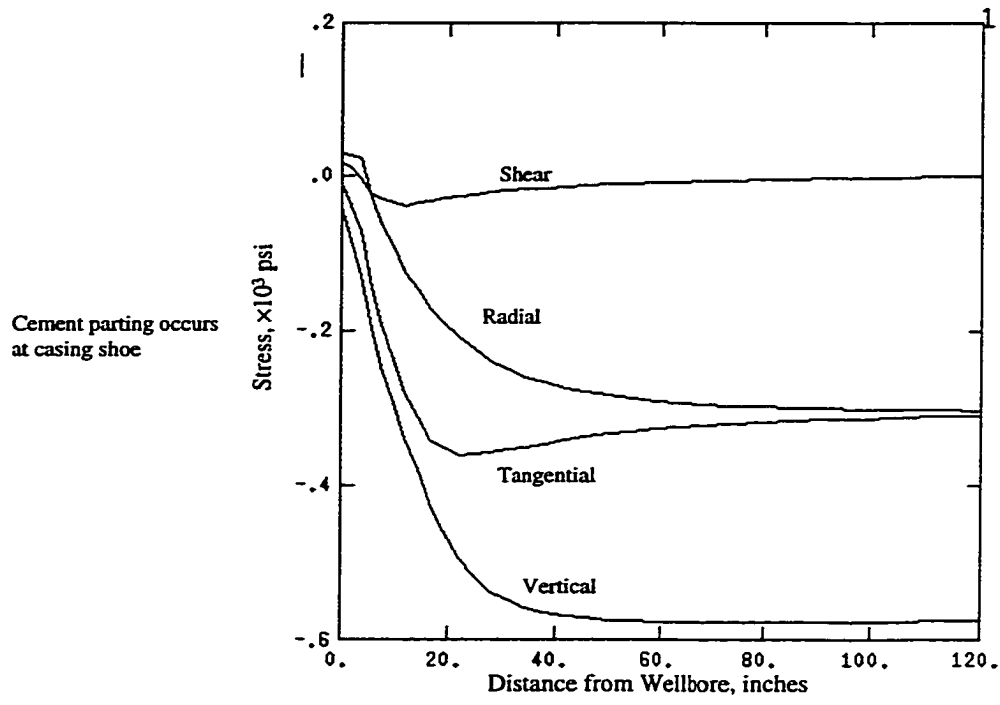


**Figure C.19 Stress distribution along Line 1 for Case 3 during LOT.**

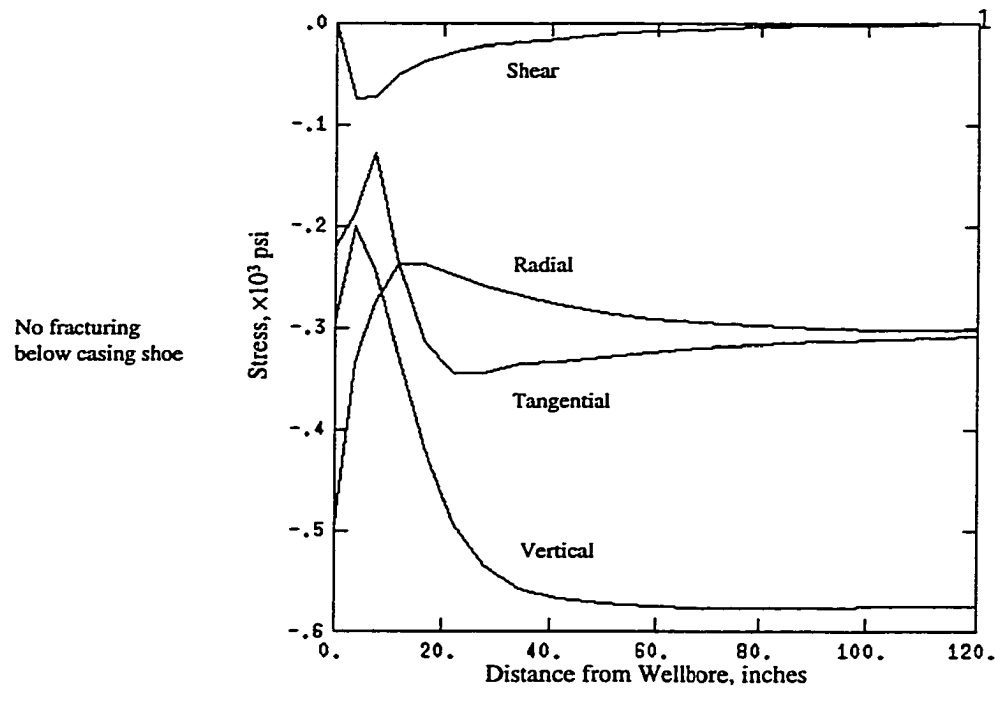


**Figure C.20 Stress distribution along Line 2 for Case 3 during LOT.**

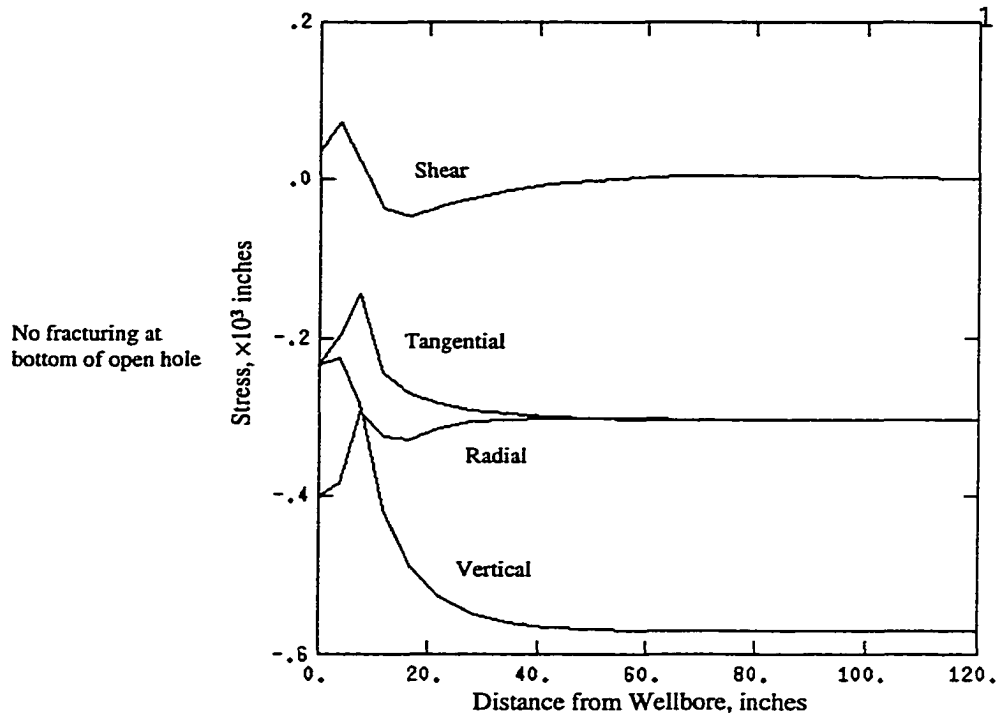


**Figure C.21 Stresses along Line 4 of Figure 5.3 for Case 3 during LOT.**

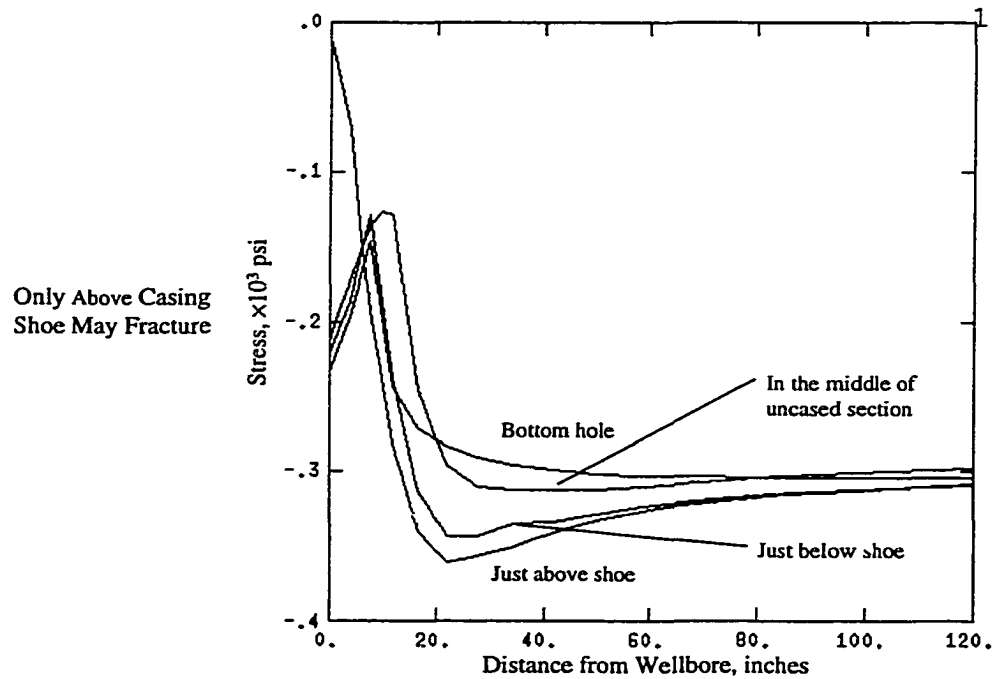


**Figure C.22 Tangential stresses along different horizontal lines (Fig. 16).**

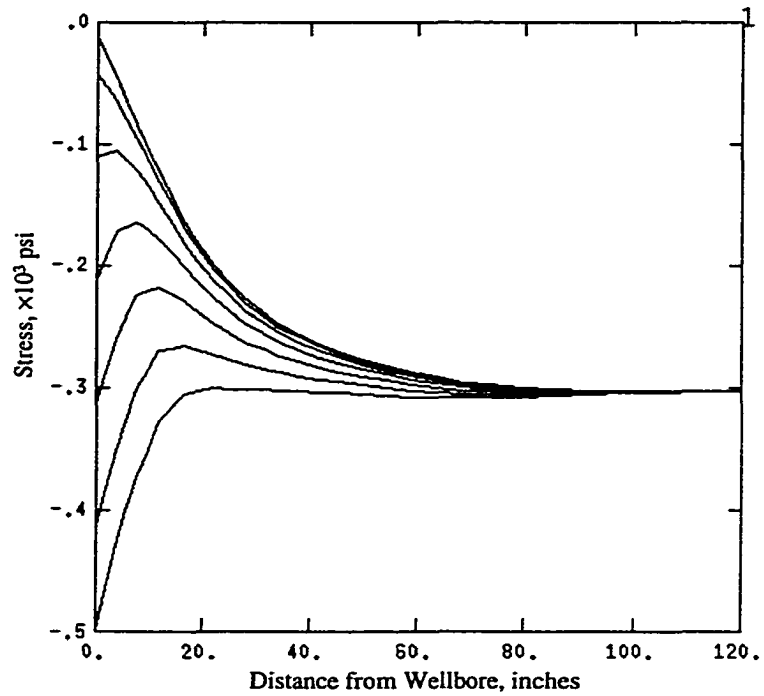


**Figure C.23 Radial stresses along Line 3 for Case 3 at different LOT pressure.**

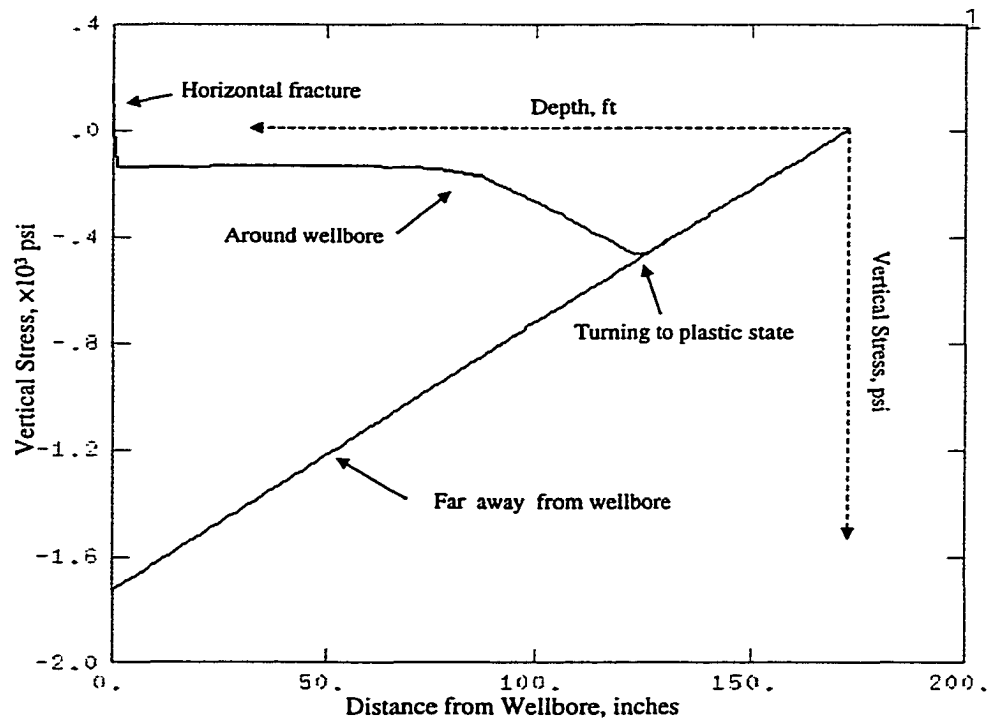


**Figure C.24 Vertical stress around wellbore and far-away. The figure shows the way to understand the figure. All the figures for following horizontal fracture analysis follow the same configuration.**

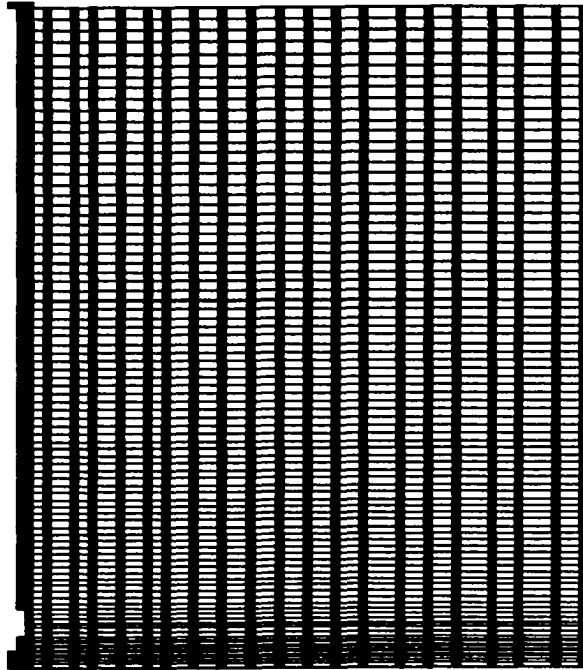


**Figure C.25** Finite elements and nodes for the analysis of horizontal fracture.

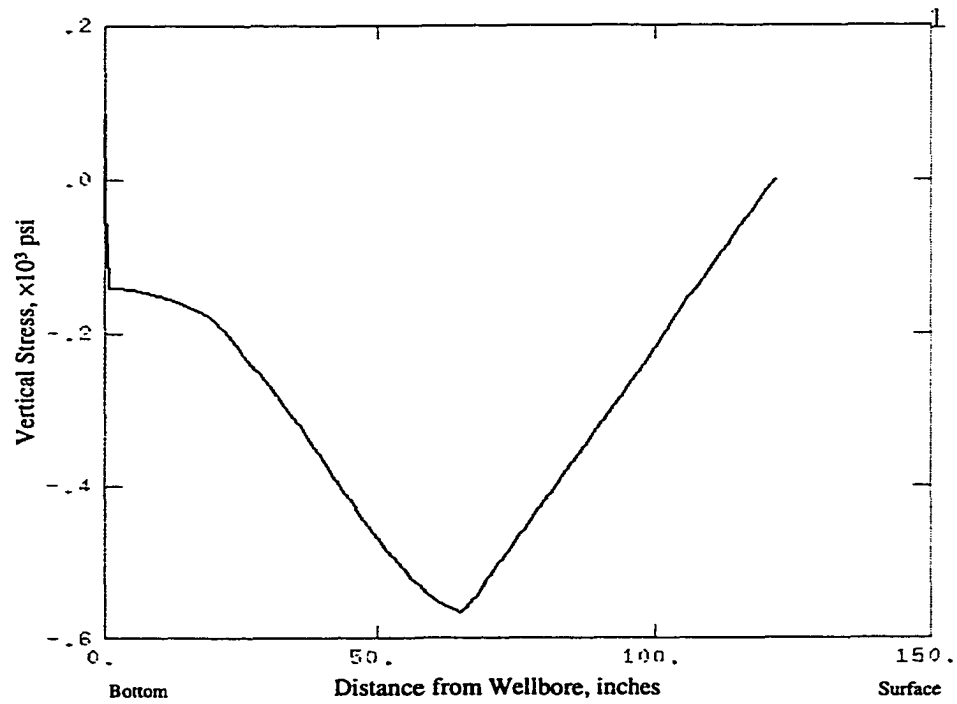


**Figure C.26** Effect of casing diameter (Table 5.1)

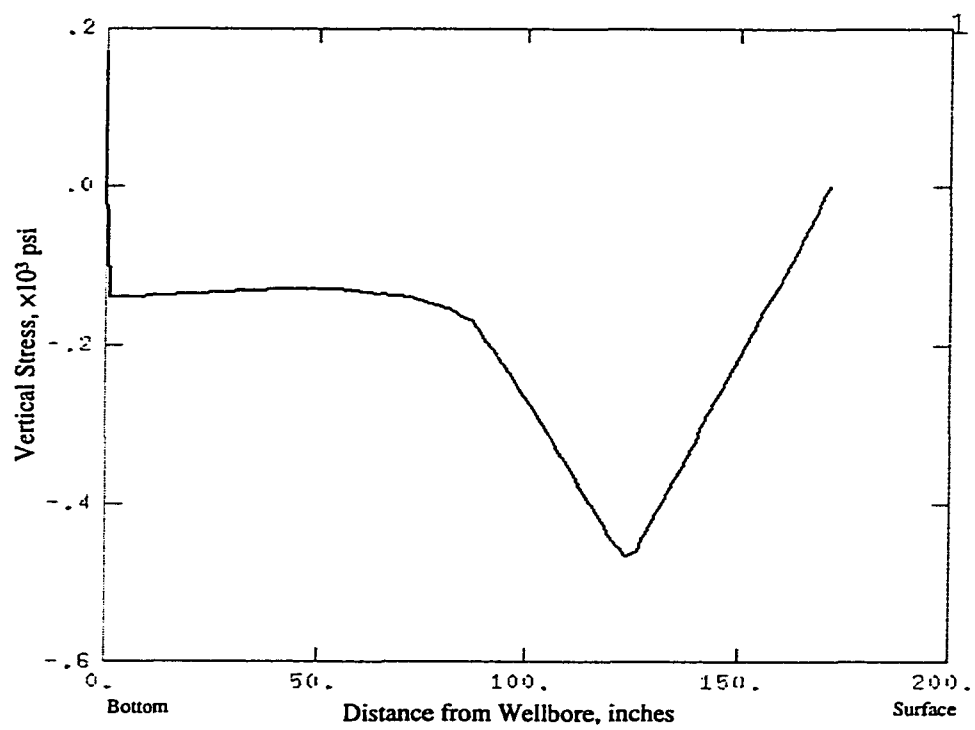


**Figure C.27 Effect of formation depth (Table 5.1)**

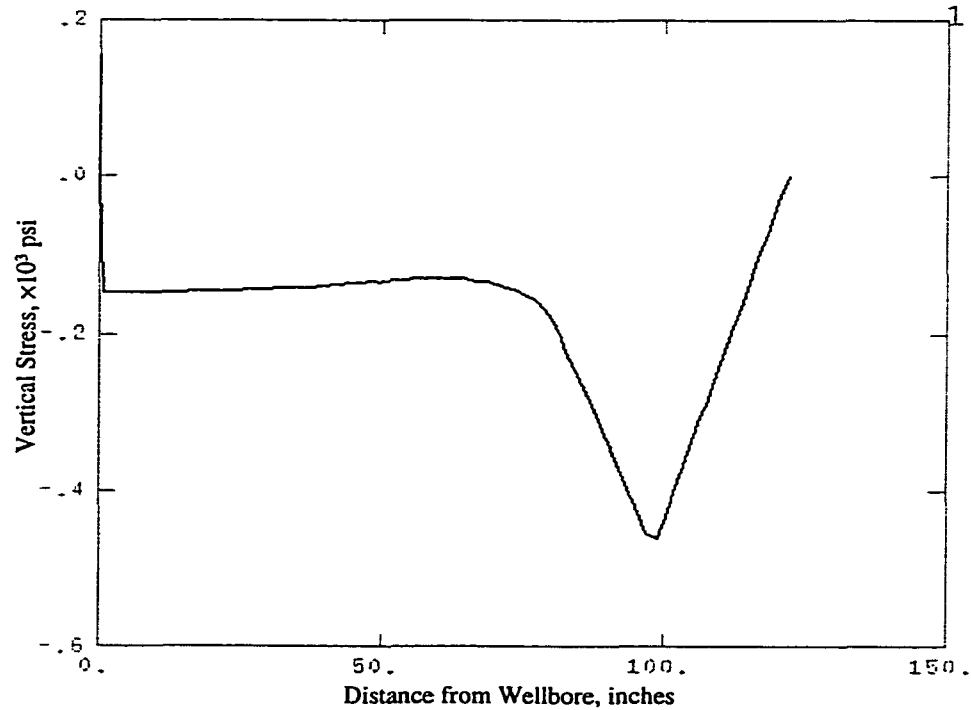


**Figure C.28 Effect of formation density (Table 5.1)**

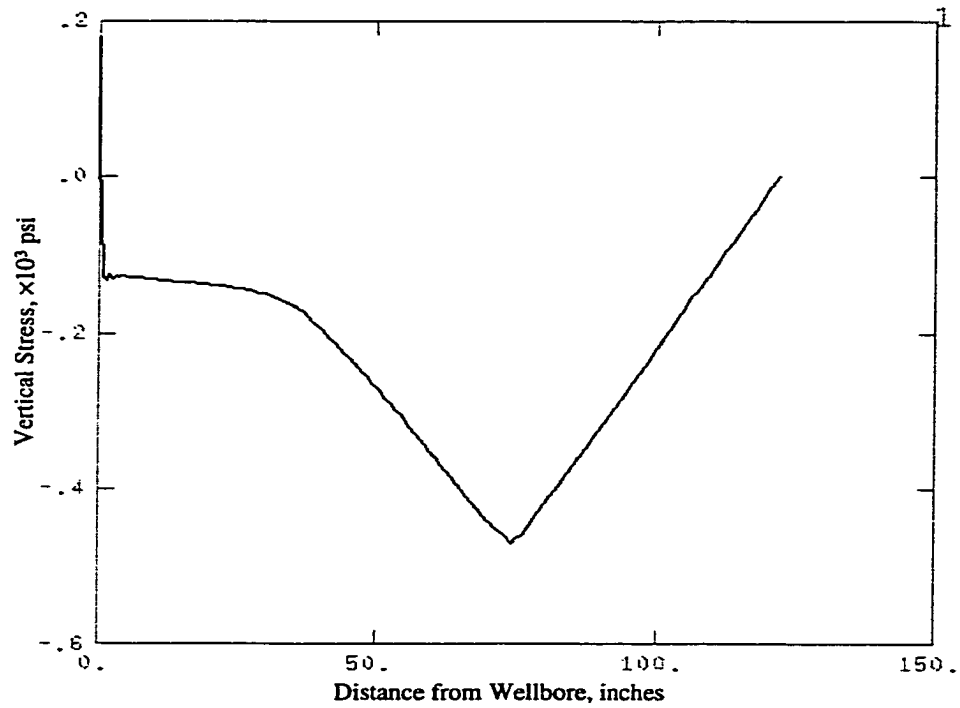


**Figure C.29 Effect of formation Young's modulus (Table 5.1)**

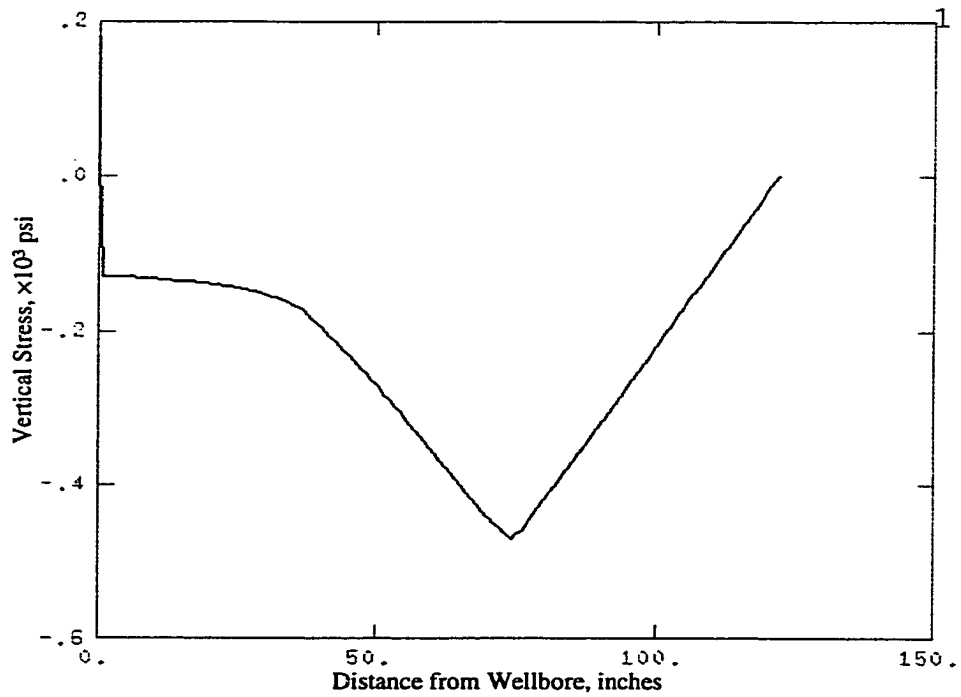


**Figure C.30 Effect of casing Young's modulus (Table 5.1)**

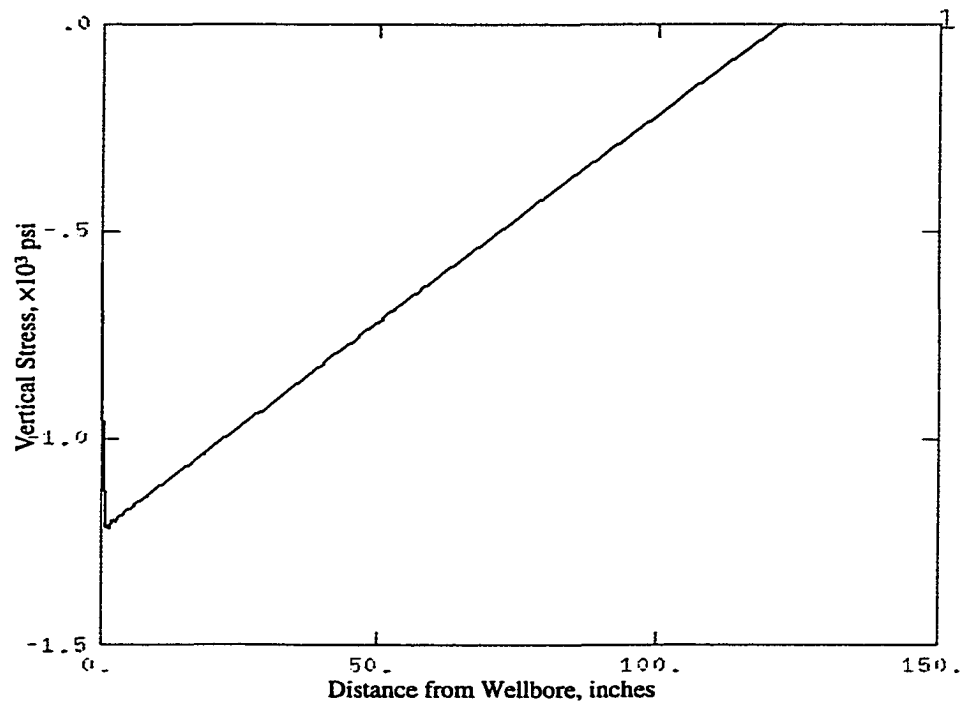


**Figure C.31 Elastic wellbore case: no vertical stress reduction around wellbore and no horizontal fracture.**

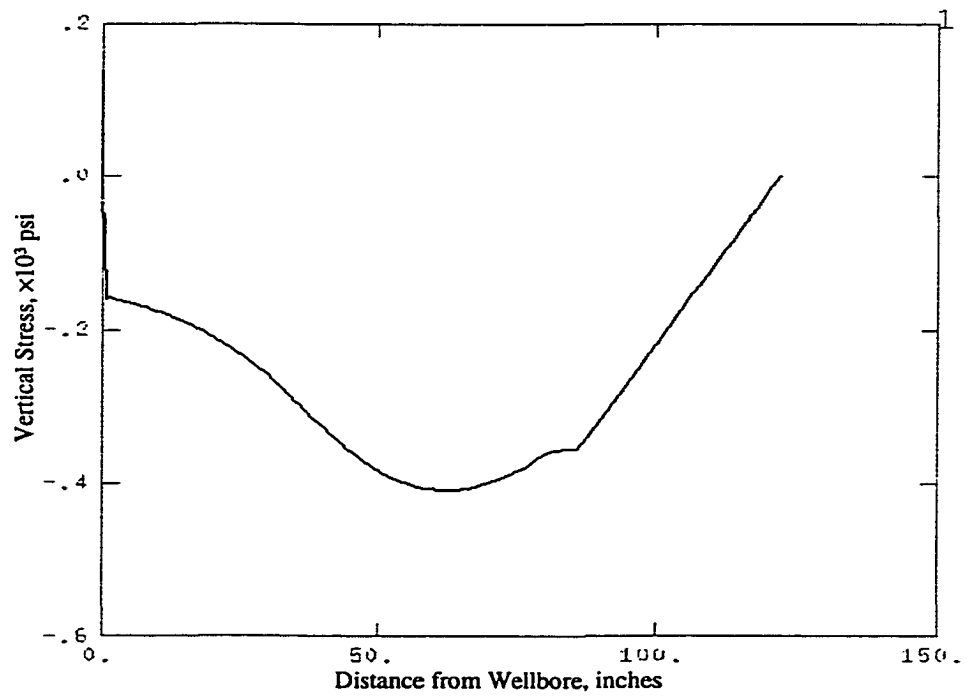


**Figure C.32 Effect of Poisson's ratio (Table 5.1)**

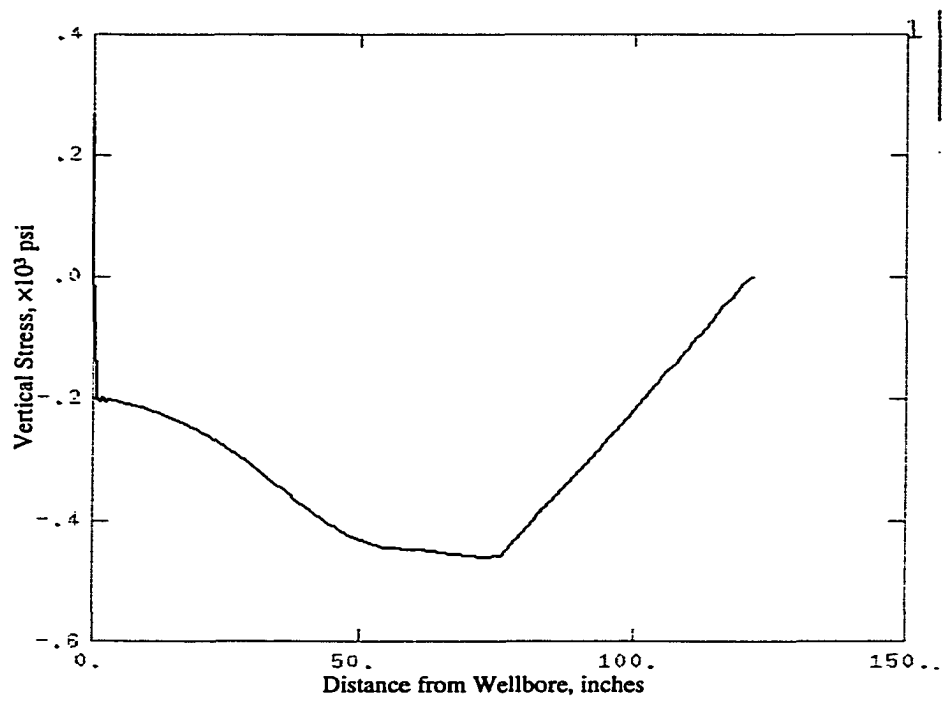


**Figure C.33 Effect of friction angle (Table 5.1)**

## APPENDIX D

### CEMENT CONTACT STRESS AT CASING SHOE

As shown in Fig. D.1(a), the contact pressure is the hydrostatic pressure of the cement slurry before cement setting. During slurry setting, the hydrostatic pressure will decrease to formation pore pressure as measured by Tinsley et al. (1980) in laboratory and Cooke et al. (1982) on field.

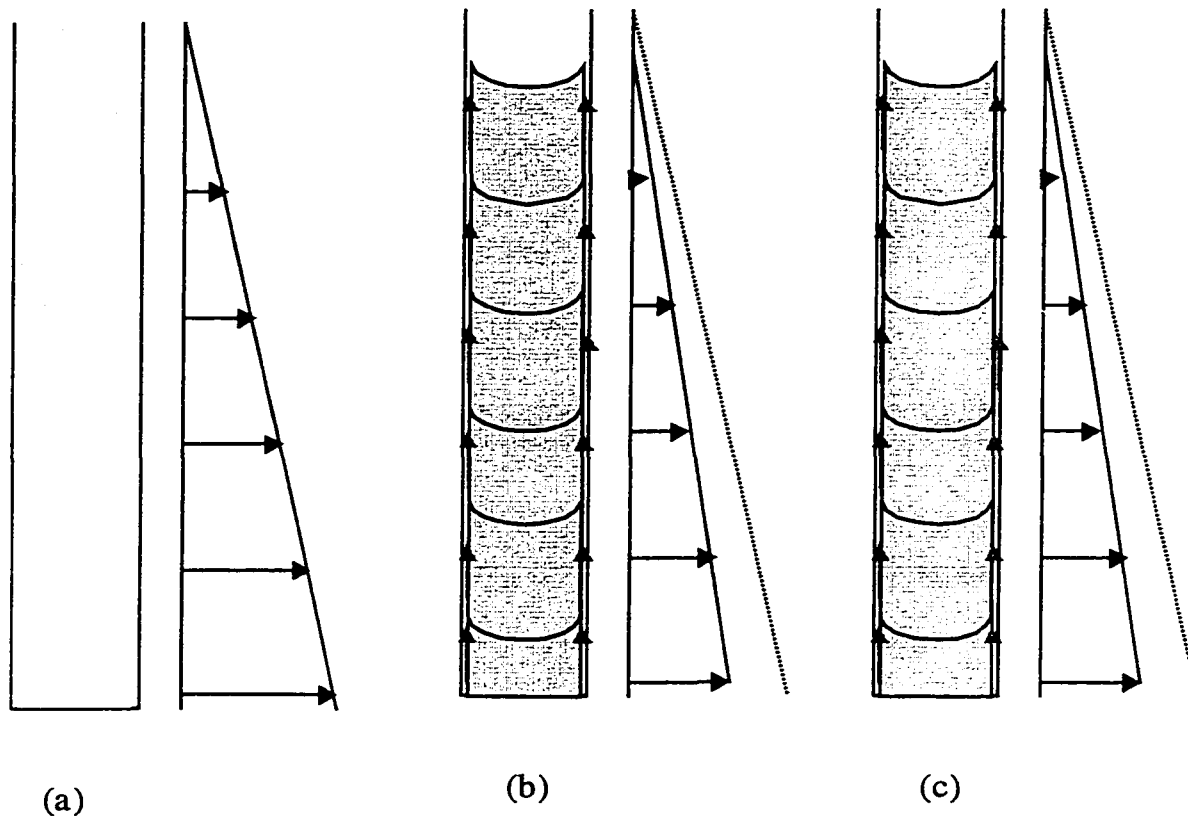


**Figure D.1** Formation of contact stress.

After cement placement, the initial cement matrix stress is zero and pore pressure is the hydrostatic pressure and equals contact pressure. During cement transition time, cement matrix and matrix stress develops. In the process, hydrostatic pressure of the slurry transforms to hydrostatic pressure of the pore water and the

effective contact pressure becomes equal to the cement matrix stress. All this happens during a slow settling of cement slurry caused by volume reduction (chemical shrinkage + filtration) opposed by increasing shear stress at the annulus walls (slurry gelation). Fig. D.1(b) shows the pressure during cement settling. The motion will stop when cement matrix can support its weight. Finally, cement matrix compressive stress reaches its final value when cement pore pressure reduces to formation pore pressure at the depth of interest, as shown in Fig. D.1(c). This final value of matrix stress would determine contact pressure and, in turn, affect the value of annulus leak-off pressure.

### D.1 Pressure Reduction in Annulus

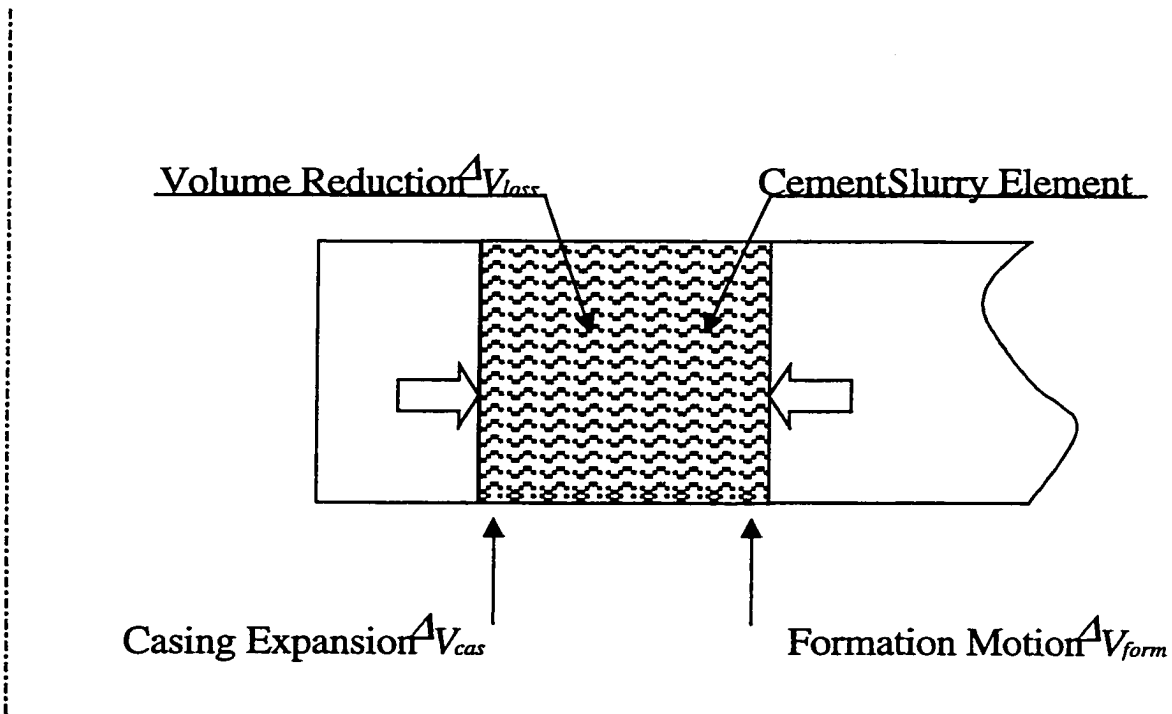


**Figure D.2** A concept of compressibility used by Tinsley et al (1980) to be modified for compensation effect from casing string and open hole.

Fig. D.2 shows a cement slurry element in the annulus between casing and formation having compressibility defined as follows:

$$C_{cem} = \frac{dV}{V dP_{de}}. \quad (D.1)$$

For a pressure reduction  $dP$ , the volume expansion  $dV$  is  $dV=CVdP$ . If the  $dV$  is treated as volume reduction due to chemical shrinkage and filtration, the resulting pressure drop is

$$dP_{de} = \frac{dV_{loss}}{V} \frac{1}{C_{cem}}. \quad (D.2)$$

The above concept was used by Sutton et al. (1984) for compressibility of cement without consideration given to elastic contribution from casing and rock. If  $dV_{ww}$  and  $dV_{cas}$  represent volumetric expansions of casing string and wellbore wall, the relation of pressure and volume becomes

$$dP_{de} = \frac{dV_{loss} - dV_{ww} - dV_{cas}}{V} \frac{1}{C_{cem}}. \quad (D.3)$$

Equation D.3 can be used to calculate pressure reduction at any depth in the annulus. Using similar concept pressure reduction at casing shoe can also be calculated.

## D.2 Pressure Reduction at Casing Shoe

Contact pressure can be calculated from initial pressure at casing shoe once we know pressure reduction there. The initial pressure is discussed, first.

### D.2.1 Initial Pressure at Casing Shoe

Initial pressure is the maximum hydrostatic pressure at casing shoe after cement placement. The maximum hydrostatic pressure can be calculated from the fluid column in the annulus above casing shoe. Casing shoe depth would decrease a little bit after the top plug is bumped since pressure in casing string will decrease with

stopping pump and shutting well in. However, as shown in the following example, the upward motion of the casing shoe is very small comparing to thousand feet of casing string for the calculation of hydrostatic pressure.

If a 11¾” N 80 (60 ppf) casing string was set at 10,000 ft, the equivalent density in the annulus is 11.4 lbm/gal, and 9 lbm/gal mud is used to displace the cement slurry. If the shut in pressure decreases to 0 psig and neglects the hydrostatic pressure in its float collar, the hydrostatic force in casing string on the top plug is  $0.052(9)(10,000)(1/4\pi(10.772)^2) = 426509$  lbf. The force on the bottom plug from the cement annulus column is  $0.052(11.4)(10,000)(1/4\pi(11.75)^2) = 642797$  lbf. The upward displacement by the force difference on cement plugs (the hydrostatic pressure from annular on the plug bottom subtracts the mud pressure on top of the plug) is

$$\begin{aligned} \Delta h_{mv} &= \frac{\Delta F D_{cas}}{A_{cs} E_{cas}} \\ &= \frac{0.052 D_{cas}^2 (\rho_{ics} A_{oc} - \rho_{mdis} A_{ic}) - P_{surc} A_{ic} D_{cas}}{A_{cs} E_{cas}} \end{aligned} \quad (D.4)$$

The displacement caused by the pressure difference is about 4 ft from Eq. D.3 using  $E_{cas} = 30E6$  psi. Although this height can be ignored for hydrostatic pressure calculation, it increases the open hole section below casing shoe and should be added to  $\Delta h$  in Eq. 6.6 for pressure reduction calculation.

### D.2.2 Compensation from Casing String Elongation

In annulus, volume reduction of the slurry element is partially compensated by the expansion of casing string and wellbore wall. Below casing shoe, casing string elongation is just another factor contributing the pressure compensation of the element.

### D.2.2.1 Elongation from Pressure Reduction

During cement setting, casing shoe pressure decreases due to volume reduction of cement slurry. As discussed above, a new stress balance is formed in casing string after the motion of casing shoe. We assume casing string is in its elastic range, so linear strain occurs.

For pressure drop,  $\Delta P_{de}$ , force reduction at the close-ended casing string is  $\Delta F_1 = A_{oc} \Delta P_{de}$ , and casing string elongation is

$$\Delta L_1 = \frac{\Delta F_1 D_{cas}}{A_{cs} E_{cas}} = \frac{A_{oc} \Delta P_{de} D_{cas}}{A_{cs} E_{cas}}. \quad (D.5)$$

### D.2.2.2 Elongation from Shear Stress

Hydrostatic pressure decrease is the result of shear stress along the outside surfaces of annulus cement slurry column. The same shear stress pulls on the casing string downward. The shear stress would make the casing string elongate.

For pressure reduction  $\Delta P_{de}$  at the casing shoe, force reduction from annulus slurry at the casing shoe is  $(A_{ww} - A_{oc}) \Delta P_{de}$ . The force acting on the casing string is about half of it, that is  $\Delta F_2 = 1/2 (A_{ww} - A_{oc}) \Delta P_{de}$ . The distribution of the shear stress along casing is complex. It is assumed as uniformly distributed along casing string to calculate casing string lengthening. The shear force on a unit length of casing string

$$\Delta f = \frac{\Delta F_2}{D_t} = \frac{(A_{ww} - A_{oc}) \Delta P_{de}}{2D_t}. \quad (D.6)$$

Where:  $D_t$  is the height of tail cement slurry since it is generally designed to set first. If tail and lead cement slurries set at the same time or only one cement slurry is on the annulus, all cement column height should be used in Eq. D.6 instead of  $D_t$ . At any

depth  $D_x$  from top tail cement slurry, the increased cross sectional force in casing string by the shear stress is

$$F(x) = \Delta f D_x = \frac{(A_{ww} - A_{oc}) \Delta P_{de}}{2D_t} D_x. \quad (D.7)$$

For the casing string element,  $\Delta x$ , at depth  $D_x$  the elongation of this element is

$$\Delta L(\Delta x) = \frac{F(x) \Delta x}{A_{cs} E_{cas}}. \quad (D.8)$$

Therefore, the total length change of all the casing string by pressure reduction  $\Delta P_{de}$

$$\begin{aligned} \Delta L_2 &= \int_0^{D_t} \frac{F(x)}{A_{cs} E_{cas}} dx + \frac{\Delta P_{de} (A_{ww} - A_{oc}) (D_{cas} - D_t)}{2A_{cs} E_{cas}} \\ &= \int_0^{D_t} \frac{(A_{ww} - A_{oc}) \Delta P_{de} D_x}{2D_t A_{cs} E_{cas}} dx + \frac{\Delta P_{de} (A_{ww} - A_{oc}) (D_{cas} - D_t)}{2A_{cs} E_{cas}} \\ \Delta L_2 &= \frac{(A_{ww} - A_{oc}) \Delta P_{de} (D_{cas} - D_t)}{2A_{cs} E_{cas}} + \frac{(A_{ww} - A_{oc}) \Delta P_{de} D_t}{4A_{cs} E_{cas}} \\ &= \frac{(A_{ww} - A_{oc}) \Delta P_{de}}{2A_{cs} E_{cas}} (D_{cas} - 0.5D_t) \end{aligned} \quad (D.9)$$

### D.2.2.3 Compensation from Total Casing String Elongation

Total elongation of casing string is the sum of the displacements caused by shear stress and pressure reduction.

$$\begin{aligned} \Delta L_{cas} &= \Delta L_1 + \Delta L_2 \\ &= \frac{A_{oc} D_{cas} \Delta P_{de}}{A_{cs} E_{cas}} + \frac{(A_{ww} - A_{oc}) \Delta P_{de}}{2A_{cs} E_{cas}} (D_{cas} - 0.5D_t) \\ \Delta L_{cas} &= \frac{\Delta P_{de}}{2A_{cs} E_{cas}} (A_{ww} (D_{cas} - 0.5D_t) + A_{oc} (D_{cas} + 0.5D_t)) \end{aligned} \quad (D.10)$$

The volumetric effect of this elongation is

$$\Delta V_{cas} = A_{ww} \Delta L_{cas} \cdot \quad (D.11)$$

We assume the area  $A_{ww} \cong A_{oc}$  since no relative motion between the casing string at shoe and the cement slurry outside it is assumed for the reason of small annulus and cement gelation.

Volume compensation coefficient,  $K_{cas}$ , is the ratio of compensated volume and the total slurry volume below casing shoe,  $V = A_{ww} \Delta h$ . Open hole section  $\Delta h$  is the height of the gap below casing shoe. Effective open hole height should be used if there are more than one wellbore diameters below casing shoe.

$$K_{cas} = \frac{\Delta V_{cas}}{V} = \frac{\Delta L_{cas}}{\Delta h} = C_{cas} \Delta P_{de} \cdot \quad (D.12)$$

$$\text{Where } C_{cas} = \frac{A_{ww}(D_{cas} - 0.5D_t) + A_{oc}(D_{cas} + 0.5D_t)}{2A_{cs}E_{cas}\Delta h} \Delta P_{de} \cdot$$

### D.2.3 Compensation from Slurry Expansion

Cement slurry expands as pressure decreases. Cement slurry compressibility consists of its components and is  $C_{cem} = C_w f_w + (1 - f_w) C_s$ . Where  $f_w$  is water volume fraction in the slurry. Cement slurry compressibility decreases during cement transition from liquid to solid. Average slurry compressibility should be used. For a pressure reduction  $\Delta P_{de}$  expanded volume of the cement slurry element below casing shoe is

$$\Delta V_{cem} = (A_{ww} \Delta h) C_{cem} \Delta P_{de} \cdot \quad (D.13)$$

Volume compensation coefficient

$$K_{cem} = C_{cem} \Delta P_{de} \cdot \quad (D.14)$$

#### D.2.4 Compensation from Wellbore Shrinkage

When pressure in a well decreases, wellbore wall will move inside and compensates some volume. Compensated volume is

$$\Delta V_{ww} = \pi d_{ww} \Delta h \Delta r_{ww} = A_{ww} \Delta h \left( \frac{4}{d_{ww}} \Delta r_{ww} \right). \quad (D.15)$$

Where  $\Delta r_{ww}$  is the displacement of a wellbore wall due to a pressure reduction,  $\Delta P_{de}$ .

$$\Delta r_{ww} = \frac{3 \Delta P_{de} d_{ww}}{4 E_{form}}. \quad (D.16)$$

Volume compensation coefficient

$$K_{ww} = \frac{4}{d_{ww}} \Delta r_{ww} = \frac{3 \Delta P_{de}}{E_{form}}. \quad (D.17)$$

Wellbore bottom will also move up when wellbore pressure decreases. If the same displacement formula is used

$$\Delta V_{wb} = A_{ww} \Delta r_{ww} = (A_{ww} \Delta h) \frac{3 \Delta P_{de} d_{ww}}{4 E_{form} \Delta h}. \quad (D.18)$$

Volume compensation coefficient  $K_{wb} = \frac{3 \Delta P_{de} d_{ww}}{4 E_{form} \Delta h}$ . If well bore diameter is

in inches and open hole section is in feet, then

$$K_{wb} = \frac{3 \Delta P_{de} d_{ww}}{48 E_{form} \Delta h}. \quad (D.19)$$

#### D.2.5 Pressure Reduction after Total Compensation

Due to volume reduction of the slurry below casing shoe, cement slurry pressure decreases. However, as shown in Fig. D.3, the pressure reduction at casing

shoe will be partly compensated by casing string elongation, slurry expansion, and wall and bottom motions. Same logic as Eq. D.3, the correlation of pressure reduction and volume change for the slurry element below casing shoe can be written as

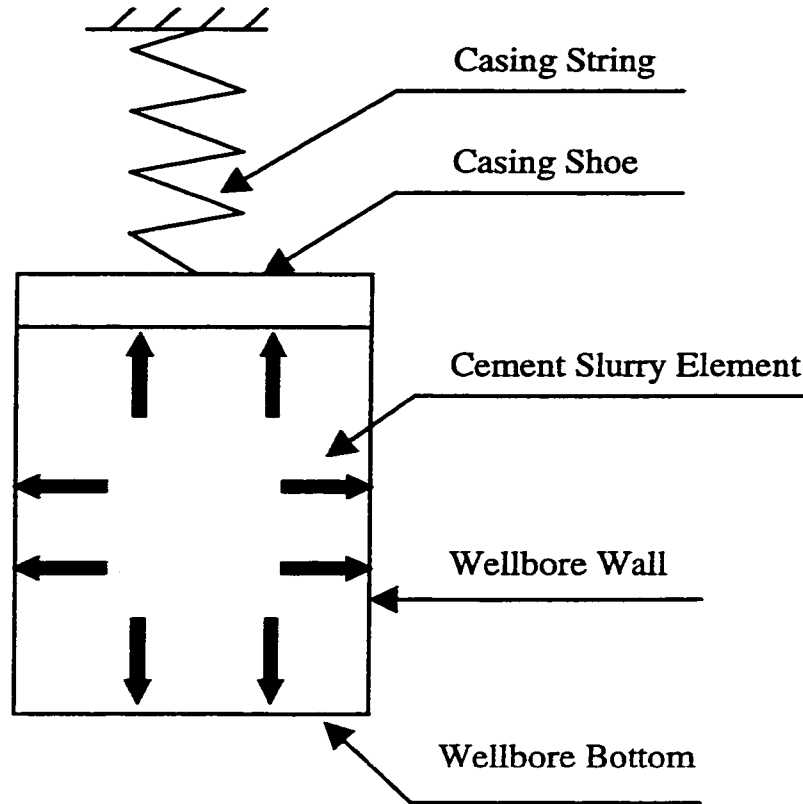


**Figure D.3** A bottomhole hydrostatic pressure drop in cement slurry below casing shoe is compensated by casing string, wellbore wall and wellbore bottom.

$$dP_{de} = \frac{dV_{loss} - dV_{ww} - dV_{wb} - dV_{cas}}{V} \frac{1}{C_{cem}} \quad (D.20)$$

$$= (K_{loss} - K_{ww} - K_{wb} - K_{cas}) / C_{cem}$$

Where  $K_{loss} = dV_{loss}/V$ . Substitute of Eqs. D.12, D.17 and D.19 into Eq. D.20 and rearrange it, we get

$$\Delta P_{de} = \frac{1}{C_{cas} + C_{cem} + C_{form}} K_{loss} \cdot \quad (D.21)$$

Where

$$C_{cas} = \frac{A_{ww}(D_{cas} - 0.5D_t) + A_{oc}(D_{cas} + 0.5D_t)}{2A_{cs}E_{cas}\Delta h}, \text{ and } C_{form} = \frac{3}{E_{form}} \left(1 + \frac{d_{ww}}{48\Delta h}\right).$$

Two limitations for this equation: one is the total elongation  $\Delta L_{cas} < \Delta h$ ; the other is  $\Delta P_{de} < P_{ics} - P_p$ .

It should be point out that an assumption is implied in derivation of Eq. D.21. That is there is no inter-volume change between elements. The assumption is right for uniform volume reduction of slurry elements and it holds approximate for the following reasons. The slurry element below casing shoe can not flow into the annulus above it since to flow into the annulus the compensated pressure has to change the shear stress direction first and then lifts the slurry in the annulus. The annulus fluid cannot also flow into the element since any flow will break the supporting shear stress and make pressure reduction almost zero from Cooke et al. (1982).

Eq. D.21 can also be derived by material balance principle. Lost volume equals compensated volume at new pressure balance.

$$\begin{aligned} & K_{cas}A_{ww}\Delta h + K_{cem}A_{ww}\Delta h \\ & + K_{ww}A_{ww}\Delta h + K_{wb}A_{ww}\Delta h = K_{loss}A_{ww}\Delta h. \end{aligned}$$

$$K_{cas} + K_{cem} + K_{ww} + K_{wb} = K_{loss}. \quad (D.22)$$

From Eq. D.22, we can also get Eq. D.21.

**APPENDIX E**  
**WELLBORE EXPANSION**

Wellbore expansion under wellbore pressure during LOT is derived here based on elastic theory. The basic mechanic equations are well discussed in most of elastic books. Obert and Duvall (1967) and Chen and Han (1988) also presented these equations.

The derivation is simplified as plain strain. Fig. 7.1 may be used as a reference ignoring the plastic zone. A cylinder with an inner radius of  $r_w$  under pressure of  $p_w$  and the outside radius extends to infinite with a pressure of  $\sigma_h$ . The rock cylinder is assumed as smooth, isotropic, homogeneous, and in elastic state.

General equilibrium equation of any element in a cylindrical coordinate system

$$\frac{d\sigma_r}{dr} - \frac{\sigma_\theta - \sigma_r}{r} = 0 \quad (\text{E.1})$$

Radial strain  $\epsilon_r$  and tangential strain  $\epsilon_\theta$  with radial displacement  $u$  at radius  $r$  can be expressed as

$$\epsilon_r = \frac{du}{dr}, \quad \epsilon_\theta = -\frac{u}{r} \quad (\text{E.2})$$

For plain strain, vertical strain  $\epsilon_z=0$ . Elastic constitutive relation of an element

$$\begin{aligned} E\epsilon_r &= \sigma_r - \mu(\sigma_\theta + \sigma_z) \\ E\epsilon_\theta &= \sigma_\theta - \mu(\sigma_r + \sigma_z) \\ E\epsilon_z &= \sigma_z - \mu(\sigma_r + \sigma_\theta) \end{aligned} \quad (\text{E.3})$$

Compatibility relation can be got from Eq. E.2,

$$\epsilon_r = \frac{d}{dr}(r\epsilon_\theta) \quad (\text{E.4})$$

Substitution of Eq. E.3 into Eq. E.4 yields

$$\frac{\sigma_r - \sigma_\theta}{r} = (1 - \mu) \frac{d\sigma_\theta}{dr} - \mu \frac{d\sigma_r}{dr}$$

Using Eq. E.1 to eliminate  $\sigma_\theta$  and  $d\sigma_\theta/dr$  in the above equation gets

$$r \frac{d\sigma_r^2}{dr^2} + 3 \frac{d\sigma_r}{dr} = 0 \quad (\text{E.5})$$

Boundary conditions for LOT can be expressed as

$$\begin{aligned} \sigma_r &= p_w, & \text{at } r &= r_w \\ \sigma_r &= \sigma_h, & \text{at } r &= \infty \end{aligned}$$

Solving Eq. E.5 at the boundary condition for  $\sigma_r$  and substituting into Eq. E.1

for  $\sigma_\theta$  yields

$$\begin{aligned} \sigma_r &= \sigma_h - (\sigma_h - p_w) \frac{r_w^2}{r^2} \\ \sigma_\theta &= \sigma_h + (\sigma_h - p_w) \frac{r_w^2}{r^2} \end{aligned} \quad (\text{E.6})$$

Radial displacement,  $u$ , can be got from Eq. E.2 by substituting Eq. E.3 and Eq. E.4. Note that Poisson's ratio  $\mu = 0.5$  and  $\sigma_z = \mu(\sigma_r + \sigma_\theta)$  for plane strain problem.

$$u = \frac{3(p_w - \sigma_h)r_w^2}{2Er} \quad (\text{E.7})$$

When the radius of  $r$  gets the value of wellbore size, Eq. E.7 reduces to the displacement at the wellbore wall

$$u_w = \frac{3(p_w - \sigma_h)r_w}{2E} \quad (\text{E.8})$$

The displacement is the motion of the wellbore wall under the action of inside pressure of  $p_w$ , outside stress of  $\sigma_h$ . Using superposition principle for the linear elastic

deformation, the displacement of an increase of wellbore pressure  $\Delta p_w$  can be derived from Eq. E.7.

$$u = \frac{3\Delta p_w r_w^2}{2Er} \quad (\text{E.9})$$

At the wellbore wall

$$u_w = \frac{3\Delta p_w r_w}{2E} \quad (\text{E.10})$$

## APPENDIX F

### FORMATION FRACTURE WIDTH AND VOLUME

As shown in Fig. 7.1, there is a plastic zone around a wellbore and outside the plastic zone is an elastic zone. Vertical stress is always overburden stress in the elastic zone and drops largely in the plastic zone. A lower wellbore pressure can open a horizontal crack in the plastic zone if it is greater than the vertical stress around the crack although it is less than in-situ overburden stress (Fig. 7.2). Since the vertical stress increases with radius in the plastic zone, higher wellbore pressure is needed to propagate the formed horizontal fracture at lower wellbore pressure. The formed fracture in the plastic zone is called plastic fracture in the dissertation since it can only be propagated with increasing wellbore pressure (Wojtanowicz and Zhou, 1998).

The plastic zone is formed during drilling operation. LOT is a further loading process to the plastic zone. According to plastic theory (Chen and Han, 1988), further loading on a plastic zone may result in a further plastic deformation or only elastic deformation depending on so-called loading type. Three loading types are loading, neutral loading and unloading (Chapter 5, Eq. 5.4). For horizontal fracturing, the further deformation is elastic since the wellbore wall is cemented and can not move inward (unloading).

Horizontal fracture size increases with wellbore pressure. Assuming a penny-shaped crack in a circular cylinder deforms in a linear elastic manner, Sneddon and Lowengrub (1969) gave the basic width equation based on plane strain condition.

$$w(r) = \frac{4(1-\mu)r_c}{\pi G} \int_{r/R}^1 \frac{df_2}{\sqrt{(f_2^2 - (r/r_c)^2)}} \int_{r_w/R}^{f_2} \frac{f_1 \Delta p(f_1) df_1}{\sqrt{f_2^2 - f_1^2}} \quad (\text{F.1})$$

Where,  $f_1$  and  $f_2$  are fractions of the length of interested place  $r$  to the total length of the crack  $R$ .  $G$  is the shear modulus of the rock and  $G=E/2(1-\mu)$ ,  $\Delta p$  is the difference of the effective fluid pressure in the crack and the closing stress of the crack.

Vertical stress increases almost linearly with distance from wellbore wall and can be expressed as (Wojtanowicz and Zhou, 1998)

$$\sigma_v = N(p_w + \frac{\sigma_0}{N-1})\left(\frac{r}{r_w}\right)^{N-1} - \frac{\sigma_0}{N-1} \quad (\text{F.2})$$

For the convenience of the integration of Eq. F.1, Eq. F.2 is simplified as a linear relation by forcing  $N=2$ .  $N=2$  corresponds to an internal friction angle of 20 degrees which is a representative value of shallow sediments around 500 ft in the Gulf of Mexico.

$$\sigma_v = 2(p_w + \sigma_0)\frac{r_c}{r_w}\left(\frac{r}{r_c}\right) - \sigma_0 \quad (\text{F.3})$$

From Eq. F.3, the vertical stress is reduced from in-situ overburden stress to  $\sigma_v=2p_w+\sigma_0$  at the wellbore wall. To make the fracture propagate to a radius of  $R$  ( $r_w \leq R \leq r_c$ ), the effective fluid pressure in the fracture should be equal to the vertical stress at the radius  $R$ . It is assumed that the fluid pressure in the fracture is constant everywhere and equals to the wellbore pressure at casing shoe since the fracture is relatively short (in plastic zone), wide in width, and low pump rate. Therefore, fracture length  $R$  can be calculated from effective wellbore pressure  $p_{LOT}$ .

$$p_{LOT} = 2(p_w + \sigma_0)\frac{r_c}{r_w}\left(\frac{R}{r_c}\right) - \sigma_0 \quad (\text{F.4})$$

$$R = \frac{(p_{LOT} + \sigma_0)r_w}{2(p_w + \sigma_0)} \quad (\text{F.5})$$

For such an effective wellbore pressure  $p_{LOT}$ , the pressure to open the fracture at any place  $r$  ( $r \leq R$ ) on the two sides of the fracture is

$$\begin{aligned} \Delta p(f_1) &= p_{LOT} - \sigma_v = p_{LOT} + \sigma_o - 2(p_w + \sigma_0) \frac{R}{r_w} \left( \frac{r}{R} \right) \\ &= A(1-f_1) \quad \text{for } r \leq R \end{aligned} \quad (F.6)$$

Where  $A = p_{LOT} + \sigma_o$ ,  $2(p_w + \sigma_0)(R/r_w) = A$  from Eq. F.5, and  $f_1 = r/R$ .

Substituting Eq. F.6 into Eq. F.1 gives the half width at radius  $r$  in a fracture propagating to  $R$ .

$$w(r) = \frac{4(1-\mu)R}{\pi G} \int_{r/R}^1 \frac{df_2}{\sqrt{(f_2^2 - (r/r_c)^2)}} \int_{r_w/R}^{f_2} \frac{f_1(A - Af_1) df_1}{\sqrt{f_2^2 - f_1^2}} \quad (F.7)$$

Integrating Eq. F.7 yields

$$\begin{aligned} w(r, R) &= \frac{8(1-\mu^2)AR}{\pi E} \left\{ \left(1 - \frac{f_{rw}}{2}\right) \left[ \sqrt{(1-f_{rw}^2)(1-f_r^2)} - \frac{f_{rw}^4 \sqrt{(1-f_r^2)^3}}{8f_r^2} \right. \right. \\ &\quad \left. \left. - \frac{f_{rw}^2}{2f_r^2} \left(1 + \frac{f_{rw}^2}{8f_r^2}\right) \left( \sqrt{(1-f_r^2)^3} - \sqrt{1-f_r^2} + f_r \arctan \frac{\sqrt{1-f_r^2}}{f_r} \right) \right] \right. \\ &\quad \left. + \frac{f_{rw}^3}{2f_r} \operatorname{arcsec} \left( \frac{1}{f_r} \right) + \frac{f_{rw}^5}{24f_r^2} \left( \sqrt{1-f_r^2} + \frac{1}{f_r} \operatorname{arcsec} \left( \frac{1}{f_r} \right) \right) \right. \\ &\quad \left. - \frac{\pi}{8} \left( \sqrt{1-f_r^2} + f_r^2 \ln \left( \frac{1 + \sqrt{1-f_r^2}}{f_r} \right) \right) \right\} \quad (F.8) \end{aligned}$$

Where and  $A = p_{LOT} + \sigma_o$ ,  $f_r = r/R$ ,  $f_{rw} = r_w/R$ , and  $R$  can be calculated in Eq. F.5. Eq. F.8 represents the shape of a horizontal fracture. Fig. 7.3 gives the plot of the horizontal fracture of the example in Chapter 7.

From Fig. 7.3, the curve of width vs. radius in plastic zone can be approximately regarded as linear, therefore the width at any radius  $r$ ,  $w(r,R)$ , can be calculated from the width at the wellbore wall,  $w(r_w,R)$ , by

$$w(r,R) = w(r_w,R) \frac{R-r}{R-r_w} \quad (\text{F.9})$$

The volume in a plastic fracture that gets to  $R$  is the integration of the opened shape. Substitution of Eq. F.9 into the volume equation yields

$$\begin{aligned} V_{ff}(R) &= \frac{2}{231} \int_{r_w}^R \int_0^{2\pi} w(r,R) r dr d\theta \\ &= \frac{1}{110} (R^2 + r_w R - 2r_w^2) w(r_w,R) \end{aligned} \quad (\text{F.10})$$

## APPENDIX G

### ANNULAR CRACK

Micro-cracks between cement and formation are closed by contact stress. To open a crack, wellbore fluid pressure should be increased to overcome the contact stress and tensile strength of the crack for penetrating fluid (Zhou and Wojtanowicz, 1999). The tensile strength is assumed as zero for soft formation.

Once a crack is opened, drilling fluid will flow into it and propagate the crack. Pressure drops along the opened crack for friction loss. The pressure drop in an annular for Bingham plastic fluid in laminar flow is expressed as (Bourgoyne et al, 1992)

$$\frac{dp_f}{dL} = \frac{\mu_p v}{1,000(d_2 - d_1)^2} + \frac{\tau_y}{200(d_2 - d_1)} \quad (G.1)$$

Where, pressure drop  $dp_f/dL$  is in unit of psi/ft. Plastic viscosity  $\mu_p$  is in centipoise. Velocity  $v$  is in feet/sec. Wellbore diameter  $d_1$  is in inches, and  $d_2 = d_1 + 2u_w$  ( $u_w$  is the displacement of wellbore under the acting of fluid pressure in the parted fracture). Yield point of the drilling fluid  $\tau_y$  is in lb/100 ft<sup>2</sup>. The relation of velocity with flow rate in gal/min is

$$v = \frac{q}{2.448(d_2^2 - d_1^2)} \quad (G.2)$$

Substituting Eq. G.2 into Eq. G.1 and simplifying the equation yields the gradient of frictional pressure loss.

$$\frac{dp_f}{dL} = \frac{\mu_p q}{39168u_w^3 d_1} + \frac{\tau_y}{400u_w} \quad (G.3)$$

Assuming the opened crack has a constant inner and outer diameter along the crack, and friction gradient is constant along the crack length  $L$ . The pressure to move the wellbore wall at the crack inlet,  $\Delta p_{wc}$ , is the difference of effective wellbore pressure at the casing shoe  $p_{LOT}$ , and the contact stress  $\sigma_c$  ( $\Delta p_{wc} = p_{LOT} - \sigma_c$ ). The pressure to move the wall at the tip of the crack is zero where the effective fluid pressure equals the contact stress. The width of the crack is the displacement of the wellbore wall,  $u_w$ . The average pressure to displace the wall,  $\Delta p_w = \Delta p_{wc} / 2$ , is used to calculate the average width of the crack.

The pressure drop on the whole crack due to friction  $p_f$  is  $p_f = p_{LOT} - \sigma_c = \Delta p_{wc}$ . Integrating Eq. G.3 and substituting the average displacement of the crack from Eq. E.8 in Appendix E gets

$$\Delta p_{wc}^2 = \frac{\mu_p q E^3 L}{16524 \Delta p_{wc}^2 r_w^3 d_1} + \frac{\tau_y E L}{300 r_w} \quad (G.4a)$$

Rearranging Eq. (G.4a) and solving for fracture length  $L$  yield

$$L = \frac{\Delta p_{wc}^2}{\frac{\mu_p q E^3}{16524 \Delta p_{wc}^2 r_w^3 d_1} + \frac{\tau_y E}{300 r_w}} \quad (G.4b)$$

Substitution the  $L$  from Eq. G.4b into the following volume equation of the crack yields

$$\Delta V_{cem} = \frac{12}{231} \pi d_1 u_w L = \frac{r_w^4 \Delta p_{wc}^3}{E^2} \left( \frac{1}{\frac{\mu_p q E^2}{8262 \Delta p_{wc}^2 r_w^2} + \frac{\tau_y r_w}{75}} \right) \quad (G.5)$$

## **APPENDIX H**

### **LOTUMS SOFTWARE**

LOTUMS, leak-off test in upper marine sediments, is developed for simulating leak-off test. The basic principle of the software was discussed in Chapter 7.

#### **H.1 LOTUMS Installation**

The file is stored in a CD with a name of LOTUMS.exe. It can be run on the CD directly. If copied on hard drive a computer with MS Windows, LOTUMS runs better from hard drive. Skilled computer user can skip this section.

To install the software just copy the file (LOTUMS.exe) from CD to the directory of one's hard drive. The detail procedure is:

- (1). Insert the disk in CD driver.
- (2). Create a directory in one's computer (using File Manager, Windows Explorer or DOS) as C:\LOTUMS.
- (3). Copy the file from CD drive to C:\LOTUMS.
- (4). Check the file LOTUMS.exe in one's C:\LOTUMS otherwise copy again.

For some computer without dynamic link library, the direct copy method may fail. The disk provides an install package to install the software on any PC. To install from the package (in the CD or copied file in one's hard drive), go to package directory and double click "setup.exe" file, the installation begins. Follow the guides of the installation to complete the installation.

#### **H.2 Use LOTUMS**

The usage of the software is very simple. Double click the file LOTUMS.exe using one's mouse from Windows Explorer to execute the program. Note that the

windows of the software may not fit one's computer screen very well but it will not affect his executing.

After the software is running on one's computer, windows appear. Users can follow the guides of the software and do leak-off test analysis following the menu of the software. Users may follow the procedure as follow.

- (1). Double click the file LOTUMS.exe on you CD or hard drive.
- (2). A flash window appears. If one is a legal user, click *Yes Button* on the window using the left button of his mouse or press and hold *Alt* key and press letter *Y* (represented as *Alt + Y*) on his keyboard if he doesn't want to use mouse. Otherwise, click *No Button* or hit *Alt + N* to end this execution. If one wants to choose any bottom or menu without mouse, he can use *Alt + ?* way. The ? here represents the underlined character on the bottom or menu, such as using *Alt + Y* to execute the bottom Yes.
- (3). The main window called "Leak-off Test Analysis Software" appear on one's screen after entering the software system. On the top of the window are menus named "File, Set Data, Stress State, Leak-off Test, Window and Help".
- (4). Click the *File* menu or *Alt+F* to enter the submenu. *Set P*rinter and *E*xit submenus are provided under the *File* menu. Click *E*xit (or *Alt + X*) to end the execution of the software. You can terminate the program any time by click the *E*xit menu. Any form of the software could be printed out on one's printer. Choose and connect the right printer using the *Set P*rinter submenu.
- (5). *Set D*ate menu provides the entrance of all the data needed for the analysis. Under the menu are five submenus named as *Set All Default*, *Well and Casing String*, *Mud and leak-off test*, *Cement Slurry and Rock*.

*Well and Casing String* submenu asks for data of well planning and casing string size. A new form will pop-up if one choose to execute the submenu. One can input data one by one or use *Set Default* button to set all provided data for the form. The default data are used for practicing. One can change the data on the form whenever he wants to. Choose *Ok* button to accept the data and terminate the form. Note that the data entered by *Set Default* don't represent they are the best values. They are just a sample of data set.

Same as *Well and Casing String* submenu, *Mud and leak-off test*, *Cement Slurry and Rock* submenus ask for data of mud and leak-off test properties, the properties of cement slurry and the properties of rock respectively.

If one don't want to set data one by one form, he can choose *Set All Default* to set all the needed data for mud, cement, rock, well and so on. He can change any data by clicking the appreciate form. Again, the data set by *Set All Default* do not mean they are the best data.

(6). After setting all the necessary data, one could do analysis through *In-situ Stress Analysis*, *Fracture Analysis* and/or *Leak-off Test analysis* submenus. One could find out whether the wellbore is in plastic state and how large the plastic region is as well as the in-situ stresses by choose *Calculate* button on the *In-situ Stress Analysis* menu. Click *Close* to end the form.

(7). *Leak-off Test* menu is the major part of the analysis. It contains *Fracture Analysis* and *LOT Analysis* submenus. On the *Fracture Analysis* form, choose button of *Fracture Analysis* to see the result of fracture way. *Fracture Shape* button shows the horizontal plastic fracture shape and size. Choose *Close* button to end the form.

LOT Analysis submenu provide leak-off test analysis. On the form of LOT Analysis, there are three command buttons named View LOT, Print, Clear, and Close. View LOT button executes calculation and draw its LOT curve on the form. Clear, Print and Close buttons clear the plots, print the form on one's printer and end the form respectively. Two frames of *LOT component* and *LOT Curve Color* are provided. LOT components include *Compressing Mud*, *Wellbore Expansion*, *Filtration*, *Cement Parting* and *Plastic Fracture*. One can watch any combination effect by check the appropriate boxes and then click View LOT. One could draw LOT curves in different color by choosing the color he likes by choosing the color option in a color frame.

*Compressing Mud* set the function of analysis of only mud compression. It gives casing test result. *Wellbore Expansion* sets the function of the analysis of the expansion of the open hole section during leak-off test. *Filtration* considers the effect of leak through any pre-existed channel or pre-existed formation fracture as well as filtration into rock pores. Changing the properties of mud on *Mud and Leak-off Test*, one'll see the effect of the filtration. Check *Cement Parting* box allow one to analyze the effect of cement parting of the leak-off test. *Plastic Fracture* adds the effect of horizontal plastic fracture on the LOT. The result of plastic fracture and filtration through the newly created surfaces will be added on the LOT curve once these boxes are checked.

(8). Menu of Window contains the current opened windows during the execution of the software. Users can shift form from one to another directly by using the submenus under the Window. Functions of multi-form operation are also provided under the Window menu. One may arrange forms in layer, horizontal and vertical.

Menu *Help* contains simple guides of using the software, and a *About* form which gives the information about the software is also provided under *Help* menu.

## APPENDIX I

### OVERBURDEN PRESSURE IN SHALLOW MARINE SEDIMENTS

#### I.1 Overburden Pressure in Shallow Marine Sediments

Overburden pressure can be calculated from rock density data available from well logs. If the bulk density ( $\rho_b$ ) is known as a function of depth, the overburden pressure for each depth interval is calculated by integrating the bulk density for each depth interval, and the overburden pressure is determined by the following equation using this procedure.

$$P_{over} = \int_0^{D_w} g \rho_w dD + \int_{D_w}^D g \rho_b dD \quad (I.1)$$

Where  $D_w$  and  $\rho_w$  are water depth and density,  $D$  and  $\rho_b$  are the vertical depth and formation density which is function of depth.

If rock density is unknown, Overburden pressure can also be assumed to be 1.0 psi/ft according to Harrison et al, 1954; Hubbert and Willis 1957.

##### I.1.1 Density Model

Bourgoyne et al (1991) presented a universal method to estimate bulk density at any depth (universal model) as

$$\rho_b = (1 - \phi_0 e^{-KD_s}) \rho_{grain} + \phi_0 e^{-KD_s} \rho_{fluid} \quad (I.2)$$

Where constants  $\phi_0$  and  $K$  are surface porosity and porosity decline constant determined graphically or by the least-square fit method.  $\rho_{grain}$  and  $\rho_{fluid}$  are the densities of sediment grain and pore fluid.  $D_s$  is the sediment's depth.

The formula fits the deep sediments in the Gulf of Mexico. However, it is not satisfied for the shallow part as shown in Fig. I.1. The parameters for Eq. I.2 are grain

density  $\rho_{grain} = 2.65$ , surface porosity  $\phi_0 = 0.77$  and porosity decline constant  $K = 323E-6$  for the Green Canyon area in the Gulf of Mexico according to Rocha (1993) and Bender et al. (1995).

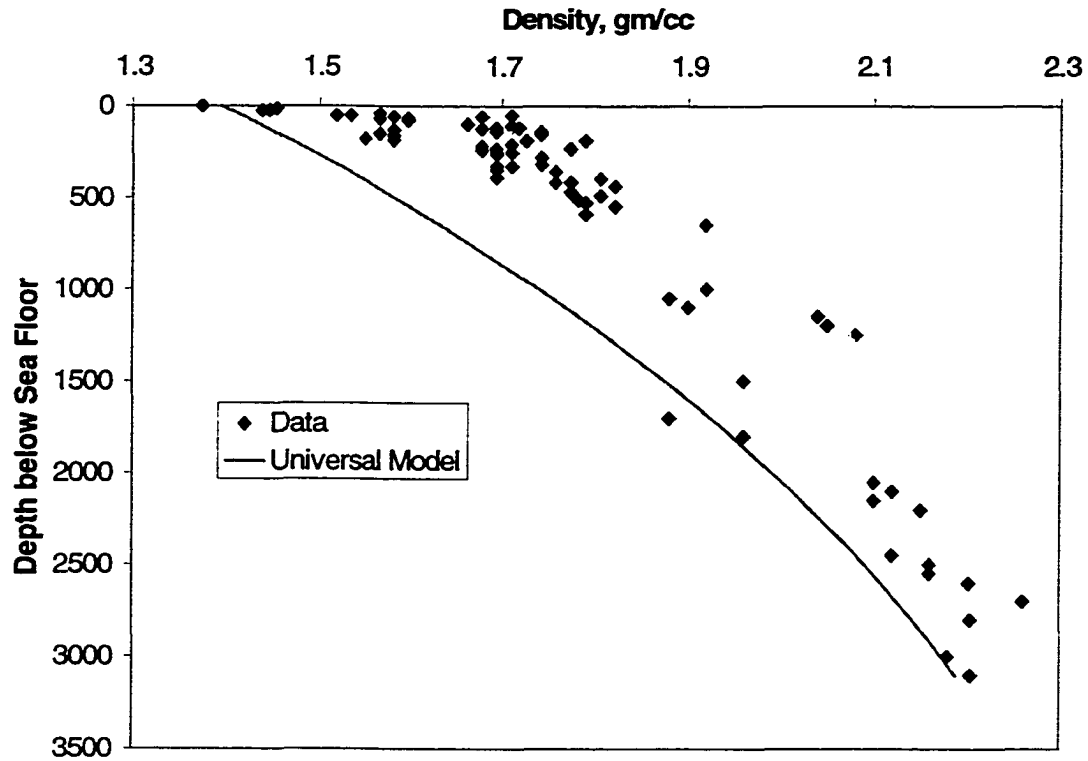


**Figure I.1 Comparison of boring data to universal model at shallow in the Green Canyon Area offshore Louisiana.**

The densities in the area from boring data are also presented in Fig. I.1. As shown in Fig. I.1, the universal model (Eq. I.2) underestimated the sediment density and therefore underestimated overburden pressure in the shallow marine sediment.

By fitting the density data in the Green Canyon area, a model is proposed for the shallow densities when only shale exists. The model provides three different formulas based on the depth as shown in Eq. I.3. The unit of density  $\rho$  is in gm/cc and the sediment depth  $D$  in feet.

$$\begin{aligned}
 \rho_1 &= 1.37(2 - e^{-D/400}) & 0 \leq D < 100 \\
 \rho_2 &= 1.65(2 - e^{-D/5500}) & 100 \leq D < 650 \\
 \rho_3 &= 1.7(2 - e^{-D/8000}) & 650 \leq D < 3000
 \end{aligned}
 \tag{I.3}$$

Fig. I.2 shows the source density data in the Green Canyon area and the calculated value from the model (Eq. I.3). In the figure, model 1, 2, and 3 are the formulas of  $\rho_1$ ,  $\rho_2$ ,  $\rho_3$  respectively.

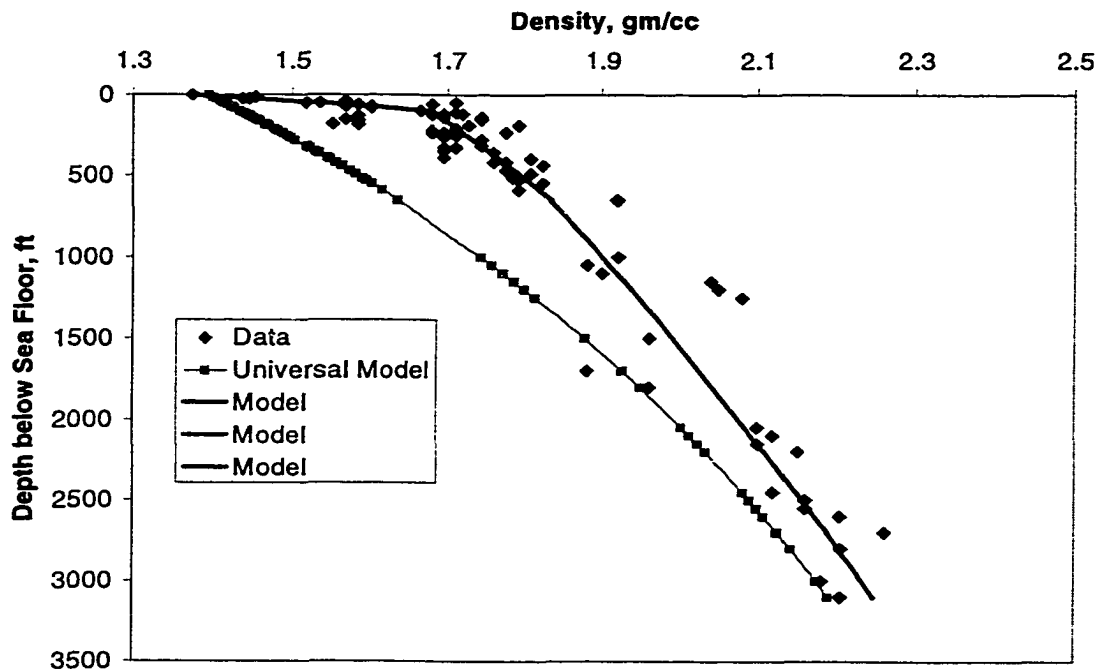


**Figure I.2 Comparison source data with new proposed model for the Green Canyon Area offshore Louisiana.**

### I.1.2 Overburden Pressure

Overburden pressure is the integration of the bulk density with depth. Substitution of Eq. I.2 into Eq. I.1, Bourgoyne's et al (1991) presented the following formula.

$$p_{over} = g\rho_w D_w + g\rho_{grain} D_s - \frac{(\rho_{grain} - \rho_{fluid}) g \phi_o}{K} (1 - e^{-KD_s})
 \tag{I.4}$$

The formula works fine for deep sediments in the Gulf of Mexico. However, in shallow marine sediments it loses its application since its basic density formula could not reflect the actual boring data. Substitution Eq. I.3 into Eq. I.1 and integration give the overburden formula in shallow marine sediments as shown in Eq. I.5.

$$\begin{aligned}
 p_{over} &= g\rho_w D_w + 1.2D_s - 240(1 - e^{-D/400}) : & 0 \leq D_s < 100 \\
 p_{over} &= g\rho_w D_w + 66.9 + 3929.5e^{-D_s/5500} + 1.4289D_s - 4001.56 : & 100 \leq D_s < 650 \\
 p_{over} &= g\rho_w D_w + 485.6 + 5888.8e^{-D_s/8000} + 1.4722D_s - 6386.19 : & 650 \leq D_s < 3000
 \end{aligned}
 \tag{I.5}$$

Where  $p_{over}$  = overburden pressure in psi.  $D_s$  = sediment depth in feet.

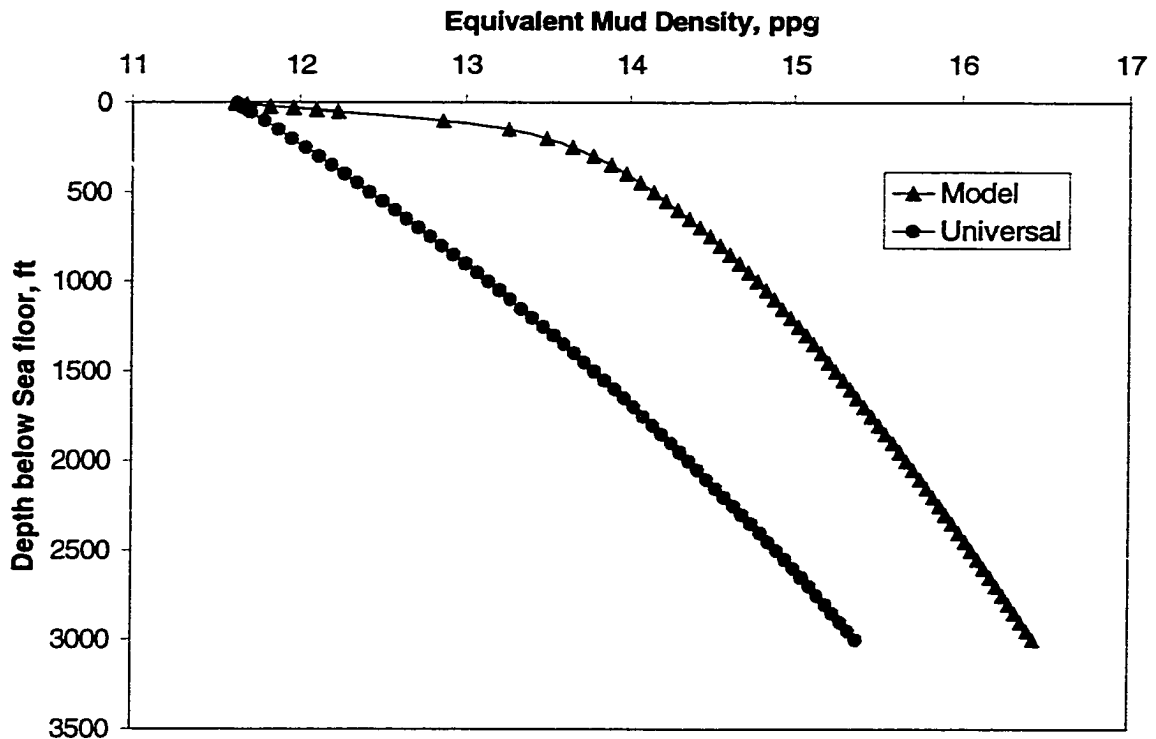


**Figure I.3 Overburden pressures from new model and Bourgoyne's in shallow marine sediments.**

Figure I.3 shows the equivalent overburden pressure gradient of the new proposed model with universal model in shallow marine sediments. The universal model in shallow underestimates the overburden pressure.

## I.2 SMS Containing Sand and Shale Sections

The boring data presented above are from the Green Canyon area in the Gulf of Mexico. All the sediments in the area from 0 to 650 ft below sea floor are clays. The model in Eq. I.3 is based on such pure soil property. However, for sediments with sand layers in shallow marine sediments, the correlation of density versus depth is not the same as Eq. I.3 as shown in Fig. I.4.

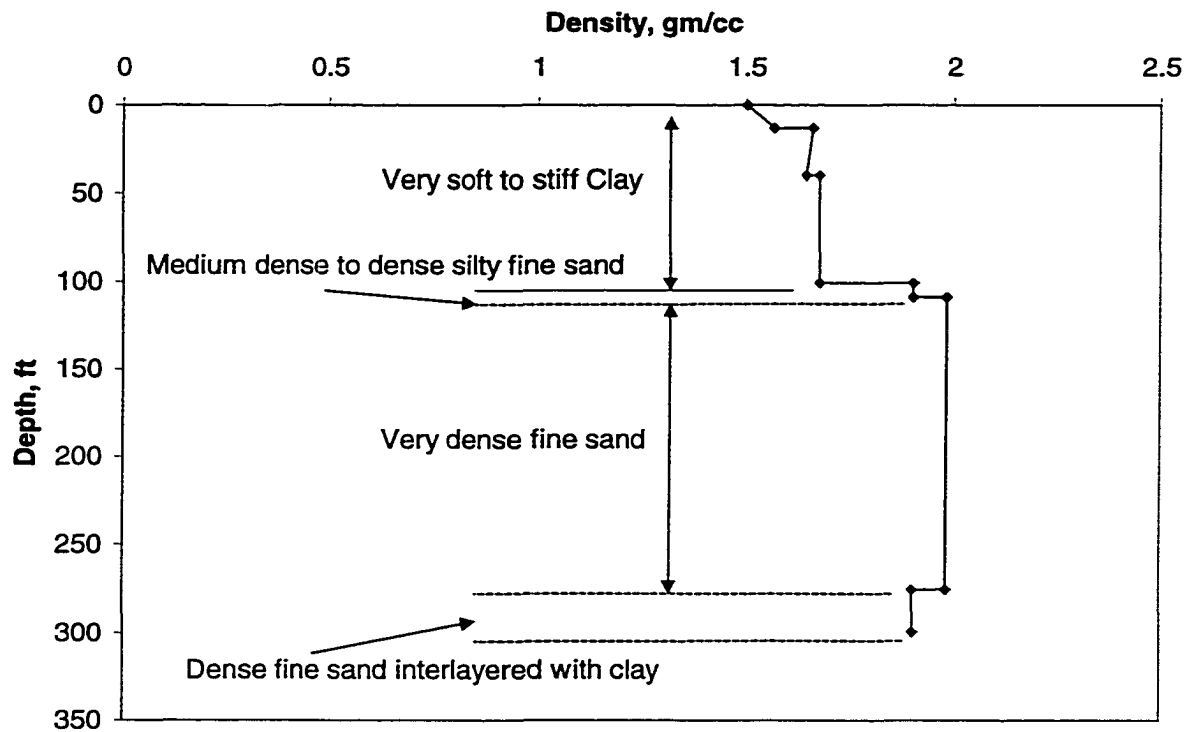


**Figure I.4** Densities of Sediments Containing Sand and Shale (Grand Isle Area).

As shown in Fig. I.4, the density of sand is approximate 1.98 gm/cc (0.86 psi/ft) and 1.90 gm/cc (0.82 psi/ft) for shaly sand. Other areas, such as Ship Shoal, Vermilion, West Delta, Grand Isle in the Gulf of Mexico support the conclusion that shallow sand density is about 1.98 gm/cc for sand and 1.90 gm/cc for shaly sand as shown in Fig. I.5.

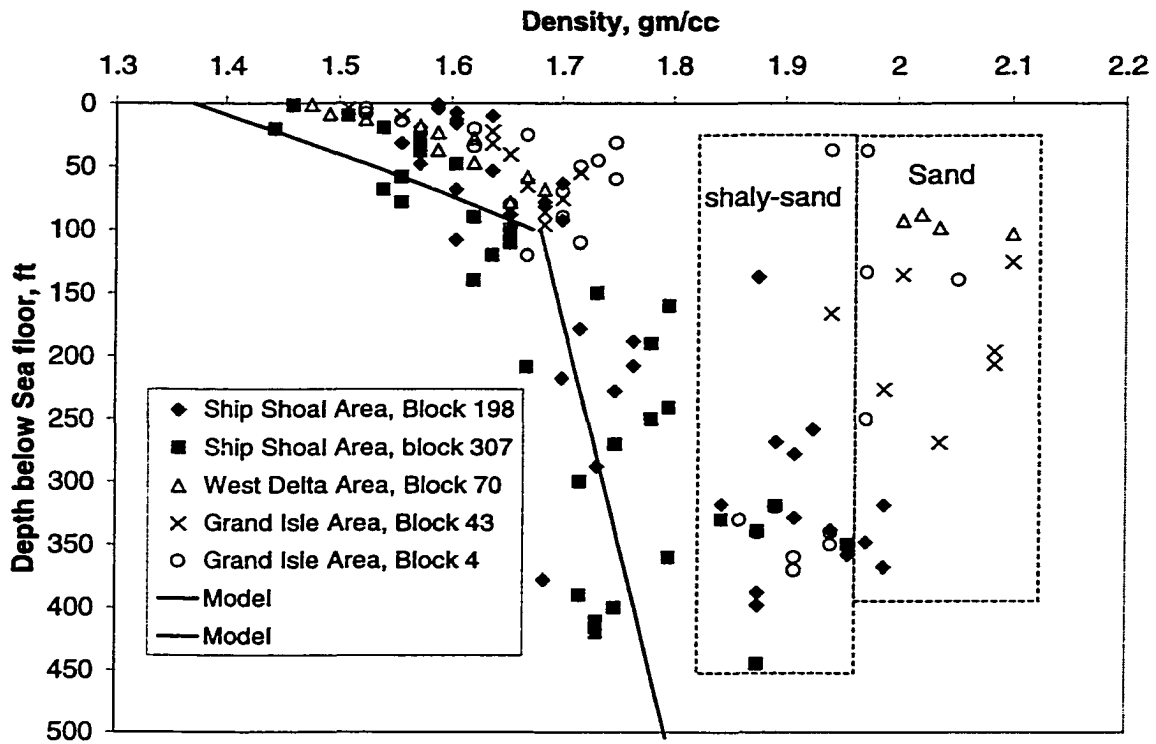


**Figure I.5 Sediments Containing Sand and Shale Section.**

Shallow marine sediment model in Eq. I.3 represents compaction of clay. However, in SMS, sand is not showing the effect of compaction as shown in Figure I.5. The model of mixture of layers of sand and shale is

$$P_{over} = P_{over-clay} + 0.86D_{sand} \quad (I.6)$$

Where  $p_{over-clay}$  = overburden pressure from Eq. I.5 with a depth of  $(D_s - D_{sand})$ .  $D_s$  and  $D_{sand}$  are the total depth of the sediment and the depth of sand respectively.

For example if an interested place is at 1000 ft below sea floor in the Green Canyon area, and the total sand depth in the 1000 ft is 400 ft. Sea water depth is 1750 ft. Then the overburden pressure from the sand is  $0.86 \cdot 400 = 344$  psi. The overburden pressure from the clay =  $66.9 + 3929.475e^{-600/5500} + 1.4289 \cdot 600 - 400 = 1.56 = 446$  psi. Sea

water density is 0.442 psi/ft, overburden from the sea water is  $0.442 \times 1750 = 773.5$  psi.

Therefore, the total overburden pressure at the place below sea floor 1000 ft is

$344 + 446 + 773.5 = 1563.5$  psi.

## VITA

Desheng Zhou, son of Lisheng Zhou and Hongyu Long, was born on November 19, 1963, in Wusheng, People's Republic of China.

He received his bachelor of engineering degree from Beijing University of Aeronautics and Astronautics in July 1985. In June 1988 and July 1992, he received his master's degree and doctoral degree in engineering from Southwest Petroleum Institute in Nanchong, People's Republic of China.

Since 1997, he has studied for his doctoral degree in petroleum engineering at Louisiana State University. The degree of Doctor of Philosophy will be conferred in December, 2000.

**DOCTORAL EXAMINATION AND DISSERTATION REPORT**

**Candidate:** Desheng Zhou

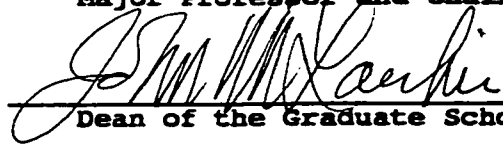
**Major Field:** Petroleum Engineering

**Title of Dissertation:** Well Integrity Mechanism, Failure, and Testing in Shallow Marine Sediments

**Approved:**



Major Professor and Chairman



Dean of the Graduate School

**EXAMINING COMMITTEE:**



Jeffrey A. Nason

Jh Roger Smith

**Date of Examination:**

August 3, 2000